DISSERTATION

MOLECULAR CHARACTERIZATION OF CANINE PERIPHERAL T-CELL LYMPHOMA

Submitted by

Lauren Harris

Department of Microbiology, Immunology, and Pathology

In partial fulfillment of the requirements

For the Degree of Doctor of Philosophy

Colorado State University

Fort Collins, Colorado

Summer 2020

Doctoral Committee:

Advisor: Anne Avery

Paul Avery
Randall Basaraba
Susan Bailey

ABSTRACT

MOLECULAR CHARACTERIZATION OF CANINE PERIPHERAL T-CELL LYMPHOMA

Peripheral T-cell lymphoma (PTCL) encompasses a heterogenous group of tumors derived from neoplastic T-cells that affect the peripheral lymphoid organs, most often the peripheral lymph nodes. PTCL is a naturally-occurring disease in multiple species, including humans and dogs. This disease is poorly understood and associated with short overall survival times in both canine and human patients. PTCL is relatively more common in dogs, and therefore the dog provides a unique opportunity to serve as a naturally occurring model. **Hypothesis:** We hypothesize that canine PTCL and a subset of human PTCL have shared pathologic features and molecular drivers; therefore, the dog will provide a useful translational model to aid in the discovery of novel, targeted therapies. We test this hypothesis by 1) characterizing tumor heterogeneity, biologic behavior, and gene expression profile of canine PTCL 2) comparing the molecular features of canine PTCL to those previously identified in human PTCL 3) identifying the normal immunological counterpart(s) of canine PTCL and 4) discovering oncogenic molecular pathways and driving genetic alterations including fusion genes.

Aim 1: Characterization of the histomorphology, clinical features, and gene expression profile of canine PTCL. Our understanding of the biologic and molecular subtypes of lymphoproliferative diseases in dogs is scarce compared to what is known about similar diseases in humans. Within the T-cell lymphoma (TCL) group, tumors can be categorized by expression of the surface antigen molecules CD4 and CD8, with the majority of TCL cases in

dogs expressing CD4. $CD4^+$ TCL has been previously associated with a poor prognosis and short overall survival times. Tumors expressing CD8 or lacking expression of CD4 or CD8 are considered rare. In an effort to better characterize these TCL phenotypes we evaluated a large number of cases with paired flow cytometry and biopsy samples to determine if tumors diagnosed as TCL by flow cytometry identified distinct lymphoma subtypes with consistent histologic and molecular features. All evaluated tumors diagnosed as $CD4^+$ TCL had a histologic pattern and cellular morphology consistent with PTCL. RNA-seq was performed on a small group of $CD4^+$ PTCL cases compared to sorted non-neoplastic $CD4^+$ lymphocytes. The gene expression pattern of $CD4^+$ TCL was similar between all cases, regardless of dog breed. We then focused on the less common $CD8^+$ and $CD4^-CD8^-$ subgroups. A small subset of $CD8^+$ and $CD4^-CD8^-$ tumors were evaluated histologically or cytologically. Tumor morphology was consistent with PTCL, but exhibited increased variation in cytologic appearance with some cases displaying marked atypia. We then evaluated the presenting clinical signs, flow cytometry, and clinical outcomes of a large group of dogs diagnosed with either $CD8^+$ or $CD4^-CD8^-$ TCLs. Dogs with either $CD8^+$ or $CD4^-CD8^-$ TCLs had aggressive clinical disease with short overall survival times. Skin lesions present at the time of diagnosis were more commonly observed in the $CD8^+$ TCL group. Mediastinal enlargement and/or hypercalcemia, clinical features previously associated with $CD4^+$ TCL, were more commonly present in patients with $CD4^-CD8^-$ TCL. Shared diagnostic and clinical features identified in both $CD4^-CD8^-$ and $CD4^+$ TCLs suggested a common pathogenesis. Conversely, $CD8^+$ TCLs exhibited unique clinical features and prognostic indicators suggesting that these tumors may have a different pathobiology.

Aim 2: Evaluation of canine PTCL as a model for human PTCL-NOS. In humans, peripheral T-cell lymphoma (PTCL), not-otherwise specified (NOS) is the most common PTCL

subgroup. Recent studies using human patient samples have identified molecular subtypes of PTCL-NOS, including PTCL-GATA3 and PTCL-TBX21. PTCL-GATA3 is associated with a worse prognosis and frequent alterations in the CDKN2A/TP53 and PTEN-PI3K signaling pathways. We identified molecular similarity to human PTCL-NOS by evaluating the gene expression profiles of a large number of canine PTCL cases by RNA-seq. We show that canine PTCL is most similar to the PTCL-GATA3 subgroup, with strong expression of GATA3 and gene enrichment for the PI3K-AKT-MTOR pathway. *In vitro* cell culture studies established a functional role for PI3K signaling in canine PTCL. Inhibition of PI3K resulted in impaired proliferation of a canine T-cell lymphoma cell line and reduced survival of primary patient-derived PTCL cells. We show that the dog may provide a unique opportunity to further investigate the pathogenesis of the PTCL-GATA3 subgroup.

Aim 3: Evaluation of canine PTCL cell of origin. Classification of hematopoietic neoplasms is in part reliant upon identification of the cell of origin, which can provide insights into the underlying pathogenesis and can have prognostic and therapeutic impact. We evaluated surface protein expression and changes in gene expression in canine PTCL to identify the normal immunological counterpart. We demonstrated that $CD4^+$ PTCL appears to be derived from a naïve single positive T-cell. This conclusion is supported by lack of expression of markers of activation (MHC class II, CD25, and T-cell receptor signaling molecules) as well as lack of upregulation of markers associated with T helper subsets. $CD4^-CD8^-$ tumors were enriched for gene signatures associated with a more immature T-cell phenotype, and therefore are thought to most likely develop from an immature, double negative, thymic precursor cell. $CD8^+$ TCLs upregulated molecules associated with activated cytotoxic T-cells, suggesting that at least a subset of $CD8^+$ TCLs may originate from a mature $CD8^+$ effector cell.

Aim 4: Discovery of fusion gene candidates in canine PTCL. Chromosome aberrations and rearrangements resulting in the formation of fusion genes are common in a wide variety of cancers. Fusion genes are particularly common drivers of hematologic malignancies (e.g., AML) and serve as useful diagnostic markers as well as therapeutic targets. We aimed to discover fusion gene candidates in canine PTCL using FusionCatcher, an RNA-seq based discovery pipeline. We identified 11 recurrent fusion genes of interest and evaluated the structural fusion events in these cases. Recurrent fusion genes involving DGKZ-MDK and LMO4 with several 5' fusion partners were particularly interesting due to their oncogenic potential. This study identifies a list of potential fusion gene candidates in canine PTCL, and lays the groundwork for future efforts to validate these targets. Identification of these potential driving fusion genes is critical for both improving diagnosis, as well as the development of targeted and personalized therapeutics.

Conclusions: This dissertation improves mechanistic understanding of the molecular and genetic drivers of canine PTCL and correlates these findings to the human counterpart of the disease. In so doing, we provide essential supporting evidence that the dog may serve as a useful and relevant, naturally occurring, translational model of hematopoietic neoplasia. In a broader sense, this work supports a comparative approach to understanding cancer biology and treatment through collaborations between veterinarians, biomedical researchers, and physicians.

ACKNOWLEDGEMENTS

Throughout my training as a scientist, pathologist, and veterinarian I have been incredibly fortunate to benefit from strong mentorship. I would like to thank my advisor, Dr. Anne Avery, for her generous guidance and support. Anne has an innate scientific curiosity, ability to ask critical scientific questions, and work ethic that I greatly admire and hope to one day emulate. Anne is a strong woman in science who is able to balance her clinical and research appointments in a unique and mutually beneficial manner. The mentorship of Dr. Avery and my time spent in her lab will have a prolonged and significant impact on my career as a scientist and a pathologist.

I would also like to thank my committee members, Drs. Paul Avery, Randy Basaraba, and Susan Bailey for their generosity with their time and for all of their insight, valuable feedback, and guidance along the way. Further, I would like to thank Dr. Ed Hoover for overseeing the T32 grant for biomedical research training for veterinarians at CSU. My support through the T32 grant was instrumental in the completion of this project and has provided me with ample opportunities for growth and development as a researcher. The work in this project could not be done without all the members of the Clinical Immunology Laboratory. Janna Yoshimoto, Rob Burnett, Emily Rout, Kelly Hughes, Julia Labadie, and Jeremy Dossey, in particular, have been answered my countless questions and have contributed significantly to this project.

During the combined residency-PhD program I was also fortunate to have worked closely with the CSU pathology faculty who all spent innumerable hours teaching me and guiding me to become a passionate and competent pathologist. Drs. EJ Ehrhart, Paula Schaffer, Gary Mason, Chad Frank, Colleen Duncan, and Deanna Dailey have spent extra time and interest in my

growth as a diagnostician and as a person. From weekend necropsy days, happy hour chats, and evening talks in the diagnostic lab I am so grateful for your endless support and encouragement.

I am incredibly thankful for my resident-mates and lab-mates who have become long-lasting friends, colleagues, and mentors. My resident-mate, Alex Byas, has been with me every step of the way and I am so grateful for her support and friendship throughout this journey. Allison Vilander, Laura Hoon-Hanks, Klaudia Polak, Kendra Andrie, Emily Rout, and Kelly Hughes are dear friends who have been commiserated with me through challenges, given me sage advice, celebrated successes, and pushed me to become a better pathologist, researcher, and person.

Finally, I would like to thank my family and friends who have always encouraged me to challenge myself and have believed in me, even when I was experiencing times of doubt. My parents have tirelessly supported me and have shown me the power of hard work, determination, and intellectual curiosity. They have instilled in me the value of education and have taught me the joy and satisfaction of being a life-long learner. I feel so incredibly fortunate to find a profession that I am truly passionate about and I would never have been able to do that without their support. My brother, James, has always encouraged me to become the best person I can be and to strive to make positive change in the world. He has been a role model throughout my life, and I couldn't imagine a better person to look up to. Lastly, I am grateful for my fiancé, Kevin, who has shared every high and every low with me throughout this journey. Thank you for encouraging me, supporting me, and believing in me.

TABLE OF CONTENTS

CHAPTER 1 – INTRODUCTION

T-cell Development and the Classification of Lymphoid Neoplasms

Overview

Lymphoma is a broad term used to describe clonal tumors of mature and immature B-cells, T-cells, and NK cells at various stages of differentiation. Classification of lymphoma is reliant on a number of diagnostic features including cellular morphology, immunophenotype, genetic abnormalities, and clinical presentation. Neoplastic cells often appear to recapitulate stages of normal B-cell or T-cell development, and therefore classification is often based, at least in part, according to the corresponding normal counterpart.

T-cells are key effectors of cell-mediated immunity and their development and differentiation involves a complex and tightly regulated series of events. T-cells are highly specialized to combat microbial pathogens, mediate immune surveillance against tumor cells, and coordinate antigen-driven responses. These cells originate from hematopoietic precursors which migrate to the thymus, differentiate, undergo selection, and eventually mature into functional T-lymphocytes (Figure 1.1).[1]

Thymic Development

T-cells arise from bone marrow progenitor cells that emigrate to the thymus to mature and undergo gene rearrangements to produce their antigen receptors.[2]As multipotent progenitors leave the bone marrow and travel to the thymus, they become progressively more restricted in their fate options.[3] Progenitor cells can be identified by expression of cell-surface markers that characterize stem cells such as CD34, and lack of the characteristic cell-surface glycoproteins of mature T-cells.[4–7] Following emigration to the thymus and interaction with thymic stromal cells,

these cells are signaled to divide and differentiate. IL-7 is secreted by thymic stromal cells and binds to the IL-7 receptor on thymocytes.[4,8–10] This interaction is critical for T-cell development. Knockdown of the IL-7 receptor experimentally or within patients who have inherited two defective IL-7R alleles results in the absence of T-cells and subsequent immunodeficiency.[8,11–13]

Thymic stromal cells are also important in promoting activation of the Notch1 pathway, a major regulator of T-cell development.[14] Notch1 is a cell-surface receptor that is expressed on the surface of thymocytes and interacts with the ligands present on thymic epithelial cells.[15–17] Notch1 is vital for T-cell commitment and inhibition of B-cell differentiation.[18,19] The critical role of Notch1 is highlighted by studies in which mice that are reconstituted with bone-marrow precursors expressing a constitutively active form of Notch completely lack B-cell development. Instead, these mice develop $CD4^+CD8^+$ double positive (DP) cells in the bone marrow.[19] Furthermore, Notch-1 deficient mice exhibit a block of T-cell development and concurrent development of B-cells within the thymus.[18]

T-lymphoblastic leukemia/lymphoma is derived from T-cell progenitors within the bone marrow and early thymic T-cell progenitors. These precursor neoplasms are typically identified by the expression markers of immaturity including: CD34, TdT, CD1a, and CD99.[20–22] Activating mutations of the NOTCH1 gene are present in greater than 50% of T-ALL patients, demonstrating deregulation of normal thymic development in these patients.[23,24]

Differentiation of progenitor cells is dependent upon temporally coordinated expression of cell surface proteins, including CD4, CD8, CD44, and CD25 on the thymocytes.[25] Progenitor cells entering the thymus do not express CD4 or CD8 and are therefore termed double-negative (DN) thymocytes.[26] DN thymocytes progress through DN1 (CD44+CD25-), DN2 (CD44+CD25+), DN3 (CD44-CD25+) and DN4 (CD44-CD25-)stages.[1,2,27] At this stage,

rearrangement of the T-cell receptor (TCR) γ, δ, and β loci can occur and DN thymocytes give rise to two distinct lineages of T-cells, distinguished by the expression of an α:β or γ:δ T-cell receptor (TCR).[28–30] This process is termed β-selection.

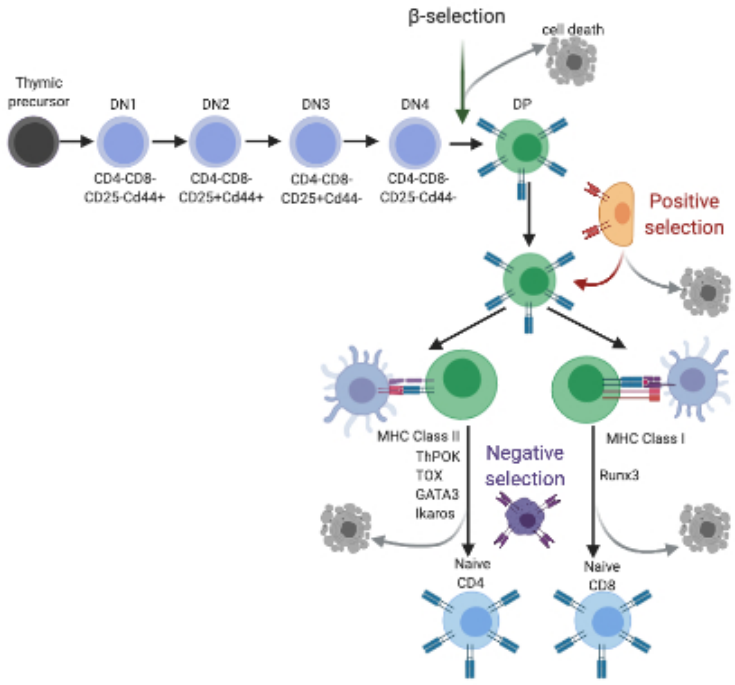

Figure 1.1 Overview of thymic T-cell development. Bone marrow derived hematopoietic progenitors migrate to the thymus. Early thymic precursors lack expression of T-cell receptor (TCR), CD4 and CD8, and are termed double-negative (DN) thymocytes. DN thymocytes undergo four stages of differentiation (DN1, $CD44^{+}CD25^{-}$; DN2, $CD44^{+}CD25^{+}$; DN3, $CD44^{-}CD25^{+}$; and DN4, $CD44^{-}CD25^{-}$). As cells progress through the DN stages, they undergo TCR gene rearrangement and B-selection, resulting in formation of the pre-TCR. Successful formation of a pre-TCR results in cell proliferation and expression of CD4 and CD8, termed double positive (DP) thymocytes. The pre-TCR α-chain is then replaced with a newly rearranged TCR α-chain, resulting in a complete αβ TCR. DP thymocytes undergo positive selection by interacting with cortical epithelial cells that express MHC class I and class II molecules and present self-peptides. A weak interaction results in apoptosis. Thymocytes that express TCRs that bind to MHC class I molecules become single positive (SP) $CD8^{+}$ T-cells and those with TCRs that bind to MHC class II molecules become SP $CD4^{+}$ T-cells. Cells further undergo negative selection, which results in removal of cells that interact too strongly with self-peptides on hematopoietic antigen presenting cells. Commitment to the CD4+ lineage is dependent upon key transcription factors ThPOK, GATA3, TOX, and Ikaros whereas commitment to the $CD8^{+}$ lineage is dependent on the transcription factor Runx3.

Commitment to a α:β or γ:δ T-cell lineage is determined by productive or non-productive rearrangements of TCR genes. TCR gene rearrangement is analogous to immunoglobulin gene rearrangements undergone during B-cell development. The β and δ chains contain V,D, and J segments. The first rearrangement for a β or δ chain joins D to J and the second rearrangement

joins V to DJ. The α and γ chains contain only V and J segments and therefore, a single rearrangement joins the V and J.[31] The process of gene rearrangement is regulated by the genes *RAG1* and *RAG2 (*recombination-activating genes), and involves the enzyme TdT which inserts the N nucleotides.[32,33] Both α:β and γ:δ T-cells begin rearranging the γ,δ, and β TCR loci at the DN stage. If an individual thymocyte is able to make a successful γ:δ receptor prior to a functional β chain, then the cell commits to become a γ:δ T-cell.[28,34] Conversely, if a functional β chain is created first this receptor chain is incorporated into a pre-TCR. The pre-TCR is formed by binding of the β chain to an invariant polypeptide termed pTα to form a superdimer.[35,36]

This pre-TCR is a rigorous test of the β chain conformation and its potential to bind the α chain to form a functional TCR. The α:β lineage is favored because the α:β lineage only requires one productive rearrangement, whereas γ:δ lineage requires two productive rearrangements.[37] Following formation of a pre-TCR, gene rearrangements are halted by suppression of *RAG1* and *RAG2*, proliferation is induced, and the thymocytes gains expression of the CD4 and CD8 co-receptors and are then termed double-positive (DP) thymocytes.[38–40] Upon progression into the DP stage, cells are allowed to continue with TCR chain rearrangement including α-chain genes and continued γ and δ gene rearrangements. At this stage, if a DP thymocyte creates an α:β receptor prior to a γ:δ receptor it will commit to α:β lineage. Alternatively, if a γ:δ receptor is created first than it will commit to the γ:δ lineage.[41] Cells with functional γ:δ rearrangements then assemble with the CD3 signaling complex and leave the thymus to enter circulation and migrate to peripheral tissues.[42] If the thymocyte fails to create a functional TCR gene rearrangement, then the cell will undergo apoptosis and be phagocytosed by thymic cortical macrophages.[43,44] Peripheral γ:δ cytotoxic T-cells of the splenic pool are

believed to be the cell-of-origin of hepatosplenic T-cell lymphomas (HSTL)[45]. A smaller fraction of HSTL, are believed to be derived from α:β cytotoxic T-cells.[20,46]

The process of TCR gene rearrangement produces a highly diverse repertoire of TCRs that can interact with MHC class I and class II isoforms. However, the TCR genes of an individual are not specific for the forms of MHC molecules expressed by that same individual. Therefore, positive selection is a necessary process that occurs to select only the thymocytes that can recognize the self-MHC complexes expressed on thymic cortical epithelial cells.[47,48] Following positive selection, DP thymocytes differentiate into single-positive (SP) CD4 or CD8 T-cells. When a DP thymocyte interacts with an MHC class I molecule, CD8 molecules are recruited. Conversely, when a DP thymocyte interacts with an MHC class II molecule, CD4 molecules are selected.[49,50] This stage of T-cell development is highly regulated by changes in gene expression and defined by detectable cell-surface phenotypes. In particular, the T-helper-inducing POZ/Krueppel-like factor (Th-POK), GATA3, TOX, and Ikaros are key regulatory transcription factors that drive the development of SP CD4 thymocytes from DP thymocytes.[47,51–56] Conversely, Runx3 directs commitment to the CD8 lineage.[57,58]

Following commitment to a SP lineage, T-cells undergo the process of negative selection. This process removes cells whose antigen receptor binds too strongly to the complexes of self-peptides and self-MHC molecules presented by cells within the thymus, including bone marrow derived dendritic cells and macrophages. This process of negative selection is critical for the elimination of potentially autoreactive T-cells and prevention of subsequent autoimmune disease.[25,59,60]

α:β T-cells that survive the processes of positive and negative selection and commit to CD4 or CD8 single positive lymphocytes, are able to leave the thymus as naïve T-cells. These

cells enter the circulation and travel to secondary lymphoid tissues. Within secondary lymphoid tissues, naïve T-cells can interact with specific antigens and become activated. Antigen-exposure triggers proliferation and further differentiation into the effector T-cell subsets.

T-cell Activation

Adaptive immune responses are coordinated to maximize exposure of lymphocytes to potential antigens. Essential to this process, are myeloid dendritic cells (DCs), which capture antigens at the site of infection and then travel to secondary lymphoid tissues to present to naïve T-cells. The dendritic cells express pathogen-derived peptides on MHC molecules. Binding of the T-cell to the dendritic cell involves binding of the T-cell LFA-1 to ICAM-1 and ICAM-2 on the DC, as well as binding of the DC LFA-1 to ICAM-3 expressed on the T-cell.[61] ICAM-3 also binds to the adhesion molecule DC-SIGN, which is uniquely expressed on activated DCs.[62,63] These cell surface interactions promote binding of the antigen receptor to the peptide-MHC complexes on the surface of a DC. The binding of the TCR and co-receptor (CD4 or CD8) with the MHC complex is necessary, but not sufficient, for T-cell activation. A co-stimulatory signal is also required and is induced by binding of the co-stimulatory receptor CD28 on T-cells to its ligand B7 on DCs.[64,65]

Upon organization of the molecules on the T-cell membrane and formation of the immunological synapse, cytoplasmic protein tyrosine kinases are activated to phosphorylate tyrosine residues in the cytoplasmic tails of the CD3 cell-surface proteins and the associated ζ chain (CD247). The phosphorylated residues are a component of the immunoreceptor tyrosine-based activation motifs (ITAMs). One of the molecules that phosphorylates the CD3 ITAMs is Lck.[66] Lck also actives ZAP-70, another protein kinase, which is necessary for the initiation of the major pathways of T-cell activation and signaling.[67] ZAP-70 initiates cell signaling pathways

including nuclear factor of activated T-cells (NFAT), activating protein-1 (AP-1), and NFκB which ultimately result in transcription of genes that promote T-cell proliferation, differentiation, and effector function.[68,69] Particularly important for T-cell proliferation is the cytokine IL-2. IL-2 works in an autocrine manner to trigger cell division.[70]

A number of T-cell neoplasms are derived from activated T-cells. Skin-homing activated T-cells are believed to be the normal counterpart to cutaneous lymphoma syndromes including mycosis fungoides, primary cutaneous CD30-positive T-cell lymphoproliferative disorders, and primary cutaneous anaplastic large cell lymphoma.[20,71]

Differentiation of Activated T-cell Subsets

Differentiation of activated T-cells is dependent upon the antigen to which they are responding. CD8 T-cells, which interact with MHC class I molecules, are particularly important for defense against intracellular pathogens, such as viruses and bacteria, as well as for tumor surveillance.[72] CD8 T-cells are considered cytotoxic and can release cytotoxins including perforin, granzymes, and granulysin to trigger cell-death via apoptosis.[73]

T-cell large granular lymphocytic leukemias (T-LGLs) are believed to be derived from a subset of $CD8^+$ α:β T-cells. A smaller portion of LGL leukemias are derived from natural killer cell lineage.[74,75] T-LGLs can express the cytotoxic effector proteins including perforin, TIA1, granzyme B, and granzyme M.[20] This neoplasm is thought to be driven by an initial exposure to an unknown antigen which results in oligoclonal LGL expansion.[76] Chronic and persistent antigen exposure results in STAT3 activation and the development of a dominant clone. This proposed pathogenesis is supported by serial studies of T-cell repertoire utilization.[77]

Effector CD4 T-cells, on the other hand, do not directly attack pathogens but rather help other cells of the immune system to perform their necessary functions and coordinate an

appropriate immune response. CD4 T-cells are therefore, termed T-helper cells. CD4 T-helper cells are highly heterogenous in their functions, cell-surface marker expression, and cytokine secretion. Classification of CD4 T-helper cell subsets is a continually evolving field with new subtypes being identified and overlapping features amongst existing subtypes. Nevertheless, there are five major T-helper subtypes identified: Th1, Th2, Th17, T follicular helper cells (Tfh), and regulatory T-cells (Treg).

Th1 cells aid in macrophage responses to intracellular bacterial and viral infections. Differentiation of Th1 cells is induced by the cytokines IL-12 and INF-γ to activate the defining transcription factor T-bet (TBX21). TBX21 regulates expression of INF-γ and can repress Th2 cytokines, Il-4 and IL-5.[78] Activated Th1 cells secrete IL-12 and INF-γ to further promote Th1 differentiation.

Th2 cells aid in the response to parasitic infections mediated by eosinophils, basophils, and mast cells. In addition, Th2 lymphocytes play a role in the repair and recovery of tissues injured by inflammatory processes. Th2 cell differentiation is induced by secretion of IL-4 which activates the major transcription factor GATA3.[79–81] GATA3 activation then promotes upregulation and secretion of IL-4 and IL-5. The balance between Th1 and Th2 T-cell subsets plays a role in determining the susceptibility to disease states, where an improper skew of Th2 cells can lead to allergy and asthma and an overactive Th1 response can result in autoimmunity.[82]

Th17 cells work to promote neutrophil-mediated responses to extracellular bacterial and fungal infections.[83–85] Th17 cell differentiation is induced by IL-6, TGF-β, Il-21, and IL-23, which promote transcription of RORγT.[86] RORγT is the master regulator of the Th17 subgroup and works to induce transcription of genes encoding IL-17 and IL-17F in naïve $CD4^+$ T helper

cells.[86] Th17 cells then secrete IL-17 and IL-6. IL-17 aids in recruiting neutrophils to sites of infection.[87]

Tfh cells interact with naïve B-cells to promote the antibody-mediated response to infection. The cytokine IL-6 promotes Tfh cell differentiation and induces expression of Bcl6, the master regulator of this subgroup.[88–91] Bcl6 is required for Tfh cells to express CXCR5, the receptor for the CXCL13 chemokine produced by the stromal cells of the B-cell follicle. The CXCR5-CXCL13 interaction allows Tfh cells to leave the T-cell areas of the secondary lymphoid tissue and migrate to the B-cell follicles.[92] Tfh cells secrete IL-21 and IL-4 which aid in class-switching, as well as formation and maintenance of the germinal center.[93,94]

Angioimmunoblastic T-cell lymphomas (AITL) are derived from Tfh cells and express the key markers BCL6, CXCR5, CD10, and CXCL13.[95–98] Patients with AITL often present with autoimmune phenomena including circulating immune complexes, cold agglutinins, hemolytic anemia, rheumatoid factor and anti-smooth muscle antibodies. Additionally, approximately half of patients have a concurrent polyclonal hypergammaglobulinemia, consistent with secondary disruption of normal B-cell physiology.[99,100]

Treg cells are unique in that they work to dampen the immune response. Tregs are induced by TGF-β in the absence of IL-6 and other pro-inflammatory cytokines.[101] Tregs express the master transcription factor FoxP3 as well as the cell-surface molecule CD25.[102] Activated Tregs secrete TGF-β and IL-10, which are important inhibitors of inflammation and immune responses.[103] Adult T-cell leukemia/lymphoma (ATLL) is postulated to be derived from $CD4^+$ $CD25^+$ FoxP3+ Tregs[104] and patients with ATLL characteristically exhibit T-cell immunodeficiency and frequent opportunistic infections[20,105–107].

Peripheral T-cell Lymphomas

Overview

Peripheral T-cell lymphomas (PTCL) encompass a heterogenous group of aggressive T-cell neoplasms. These neoplasms are uncommon, comprising 5-20% of all non-Hodgkin lymphomas (NHL).[20,108] This group of neoplasms includes tumors classified as angioimmunoblastic T-cell lymphoma, ALK^+ anaplastic large cell lymphoma, ALK^- anaplastic large cell lymphoma, adult T-cell leukemia/lymphoma (ATLL) and extranodal NK/T cell lymphoma of nasal type. Approximately 30-50% of PTCL cases do not correspond specifically to defined T-cell entities in the World Health Organization classification and are therefore categorized as PTCL, not otherwise specified (NOS).[20,109,110] Advances in the understanding of the underlying pathobiology of PTCL-NOS and development of targeted treatments have been limited by the disease heterogeneity, rarity, and lack of appropriate animal model systems.[111]

PTCL-NOS affects older patients with a median age of 60 years at the time of presentation and more commonly affects males, with a reported 2:1 male-to-female ratio.[109] Patients most often exhibit peripheral lymph node involvement. Advanced disease stages are common at the time of presentation. Patients typically exhibit poor overall responses to anthracycline-based chemotherapeutic protocols such as combination cyclophosphamide, doxorubicin hydrochloride, vincristine sulfate, and prednisone (CHOP) chemotherapy, which is considered the standard of care.[110]

Molecular Classification of PTCL-NOS

Because PTCL-NOS encompasses a group of tumors that do not correspond to other defined entities defined by the World Health Organization classification, cases can exhibit a broad spectrum of cytologic, histologic, and molecular features. Recent gene expression profiling

studies have improved the ability to further classify these cases. Firstly, genetic profiling studies have identified a small subset of cases previously classified as PTCL-NOS that exhibit features of Tfh cell origin, leading to the development of new distinction within the WHO classification termed follicular T-cell lymphoma (PTCL-Tfh). These cases exhibit some morphological, immunophenotypic, genetic, and clinical overlap with AITL but also have a number of unique, distinctive features precluding inclusion in the AITL phenotype.[20,112] Overlapping features between AITL and PTCL-Tfh include genetic alterations associated with Tfh origin such as *TET2*, *RHOA*, *DNMT3A*, *IDH2* mutations[113–116] as well as expression of Tfh cell phenotypic markers CD4, CD10, CXCL13, and BCL6.

The PTCL-NOS cases that cannot be reclassified as Tfh cell origin can be classified into two major subgroups based on GATA3 or TBX21 molecular signatures, termed PTCL-GATA3 and PTCL-TBX21.[117–119] PTCL-GATA3 is associated with a worse prognosis and a 5-year OS of 19% compared to PTCL-TBX21, which has a 5-year OS of 38%. The majority of cases within the PTCL-GATA3 group exhibit a $CD4^{+}CD8^{-}$ immunophenotype.[120] Histologically, PTCL-GATA3 group displays a monotonous pattern of intermediate to large cells with a minimal inflammatory background.[120] The GATA3 phenotype is enriched in gene signatures related to cell proliferation including MYC, PI3K-ATK-MTOR, and β-catenin. PTCL-GATA3 also exhibits increased genetic abnormalities including frequent loss or mutation of tumor suppressor genes involving the CDKN2A, TP53, RB1 and PTEN-PI3K pathways. Co-occurrence of impaired TP53 signaling and loss of PTEN are significantly associated with PTCL-GATA3. This combination of tumor suppressor gene aberrations is infrequent in other PTCL-NOS subtypes and other T-cell NHLs.[119] Simultaneous amplifications of STAT3 and MYC were also identified in a subset of PTCL-GATA3 cases.[119] Similarly, recurrent gene fusions and alterations involving

components of the T-cell receptor signaling pathways including *VAV1*, *ITK*, *SYK, PTPRC, PLCGI* or proliferation pathways including *TP63, CDKN2A, PTEN,* and *TP53* have been described by multiple groups in a proportion of PTCL-NOS cases.[119,121–124]

Alternatively, PTCL-TBX21 exhibits a more heterogenous immunophenotype with half of cases being $CD4^{+}CD8^{-}$ immunophenotype, approximately a third of cases being $CD8^{+}CD4^{-}$, and fewer $CD4^{-}CD8^{-}$ or $CD4^{+}CD8^{+}$ cases.[120] These tumors are exhibit by a polymorphous histologic appearance characterized by variably-sized neoplastic cells admixed with high numbers of inflammatory cells including small lymphocytes, eosinophils, plasma cells, and histiocytes. A portion of PTCL-TBX21 cases have a lymphohistioyctic pattern comprised of atypical small neoplastic cells admixed with aggregates of epithelioid histiocytes.[120] The TBX21 phenotype is enriched in the INF-γ and NF-κB gene signatures. PTCL-TBX21 generally exhibits fewer genetic aberrations, and those present primarily involve cytotoxic effector genes or regulators of DNA methylation.[119] A higher proportion of cases within the TBX21 subgroup also exhibit upregulation of transcripts associated with cytotoxic T-cells as well expression of T-cell restricted intracellular antigen-1 (TIA-1) and/or granzyme B by immunohistochemistry.[120]

Novel Therapies for PTCL-NOS

Conventional treatment for PTCL-NOS involves anthracycline based chemotherapy, like CHOP. CHOP-based protocols, however, typically do not result in durable remission and relapse or refractory disease is common.[110] Targeted and personalized therapies are therefore an important and emerging field for improved outcomes for patients with PTCL-NOS.

Platelet-derived growth factor receptors (PDGFRs) are tyrosine kinase receptors critical for regulation of a number of cellular processes including cellular proliferation, development, differentiation, and inflammatory responses.[125] Aberrant PDGFR has been identified in a number

of cancers and receptor tyrosine kinase (RTK) inhibitors have been developed as a targeted therapeutic approach.[125,126] PDGFRs activation can result in stimulation of multiple signaling cascades including MAPK, PI3K, and PLCγ pathways.[127] PTCL-NOS has been shown to overexpress PDGFRα and PDGFR activity has been shown to promote neoplastic cell proliferation.[128,129] The PDGFR inhibitor, imatinib mesylate, was shown to effectively inhibit growth of PTCL-NOS primary cells. In a small clinical trial involving 12 patients with refractory or relapsed PTCL, however, treatment with imatinib, a tyrosine kinase inhibitor that targets PDGFR, resulted in no clinical improvement with short overall survival and progression-free survival times. Targeted treatment of PDGFRs via imatinib, therefore, is considered not effective for the treatment of PTCL-NOS.[130]

The PI3K-AKT-MTOR pathway is an important pathway involved in cell growth, survival, and proliferation.[131,132] Activation of this pathway controls many hallmarks of cancer including cell cycle, metabolism, motility and genomic instability.[133] PI3K signaling can also contribute to alterations in the microenvironment that promotes tumor growth including angiogenesis.[134–136] The PI3K pathway has been shown to be among the most frequently altered pathways in human tumors, with frequent mutations in PIK3CA and PTEN, a negative regulator of PI3K-AKT.[137] Alteration of this pathway has been shown to be involved in PTCL-NOS pathogenesis, particularly within the PTCL-GATA3 subgroup.[117,119] Duvelisib (IPI-145) is an oral inhibitor of PI3K. Treatment of patients with refractory or relapsed PTCL with duvelisib resulted in a 50% response rate and 3 complete responses.[138] Duvelisib is also a potent inducer of cell death within 4 TCL lines with constitutively phosphorylated AKT (pAKT). In a patient-xenograft mouse model, administration of duvelisib resulted in shifting of tumor-associated macrophages from the immunosuppressive M2-phenotype to the inflammatory M1-phenotype.

Duvelisib and other combination therapies that target the PI3K-AKT-MTOR axis are therefore considered promising new therapeutics for patients with PTCL-NOS.[138]

Subsets of PTCL including AITL and PTCL-Tfh have been shown to exhibit mutations in epigenetic regulators, including *TET*, *DNMT2*, and *IDH*. Drugs targeting epigenetic regulators, particularly histone deacetylase (HDAC) inhibitors, are therefore of interest to treat these subtypes of PTCL. Patients receiving HDAC inhibitors such as romidepsin and belinostat have exhibited strong response rates.[139] HDAC inhibitors, particularly as part of a combination therapy protocol, are therefore of interest in patients with T-cell neoplasms that exhibit altered epigenetic regulation.

Another therapeutic target of interest in the treatment of PTCL is CD30. CD30 is a transmembrane glycoprotein receptor that is a member of the tumor necrosis factor superfamily.[140] CD30 promotes cell growth and survival primarily through NFκB signaling pathways.[141] CD30 is expressed by a wide variety of lymphomas, to varying degrees. Anaplastic large cell lymphoma (ALCL) and the Reed-Sternberg cells found in classic Hodgkin lymphoma exhibit marked upregulation of CD30.[20,140] A subset of PTCL-NOS have been shown to express the CD30 antigen.[142] A novel CD30 antibody-drug conjugate, brentuximab vedotin, has undergone several clinical trials enrolling patients with ALCL, AITL, or PTCL-NOS with variable levels of surface and soluble CD30 expression.[143–145] Targeted CD30 treatment resulted in strong response rates ranging from 33-86% with the highest overall response rates seen in patients with ALCL. The duration of responses, however, were variable and there was no apparent correlation between response and CD30 expression. Discrepancies in response rates and CD30 expression has been attributed to the sensitivity of the diagnostically available immunohistochemistry and contributions of activated T-cells within the microenvironment.[139]

Further investigation into the role of CD30 in TCL pathobiology and mechanisms in which CD30-targeted immunotherapy may alter disease progression are needed to better understand the potential impact of this method of treatment.

PTCL-NOS remains a highly aggressive disease with poor outcomes in patients receiving traditional CHOP chemotherapy. While there have been advances in our understanding of the molecular drivers of these tumors and development of new therapies, significant improvement in treatment and survival of patients still trails that of other lymphoproliferative diseases. Further understanding of the pathogenesis and response to treatment of this diverse group of neoplasms is therefore needed.

Canine T-cell Lymphomas

Overview

Lymphoma is among the most common types of cancer affecting dogs, comprising approximately 6% of all neoplasms and approximately 90% of all hematopoietic tumors.[146,147] The estimated incidence of canine lymphoma is between 20-107 cases per 100,000[148–150] which is higher than that report in humans (19.6 cases per 100,000).[151] Canine NHLs can be classified using a modified WHO classification[152] and there is strong evidence that specific dog breeds have distinct predispositions for the development of unique subtypes of non-Hodgkin's lymphomas (NHLs).[150,153–155] The current classification of canine NHLs relies heavily on histomorphologic and cytologic features. Characterization of the molecular and genetic phenotypes and elucidation of the underlying pathogenesis of these canine lymphoma subtypes is therefore needed for more accurate tumor classification, development and utilization of targeted therapies, and better evaluation of the potential for a naturally occurring canine model of NHL.

Similar to humans, B-cell lymphomas are the more common than T-cell lymphomas in dogs and diffuse large B-cell lymphoma is the most common subtype in both species. In dogs however, the next most common subtypes are PTCL, nodal marginal zone lymphoma, and T-zone lymphoma.[156] Because of the relative increased incidence of PTCL in dogs compared to humans, the dog may serve as a valuable and naturally occurring translational model for this uncommon but highly aggressive disease.

Canine Peripheral T-cell Lymphoma

PTCL is among the most common subtypes of naturally-occurring NHL in dogs, comprising approximately 15% of all NHLs in this species.[156–159] The majority of PTCL cases in dogs fall within the category of PTCL-NOS[160], with rare reports of other PTCL subtypes, including anaplastic large cell lymphoma.[158,161,162] Dogs affected by PTCL-NOS exhibit similar clinical and diagnostic features to human patients. Dogs are typically diagnosed at middle to older age with a slight male predominance.[109,159,163] Canine patients often present in advanced stages with multicentric peripheral lymph node involvement, although any organ can be affected. In dogs, mediastinal involvement is seen in 30-40% of cases and patients often present with concurrent paraneoplastic hypercalcemia.[163] The Boxer breed is among the most common breeds affected by PTCL-NOS, comprising 19-26% of cases.[158,163,164]

PTCL-NOS is an aggressive disease in dogs with median overall survival times ranging from 159-162 days.[153,163,165] Dogs are typically treated with anthracycline-containing regimens, most often comprised of CHOP based protocols with variable initial response and poor overall prognosis.[163]

The diagnosis of PTCL-NOS can be made based on a combination of histology, flow cytometry, and PCR for antigen receptor rearrangement (PARR) assay. Similar to PTCL-NOS in

humans, canine tumors exhibit clonal T-cell receptor (TCR) gene rearrangement. Using flow cytometry, the majority of PTCL-NOS cases are characterized by a homogenous expansion of intermediate to large sized T-cells identified by expression of T-cell markers CD3 and/or CD5 and lack of expression of B-cell marker CD21. The majority of PTCL-NOS cases express the T-cell subset antigen CD4 with fewer cases being $CD8^+$ or $CD4^-CD8^-$. Loss of CD5 expression and low expression of MHC class II are common features of this neoplasm.[163] Histologically, these tumors are comprised of intermediate to large cells that are arranged in diffuse sheets that efface normal nodal architecture. Nuclei are of the neoplastic population can be irregular with variable chromatin pattern, prominent nucleoli, and variable mitotic rates.[152,156,163,166]

The molecular and genetic features of PTCL-NOS in dogs are not well-understood. Exome sequencing of Boxer dogs with TCL identified frequent mutations in the PTEN-mTOR pathways.[167] Interestingly, the PTEN-PI3k-AKT-MTOR pathway has been shown to be a driving pathway of human PTCL-GATA3, and frequent mutations of PTEN has also been identified in human PTCL.[119] Further investigation of the molecular drivers of canine PTCL-NOS is needed to better understand the pathogenesis underlying this aggressive disease in both human and canine patients.

A Canine Model of Naturally Occurring Cancers

Murine models are the mainstay animal model for cancer research and provide an invaluable tool for elucidating the mechanisms of cancer biology and oncogenesis. However, many novel therapeutics which exhibit strong results in rodent models fail in human patients. In fact, the success rate of oncologic clinical trials has been reported to be as low as 3.4%.[168] The variable results in mice versus human patients may be due, at least in part, to the lack of tumor and microenvironmental heterogeneity, genomic instability, immune surveillance, and recurrence

and/or metastasis within the conventional mouse models.[169] Therefore, a more relevant animal model that better represents human disease would be of tremendous value in effectively translating novel therapies into human patients.

The dog has been proposed as a naturally occurring model for a number of human tumors based on shared clinical, diagnostic, and molecular features.[170] Dogs provide a unique model for cancer research since tumors are able to grow over a long time period and in the presence of an in-tact immune system. Canine tumors additionally exhibit heterogeneity between individuals, as well as within the same individual. Furthermore, affected dogs can develop resistant or recurrent disease and exhibit variable responses to therapeutic agents.[170] Companion dogs also share daily environmental and lifestyle exposures with their owners. Together, these features make the canine translational model an attractive one, as they offer an opportunity to better recapitulate natural disease than genetically-induced rodent models.

Logistically, clinical trials in dogs are feasible, particularly within veterinary teaching hospitals that benefit from large caseloads and clinical researchers on staff. The establishment of inter-institutional and multidisciplinary consortiums and working groups, such as the Canine Comparative Oncology Trials Consortium,[169] represents exciting possibilities for development of large-scale trials that limit the biases of geographic, socioeconomic, and institutional factors. The lack of gold-standard veterinary treatments allows for the unique design of trials to evaluate early implementation of novel therapies. This may provide an advantage over human clinical trials in which patients have already failed standard treatment protocols.

The dog offers a naturally occurring model for a number of cancer subtypes including lymphoma, osteosarcoma, melanoma, prostate carcinoma, lung carcinoma, mammary carcinoma, and soft tissue sarcoma.[170] Among the most studied and accepted models is canine

osteosarcoma.[171] Osteosarcoma is a bone tumor that affects adolescent children as well as older, large-breed dogs. Similar to PTCL-NOS, osteosarcoma is a relatively uncommon, but highly aggressive tumor in people. Both osteosarcoma and PTCL-NOS occur relatively more frequently in the dog, and therefore offer a unique canine patient population to study these diseases. Recent studies have identified a novel agent, Losartan, to suppress pulmonary metastases in canine patients with osteosarcoma leading to combined clinical trials in canine and human patients (NCT03900793).[172,173]

Further development and implementation of the dog as a naturally occurring disease model is dependent on molecular studies to evaluate mechanistic similarities between canine and human tumors. Through the identification of shared molecular drivers and oncogenic signaling pathways, we may foster a unique opportunity to evaluate targeted therapies in the dog at an earlier clinical timepoint than would be otherwise possible in typical trials involving human patients. This opportunity may facilitate faster and more efficient identification of promising treatment options and thereby allow more effective translation into human patients.

Conclusions

In this thesis we aim to characterize the clinical and molecular features of PTCL in dogs. In so doing, we seek to determine if this naturally occurring disease in dogs may provide a useful model to study PTCL-NOS in people. Specific goals of this work include: 1) characterization of the histomorphology, clinical features, and gene expression pattern of canine PTCL 2) evaluation of the molecular similarities between canine and human PTCL-NOS 3) investigation into the cell of origin of canine PTCL and 4) identification of genetic drivers of canine PTCL-NOS, including novel fusion gene candidates.

CHAPTER 2 – CHARACTERIZATION OF THE HISTOMORPHOLOGY, CLINICAL FEATURES, AND GENE EXPRESSION PROFILE OF CANINE PTCL

Summary

T-cell lymphomas (TCL) are a diverse group of neoplasms with variable diagnostic features, pathophysiology, therapeutic responses, and clinical outcomes. In dogs, TCL includes indolent and aggressive tumors such as T-zone lymphoma (TZL) and peripheral T-cell lymphoma (PTCL), respectively. TCL phenotypes can be categorized by expression of the surface antigen molecules CD4 and CD8, identified by flow cytometry. The majority of TCL cases are $CD4^+$, with far fewer cases being $CD8^+$ or $CD4^-CD8^-$. The clinical features of $CD4^+$ TCLs have been previously described. The histomorphology and gene expression profile of tumors classified as $CD4^+$ TCL, however, has not been well characterized and it remains uncertain if this group of tumors represents a uniform population or encompasses a more heterogenous group of diseases. Furthermore, the less common TCL phenotypes are poorly understood with little to no information about histomorphology, clinical features, and prognosis. In this chapter, we aim to first determine if tumors diagnosed as $CD4^+$ TCL by flow cytometry identify a distinct lymphoma subtype with consistent histologic and molecular features. Seventy-three cases of nodal TCL with paired flow cytometry and histopathology were evaluated. The majority of cases (82.2%) were characterized as $CD4^+$ TCL by flow cytometry. Fewer cases were classified as $CD8^+$ TCL (6.8%) or $CD4^-CD8^-$ TCL (11.0%). All cases, regardless of immunophenotype, exhibited conserved histologic features consistent with the WHO classification of PTCL. Histologic subsets of PTCL corresponding to immunophenotypic features were not identified. RNA-seq was then performed on a subset of $CD4^+$ PTCL cases

(n=6) and compared with sorted control $CD4^+$ T-cells. The gene expression pattern of $CD4^+$ PTCL was similar between all cases regardless of breed.

Given the rarity of the $CD8^+$ and $CD4^-CD8^-$ PTCL cases, we then sought to evaluate a second cohort of patients to further characterize these less common PTCL phenotypes. We describe and correlate the presenting clinical signs, flow cytometry, and outcomes of 119 dogs diagnosed with nodal, non-TZL, $CD8^+$ or $CD4^-CD8^-$ TCL by flow cytometry. Skin lesions present at the time of diagnosis were more commonly observed in the $CD8^+$ TCL group. Mediastinal enlargement and/or hypercalcemia were more commonly seen in the $CD4^-CD8^-$ TCL group. Dogs with either $CD8^+$ or $CD4^-CD8^-$ TCLs had aggressive clinical disease with median overall survival (OS) times of 198 days and 145 days, respectively. In both groups, neoplastic cell size determined by flow cytometry ranged from small to large, and large cell size was associated with shorter OS times. In this chapter, we first demonstrate the ability of flow cytometry to identify a subtype of T-cell lymphoma, $CD4^+$ PTCL, with a uniform histomorphology and gene expression profile. We then show that $CD4^-CD8^-$ TCLs share clinical and diagnostic features with the more common $CD4^+$ TCLs, suggesting a mutual pathogenesis. $CD8^+$ TCLs, on the other hand, exhibit unique clinical features and prognostic indicators suggesting that these tumors may be have a different etiology.

Introduction

Lymphoma is the most common hematopoietic malignancy in dogs and encompasses a broad spectrum of diseases with diverse mechanisms of oncogenesis, diagnostic criteria, and biologic behaviors.[149,156] Flow cytometry is a powerful non-invasive tool used to differentiate clinically significant subtypes of lymphoma by objectively evaluating cell size, cell complexity, and the expression of multiple surface antigens. The utility of flow cytometry is particularly evidenced by T-zone lymphoma (TZL) which is routinely diagnosed by flow cytometry based on an expansion of small to intermediate sized $CD3^+CD5^+$ T-cells with characteristic loss of the pan-leukocyte marker CD45.[160,174] Diagnosis of T-zone lymphoma by flow cytometry has been shown to reliably predict a distinct histologic pattern and cytomorphology consistent with the disease entity.[160,174] T-zone lymphoma is an indolent T-cell lymphoma that is clinically important to distinguish from more aggressive types of peripheral T-cell lymphomas.[163]

$CD4^+$ TCL is the most common subtype of TCL in dogs.[5] The clinical presentation and outcome of dogs diagnosed with $CD4^+$ TCL by flow cytometry have been previously described.[163] In this study, the most common immunophenotype of neoplastic cells was $CD3^+CD4^+CD45^+CD21^-$ with low levels of MHC class II expression, and variable expression of CD5. This phenotype has been associated with poor clinical outcomes independent of the treatment protocol with a median progressive free interval (PFI) of 91-108 days and overall survival (OS) of 159-160 days.[163,164] Clinically, patients with this immunophenotype often present with a mediastinal mass and/or hypercalcemia.[163,164] Boxer dogs are overrepresented in the $CD4^+$ PTCL population, comprising approximately 19-26% of cases.[153,163,165]

In the current study we assessed the correlation between flow cytometry and histomorphology of a large group of nodal, non-TZL, TCL cases and then evaluated the gene

expression pattern of the most common immunophenotype, $CD4^+$ TCL. Currently in veterinary medicine, it is far more common to diagnose lymphoma by cytology and flow cytometry than biopsy, and therefore this study provides the unique opportunity to directly correlate the immunophenotype to histology. Understanding the spectrum of histologic changes associated with specific antigen expression may also provide insight into the disease process and lay the groundwork for future studies that rely on flow cytometry to identify lymphoma subtypes.

The cytomorphology and histomorphology of $CD4^+$ TCLs (excluding T-zone lymphoma) have been previously classified as peripheral T-cell lymphoma not-otherwise specified (PTCL-NOS)[156,163,165], lymphoblastic lymphoma[163,165], pleomorphic mixed small, medium, and large cell[166], or pleomorphic large cell type[166]. In these studies, a range of classification criteria (World Health Organization (WHO) classification, Kiel classification) and sample preparation (cytology, histology) were used.

Nodal TCLs with other immunophenotypes, including $CD8^+$ and $CD4^-CD8^-$ lymphomas, are less common[164,165] and not well characterized in dogs. Studies focused on histologic and cytologic characterization of canine lymphomas using a variety of classification schemes other than the contemporary WHO standard, have included small numbers of $CD8^+$ and/or $CD4^-CD8^-$ TCLs. $CD8^+$ TCLs involving the lymph node have been classified as mycosis fungoides, pleomorphic large cell, pleomorphic mixed cell, unclassifiable plasmacytoid, plasmacytoid, and unclassifiable high-grade.[166,175,176] $CD4^-CD8^-$ TCLs have been previously classified as lymphoblastic and PTCL.[166] The clinical features and biologic behavior of these uncommon nodal $CD8^+$ and $CD4^-CD8^-$ TCL subtypes are poorly described and it remains uncertain if T-cell immunophenotype can be used to identify TCL subtypes with unique clinical presentations or survival times.

The goals of this chapter were to 1) evaluate the heterogeneity of histomorphologies and gene expression within a group of tumors diagnosed as $CD4^+$ TCL by flow cytometry 2) determine if less common TCL immunophenotypes can be reliably distinguished from $CD4^+$ TCL by histology and 3) characterize the presenting clinical signs, flow cytometry profiles, and clinical outcomes associated with the rare TCL subtypes.

Materials and Methods

Case Selection for Flow Cytometry-Histopathology Correlation

Cases with a T-cell phenotype (expression of the T-cell antigens CD3 or CD5, lack expression of the B-cell antigen CD21, and variable expression of the T-cell subset antigens, CD4 and CD8) were identified through Aratana Therapeutics T-CHOMP and T-LAB clinical studies. Samples used in this study were collected between 2014 and 2015 from dogs presenting to veterinary specialty clinics throughout the United States with suspicion of lymphoproliferative disease. Dogs were selected for this study in two phases. During the first phase, fine needle aspirates for flow cytometry were taken simultaneously with a biopsy for histopathologic evaluation. All samples were obtained from peripheral lymph nodes. During the second phase of the study, flow cytometry was performed first and dogs with an indolent lymphoma (TZL immunophenotype) and B-cell lymphoma were excluded. TZL lymphoma was identified based on a neoplastic population composed of small to intermediate cells which expressed CD3, CD5, and lost expression of CD45. Dogs with a non-TZL TCL were then entered into the clinical study and a pre-treatment lymph node biopsy was obtained. Thus, the cases in this study represent the diversity of phenotypes and histologies that might be present in nodal TCL not classified as TZL. During the first phase of the trial, ten TZL cases were evaluated and independently diagnosed by both histomorphology and flow cytometry.

Flow Cytometry

Routine diagnostic flow cytometry was performed by the Colorado State University Clinical Immunology Laboratory (CSU-CI) on all cases as previously described.[160] Flow cytometry was reviewed for lymph node aspirates of 73 cases of TCL, and compared to lymph node aspirates from 20 healthy dogs utilized for IACUC approved surgical continuing education courses, and 20 cases of $CD4^+$ T-zone lymphoma submitted to the CSU-CI for routine diagnostics. Cases of T-zone lymphoma were selected based on $CD45^-CD3^+CD4^+CD5^+CD21^{hi}$ immunophenotype.[160,174] Although T-zone lymphomas can express CD4, CD8, neither or rarely both subset antigens, for this study CD4-expressing cases were examined. The following features of the neoplastic populations and control $CD4^+$ and $CD8^+$ T-lymphocytes were evaluated: cell size by forward scatter on a linear scale, MHC class II median mean fluorescence intensity (MFI), CD25 median MFI, and expression of CD5.

Histopathology

Two pathologists (Lauren J Harris, Kelly L Hughes) were blinded to the flow cytometry parameters and independently evaluated whole lymph node or lymph node core biopsies. Biopsies were subtyped according to the WHO classification for canine lymphoma and scored for histologic features (summarized in Table 2.1). Hematoxylin and eosin stain, CD3 immunohistochemistry, and CD79a immunohistochemistry were reviewed in every case. WHO classification and scores of histologic features were compared between pathologists and in cases of discrepancy a third pathologist (EJ Ehrhart) was consulted for a consensus diagnosis.

Table 2.1. Summary of Criteria for Histologic Characterization

Feature	Criteria		
Size	Small: 1.5x RBC	Intermediate: 1.5-2x RBC	Large: >2x RBC
Percent necrosis	0-10%	10-20%	>20%
Number of tingible body macrophages	None	Few	Many
Fibrosis	Mild	Moderate	Marked
Neovascularization	Mild	Moderate	Marked
Nuclear Shape	Round	Indented	Pleomorphic
Chromatin Pattern	Condensed	Stippled	Vesicular
Nucleolar Prominence	Unapparent	Small and distinct	Large and prominent
Cytoplasm Color	Eosinophilic	Basophilic	Amorphous
Cytoplasm Character	Smooth, even	Scant	Flocculent
Mitotic Rate	Mitoses per ten 400x fields		

RBC=diameter of a resident red blood cell

Immunohistochemistry

CD3 and CD79a expression were evaluated by immunohistochemistry in all biopsies included in the flow cytometry-histopathology correlation study. Three-micron sections of formalin fixed paraffin embedded tissues were mounted on positively charged slides along with positive control tissue. Slides were deparaffinized and hydrated through two changes of xylene, two changes of 100% alcohol, and one change of 95% alcohol to water. Heat induced epitope retrieval (HIER) was performed using citrate buffer, pH = 6, for 30 seconds at 125 C using a Dako Pascal pressure cooker. CD3 (courtesy of Dr. Moore, UC Davis) at 1:50 dilution or CD79a (Biocare, Pacheco, CA) at 1:100 were applied for 60 minutes at room temperature. After rinsing, Promark Mouse on Canine Polymer (Biocare, Pacheco, CA) was applied for 60 minutes. After rinsing, Betazoid DAB (Biocare, Pacheco, CA) was applied for 5 minutes. Slides were then rinsed thoroughly and counterstained using Mayer's Hematoxylin for 30 seconds. Slides were dehydrated and cleared using graded alcohol and xylene and coverslipped with tape coverslips. Negative controls were incubated in diluent consisting of Tris-buffered saline with carrier protein

and homologous nonimmune sera. All sequential steps of the immunostaining procedure were performed on negative controls following incubation.

Flow Cytometry-Histology Correlation Statistical Analysis

All statistical analyses were performed using GraphPad Prism version 5.0 for Windows (GraphPad Software, San Diego California, USA). Nonparametric Mann-Whitney U tests were used to compare flow cytometric parameters amongst samples. Nonparametric correlations between flow cytometry and histologic features were determined using Spearman's correlation matrix.

RNA-Seq

Lymph node aspirates from 6 dogs submitted to the CSU-CI for routine diagnostics and diagnosed with $CD4^+$ PTCL by flow cytometry were selected for RNA-seq. Patients were naïve to treatment at the time of sample submission. The 6 patient samples selected for RNA-seq were not enrolled in the above-mentioned T-LAB and T-CHOMP clinical studies, and were therefore not included in the group of samples evaluated for flow cytometry-histopathology correlation. Patient information is summarized in Table 2.3. Aspirates from selected cases had a purity of greater than 88% neoplastic cells. Control $CD4^+$ T lymphocytes were harvested from lymph nodes of 6 healthy dogs utilized for IACUC approved surgical continuing education courses. $CD4^+$ T lymphocytes were sorted using a MoFlo cell sorter (Beckman Coulter, Brea, CA). RNA was extracted from the 6 individual $CD4^+$ PTCL cases. RNA from sorted $CD4^+$ lymphocytes from six total dogs were pooled in groups of two to obtain three control samples. RNA extraction was performed using the Purelink RNA mini Kit (Thermo Fisher Scientific, Waltham, MA) and quality was measured with an Agilent 2100 Bioanalyzer System. All samples had a RIN value greater than 8.80. RNA was shipped to Novogene Corporation Inc (Sacramento, CA) where the

libraries were constructed and sequenced. Briefly, mRNA was enriched using oligo(dT) beads and randomly fragmented. Random hexamer primer and reverse transcriptase were used for first strand cDNA synthesis followed by second strand synthesis via custom synthesis buffer (Illumina, San Diego, CA), dNTPs, RNAse H, and Escherichia coli polymerase I. Double-stranded cDNA fragments were purified and end-repaired by A-tailing and ligation of sequencing adapters. cDNA inserts were selected and enriched via PCR. Transcriptome sequencing was carried out on an Illumina Hiseq PE150 platform and generated 150bp paired-end raw reads. Sequences were aligned to the CanFam3.1 genome using TopHat2.[19] HTSeq[20] and DESeq2[21] software were used to quantify reads and normalize gene expression levels measured as fragments per kilobase of transcript sequence per millions of base pairs sequenced (FPKM). P-values were determined using a negative binomial distribution. A Benjamini-Hochberg procedure was used to correct p-values and padj<0.05 was considered the differentially expressed gene screening standard. The Broad Institute tool, Morpheus[22], was used to perform hierarchical clustering (Euclidean, average linkage) and create heatmaps based on the differentially expressed genes. The RNA-seq data in this publication have been deposited in NCBI's Gene Expression Omnibus[25] and are accessible through GEO Series accession number GSE122347.

Case Selection of $CD8^+$ and $CD4^-CD8^-$ TCLs

To determine the distribution of nodal lymphoma subtypes diagnosed at the Colorado State University Clinical Immunology Laboratory (CSU-CI), the CSU-CI database was searched for canine lymph node aspirates submitted between 2012-2017. Cases with a final diagnosis of B-cell lymphoma, $CD4^+$ TCL, $CD8^+$ TCL, $CD4^-CD8^-$ TCL, $CD4^+CD8^+$ TCL or T-zone lymphoma were selected. Duplicate samples from the same patient with consistent diagnoses

were eliminated, as were patients that were involved in studies that recruited dogs with specific lymphoma immunophenotypes.

Subsequently, cases with a diagnosis of either $CD8^+$ or $CD4^-CD8^-$ TCL were chosen for further evaluation. T-cell lymphoma cases were identified by a discrete population of T-cells with a single phenotype which comprised the majority of the sample, or a population of T-cells which exhibited at least one feature of aberrancy including: loss of both CD4 and CD8 T-cell subset antigens, loss of CD5 expression, marked decrease in MHC class II expression, or large cell size (greater than or equal to 1.3 times the size of normal T-lymphocytes). $CD8^+$ and $CD4^-CD8^-$ TCLs were characterized by CD3 and/or CD5 expression, lack of expression of CD21, and either $CD8^+CD4^-$ or $CD4^-CD8^-$ T-cell subset antigen expression patterns. Cases with morphology consistent with large granular lymphocytes (LGL-leukemia) and cases with a diagnosis of T-zone lymphoma, identified by the characteristic loss of the pan-leukocyte marker CD45, were excluded from evaluation. Medical records for 120 of these cases were obtained for further evaluation. One case with a concurrent B-cell lymphoma was subsequently excluded from the case series, resulting in a total of 119 cases.

Medical Record Evaluation

Medical records from patients that met inclusion criteria were acquired from the referring veterinarians. The patient age, sex, breed, date of diagnosis, type of treatment (categorized as: no treatment, corticosteroid treatment only, single-agent chemotherapy, or multi-agent chemotherapy), and date of last contact/euthanasia/death were extracted from the medical records. Patients in which the treatment regime or intention to treat was not clear in the medical record (n=5) and patients who were enrolled in a novel immunotherapy clinical trial (n=5) were removed from the group used to evaluate the effect of treatment on overall survival. Patients who

received a single injection of L-asparaginase and then were treated with CCNU alone or prednisone alone were categorized as single agent or corticosteroid alone, respectively. The presence or absence of the following clinical signs was also evaluated at the time of initial flow cytometry diagnosis: peripheral lymphadenopathy, abdominal lymphadenopathy, hepatomegaly, splenomegaly/splenic nodules, gastrointestinal involvement (including gastrointestinal mass, thickened intestines, and/or clinical diagnosis of protein-losing enteropathy), skin lesions, cranial mediastinal enlargement/sternal lymphadenopathy, and hypercalcemia. Where applicable, the diagnostic method used to identify these clinical abnormalities was also recorded. In cases where the presence or absence of the clinical sign was unknown, the patient was excluded from analysis of that particular feature. The patient's complete blood count (CBC) at the time closest to flow cytometry diagnosis was reviewed for hematologic abnormalities. Anemia was classified as mild (hematocrit (HCT) 30-36%), moderate (HCT 20-30%), or marked (HCT <20%). Thrombocytopenia was characterized as mild (100,000-175,000 platelets/uL), moderate (30,000-100,000 platelets/uL), or marked (<30,000 platelets/uL) if there were no platelet clumps identified on blood smear review. Lymphocytosis was classified as mild (5,000-10,000 lymphs/uL), moderate (10,000-30,000 lymphs/uL) or marked (>30,000 lymphs/uL).

Cytology

Of the 119 cases included the $CD8^+$ and $CD4^-CD8^-$ outcome study, only 4 cases (3 $CD4^-CD8^-$ TCL and 1 $CD8^+$ TCL) had cytology samples available at the CSU Veterinary Diagnostic Laboratory. To obtain additional cases for cytologic review, the CSU-CI database was searched for cases with concurrent flow cytometry and cytology where the slides were available at the CSU Veterinary Diagnostic Laboratory. Ten cases of $CD8^+$ TCL and 10 cases of $CD4^-CD8^-$ TCL were randomly selected for evaluation. Cases were classified as $CD8^+$ TCL and $CD4^-CD8^-$ TCL

by flow cytometry using the same criteria described above. Fine needle aspirations from the 24 total cases were evaluated by two clinical pathologists (EDR, PRA). Pathologists were blinded to the immunophenotype. Additionally, for cytologic comparison, ten $CD4^+$ nodal TCL samples with concurrent flow cytometry and cytology were randomly selected and reviewed.

Statistical Analysis-Retrospective outcome study

All statistical analyses were performed using GraphPad Prism version 8.0 for Windows (GraphPad Software, San Diego California, USA) and R version 3.5.3. Fischer's exact test was used to compare categorical parameters and non-parametric Wilcoxon rank-sum test was used to compare continuous parameters between TCL phenotypes. Overall survival (OS) was calculated in days from the time of diagnosis by flow cytometry until time of death or censor by Kaplan Meier method. Dogs still alive or lost to follow-up at the time of data analysis were censored at the last date of contact. The following potential clinical prognostic factors were evaluated: abdominal lymphadenopathy, sternal lymphadenopathy or mediastinal enlargement, cutaneous involvement, splenomegaly or splenic nodules, hepatomegaly, hypercalcemia, anemia, age and treatment (multi-agent chemotherapy, single-agent chemotherapy, corticosteroids alone or no therapy). All clinical parameters were categorized as present or absent at the time of diagnosis. To evaluate age, patients were divided into 'old' and 'young' categories, with 'old' defined as ≥10 years of age at the time of diagnosis. The following flow cytometry features of the neoplastic population were also evaluated: cell size as determined by forward scatter, MHC class II expression (MFI), and CD5 expression. Cases with a median neoplastic cell size greater than or equal to 1.3 times the median size of control T-cells from normal dogs were considered large. Cases with a median cell size less than 1.3 times the median size of control T-cells from normal dogs were considered small. MHC class II expression was categorized as high (greater than or

equal to the median MFI of control T-cells from normal dogs) or low (less than the median MFI of control T-cell from normal dogs). Cases were categorized as CD5 positive or CD5 negative, as determined by complete loss of CD5 expression based on MFI and interpretation of the flow cytometry plots. The impact on survival was determined by log rank test (p-value) and Cox proportional hazard model (Hazard Ratio [HR] and 95% confidence interval [CI]). Multivariable analysis was not performed due to insufficient sample numbers available for evaluation. A p-value less than 0.05 was considered significant.

Results

Flow cytometry-Histopathology Correlation

Flow cytometry features of canine nodal TCL

The 73 nodal TCL cases fell into 3 immunophenotypic categories: $CD4^+$ TCL (82.3%), $CD8^+$ TCL (6.9%), and $CD4^-CD8^-$ TCL (11.0%). The demographics of TCL patients are summarized in Table 2.2.

Table 2.2. Patient Demographics of Flow Cytometry-Histopathology Study

Parameter	$CD4^+$ PTCL (n=60)	$CD8^+$ PTCL (n=5)	$CD4^-CD8^-$ PTCL (n=8)	CNTRL CD4+/CD8+ (n=20)	TZL (n=20)
Age (years)					
Median (range)	7 (3-13)	11 (8-12)	6.5 (4-8)	1 (1-1)	10 (8-14)
Sex					
Male	3 (5%)	0 (0%)	0 (0%)	5 (25%)	1 (5%)
Neutered Male	34 (57%)	0 (0%)	4 (50%)	0 (0%)	8 (40%)
Female	2 (3%)	1 (20%)	0 (0%)	15 (75%)	0 (0%)
Female Spayed	21 (35%)	4 (80%)	4 (50%)	0 (0%)	11 (55%)
Breed					
Mixed breed	18 (30%)	0 (0%)	2 (25%)	10 (50%)	6 (30%)
Boxer	16 (27%)	2 (40%)	1 (13%)	0 (0%)	0 (0%)
Golden Retriever	8 (13%)	1 (20%)	2 (25%)	0 (0%)	8 (40%)
Lab	4 (7%)	0 (0%)	1 (13%)	0 (0%)	0 (0%)
Other	14 (23%)	2 (40%)	2 (25%)	10 (50%)	6 (30%)

$CD4^+$ TCL cases had a $CD3^+CD4^+CD8^-$ phenotype consistent with that previously associated with aggressive clinical disease.[163] By flow cytometry, cells with the $CD4^+$ TCL phenotype were significantly larger based on forward scatter determined on a linear scale (median=530) compared to control $CD4^+$ lymphocytes (median=375; p-value<0.0001), control $CD8^+$ lymphocytes (median=379; p-value<0.0001) and $CD4^+$ TZL cells (median=406; p-value<0.0001) (Figure 2.1a). $CD4^+$ TCL cells exhibited low MHC Class II expression (median MFI=0.80) compared to control $CD4^+$ lymphocytes (median MFI=12.15; p-value<0.0001), control CD8+ lymphocytes (median MFI=17.03, p-value<0.0001) and $CD4^+$ TZL cells (median MFI=26.48; p-value<0.0001) (Figure 2.1b). CD25 expression in $CD4^+$ TCL (median MFI=0.1) was similar to that of control T-cell subsets, while CD25 expression was increased in $CD4^+$ TZL cells (median MFI=0.56; p-value<0.001) (Figure 2.1c). Nineteen of the 60 $CD4^+$ TCL cases (31.7%) exhibited complete loss of CD5 expression and 6 cases (10.0%) exhibited partial downregulation of CD5. Consistent with previous studies,[163] dogs diagnosed with $CD4^+$ TCL were a median age of 7 years and mixed breeds (30%), Boxers (27%), and Golden Retrievers (13%) were the most common breeds. Male dogs, the majority of which were neutered, composed 62% of the population (Table 2.2).

$CD8^+$ TCL cases expressed the T-cell antigen CD3, the T-cell subset marker CD8, and lacked expression of CD4 ($CD3^+CD4^-CD8^+$). These tumors exhibited variable expression of CD5 (3 out of 5 $CD5^+$; 2 out of 5 $CD5^-$). $CD8^+$ TCL cells did not differ significantly in size (median=524), MHC class II expression (median MFI=1.79) or CD25 expression (median MFI=0.1) from $CD4^+$ TCL cases. $CD8^+$ TCL cases were significantly older at the time of diagnosis with a median age of 11 years (p-value=0.005) and all 5 cases were female. Similar to $CD4^+$ TCL, 2 of the 5 $CD8^+$ TCL cases were Boxer dogs and 1 was a Golden Retriever.

$CD4^-CD8^-$ cases lacked expression of CD4 or CD8 ($CD4^-CD8^-$) and the majority expressed CD3. One $CD4^-CD8^-$ TCL case lacked CD3 expression but exhibited CD5 positivity, confirming T-cell origin. Within this group of TCLs there was variable expression of CD5 (4 out of 8 $CD5^+$, 4 out of 8 $CD5^-$). $CD4^-CD8^-$ TCL cells did not differ significantly in cell size (median=495.51), CD25 expression (median MFI=0.105), or MHC class II expression (median MFI=0.605) compared to $CD4^+$ TCL. The median age of patients diagnosed with $CD4^-CD8^-$ PTCL was 6.5 years and was not significantly different from $CD4^+$ TCL cases. Two of the 8 total $CD4^-CD8^-$ TCL cases were mixed breed dogs, 1 was a Boxer dog, and 2 were Golden Retrievers.

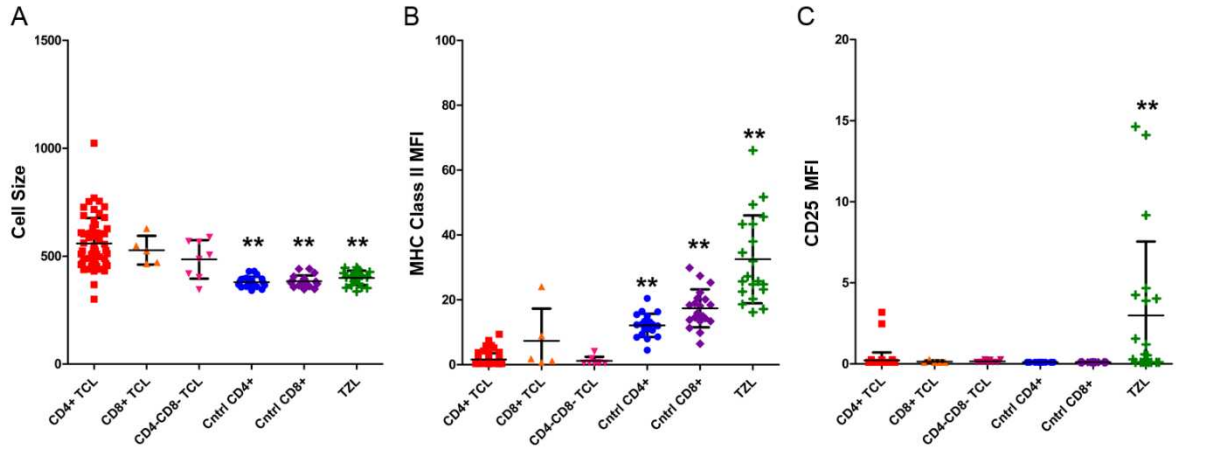

Figure 2.1. Flow cytometry features of PTCL. $CD4^+$ PTCL cells were significantly larger than control $CD4^+$ T-cells, control $CD8^+$ T-cells, and TZL cells. Cell size was determined by forward scatter on a linear scale (A). $CD4^+$ TCL had low levels of MHC class II expression (median fluorescence intensity) compared to control $CD4^+$ T-cells, control $CD8^+$ T-cells, and $CD4^+$ TZL cells (B). $CD4^+$ TCL had low levels of CD25 expression (median fluorescence intensity) compared to $CD4^+$ TZL cells (C). (Mean ± SD , **=p<0.001).

Control $CD4^+$ and $CD8^+$ lymphocytes were evaluated in healthy, young hound and mixed-breed dogs (Table 2). This population was uniformly 1 year of age, predominantly female (75%), and all dogs were intact. Cases of TZL were significantly older than $CD4^+$ PTCL (p-value<0.001) and $CD4^-CD8^-$ PTCL (p-value=0.004). $CD8^+$ PTCL cases did not differ significantly in age from TZL cases (p-value=0.83). Golden Retrievers comprised 40% of the TZL cases.

Correlations between flow cytometry phenotype and histomorphology

Of the 73 total cases, 70 tumors had diagnostic quality histologic preparations adequate for subtyping. The three tumors with insufficient sample were diagnosed as $CD4^{-}CD8^{-}$ TCL by flow cytometry. All evaluated cases were classified as PTCL-NOS, regardless of immunophenotype. All tumors were characterized by sheets of intermediate to large lymphocytes that diffusely infiltrated and effaced the nodal architecture and often invaded the fibrous capsule and perinodal adipose tissue. Neoplastic cells had moderate amounts of eosinophilic cytoplasm. Nuclei were 2 to 3 times the size of the diameter of an erythrocyte and round to indented or pleomorphic in shape. Most cases had open chromatin with 1-3 small distinct nucleoli, and a high mitotic index (median 49.42; range 10-118 per ten 400x fields). Throughout all cases there were few to moderate scattered tingible body macrophages, low levels of tumor necrosis (less than 20% examined cross sectional area), and mild fibroplasia. Neovascularization was generally not a prominent feature of these neoplasms (Figure 2.2).

Cases of $CD8^{+}$ and $CD4^{-}CD8^{-}$ TCL could not be reliably distinguished from $CD4^{+}$ TCL by histology. In the single $CD4^{-}CD8^{-}$ PTCL case that lost expression of CD3 based on flow cytometry, approximately 40% of neoplastic cells exhibited positive membranous immunoreactivity to the CD3 antibody with immunohistochemistry. This finding is interpreted as a result of the intracellular binding of the CD3 antibody used in immunohistochemistry compared to the cell-surface binding of the CD3 antibody used for flow cytometry. Two of 5 $CD8^{+}$ TCL tumors had unique histologic features. In one case, cells had markedly expanded lacy to vacuolated cytoplasm. Cell size, nuclear characteristics, and tumor pattern of this neoplasm was still consistent with that previously described in other cases of PTCL-NOS. Another $CD8^{+}$ PTCL case exhibited pronounced tumor-associated fibroplasia that multifocally dissected

between neoplastic lymphocytes. A diagnosis of angioimmunoblastic lymphoma was considered in this case, however, because neoplastic cellular morphology was consistent with other cases of PTCL, a consensus diagnosis of PTCL was agreed upon. Because of the small sample size of $CD8^+$ TCLs (n=5), conclusions of whether these unique histologic features represent distinct entities or variations within the PTCL subgroup cannot be definitively determined.

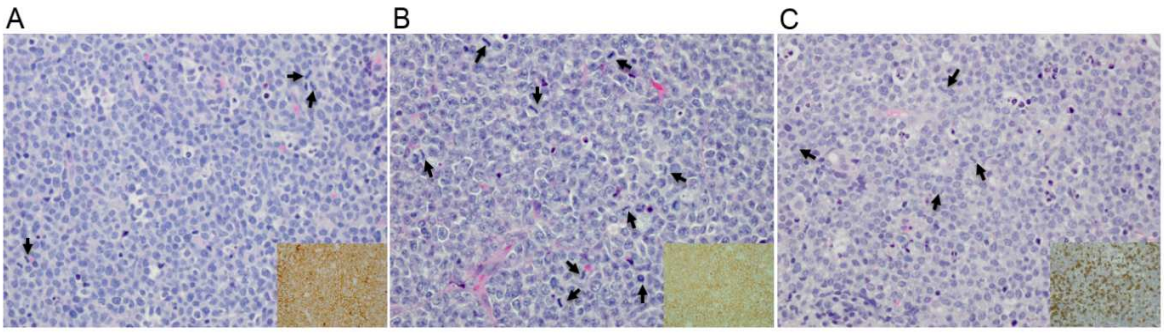

Figure 2.2. Histomorphology of PTCL. Tumors diagnosed as PTCL exhibited consistent histologic features including sheets of intermediate to large size cells with round to indented to pleomorphic nuclei, open chromatin, 1-3 small discrete nucleoli, and high mitotic rates (arrows) (A-C). Tumors diagnosed as $CD4^+$ PTCL (A), $CD8^+$ PTCL (B), and $CD4^-CD8^-$ PTCL(C) could not be classified into distinct histologic subgroups. Insets are CD3 immunohistochemistry demonstrating diffuse positive membranous immunoreactivity. A single $CD4^-CD8^-$ PTCL exhibited loss of CD3 by flow cytometry. In this case approximately 40% of neoplastic T-cells were CD3-positive by immunohistochemistry (C). 400x magnification.

Based on the consistency of the categorically evaluated histologic features throughout all examined cases, statistical evaluation of the categorical features with flow cytometry parameters was not pursued. Spearman's rank correlation coefficients did identify a weak to moderate correlation between neoplastic cell size as determined by forward scatter via flow cytometry and mitotic rate per ten 400x fields (ρ=0.418, p-value<0.001).

RNA-seq

Flow Cytometry Identifies a Consistent Gene Expression Profile

RNA-seq was performed on lymph node aspirates from 6 dogs diagnosed with $CD4^+$ TCL ($CD4^+CD8^-CD5^{+/-}ClassII^{lo}$) based on flow cytometry and compared to sorted $CD4^+$ T-cells from lymph nodes of young, healthy, hound dogs. The selected cases were representative of the

$CD4^+$ TCL patient population based on clinical presentation and flow cytometric features. Three of the selected cases were Boxers and three cases were non-Boxer breeds (Cavalier King Charles Spaniel, Rhodesian Ridgeback, and a Collie dog). Two of the cases exhibited loss of CD5 expression. One case had a mediastinal mass, one case was hypercalcemic, and one case had both a mediastinal mass and hypercalcemia (Table 2.3).

Table 2.3. Summary of Patient Information for individuals with RNAseq analysis

Sample name	Breed	Age	Sex	Mediastinal Mass	Hypercalcemia
BOXER1	Boxer	6	MC	No	No
BOXER2	Boxer	8	FS	No	No
BOXER3	Boxer	6	MC	Yes	No
OTHER1	Cavalier King Charles Spaniel	3	FS	No	Yes
OTHER2	Rhodesian Ridgeback	4	FS	Yes	Yes
OTHER3	Collie	11	MC	No	No
CNTRL1a	Hound	1	F	No	No
CNTRL1b	Hound	1	F	No	No
CNTRL2a	Hound	1	F	No	No
CNTRL2b	Hound	1	F	No	No
CNTRL3a	Hound	1	F	No	No
CNTRL3b	Hound	1	F	No	No

RNA extracted from lymph nodes from CNTRL dogs 1a and 1b were combined for a single CNTRL1 sample, CNTRL2a and 2b were combined for a single CNTRL2 sample, and CNTRL3a and 3b were combined for a single CNTRL3 sample. MC=male castrated; FS=female spayed; F=female.

5011 genes were significantly differentially expressed (padj<0.05) when comparing $CD4^+$ PTCL cases to control $CD4^+$ lymphocytes (Figure 2.4a,b). Surface protein expression characterized by flow cytometry correlated with gene expression including decreased expression of CD5, CD25, and MHC class II molecules (DLA DRA, DLA DRB1, DLA DQA1, DLA DQB1)[29] as well as the MHC class II transactivator, CIITA (Figure 2.3a-e). Hypercalcemia is a common clinical presentation in dogs with $CD4^+$ PTCL and this process is driven by

paraneoplastic production of parathyroid hormone-like hormone (PTHLH).[30] PTHLH expression was increased in all cases regardless of presence of clinical hypercalcemia.

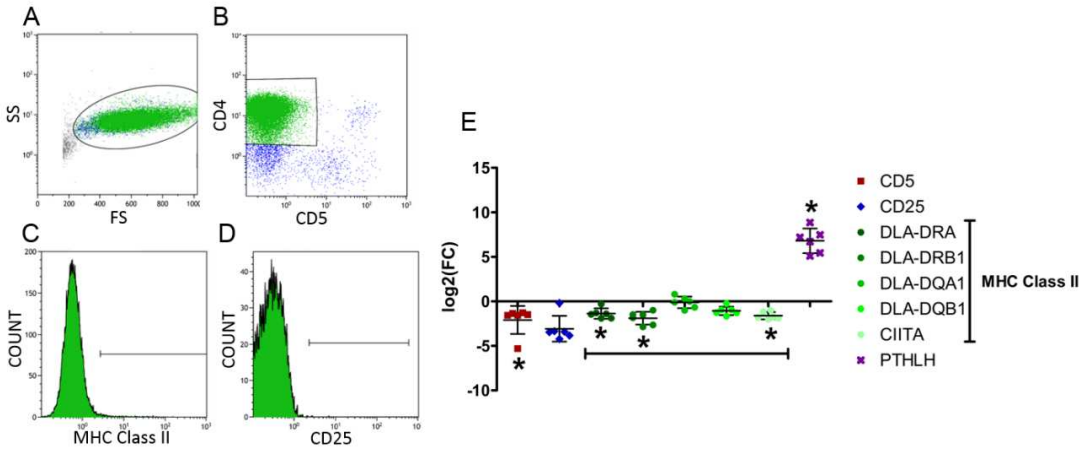

Figure 2.3. Flow cytometry cell surface protein expression is consistent with gene expression. $CD4^+$ PTCL is characterized by enlarged cell size determined by forward scatter (A), expression of the T-cell subset marker CD4 and frequent loss of T-cell marker CD5 (B). $CD4^+$ PTCL exhibits low levels of MHC class II (C) and CD25 (D). RNAseq derived differential gene expression of PTCL cases compared to control $CD4^+$ T-cells demonstrated that expression of CD5, CD25, and MHC class II molecules (DLA-DRA, DLA-DRB1, DLA-DQA1, DLA-DQB1, and CIITA) corresponded with cell surface protein expression (E). Parathyroid hormone like hormone (PTHLH) expression was increased in all patients, regardless of presence of clinical hypercalcemia (Mean ± SD, *=Padj<0.05).

Hierarchical clustering of samples resulted in distinct separation of control lymphocytes and PTCL cases with intermixing of PTCL from Boxer and non-Boxer dogs (Figure 2.4a). In fact, only 82 genes were significantly differentially expressed when comparing tumor samples from Boxers and non-Boxer dogs (Figure 2.4c). Interestingly, one of the most overexpressed genes in PTCL in all 3 Boxers compared to PTCL in non-Boxer dogs was ROS proto-oncogene 1 (ROS1) (log(fold change)=4.15; padj= <0.001). ROS1 is a receptor tyrosine kinase oncogene that has been shown to undergo genetic rearrangements in a variety of human cancers.[31] Overall, it does not appear that the gene expression profile of $CD4^+$ PTCL in Boxer dogs is markedly different from that of $CD4^+$ PTCL in other breeds, despite overrepresentation of Boxers within the patient population.

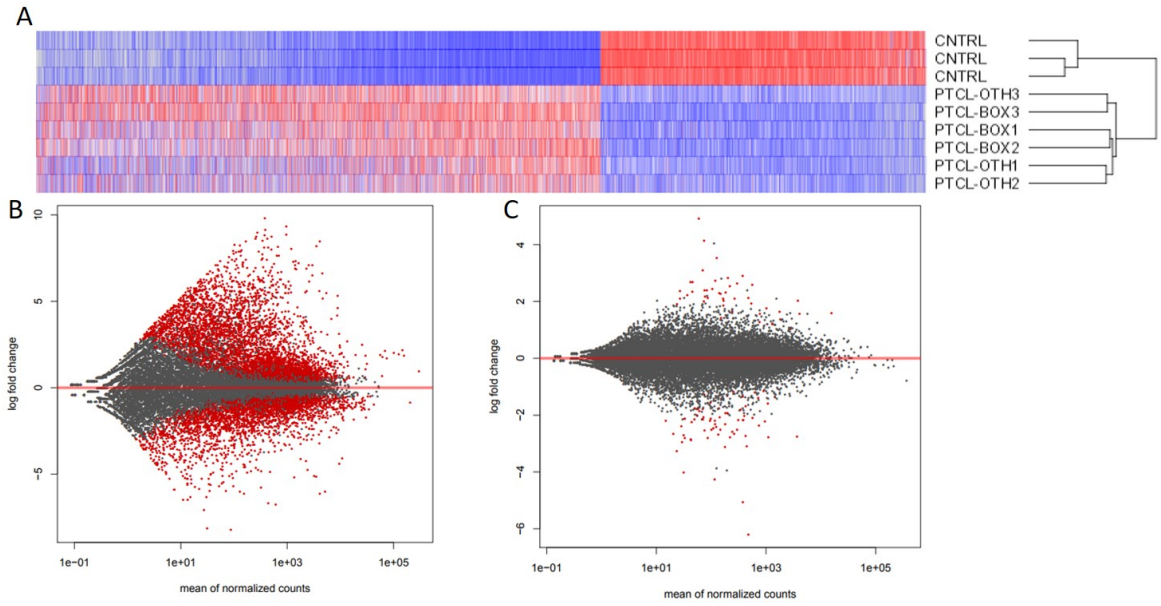

Figure 2.4. Gene expression profile of CD4$^+$ PTCL. Hierarchical clustering (average Euclidean distance) of differentially expressed genes (Padj<0.05) identified distinct separation of control and PTCL case samples. There was intermixing of PTCL cases from Boxer dogs and other breeds (A). MA-plots showed global differential gene expression of all PTCL cases compared to CD4$^+$ T-cell controls (B) and PTCL cases from Boxer dogs compared to PTCL cases from other dog breeds (C). Significantly differentially expressed genes (Padj<0.05) are highlighted in red.

CD8$^+$ and CD4$^-$CD8$^-$ Outcome Study

Given the low numbers of CD8$^+$ and CD4$^-$CD8$^-$ TCLs within the population evaluated in the flow cytometry:histopathology correlation study, we next sought to evaluate the flow cytometry and clinical features of a larger group of these uncommon phenotypes. We aimed to better determine if CD8$^+$ and CD4$^-$CD8$^-$ tumors represent distinct biological entities with unique pathogeneses and clinical behaviors or conversely, if these tumors are part of the larger single group of TCL neoplasms that includes CD4$^+$ TCL.

In dogs, $CD8^+$ and $CD4^-CD8^-$ TCLs involving the lymph node are rare (Figure 2.5). Between 2012 and 2017, a total of 11,746 unique cases of canine lymphoma involving the lymph node were diagnosed at the CSU-CI laboratory. Of this population, the majority of cases were diagnosed as B-cell lymphoma. $CD4^+$ TCL was the next most common phenotype followed by T-zone lymphoma. $CD4^-CD8^-$ TCL and $CD8^+$ TCL comprised 2.6% and 2.3% of cases respectively.

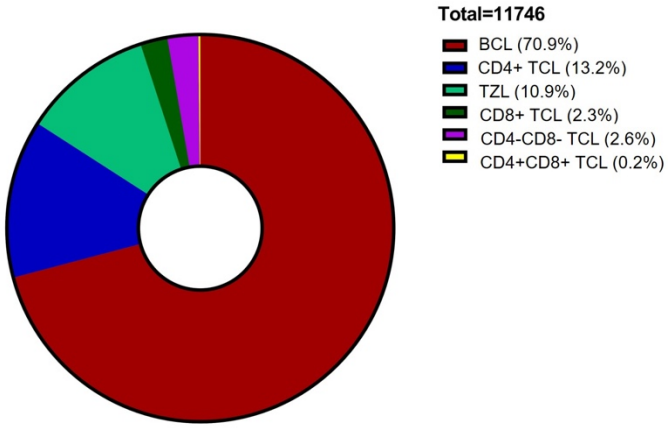

Figure 2.5. Immunophenotypic distribution of canine nodal lymphoid neoplasms. The immunophenotypic distribution of canine lymphoid neoplasia characterized by flow cytometry performed on lymph node aspirates between 2012-2017. B-cell lymphoma (BCL) is the most common immunophenotype, followed by $CD4^+$ T-cell lymphoma (TCL) and T-zone lymphoma (TZL). $CD8^+$ TCL, $CD4^-CD8^-$ TCL, and $CD4^+$ $CD8^+$ TCL are uncommon phenotypes.

Patient Demographics:

During this timeframe, a total of 561 cases met inclusion criteria for this study and medical records for 119 of these cases were obtained. Within this study group, 59 cases were categorized as $CD4^-CD8^-$ TCL and 60 cases were categorized as $CD8^+$ TCL. Patient demographics are summarized in Table 2.4. Significantly more patients diagnosed with $CD8^+$ TCL were categorized as older (≥10 years) than those diagnosed with $CD4^-CD8^-$ TCL ($p=0.0130$). There was a significantly different sex distribution between $CD8^+$ TCL cases and $CD4^-CD8^-$ TCL cases ($p=0.0045$), with $CD4^-CD8^-$ TCL having a male (62.7%) predominance

and $CD8^+$ TCL having a female (63.3%) predominance. The most common breeds affected by $CD4^-CD8^-$ or $CD8^+$ TCLs were mixed breeds, Boxers, Golden Retrievers, and Labrador Retrievers. There was no difference in breed distribution between the two immunophenotypes (p=0.8557).

Table 2.4. Summary of patient demographics

Immunophenotype	**$CD4^-CD8^-$ TCL**	**$CD8^+$ TCL**
Age, yrs (median; range)	8 (3-15)	10 (1-15)
Sex (number; percent)		
Female Spayed	22 (37%)	36 (60%)
Female Intact	0 (0%)	2 (3%)
Male Castrated	32 (54%)	19 (32%)
Male Intact	5 (8%)	3 (5%)
Breed (number; percent)		
Mixed Breed	13 (22%)	12 (20%)
Golden Retriever	10 (17%)	7 (12%)
Boxer	7 (12%)	7 (12%)
Labrador Retriever	5 (8%)	8 (13%)
Other	24 (41%)	26 (43%)

Clinical Signs:

Presenting clinical signs are summarized in Table 2.5. Most cases of $CD4^-CD8^-$ and $CD8^+$ TCLs in this study presented with peripheral lymphadenopathy, consistent with the inclusion criteria of lymph node sample. Abdominal lymphadenopathy was present in 81% of evaluated $CD4^-CD8^-$ TCLs and 56% of evaluated $CD8^+$ TCLs. Few cases demonstrated enlarged abdominal lymph nodes in the absence of reported peripheral lymph node involvement (1 $CD8^+$ TCL and 4 $CD4^-CD8^-$ TCLs). More commonly, dogs with peripheral lymphadenopathy had concurrent abdominal lymphadenopathy (17 $CD8^+$ TCLs and 25 $CD4^-CD8^-$ TCLs). Abdominal lymph node involvement was most often identified by abdominal ultrasound, with rare cases identified by abdominal radiographs (n=2). The presence of hepatomegaly was unknown in about half of the evaluated dogs and of those where is was evaluated, 50% (n=18) of cases in the

$CD8^+$ group and 47% (n=16) of cases in the $CD4^-CD8^-$ TCL group were affected. Similarly, splenomegaly and/or splenic nodules affected 52% (n=17) and 53% (n=18) of evaluated cases in the $CD8^+$ and $CD4^-CD8^-$ TCL groups, respectively. Hepatomegaly and/or splenic changes were most often identified by abdominal ultrasound with fewer cases identified by abdominal radiographs (n=6), computed tomography (n=1), or abdominal palpation (n=2). The cause of liver or splenic enlargement was not definitively determined by cytology or histology. Gastrointestinal involvement was uncommon among both TCL groups (n=6) and included the presence of a gastrointestinal mass (n=2), thickened intestines (n=3), or clinical diagnosis of protein-losing enteropathy (n=1).

Table 2.5. Summary of patient clinical signs and laboratory abnormalities

	$CD4^-CD8^-$ nTCLs (n=59)			$CD8^+$ nTCLs (n=60)			
Clinical Signs	**% Affected**	**# Affected**	**# Evaluated**	**% Affected**	**# Affected**	**# Evaluated**	**p-value[+]**
Peripheral Lymph Nodes	93%	55	59	98%	59	60	0.2068
Abdominal Lymph Nodes	81%	29	36	56%	18	32	0.0380
Hepatomegaly	47%	16	34	50%	18	36	0.8161
Splenomegaly	53%	18	34	52%	17	33	0.9999
Gastrointestinal	14%	4	28	8%	2	26	0.6702
Skin/Mucocutaneous	10%	6	59	43%	26	60	<0.0001
Sternal LN/Mediastinum	60%	21	35	13%	5	40	<0.0001
Hypercalcemia	29%	16	55	4%	2	54	0.0005
Complete Blood Count							
Mild anemia	11%	5	44	10%	4	41	
Moderate anemia	14%	6	44	15%	6	41	0.9999[++]
Severe anemia	0%	0	44	0%	0	41	
Mild thrombocytopenia	27%	12	44	7%	3	41	
Mod. thrombocytopenia	11%	5	44	10%	4	41	0.0323[++]
Severe thrombocytopenia	0%	0	44	0%	0	41	
Mild lymphocytosis	11%	5	44	15%	6	41	
Mod. lymphocytosis	2%	1	44	2%	1	41	0.4188[++]
Severe lymphocytosis	2%	1	44	7%	3	41	

[+]Wilcoxon rank-sum test was performed to compare clinical features between $CD4^-CD8^-$ TCLs and $CD8^+$ TCLs.
[++]Complete blood count parameters were grouped to compare all cases with anemia, thrombocytopenia, or lymphocytosis.

Skin lesions were significantly more common in $CD8^+$ TCL patients, with 43% (n=26) of the $CD8^+$ TCL cohort exhibiting skin lesions clinically suspicious for cutaneous lymphoma. Within the $CD8^+$ TCL group, 73% (n=19) of the patients with skin lesions had mucocutaneous

involvement. Thirteen of the 26 cases of $CD8^+$ TCL with cutaneous lesions were confirmed to be cutaneous lymphoma by cytology or histology. Nine of those cases were described specifically as epitheliotropic, 1 case was described as non-epitheliotropic, and epitheliotropism was unknown in the remaining cases. In contrast, only 10% (n=6) of cases classified as $CD4^-CD8^-$ TCL presented with concurrent cutaneous involvement. Of these 6 total $CD4^-CD8^-$ TCL patients with cutaneous involvement, 1 dog had gingival involvement and the other 5 had generalized lesions. Two of the 6 cases within the $CD4^-CD8^-$ TCL group were confirmed to be cutaneous lymphoma by cytology or histology. Epitheliotropism was unknown in all the $CD4^-CD8^-$ TCL cases with cutaneous lesions. The presence of skin lesions was not significantly associated with cell size ($p=0.6785$), expression of MHC class II ($p=0.6841$), or CD5 expression ($p=0.8287$) evaluated by flow cytometry.

Cranial mediastinal enlargement and/or sternal lymphadenopathy was seen significantly more commonly in $CD4^-CD8^-$ TCLs, affecting 60% (n=21) of evaluated cases. Mediastinal enlargement or sternal lymphadenopathy were diagnosed by thoracic radiographs in all cases, with no additional diagnostics performed. Similarly, hypercalcemia affected 29% (n=16) of $CD4^-CD8^-$ TCL cases and was more frequently present at the time of diagnosis than in $CD8^+$ TCLs.

Complete blood counts (CBC) were available for review in 85 total cases (41 $CD8^+$ TCLs and 44 $CD4^-CD8^-$ TCLs) (Table 2.5). In general, CBC abnormalities were uncommon at the time of diagnosis. The most common changes included a mild to moderate anemia, mild to moderate thrombocytopenia, and mild lymphocytosis (5,000-10,000 lymphs/uL). Cases with mild to moderate neutrophilia in conjunction with mild to absent lymphopenia were common and interpreted as most consistent with a stress leukogram and not further evaluated. Two patients with $CD4^-CD8^-$ TCL were mildly neutropenic (1,920 and 1,940 neutrophils/uL) and this finding

was not further explored. Moderate to marked lymphocytosis (>10,000 lymphs/uL), consistent with neoplastic involvement of the blood, was seen in 3 $CD8^+$ TCLs and 1 $CD4^-CD8^-$ TCL.

Flow Cytometry

All cases were evaluated for relative cell size based on median forward light scatter, MFI of MHC class II, and expression of CD5 (Figure 2.6, Table 2.6). There was no significant difference in cell size between $CD8^+$ TCLs and $CD4^-CD8^-$ TCLs (p=0.3862), and neoplastic cell size ranged from small (less than 1.3 times the size of normal T-cells) to large (greater than or equal to 1.3 times the size of normal T-cells). The expression level of MHC class II was significantly lower in $CD4^-CD8^-$ TCLs, compared to $CD8^+$ TCLs (p=0.0470). The number of $CD4^-CD8^-$ cases that were classified as low MHC expression (MFI less than normal T-cells), however, was not significantly different from $CD8^+$ cases (p=0.0674). Loss of CD5 expression was observed significantly more often in $CD4^-CD8^-$ tumors compared to $CD8^+$ tumors (p=0.0188).

Table 2.6. Summary of flow cytometry features

Immunophenotype	**Size**		**MHC class II**		**Loss of CD5 Expression**	
	Median	IQR^+	Median	IQR^+	Number	Percentage
$CD4^-CD8^-$ TCL	478	424-567	2.16	0.60-9.41	25	42%
$CD8^+$ TCL	463	412-529	5.60	1.40-17.16	13	22%
Normal T-cells	387	373-412	13.78	9.81-18.52	0	0%

$^+$IQR=interquartile range

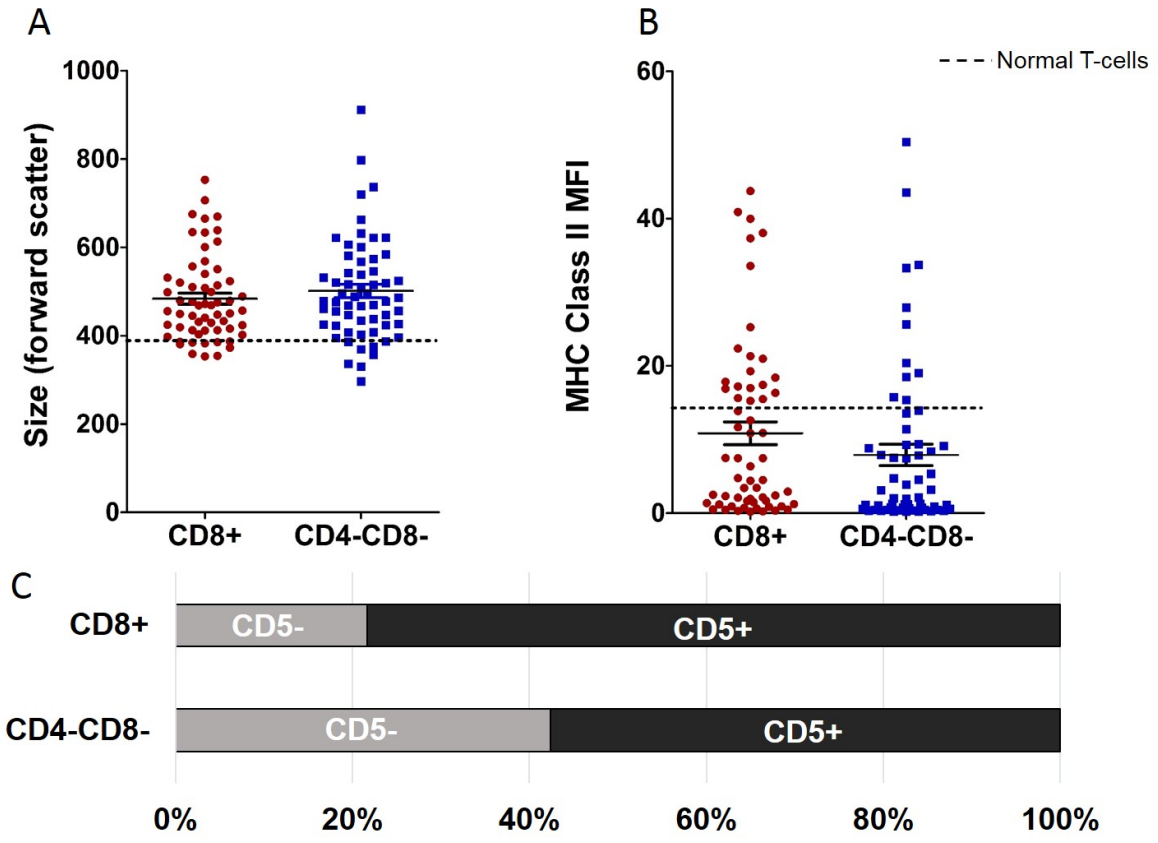

Figure 2.6. Flow cytometric features of $CD8^+$ and $CD4^-CD8^-$ TCLs. (A) The median neoplastic cell size as determined by forward scatter is depicted for each case. There is no significant difference in neoplastic cell size between $CD8^+$ and $CD4^-CD8^-$ TCLs. The median cell size of normal T-cells is represented by the dotted line. (B) The MHC class II median fluorescence intensity (MFI) on neoplastic T-cells is depicted for each case. There is variable expression of MHC class II expression in both $CD8^+$ and $CD4^-CD8^-$ TCLs, with some cases exhibiting very low expression and others with higher levels compared to normal T-cells (dotted line). (C) The percent of cases within each immunophenotypic group that have lost expression of CD5 is provided. Loss of CD5 expression was more commonly seen in $CD4^-CD8^-$ TCLs (p-value=0.0188).

Cytology

Lymph node aspirates from eleven patients diagnosed with $CD8^+$ TCL by flow cytometry and thirteen patients diagnosed with $CD4^-CD8^-$ TCL by flow cytometry were independently and blindly evaluated by two clinical pathologists (Emily D. Rout, Paul R. Avery) and compared to cytology from ten cases of $CD4^+$ PTCL (representative examples in Figure 2.7). The ten randomly-selected $CD4^+$ PTCL cases were morphologically similar and samples contained an expanded population of intermediate-sized lymphocytes with round to oval, occasionally indented nuclei, fine chromatin, absent to rarely one faint nucleolus, and moderate amounts of

pale blue cytoplasm (Figure 2.7a). In comparison, $CD8^+$ and $CD4^-CD8^-$ TCLs were highly variable and there were no apparent trends in cytomorphology that correlated to immunophenotype. Approximately half of the $CD8^+$ and $CD4^-CD8^-$ TCL cases had similar morphology to $CD4^+$ PTCL cases, but remaining cases were variable and often displayed more cellular pleomorphism. These cases tended to have round to indented nuclei and moderate amounts of cytoplasm similar to $CD4^+$ PTCL, but the nuclear chromatin was often coarser to irregularly clumped with more prominent nucleoli and the cytoplasm could become quite basophilic. Five cases had marked anisocytosis and anisokaryosis. In a small number of cases, neoplastic cells had one to a few, small, clear, discrete cytoplasmic vacuoles. Four $CD8^+$ TCLs and 3 $CD4^-CD8^-$ TCLs had rare to small numbers of neoplastic lymphocytes with few fine azurophilic cytoplasmic granules.

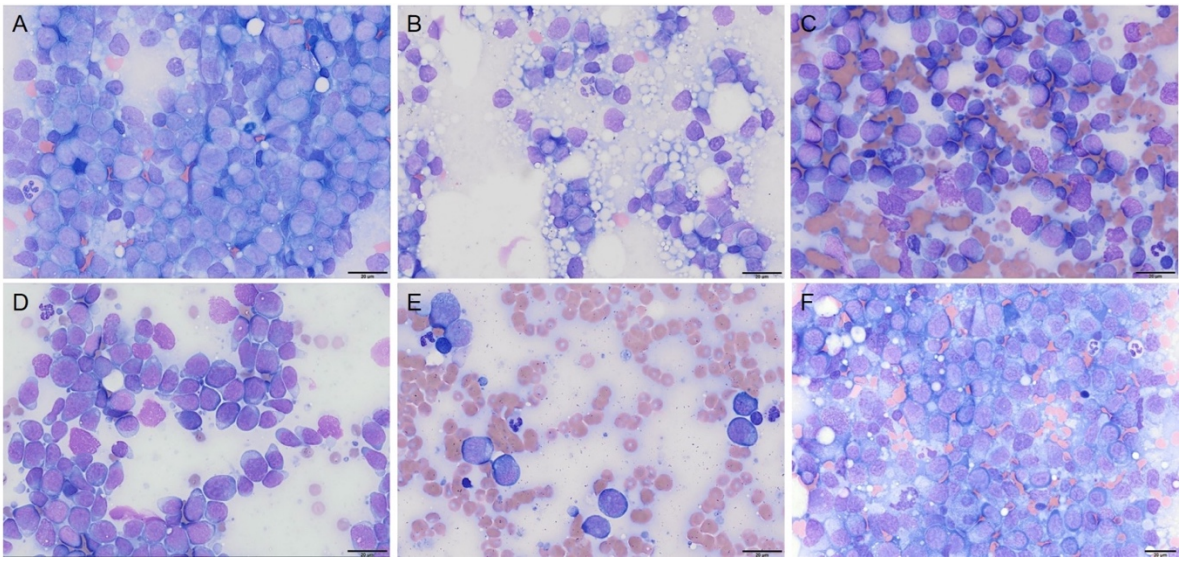

Figure 2.7. Cytomorphology of canine $CD4^+$, $CD8^+$ and $CD4^-CD8^-$ T-cell lymphoma (TCL). Direct smears of fine-needle lymph node aspirates from a representative $CD4^+$ peripheral TCL case (A) and $CD8^+$ (B, D) and $CD4^-CD8^-$ (C, E, F) TCL cases with variable cytomorphology are shown; Wright Giemsa stain, 50X. (A) Ten $CD4^+$ peripheral TCLs were reviewed for comparison to $CD8^+$ and $CD4^-CD8^-$ TCLs and an example is shown here. The cells were intermediate sized with round to indented nuclei, fine chromatin, rare faint nucleoli and moderate amounts of pale blue cytoplasm. A subset of $CD8^+$ and $CD4^-CD8^-$ TCL cases had similar morphology to $CD4^+$ peripheral TCL (B), while remaining cases were more variable (C-F). These cases demonstrated more anisocytosis with some lymphocytes exceeding 20 µm in diameter, frequently coarser to irregularly clumped chromatin, and increased cytoplasmic basophilia. Small numbers of cells had small clear cytoplasmic vacuoles (D, F). One case had prominent nucleoli up to 8 µm in diameter (F).

Clinical Outcome

Of the 119 cases evaluated, 9 cases died, 47 were humanely euthanized, and 63 cases were lost to follow up (median follow-up time: 64 days). All 9 cases that died had progressive disease and were interpreted as a lymphoma-related death. Of the 47 cases that were humanely euthanized, 42 cases were euthanized due to progressive disease and declining quality of life. Four $CD8^+$ cases were euthanized with clinical signs of unconfirmed etiologies including: hemoabdomen (n=1), pleural effusion (n=1), pulmonary nodules (n=1), and renal failure (n=1). A single $CD4^-CD8^-$ case was euthanized with renal failure.

$CD8^+$ TCLs and $CD4^-CD8^-$ TCLs were associated with poor clinical outcomes, with a median overall survival (OS) of 198 days (range 1-471 days) and 145 days (range 1-770 days), respectively (Figure 2.8a). Significant differences in survival between patients with tumors classified as $CD8^+$ TCLs versus $CD4^-CD8^-$ TCLs were not identified.

Log-rank and Cox proportional hazards univariable analyses were performed independently for both tumor subtypes and the results are summarized in Tables 2.7 and 2.8. For both subtypes, large cell size (≥1.3 times normal T-cells) determined by forward scatter was associated with shorter overall survival. Combined, cases with large cell size had a median OS of 61 days (range 1-541 days) versus 257 days (range 1-770) for those with small cell size (p=0.0002; Figure 2.8b). Neither MHC class II or CD5 expression levels had significant impact on OS.

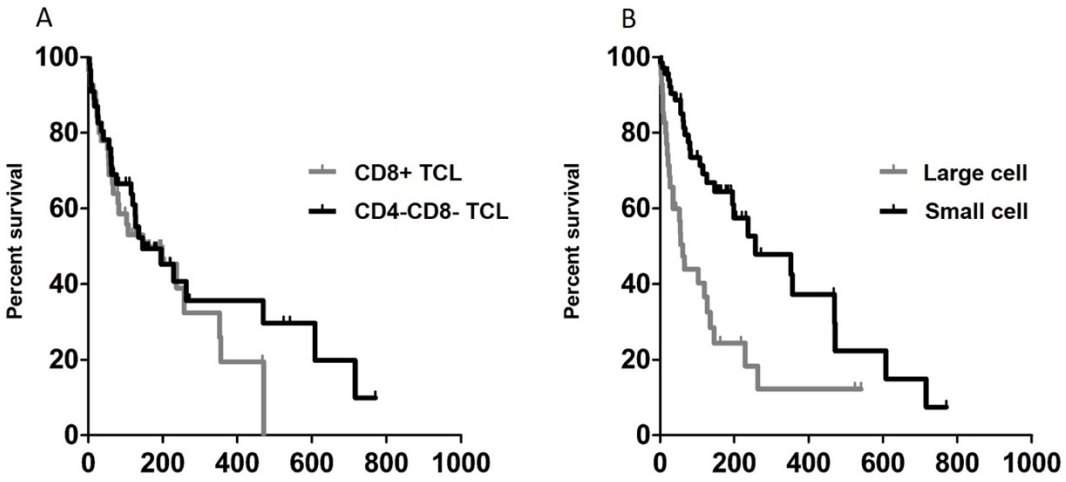

Figure 2.8. Overall survival of patients with $CD8^+$ and $CD4^-CD8^-$ TCLs. (A) Kaplan Meier curves depicting overall survival from time of flow cytometry diagnosis for each immunophenotypic group are provided. There is no significant difference in overall survival between patients with $CD8^+$ and $CD4^-CD8^-$ TCLs. The median survival times were 198 days and 145 days for $CD8^+$ and $CD4^-CD8^-$ cases, respectively. (B) Neoplastic cell size measured by forward scatter by flow cytometry is associated with a shorter overall survival in patients with $CD8^+$ and $CD4^-CD8^-$ TCLs (p=0.0002). The median survival time for cases classified as large cell was 61 days, while those classified as small cell was 257 days.

Among dogs with $CD8^+$ TCL, the presence of hepatomegaly, anemia, or abdominal lymphadenopathy at the time of diagnosis were associated with a shorter OS (Table 2.7). Abdominal lymphadenopathy, hepatomegaly, or anemia did not significantly impact survival in the $CD4^-CD8^-$ TCL group (Table 2.8) or the combined group of $CD8^+$ and $CD4^-CD8^-$ TCLs. The presence of cranial mediastinal enlargement/sternal lymphadenopathy, skin lesions, splenomegaly, hypercalcemia or age of the patient did not impact overall survival in $CD8^+$ and $CD4^-CD8^-$ TCLs.

Chemotherapeutic regimes used to treat the dogs in this retrospective study were widely variable in the combination of agents used, dosages, and frequency of administration. Consequently, to evaluate the impact of chemotherapy on survival, treatment protocols were assigned to the following broad categories: no treatment, corticosteroid therapy only, single-agent therapy, or multi-agent therapy. Corticosteroid therapy included treatment with prednisone,

prednisolone, and/or dexamethasone only. Single-agent therapy included a single chemotherapeutic agent with or without concurrent corticosteroid therapy. Single agents used included CCNU and chlorambucil. Multi-agent therapy included two or more chemotherapeutic agents with or without corticosteroid therapy. Five patients were enrolled in a double-blinded clinical trial evaluating a monoclonal antibody and may have additionally received this novel therapeutic. All dogs enrolled in this immunotherapy trial (n=5) and patients in which the therapeutic protocol was unclear in the medical record (n=5) were removed from this outcome evaluation.

Within both TCL subgroups, dogs treated with chemotherapy (single-agent or multi-agent) had a significantly prolonged survival compared to those receiving no treatment or corticosteroids alone. (Table 2.7 and 2.8). No significant difference in overall survival was observed in patients treated with single-agent or multi-agent chemotherapy in either subgroup.

Table 2.7. Summary of survival analysis for selected clinical and immunophenotypic characteristics of $CD8^+$ TCLs.

Variable	Condition		MST (d)	P-value	Hazard ratio (B/A)	CI, hazard ratio
Abdominal LN	A	Absent (n=14)	198	**0.076**	**2.92**	**1.02-8.42**
	B	Present (n=18)	67			
Sternal LN/Mediastinal mass	A	Absent (n=35)	103	0.717	1.80	0.23-14.39
	B	Present (n=5)	Undefined			
Cutaneous involvement	A	Absent (n=34)	80	0.251	0.70	0.33-1.49
	B	Present (n=26)	198			
Splenic changes	A	Absent (n=16)	55	0.351	0.86	0.26-2.89
	B	Present (n=17)	107			
Hepatomegaly	A	Absent (n=18)	257	**0.018**	**5.82**	**1.46-23.51**
	B	Present (n=18)	65			
Hypercalcemia	A	Absent (n=52)	107	0.376	Undefined	Undefined
	B	Present (n=2)	Undefined			
Treatment-Chemo vs None	A	Multi/Single (n=45)	237	**0.002**	**6.92**	**2.09-22.87**
	B	Steroids/None (n=12)	19			
Treatment - Single vs Multi	A	Multi-agent (n=34)	237	0.324	0.60	0.21-1.67
	B	Single-agent (n=11)	257			
Anemia	A	Absent (n=31)	237	**0.001**	**6.64**	**2.13-20.69**
	B	Present (n=10)	54			
Age	A	Years >10 (n=35)	198	0.243	1.60	0.72-3.57
	B	Years <10 (n=25)	80			
Cell Size	A	Small (n=40)	237	**0.002**	**3.54**	**1.52-8.26**
	B	Large (n=20)	54			
CD5 Loss	A	CD5+ (n=47)	147	0.761	0.87	0.36-2.07
	B	CD5- (n=13)	237			
Class II MHC	A	High (n=30)	352	0.562	0.80	0.37-1.72
	B	Low (n=30)	147			

Table 2.8. Summary of survival analysis for selected clinical and immunophenotypic characteristics of $CD4^{-}CD8^{-}$ TCLs.

Variable	Condition		MST (d)	p-value	Hazard ratio (B/A)	CI, hazard ratio
Abdominal LN	A	Absent (n=7)	145	0.867	2.03	0.57-7.25
	B	Present (n=29)	126			
Sternal LN/Mediastinal mass	A	Absent (n=14)	229	0.179	0.38	0.13-1.11
	B	Present (n=21)	469			
Cutaneous involvement	A	Absent (n=23)	135	0.769	1.51	0.51-4.44
	B	Present (n=6)	115			
Splenic changes	A	Absent (n=16)	145	0.707	0.73	0.25-2.15
	B	Present (n=18)	263			
Hepatomegaly	A	Absent (n=18)	263	0.648	1.05	0.36-3.01
	B	Present (n=16)	195			
Hypercalcemia	A	Absent (n=39)	145	0.686	0.76	0.30-1.89
	B	Present (n=16)	229			
Treatment: Chemo vs none	A	Multi/Single (n=40)	145	**0.050**	**3.09**	**1.00-9.54**
	B	Steroids/None (12)	56			
Treatment: Multi vs Single	A	Multi (n=37)	195	0.937	0.92	0.12-6.99
	B	Single (n=3)	145			
Anemia	A	Absent (n=33)	469	0.847	1.14	0.31-4.16
	B	Present (n=10)	195			
Age	A	Old (n=21)	126	0.351	0.70	0.32-1.50
	B	Young (n=38)	229			
Cell Size	A	Small (n=34)	469	**0.005**	**2.96**	**1.34-6.55**
	B	Large (n=25)	119			
CD5 Loss	A	CD5+ (n=34)	127	0.351	1.43	0.67-3.04
	B	CD5- (n=25)	469			
Class II MHC	A	High (n=24)	126	0.712	0.87	0.40-1.87
	B	Low (n=35)	229			

Discussion

In this study we first investigated the correlations between immunophenotype by flow cytometry and histomorphology of nodal TCLs. Within this cohort of nodal TCL patients with paired histology and flow cytometry, approximately 80% were categorized as $CD4^{+}$ PTCL and the remaining cases were classified as $CD8^{+}$ PTCL or $CD4^{-}CD8^{-}$ PTCL. The study population was representative of dogs with non-TZL TCL lymphoma presenting to specialty veterinary hospitals with enlarged peripheral lymph nodes. The less common T-cell phenotypes ($CD8^{+}$,

$CD4^-CD8^-$) could not be reliably differentiated from $CD4^+$ PTCL based on histomorphology alone. All tumors within the evaluated cohort were characterized by a diffuse infiltration of intermediate to large cells with pleomorphic nuclei and high mitotic rates. This finding may suggest that these tumors are part of the same disease entity regardless of immunophenotype. Alternatively, this finding may indicate that histomorphology alone is not a sensitive and reliable test to delineate biologically significant subtypes of nodal TCLs. Flow cytometry may be used to further divide this histologic entity into different immunophenotypic subtypes of PTCL.

A histologic diagnosis of lymphoblastic lymphoma (LBL) was considered in few cases, but ultimately these tumors were classified as PTCL based on cell size, pleomorphic nuclear shape, and intertumoral variation in chromatin staining and nucleolar prominence. Lymphoblastic is a loosely defined term in veterinary medicine with variable interpretations by both clinical and anatomic pathologists.[152] Histologically, LBL and PTCL exhibit overlapping morphologic features including intermediate cell size, variably round to oval to irregularly indented nuclei, and high mitotic rates.[152] Differentiation between the histomorphology of these neoplasms has been reliant on nucleolar prominence and number and conspicuousness of mitotic figures.[152] Because there was moderate to marked variation of these histologic features within an individual tumor sample, the authors felt that these features could not be used to reliably differentiate morphologically distinct subtypes and were consistent with the morphologic features described for PTCL-NOS by the WHO classification system in both dogs and humans. According to the WHO classification, LBL is a precursor T-lymphocyte neoplasm which typically expresses TdT and CD34[20], markers of immature lymphoblasts. Cases of PTCL do not express CD34[163], a commonly used marker of acute leukemias in dogs.[177] Evaluation of TdT expression has not yet been optimized for canine diagnostics by flow cytometry or immunohistochemistry. Further

development of markers of immaturity for canine lymphocytes would be useful to more reliably differentiate tumors of precursor versus mature lymphocyte origins.

We next performed gene expression profiling focused on the most common immunophenotype of PTCL. $CD4^+$ PTCL exhibited consistent changes in gene expression between tumor samples from different dogs. Homogeneity within the gene expression profile of PTCL from different patients is promising for investigation into novel therapeutics and clinical trial design. PTCL in Boxer dogs, who are overrepresented in the patient population, did not exhibit a distinct overall gene expression profile from PTCL in other breeds. However, one gene that was significantly differentially expressed in Boxer dogs was ROS1. ROS1 is a receptor tyrosine kinase often involved in chromosomal translocations and oncogenic fusion gene formation in human cancers.[31] In a preliminary analysis, ROS1 fusion gene transcripts were not identified in canine $CD4^+$ PTCL (data not shown).

$CD8^+$ and $CD4^-CD8^-$ TCLs involving the lymph nodes are rare in dogs, comprising 2.3% and 2.6% of all nodal lymphomas respectively. The distribution of nodal lymphoma immunophenotypes in dogs from the CSU-CI database described in this study closely mimics the distribution reported by Martini et al, demonstrating inter-institutional consistency.[178] Because these lymphoma subtypes are uncommon, the clinical features and biologic behavior has not previously been well described. In the third part of this chapter, we performed a retrospective study to describe the clinical features of a large group of individuals diagnosed with $CD8^+$ and $CD4^-CD8^-$ TCLs by flow cytometry. In general, patients with either $CD8^+$ or $CD4^-CD8^-$ TCL had poor clinical outcomes with median overall survival times of 198 and 145 days, respectively. There was no significant difference in survival between patients diagnosed with $CD8^+$ versus

$CD4^-CD8^-$ TCLs and these survival times are similar to that previously reported for $CD4^+$ TCLs (159-162 days).[158,163,164]

$CD8^+$ and $CD4^-CD8^-$ TCLs had widely variable cytomorphology, with inconsistent cell size, chromatin pattern, cytoplasmic basophilia and presence of nucleoli. Similarly, by flow cytometry both $CD8^+$ and $CD4^-CD8^-$ neoplastic cells ranged in size from small to large. Cell size determined by flow cytometry did have a prognostic impact, with tumors comprised of large cells measuring greater than or equal to 1.3 times the median size of normal T-cells having a shorter overall survival. Nevertheless, the median overall survival of patients with small cell size was 257 days. This overall survival time is still much shorter than that expected for an indolent disease,[10,12] despite the small cell size. These results support the finding that cell size is prognostic only within specific subtypes of lymphoma[163], but not as an indicator of indolent disease when the subtype is unknown. Therefore, these findings highlight the importance of ancillary diagnostics, specifically flow cytometry, to phenotype canine lymphoma cases in order to provide accurate prognostic information and inform treatment decisions.

Concurrent skin lesions, suspicious for or confirmed to be cutaneous lymphoma were more commonly seen in $CD8^+$ TCLs. This finding is consistent with previous reports demonstrating that canine cutaneous epitheliotropic lymphoma is most typically comprised of neoplastic $CD8^+$ T-cells.[178,179] Of the $CD8^+$ TCL cases with skin involvement, 73% had mucocutaneous localization. Cases with skin lesions did not exhibit distinct trends in cell size, expression of MHC class II, or CD5 expression evaluated by flow cytometry.

The presence of hepatomegaly, anemia, or abdominal lymphadenopathy were associated with shorter overall survival times in cases of $CD8^+$ TCL. In dogs, hepatosplenic lymphoma is a rare form of T-cell lymphoma characterized by infiltration of the liver and/or spleen in the

absence of peripheral lymph node involvement.[20,180] Hepatosplenic lymphoma in dogs can be comprised of $CD8^+$ or $CD4^-CD8^-$ T-cells.[180] Of the 18 $CD8^+$ TCLs in this study with hepatomegaly, one patient had abdominal lymphadenopathy in the absence of peripheral lymphadenopathy. All other $CD8^+$ TCLs and all cases of $CD4^-CD8^-$ TCL with hepatomegaly in this study had concurrent peripheral lymphadenopathy, making a diagnosis of hepatosplenic lymphoma less likely.

The few cases of $CD8^+$ and $CD4^-CD8^-$ included in the flow cytometry-histopathology correlation study were classified as PTCL-NOS by histology. Therefore, we hypothesize that the majority of cases within the larger cohort of patients would also fall with the histologic classification of PTCL-NOS. A subset of cases in the current study were classified as small to intermediate in size by flow cytometry. This feature could be also be consistent with a classification of lymphoblastic lymphoma. Both PTCL and lymphoblastic lymphoma carry poor prognoses in dogs[6], consistent with the overall survival times of patients evaluated in this study.

Presence of cranial mediastinal/sternal lymph node enlargement and/or hypercalcemia were more frequent in the $CD4^-CD8^-$ TCL subgroup. These clinical features have been previously associated with $CD4^+$ TCLs[163], suggesting clinical similarity between these two entities. $CD4^-CD8^-$ TCLs also exhibit flow cytometry features characteristic of $CD4^+$ TCLs, including frequent low MHC class II expression and loss of CD5 expression.[163] Furthermore, a subset of $CD4^-CD8^-$ cases had cytomorphology similar to $CD4^+$ TCL. It is possible that at least a subset of $CD4^-CD8^-$ TCLs are part of the same, or closely related PTCL entity as $CD4^+$ PTCL. We hypothesize that $CD4^-CD8^-$ TCLs may arise from a thymic precursor prior to expression of CD4 and CD8, while $CD4^+$ TCLs arise from a slightly more mature thymocyte or naïve single

positive T-cell that has committed to the CD4 lineage. Alternatively, $CD4^{-}CD8^{-}$ TCLs may represent a variant of $CD4^{+}$ TCL, that has lost expression of CD4.

In this study, approximately 63% of dogs with $CD8^{+}$ TCL were female and approximately 63% of dogs with $CD4^{-}CD8^{-}$ TCLs were male. $CD4^{+}$ TCL in dogs also has a male predominance with 56-62% of affected patients being male.[159,163] In human patients, PTCL-NOS, which we hypothesize to be similar to canine $CD4^{+}$ TCL, has a reported male to female ratio of 2:1.[20] The pathobiology underlying this sex predilection is not yet understood.

Evaluation of the impact of treatment on overall survival is limited by the retrospective nature of this study. Within the patient group, a wide range in chemotherapy protocols were used with marked variations in drug combinations, dosages, and frequency of administration. Consequently, patients were divided into broad treatment categories (no treatment, corticosteroids only, single-agent, multi-agent) to evaluate impact of treatment on survival. Complicating the treatment evaluation, was inherent bias in treatment decisions based on disease severity at the time of presentation to the veterinarian, response to initial treatment, and/or financial and personal considerations of clients. With these limitations in mind, we did find that patients treated with single-agent or multi-agent chemotherapy protocols had a prolonged survival compared to those not receiving treatment or only receiving corticosteroid therapy. This finding was consistent in both $CD8^{+}$ and $CD4^{-}CD8^{-}$ TCL subgroups. A significant difference in survival was not observed between patients treated with multi-agent compared to single-agent chemotherapy regimens. The clinical significance of this finding is uncertain, given the limited power and sample size in this analysis. In this group of patients, CCNU was the most frequently administered single-agent therapeutic, and this drug has been shown to improve outcome in canine patients with cutaneous lymphoma.[28,29]

In human patients, PTCL is a heterogeneous disease with the majority of tumors classified into a 'not-otherwise specified' subgroup (PTCL-NOS) of uncertain pathobiology.[30] Similar to dogs, PTCL-NOS in people is an aggressive disease with poor responses to conventional chemotherapy and 5-year overall survival rates of only 32%.[31] The majority of nodal PTCL-NOS in people are $CD4^+$, however cases can also be $CD8^+$, $CD4^-CD8^-$, or rarely $CD4^+CD8^+$.[32] In people, $CD8^+$ PTCL-NOS is more commonly associated with extranodal disease.[33] Similarly, extranodal T-cell lymphoma in dogs is most commonly $CD8^+$ or $CD4^-CD8^-$.[178] Gene expression profiling in human PTCL-NOS has identified subgroups with expression profiles similar to mature, activated $CD4^+$ T-cells or less commonly, $CD8^+$ T-cells. In this human study, however, the tumors classified as $CD4^+$ 'helper-like' or $CD8^+$ 'cytotoxic-like' subgroups did not correlate with protein expression of CD4 or CD8 as evaluated by immunohistochemistry.[32] Consequently, the utility of classifying PTCL cases in humans based on surface expression of CD4 and CD8 molecules is uncertain.

In this chapter, we first describe the ability of flow cytometry to identify a distinct molecular and histologic entity: $CD4^+$ PTCL. Less common immunophenotypes ($CD8^+$, $CD4^-CD8^-$) could not be distinguished histologically from $CD4^+$. We then describe the clinical characteristics of two uncommon nodal TCL phenotypes in dogs. Due to the rarity of these TCL subtypes, previous reports of the clinical features and biologic behavior are limited, preventing accurate prognostication of patients diagnosed with these tumors. We demonstrate that $CD8^+$ and $CD4^-CD8^-$ nodal TCLs have an aggressive behavior with overall survival times similar to that of the more common $CD4^+$ PTCL. Furthermore, based on similar presenting clinical signs, cytomorphology and flow cytometry features, we suggest that at least a subset of $CD4^-CD8^-$ tumors may share a common pathogenesis to $CD4^+$ PTCL. $CD8^+$ TCLs exhibited more variable

cytomorphology, as well as differences in clinical presentations and prognostic features. These findings imply that this entity may have a different pathophysiology to the more common $CD4^+$ TCL. Within both $CD8^+$ and $CD4^-CD8^-$ TCL groups, cell size was prognostic, and cases comprised of large cells determined by flow cytometry exhibited significantly decreased overall survival times. Importantly, however, even cases classified as small cell exhibited aggressive disease with shorter overall survival times than that reported for indolent lymphomas.[10,12,34,35] This study lays the groundwork for further investigation into the molecular pathways driving these aggressive neoplasms and highlights the utility of flow cytometry in identifying and classifying prognostically-significant lymphoma subtypes.

CHAPTER 3 – EVALUATION OF CANINE PTCL AS A MODEL FOR HUMAN PTCL-NOS

Summary

Peripheral T-cell lymphoma (PTCL), not-otherwise specified (NOS) is the most common PTCL subgroup and includes a heterogenous group of tumors derived from neoplastic T-cells. PTCL-NOS is a poorly understood and aggressive disease with grave clinical outcomes and limited therapeutic options. Molecular subtypes of PTCL-NOS including PTCL-GATA3 and PTCL-TBX21 have recently been identified. PTCL-GATA3 is associated with a worse prognosis and greater genomic complexity including frequent loss of tumor suppressor genes associated with the CDKN2A/TP53 and PTEN-PI3K pathways. Despite these advances, characterization of the underlying pathogenesis and identification of novel therapies trails that of other hematopoietic tumors. The dog presents a unique opportunity to study a naturally-occurring translational model of PTCL-NOS. PTCL is one of the most common subtypes of non-Hodgkin's lymphoma in dogs. The clinical and diagnostic features of this canine neoplasm have been previously described; however, molecular characterization remains largely unexplored. In this chapter, we evaluate the gene expression prolife of canine PTCL by RNA-seq. We compare gene expression profiles of human and canine PTCL-NOS, and identify molecular similarities between the neoplasms in these two species. We show that canine PTCL is similar to the PTCL-GATA3 subgroup with strong expression of GATA3 and enrichment for the PI3K-AKT-MTOR pathway. We also demonstrate a functional role for PI3K signaling in canine PTCL by showing that inhibition of PI3K results in impaired proliferation in a canine T-cell lymphoma cell line as well diminished cell survival of primary patient-derived PTCL cells in short-term cell culture.

Results support the dog as a potentially valuable naturally-occurring model of PTCL-NOS to investigate the pathogenesis of the PTCL-GATA3 subgroup.

Introduction

Peripheral T-cell lymphomas (PTCL) encompass a heterogenous group of aggressive neoplasms derived from T-lymphocytes. These neoplasms are uncommon, comprising 5-20% of all non-Hodgkin lymphomas (NHL).[20,108] At least 25% of PTCL cases do not correspond specifically to defined T-cell entities in the World Health Organization classification and are therefore categorized as PTCL, not otherwise specified (NOS).[20,109,110] Advances in the understanding of the underlying pathobiology and development of targeted treatments have been limited by intrinsic disease heterogeneity, rarity, and lack of useful animal model systems.

In contrast to humans, PTCL is among the most common NHL subtypes in dogs, comprising approximately 15% of all naturally-occurring NHLs cases in this species.[156–159] The majority of PTCL cases in dogs fall within the category of PTCL-NOS[160], with rare reports of other PTCL subtypes, including anaplastic large cell lymphoma.[158,161,162] Dogs affected by PTCL-NOS exhibit similar clinical and diagnostic features to human patients. Dogs are typically diagnosed at middle to older age, with an average age of approximately 7 years old. Similarly, PTCL-NOS most often affects adult patients, with a median age of presentation of 60 years.[109] There is a male predominance in both species.[109,159,163] Both human and canine patients typically present in advanced stages with multicentric peripheral lymph node involvement, although any organ can be affected. Unlike in human patients, mediastinal involvement is seen in 30-40% of canine cases.[163] Dogs and people with PTCL-NOS are typically treated with anthracycline-containing regimens, most often comprised of cyclophosphamide, doxorubicin, vincristine, and prednisone (CHOP), with variable initial response and poor overall prognosis.[109,163]

Similar to PTCL-NOS in humans, canine tumors exhibit clonal T-cell receptor (TCR) gene rearrangement. The majority of PTCL-NOS cases are $CD4^+$ with fewer cases being $CD8^+$ or $CD4^-CD8^-$. Loss of CD5 expression is common in both species.[163,181] Histologically, these tumors are comprised of sheets of intermediate to large cells which often efface normal tissue architecture. Neoplastic cells typically have cleaved or oval nuclei and the mitotic rate can be variable but most often is considered high.[152]

Gene expression profiling has improved the understanding of PTCL-NOS in humans and has identified two major molecular subgroups: (1) the GATA3 subgroup, which is enriched for MYC, PI3K-ATK-MTOR, and ß-catenin gene signatures; and (2) the TBX21 subgroup which is enriched for INF-γ and NF-kB signaling. The GATA3 signature is associated with a worse prognosis.[117,118] Similar gene expression profiling experiments have not yet been performed in canine PTCL-NOS.

In this study, we evaluate the gene expression profile of 33 canine PTCL cases compared to sorted control CD4 and CD8 T-cells from the lymph nodes of healthy dogs. We identify molecular similarities between human and canine PTCL-NOS. Canine PTCL-NOS is most similar to the GATA3 subgroup with upregulation of the GATA3-associated gene signature as well as enrichment of the PI3K-AKT-MTOR signaling axis. Shared molecular signatures between human and canine PTCL-NOS, suggests that the dog has potential as a valuable naturally-occurring translational model to further investigate the pathogenesis of PTCL-NOS. The dog may also serve as a unique model-system to evaluate responses to novel, targeted therapeutics to improve personalized/precision medicine strategies.

Materials and Methods

Case selection for RNA-Seq

Fine needle tissue aspirates from 33 dogs submitted to the Colorado State University-Clinical Immunology laboratory for routine diagnostics and diagnosed with $CD4^+$, $CD4^-CD8^-$, or $CD8^+$ PTCL by flow cytometry were selected for RNA-seq. PTCL cases were identified by uniform expansion of T-cells characterized by expression of the pan-leukocyte marker CD45, the T-cell markers CD3 with or without CD5, and lack of expression of the B-cell marker CD21. Cases exhibited variable expression of T-cell subset antigens, CD4 and CD8. Median purity of neoplastic cells was 91.5% (range 63-99%). Prior studies from our laboratory have demonstrated that T-cell lymphomas with these flow cytometric features are histologically classified as PTCL NOS.

Control $CD4^+$ and $CD8^+$ T lymphocytes were harvested from lymph nodes of healthy dogs utilized for IACUC approved surgical continuing education courses. T-cell subsets were sorted by a MoFlo cell sorter (Beckman Coulter, Brea, CA) using positive selection with anti-CD4 (clone YKIX302.9) or anti-CD8 (clone YCATE55.9). Sorted populations were re-analyzed for purity and were used if greater than 90% of the cells were the desired population.

RNA Extraction and Sequencing

RNA extraction was performed using the Purelink RNA mini Kit (Thermo Fisher Scientific, Waltham, MA) and quality was measured with an Agilent 2100 Bioanalyzer System. All samples had a RIN value greater than 6.3 (median RIN 8.45; range 6.3-9.8). RNA was shipped to Novogene Corporation Inc (Sacramento, CA) where the libraries were constructed and sequenced using an Illumina Hiseq PE150 platform.

Differential Gene Expression

Sequences were aligned to CanFam3.1 genome using HISAT2.[182] HTseq[183] and DESeq2[184] were then used to quantify reads, normalize gene expression, and evaluate differentially expressed genes between tumor samples and controls. P-values were determined using a negative binomial distribution. A Benjamini-Hochberg procedure was used to correct p-values and padj<0.05 was considered the differentially expressed gene screening standard.

Clustering

Samples were clustered by FPKM using hierarchical clustering distance method with the function of heatmap, SOM (Self-organization mapping) and kmeans. Silhouette coefficient was used to adapt the optimal classification with default parameters in R. The Broad Institute tool, Morpheus[185], was used to visualize heatmaps using one minus Pearson's correlation and average linkage.

Correlation of canine and human gene expression profiles

Differential gene expression between human PTCL-NOS samples and sorted $CD4^+$ control human T-cells was evaluated using microarray analysis previously carried out by Piccagula et al (geo accession number GSE6338).[128] Differential gene expression between human PTCL-NOS patient biopsies and sorted $CD4^+$ T-cells was performed using GEO2R analysis software. The top 200 significantly upregulated and 200 significantly downregulated genes were selected for comparison. The log2foldchange(FC) of those selected genes were identified in both human and canine samples. Human genes which are not annotated in the canine genome were removed from the analysis. Comparison of the log2FC of the selected genes in human and canine samples was compared using a heatmap created by the Morpheus tool[185] and gene set enrichment analysis (GSEA).[186] The gene set used for GSEA analysis was pre-ranked based on the log2FC.

Pathway Enrichment Analysis

Gene set enrichment analysis (GSEA)[186] was used to compare canine PTCL gene expression profiles to various molecular signatures. The list of significantly differentially expressed genes in $CD4^+$ PTCL compared to control $CD4^+$ was ranked based on log2FC. The pre-ranked gene list was then compared to gene sets identified in the molecular signature database (MSigDB) v7.0.[187] Gene sets with an FDR q-value <0.05 were considered significantly enriched.

Immunohistochemistry

Six PTCL cases were selected from submissions to the CSU Diagnostic Laboratory for biopsy or post-mortem examination. Cases were identified based on histomorphology consistent with PTCL-NOS and confirmed T-cell origin by flow cytometry, immunohistochemistry, and/or clonal T-cell receptor rearrangement. Normal canine lymph node was used as a positive control. A canine cutaneous mast cell tumor[18] served as an additional positive control for the CD30 antibody. HIER was performed on a Leica Bond-Max or Leica Bond III IHC stainer using Bond Epitope Retrieval Solution 2 (Bond Epitope Retrieval Solution 2, Leica Biosystems Newcastle Ltd, Newcastle Upon Tyne, United Kingdom) for 30 minutes. The monoclonal anti-human CD30 antibody (clone Ber-H2, Dako North America Inc., Carpinteria, CA) at 1:20 dilution or monoclonal anti-mouse GATA3 antibody (clone 1A12-1d9, Invitrogen, Waltham, MA) at 1:500 dilution was applied. Labeling was performed on an automated staining platform (Bond-Max, Leica Biosystems Newcastle Ltd, Newcastle Upon Tyne, United Kingdom). Fast Red (Fast Red Substrate System, Dako North America Inc., Carpinteria, CA) was used as a chromogen and slides were counterstained with hematoxylin. Negative controls were incubated in diluent consisting of Tris-buffered saline with carrier protein and homologous nonimmune sera. All

sequential steps of the immunostaining procedure were performed on negative controls following incubation. Expression of phosphorylated AKT was evaluated using the rabbit monoclonal phosph-AKT antibody (Ser473, D9E, XP, Cell Signaling Technology, Danvers, MA) at 1:50 dilution with the mouse and rabbit specific HRP/DAB (ABC) detection IHC kit (ab64264, abcam, Cambridge, United Kingdom).

Western Blot

$CD4^+$ PTCL and T-zone lymphoma cases were identified based on flow cytometry. $CD4^+$ PTCL was characterized by a uniform expansion of $CD45^+CD3^+CD5^{+/-}CD4^+CD8^-CD21^-$ T-cells. Cases of T-zone lymphoma were selected based on $CD45^-CD3^+CD4^+CD5^+CD21^{hi}$ immunophenotype.[160,174] Protein was extracted from fine needle aspirations of affected lymph nodes using Invitrogen cell extraction buffer (FNN0011, ThermoFisher Scientific, Waltham, MA) supplemented with 1mM PMSF and Halt protease/phosphatase inhibitor cocktail (ThermoFisher Scientific, Waltham, MA). Total protein concentrations were measured using Pierce BCA protein assay kit (ThermoFisher Scientific, Waltham, MA). Samples were resuspended to an equal total protein per sample using deionized water. NuPAGE LDS sample buffer (ThermoFisher Scientific, Waltham, MA) and NuPAGE reducing agent (ThermoFisher Scientific, Waltham, MA) were added to the samples and they were subsequently heated at 70°C for ten minutes. Gel electrophoresis was performed using NuPAGE Novex 12% Bis-Tris MiniGel (ThermoFisher Scientific, Waltham, MA). A Novex sharp pre-stained protein standard (ThermoFisher Scientific, Waltham, MA) and MagicMark XP western protein standard (ThermoFisher Scientific, Waltham, MA) were used as protein standards. The iBlot 2 dry blotting system (ThermoFisher Scientific, Waltham, MA) was used for membrane transfer. The protein-bound membrane was blocked with 5% non-fat dried milk for 1 hour and subsequently

washed in tris-buffered saline and polysorbate 20 (TBST) buffer. The membrane was exposed to the primary antibodies PDGFRB (28E1, 3169, rabbit monoclonal, diluted 1:1000, Cell Signaling Technologies, Danvers, MA) or B-actin (4967L, rabbit monoclonal, diluted 1:1000, Cell Signaling Technologies, Danvers, MA) at 4°C overnight. Membranes were then washed with TBST and incubated for 30 minutes at room temperature with the secondary antibody (goat anti-rabbit HRP, diluted 1:5000, ab6721, abcam, Cambridge, United Kingdom). The membrane was washed again with TBST and visualized using a chemiluminescent visualizer.

Cell Culture

The canine T-cell lymphoma cell line, OSW[188], and primary $CD4^+$ PTCL cells obtained from fine-needle aspirations of peripheral lymph nodes were grown under standard conditions (37 °C, 5% carbon dioxide) in RPMI1640 medium supplemented with 10% fetal bovine serum, 0.05µmol/ml 2-mercaptoethanol (Milipore Sigma, St. Louis MO), 1 x minimum essential medium (MEM), 78 non-essential amino acids (Milipore Sigma, St. Louis MO), 100U/mL penicillin and 100µg/mL streptomycin (Milipore Sigma, St. Louis MO), 1 x Glutamax (Gibco, Waltham MA), 10mM Corning HEPES (Media Tech Inc, Manassas VA) and 1mM sodium pyruvate (Gibco, Waltham MA). $CD4^+$ PTCL cases were selected as described above.

Proliferation Assays

Neoplastic cells were washed with HBSS (Milipore Sigma, St. Louis, MO) and then labelled for carboxyfluorscein succinimidyl ester (CFSE, 5µM, Invitrogen, Waltham, MA) for 5 minutes and washed as previously described.[189] Cells were then resuspended in RPMI-10 supplemented as described above. Cells were incubated in 96-well round bottom cell culture plates at a concentration of 5×10^5 cells per well for primary neoplastic lymphocytes or in a 48-well round bottom cell culture plate at a concentration of 2×10^5 cells per well for OSW cell

line. To determine the total cell count, a known amount of CountBrite beads were added prior to sample acquisition, and cells were enumerated based on bead recovery and amount of sample remaining at the time of harvest. Cells were harvested at 6 or 24 hour time points over a total time frame of 48hrs to 7 days. Harvested cells were washed twice with 150µL of flow buffer (PBS-2% FBS-0.1%NaAZ) and resuspended in 25µL of flow buffer with or without 25µL of a cocktail of antibodies in flow buffer. For primary patient samples, surface antigens used included: CD5-APC (rat anti-dog T cell, clone YKIX322.2, Bio-Rad, Hercules CA), CD4-pacblue (rat anti-dog CD4 T-cell, clone YKIX302.9, Bio-Rad, Hercules CA) and CD8-A700 (rat anti-dog CD8 T cell, clone YCATE 55.9, Bio-Rad, Hercules CA). OSW cell line was not stained with surface antigens. Samples were incubated for 15 minutes in the dark at room temperature and resuspended in 100µL of flow buffer and 100µL of 10µg/mL of propidium iodide (PI) for identification of dead cells. Samples were acquired on a 3-laser Coulter Gallios and analyzed with Kaluza software (Beckman Coulter, Brea, CA).

Cell Death Assays

Cell death was measured by annexin V expression and PI measured by flow cytometry. An Annexin V:FITC assay kit (ANNEX100F, Bio Rad, Hercules CA) was used according to manufacturer's instructions. Briefly, cells were washed in cold PBS and resuspended in binding buffer. Cells were stained with the Annexin V: FITC antibody for 15 minutes in the dark at room temperature. Following staining, cells were washed with binding buffer and resuspended in binding buffer (0.01M Hepes (pH 7.4), 0.14M NaCl, and 2.5 mM CaCl2 solution) and PI. Samples were acquired on a 3-laser Coulter Gallios and analyzed with Kaluza software (Beckman Coulter, Brea, CA).

Cellular stimulation or inhibition assays

Neoplastic T-cells were stimulated with 2.5 μg/mL phytohaemagglutinin (PHA) (Milipore Sigma, St. Louis MO) or 1ng/mL, 2 ng/mL, or 4ng/mL human recombinant platelet derived growth factor-BB (PDGF-BB) (Sigma-Aldrich, St. Louis MO). For PI3K inhibition assays, neoplastic T-cells were treated with 50 μM LY294002 (Cell Signaling Technology, Danvers MA) or equivalent volume of DMSO.

Statistical analysis

Statistical analyses were performed in GraphPad Prism 8.0. Evaluation of changes in total cell number and CFSE median fluorescence intensity (MFI) over short term culture was performed using multiple t-test analysis, resulting in an individual comparison per timepoint. Total cell death in short term cultures was compared using a Wilcoxon matched-pairs signed rank test.

Results

Canine patient demographics

Fine-needle tissue aspirates from thirty-three canine patients diagnosed with PTCL by flow cytometry were selected for RNA-seq. Patient demographics are described in Table 3.1. The mean age at the time of flow cytometry diagnosis was 8 years (range 3-14 years) and the majority of patients were castrated males (70%). The most common breeds were mixed breed (24%), Boxer (18%), and golden retriever (15%), consistent with the previous reports of increased incidence of aggressive PTCLs in the Boxer and golden retriever breeds.[153,158,163,164] The majority of samples were obtained from fine-needle aspirates of the lymph node. Few samples were obtained from the mediastinum, pleura, or bone.

Table 3.1 Demographics of patients selected for RNA-seq

Immunophenotype	Breed	Sex	Age (years)	Site Sampled
CD4+CD8-CD3+CD5+	Mixed	Male castrated	6	Lymph node
CD4+CD8-CD3+CD5+	Boxer	Female spayed	4	Mediastinum
CD4+CD8-CD3+CD5+	German Shephard	Female spayed	6	Bone
CD4+CD8-CD3+CD5+	Labrador Retriever	Male castrated	7	Pleura
CD4+CD8-CD3+CD5+	Chesapeake Bay Retriever	Male castrated	6	Lymph node
CD4+CD8-CD3+CD5+	Rhodesian Ridgeback	Male castrated	3	Mediastinum
CD4+CD8-CD3+CD5+	Boxer	Male castrated	9	Lymph node
CD4+CD8-CD3+CD5+	Boxer	Female spayed	10	Lymph node
CD4+CD8-CD3+CD5+	Goldendoodle	Male castrated	11	Lymph node
CD4+CD8-CD3+CD5+	Golden Retriever	Male castrated	7	Lymph node
CD4+CD8-CD3+CD5+	Mixed	Male castrated	11	Lymph node
CD4+CD8-CD3+CD5+	Golden Retriever	Male castrated	5	Lymph node
CD4+CD8-CD3+CD5+	Shetland Sheepdog	Male castrated	8	Lymph node
CD4+CD8-CD3+CD5+	Presa Canario	Female spayed	6	Lymph node
CD4+CD8-CD3+CD5+	Miniature Australian Shephard	Male castrated	5	Lymph node
CD4+CD8-CD3+CD5+	Shiatzu	Male castrated	11	Lymph node
CD4+CD8-CD3+CD5+	Boxer	Female spayed	9	Lymph node
CD4+CD8-CD3+CD5+	Mixed breed	Male castrated	12	Lymph node
CD4+CD8-CD3+CD5-	Boxer	Male castrated	5	Lymph node
CD4+CD8-CD3+CD5-	Golden retriever	Male castrated	10	Lymph node
CD4+CD8-CD3+CD5-	Golden retriever	Male castrated	4	Lymph node
CD4+CD8-CD3+CD5-	Dogue de Bordeaux	Male castrated	5	Lymph node
CD4+CD8-CD3+CD5-	Mixed breed	Male castrated	6	Lymph node
CD4+CD8-CD3+CD5-	Boxer	Male castrated	7	Lymph node
CD4+CD8-CD3+CD5-	Australian Shephard	Male castrated	10	Lymph node
CD4+CD8-CD3+CD5-	Golden Retriever	Female spayed	10	Lymph node
CD4-CD8-CD3+CD5+	Cavalier King Charles Spaniel	Female spayed	4	Lymph node
CD4-CD8-CD3+CD5+	Mixed	Female spayed	4	Lymph node
CD4-CD8-CD3+CD5-	Pomeranian	Male castrated	11	Lymph node
CD4-CD8+CD3+CD5+	Mixed	Female spayed	12	Lymph node
CD4-CD8+CD3+CD5+	Mixed	Male castrated	6	Lymph node
CD4-CD8+CD3+CD5+	Mixed	Female spayed	14	Lymph node
CD4-CD8+CD3+CD5+	Lhasa Apso	Male castrated	Unknown	Lymph node

Cases fell into three immunophenotypic categories: $CD4^+CD8^-$, $CD4^-CD8^+$, and $CD4^-CD8^-$ (Figure 3.1 A-C). The majority of cases (26 individuals, 79%) were $CD4^+CD8^-$ PTCLs. Eight of those 26 total $CD4^+CD8^-$ PTCLs exhibited loss of the T-cell marker CD5. Fewer cases were $CD4^-CD8^+$ PTCLs (4 individuals, 12%) or $CD4^-CD8^-$ PTCLs (3 individuals, 9%). A single $CD4^-CD8^-$ exhibited loss of CD5. All cases expressed the pan-leukocyte marker CD45, thereby excluding a diagnosis of indolent T-zone lymphoma.

Gene expression profile of canine PTCL

The surface protein expression of T-cell subset markers CD4 and CD8 used to classify the PTCL cases and sort the control T-cells correlated strongly with the gene expression levels of these molecules (Figure 3.1).

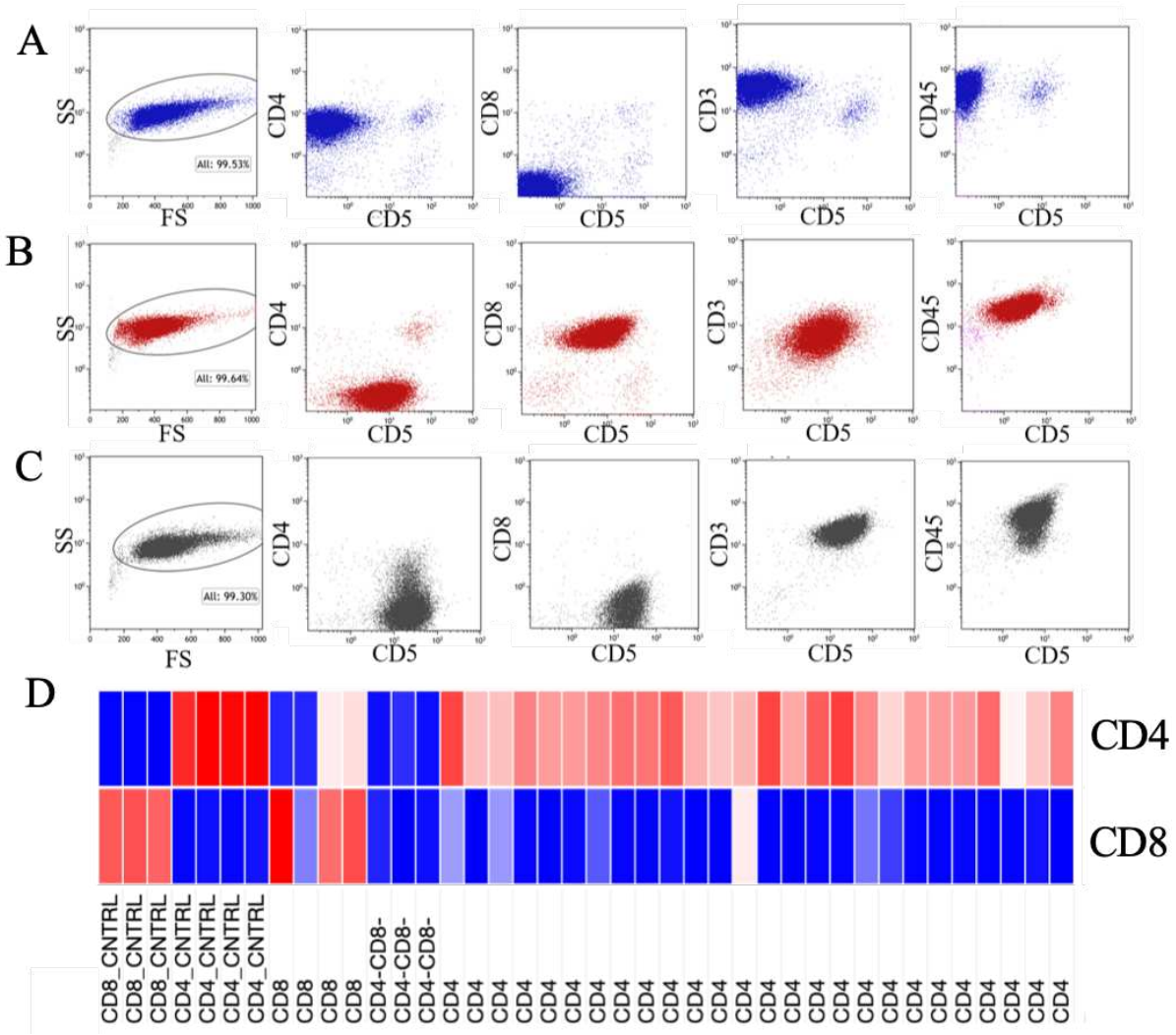

Figure 3.1. Correlation between surface molecule expression and gene expression. The flow cytometry plots used to classify $CD4^+$ TCL (A), $CD8^+$ TCL (B), and $CD4^-CD8^-$ TCL (C). Corresponding gene expression of CD4 and CD8a (D) demonstrate correlation to the surface protein level. Red denotes relative increased expression levels and blue denotes decreased expression levels. SS=side scatter; FS=forward scatter; DN=double negative, $CD4^-CD8^-$.

Hierarchical clustering and principle component analysis were performed to evaluate clustering of neoplastic and control samples using significantly differentially expressed genes (Figure 3.2). Control $CD4^+$ and $CD8^+$ T-cells clustered separately from neoplastic samples. Control cells further exhibited distinct $CD4^+$ and $CD8^+$ subgroups. The $CD4^+$ PTCL and $CD8^+$ PTCL appear to form two distinct molecular groups, with the $CD8^+$ PTCLs clustering more closely with the control T-cells. Two of the 3 $CD4^-CD8^-$ PTCLs clustered with the $CD8^+$ PTCLs and 1 $CD4^-CD8^-$ PTCL clustered with the $CD4^+$ PTCLs. Distinct clinical features were not identified to differentiate between the $CD4^-CD8^-$ PTCL that clustered with the $CD4^+$ PTCLs verses those that clustered with the $CD8^+$ PTCLs.

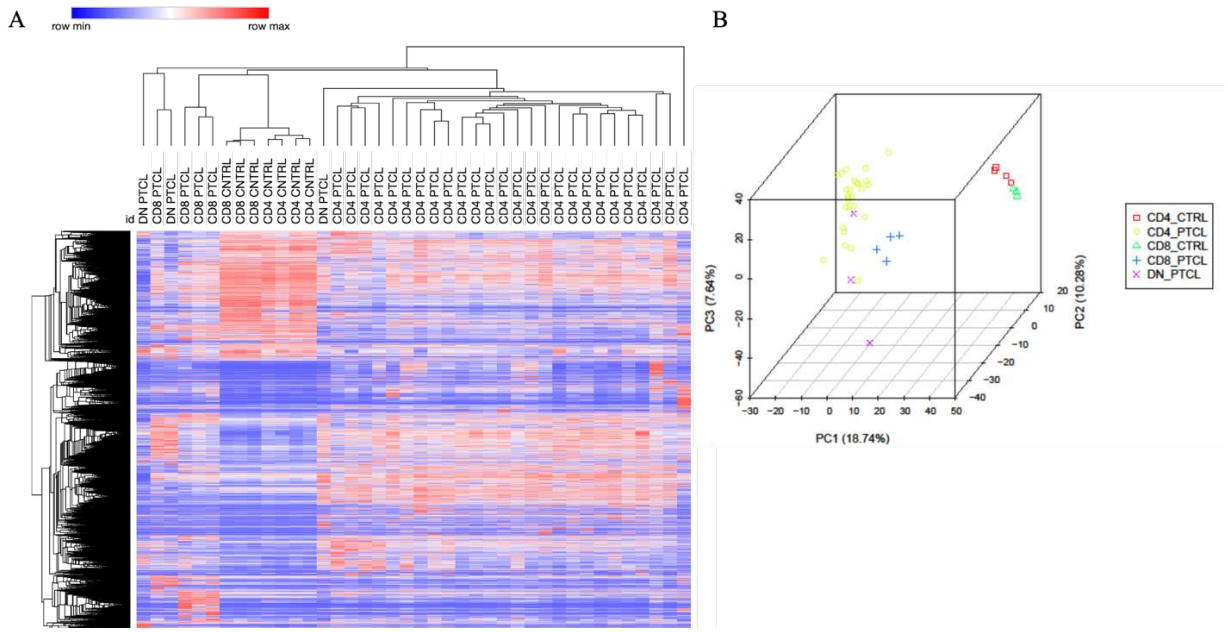

Figure 3.2 Hierarchical clustering of canine PTCL and control T-cells. Heatmap showing hierarchical clustering with red denoting upregulated genes and blue denoting downregulated genes(A) and principle component analysis (PCA) (B). Control T-cells and PTCL samples formed distinct groups in both the heatmap and PCA plot, with $CD4^+$ and $CD8^+$ T-cell subgroups. The $CD4^+$ and $CD8^+$ PTCL cases clustered separately, as two distinct groups. Two $CD4^-CD8^-$ (DN) PTCL cases clustered with the $CD8^+$ PTCL subgroup and one DN PTCL clustered with the $CD4^+$ PTCL subgroup. $CD8^+$ PTCL cases clustered more closely with control samples than the $CD4^+$ PTCL subgroup.

Comparison of human and canine gene expression profiles

We next sought to evaluate the molecular similarity between human and canine PTCL-NOS. Given the uniform clustering pattern and relative increased incidence within the canine population, subsequent studies focused on the $CD4^+$ PTCL subgroup in the dog. The top 200 upregulated and 200 downregulated genes in human PTCL-NOS cases compared to sorted human $CD4^+$ control T-cells were identified using a previous microarray study by Piccaluga et

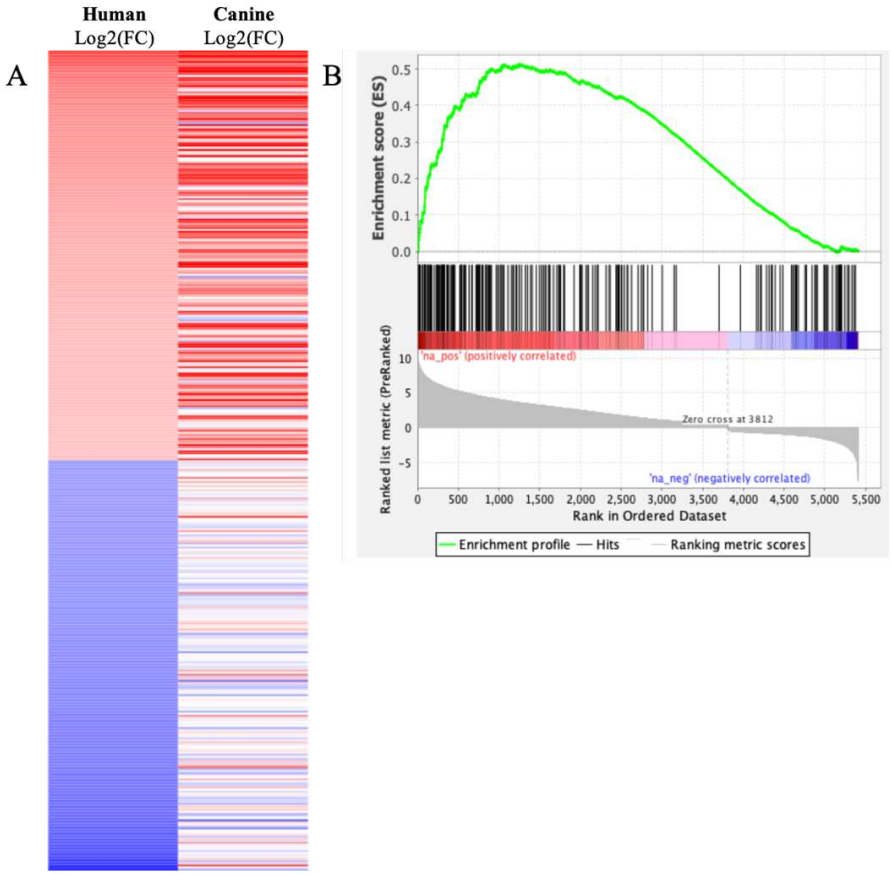

Figure 3.3 Canine PTCL is molecularly similar to the human counterpart. The top 200 upregulated and 200 downregulated genes in human PTCL-NOS cases compared to sorted human CD4+ control T-cells were identified using a previous microarray study by Piccaluga et al. (2007) and GEO2R analysis. (A) A heatmap in which each vertical line indicates a human gene ranked in increasing order of differential expression compared to normal CD4 T-cells (left) and the relative expression levels of the equivalent dog genes (right) (B) The acquired list of differentially expressed genes in human PTCL-NOS was compared to canine PTCL using Gene Set Enrichment Analysis (GSEA). GSEA assesses how the genes of each gene set are distributed across a ranked list by walking down a ranked list of genes and increasing the running-sum statistic when a gene belongs to the set and decreasing it when the gene does not. The enrichment score (top) reflects the degree to which the genes in a gene set are overrepresented at the top or bottom of the entire ranked list of genes. The hits (middle) are shown as vertical lines that represent the location of the canine genes in the ranked set of all genes. The ranking metric scores (bottom) is the signal to noise ratio for each gene used to position the gene in the ranked list. A statistically significant enrichment was identified (P-value <0.001; FDR q-value<0.001).

al.[128] This study was chosen because it included a control and experimental group analogous to the canine samples in our current study. The log2FC of the identified genes were compared between human and canine samples (Figure 3.3). The most significantly upregulated genes in the human PTCL-NOS cases were similarly upregulated in the canine samples. Upregulated genes in both human and canine samples were enriched for extracellular matrix organization, vesicle-mediated transport, signaling by receptor tyrosine kinases, regulation of insulin-like growth factor, and platelet activation signaling and aggregation using the gene set enrichment analysis (GSEA)[186] REACTOME pathway analysis (FDR<0.05).[190–192] Using GSEA, the canine GEP was significantly enriched for the top 200 upregulated and 200 downregulated genes in human PTCL-NOS (p-value <0.001; FDR q-value<0.001) (Figure 3.3 B).

CD30 expression in canine PTCL

CD30 is a useful cell-surface marker that is expressed by a number of lymphoproliferative diseases including neoplastic B-cells in classical Hodgkin's lymphoma and neoplastic T-cells in anaplastic large cell lymphoma.[20] A subset of PTCL-NOS is human patients has also been shown to express CD30, and stratification of PTCL-NOS based on CD30 expression has been proposed.[142] CD30 expression was therefore evaluated in canine PTCL. $CD4^+$ PTCL cases exhibited significant down-regulation of CD30 compared to control $CD4^+$ T-cells (log2FC=-2.9605, FDR q-value=8.21×10^{-7}). A single $CD4^+$ PTCL case had increased expression of CD30 (Figure 3.4 A). Interestingly, this case clustered as an outlier from the other $CD4^+$ PTCLs using hierarchical clustering (Figure 3.2 A, far right). All evaluated cases (n=6) of PTCL did not exhibit CD30 expression by immunohistochemistry (Figure 3.4 D). Within a non-neoplastic control lymph node, few individual lymphocyte exhibited positive immunoreactivity to CD30 (Figure 3.4 C) and a canine mast cell tumor, which have been previously shown to

express CD30[193], exhibit diffuse positive immunoreactivity to the CD30 antibody, serving as positive controls (Figure 3.4 B).

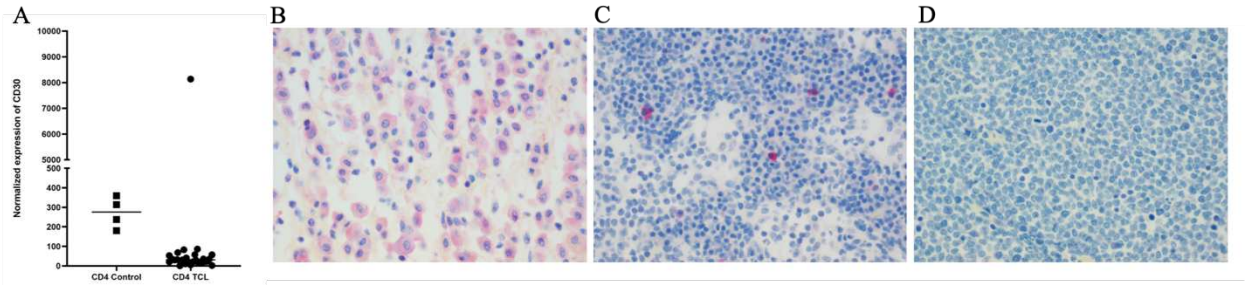

Figure 3.4. Most canine PTCLs do not express CD30. Normalized gene expression of canine CD4$^+$ PTCL cases compared to sorted control CD4$^+$ T-cells. The majority of cases exhibit down-regulation of the CD30 gene. One case exhibited upregulation of CD30 (A). Neoplastic mast cells in a canine cutaneous mast cell tumor demonstrate diffuse positive cytoplasmic staining (positive control) (B). In a normal lymph node there are few scattered cells with positive cytoplasmic staining (D). All six PTCL cases tested were negative for CD30 expression. A representative photomicrograph of one of the six tested cases is presented (D). 400x magnification

Human PTCL-NOS has been previously shown to express platelet-derived growth factor alpha (PDGFRA) and PDGFR activation is thought to play a role in proliferation of the neoplastic T-cells.[129] PDGFR expression and activation were subsequently evaluated in canine CD4$^+$ PTCL cases (Figure 3.5). Canine CD4$^+$ PTCL cases upregulate PDGFRA and PDGRB compared to control CD4$^+$ T-cells and canine PTCL cases were enriched for the activation of the PDGF pathway[190–192] using GSEA pathway enrichment analysis (FDR q-value<0.001). Protein expression of PDGRFA and PDGRB was confirmed by immunohistochemistry and western blot, respectively.

Primary CD4$^+$ TCL cells isolated from fine-needle aspiration of affected lymph nodes were grown in short term culture with the addition of exogenous PDGF, phytohemagglutinin (PHA), or no stimulation. Cellular proliferation was assessed by quantification of CFSE over a 7-day time-course. CFSE was measured by flow cytometry. Addition of exogenous PDGF did not stimulate proliferation in short-term culture of primary

CD4$^+$ PTCL cells. PHA non-specifically binds sugars on glycosylated surface proteins, including the TCR. Following PHA-stimulation, proliferation was induced in primary canine PTCL cells.

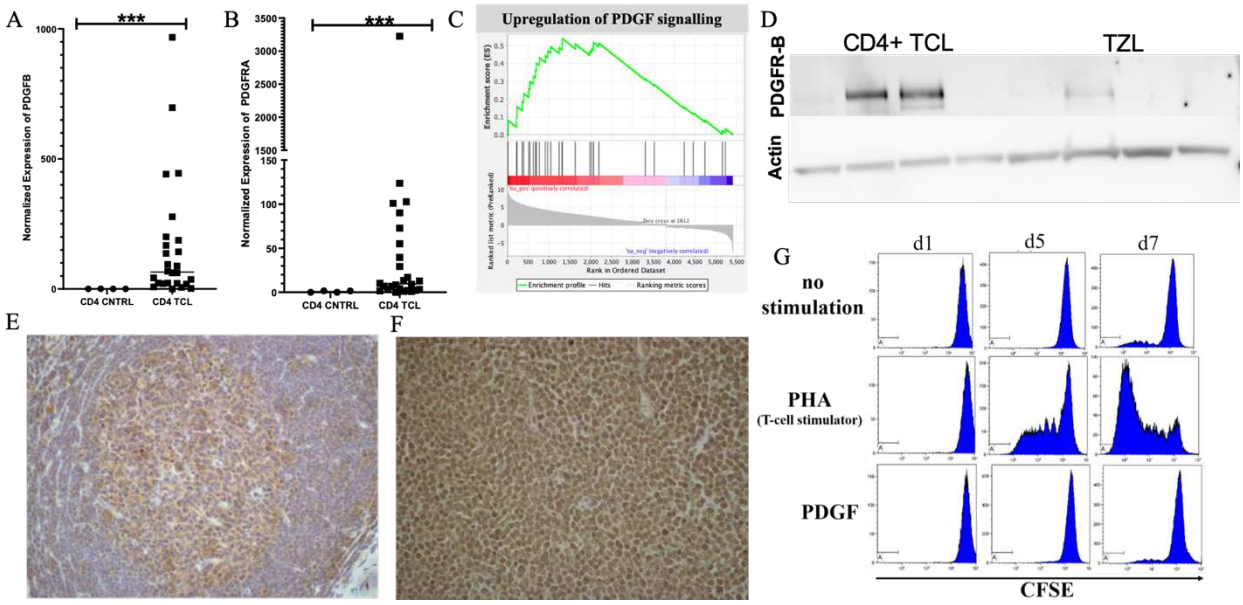

Figure 3.5. Canine PTCL expresses platelet-derived growth factor receptors alpha and beta. (A,B) Normalized gene expression of PDGFRB (A) and PDGFRA (B) in canine CD4$^+$ PTCL cases compared to sorted control CD4$^+$ T-cells. The majority of cases exhibit upregulation of PDGFRA and PDGFRB. (C) There is significant (FDR q-value<0.001) enrichment of PDGF signaling pathways in canine PTCL. Pathway enrichment was performed using GSEA. Two out of four evaluated canine CD4$^+$ PTCLs strongly expressed PDGFRB protein using western blot analysis compared to cases of indolent T-zone lymphoma. Canine PTCL cases (n=6) (F) exhibited strong, diffuse, expression of PDGFRA compared to control lymph node (E). The germinal center of the control lymph node exhibits increased PDGFRA expression. Primary CD4$^+$ TCL cells were stimulated with PHA and PDGF in short-term (7-day) cell culture (G). TCL cells stimulated with PHA underwent proliferation, exhibited by loss of CFSE expression over time. TCL cells stimulated with PDGF, however, did not proliferate.

Canine CD4$^+$ PTCL is molecularly similar to PTCL-GATA3

Molecular characterization of PTCL-NOS has recently identified distinct subgroups named PTCL-GATA3 and PTCL-TBX21. Differentiation of these molecular subgroups is determined by respective expression of GATA3 and TBX21, as well as their associated genes.[117] Additional genes included within the GATA3 group include CCR4, IL18RA, CXCR7, IK, MSH6, EGR1, CAT, and SEPTIN6 and target genes within the TBX21 group include EOMES,

CXCR3, IL2RB, CCL3, and IFNG.[117] Expression of these key markers within canine PTCL is illustrated in Figure 3.6. $CD4^+$ canine PTCL samples exhibited upregulation of genes associated with the GATA3 subgroup, as well as diffuse, strong, positivity for GATA3 via

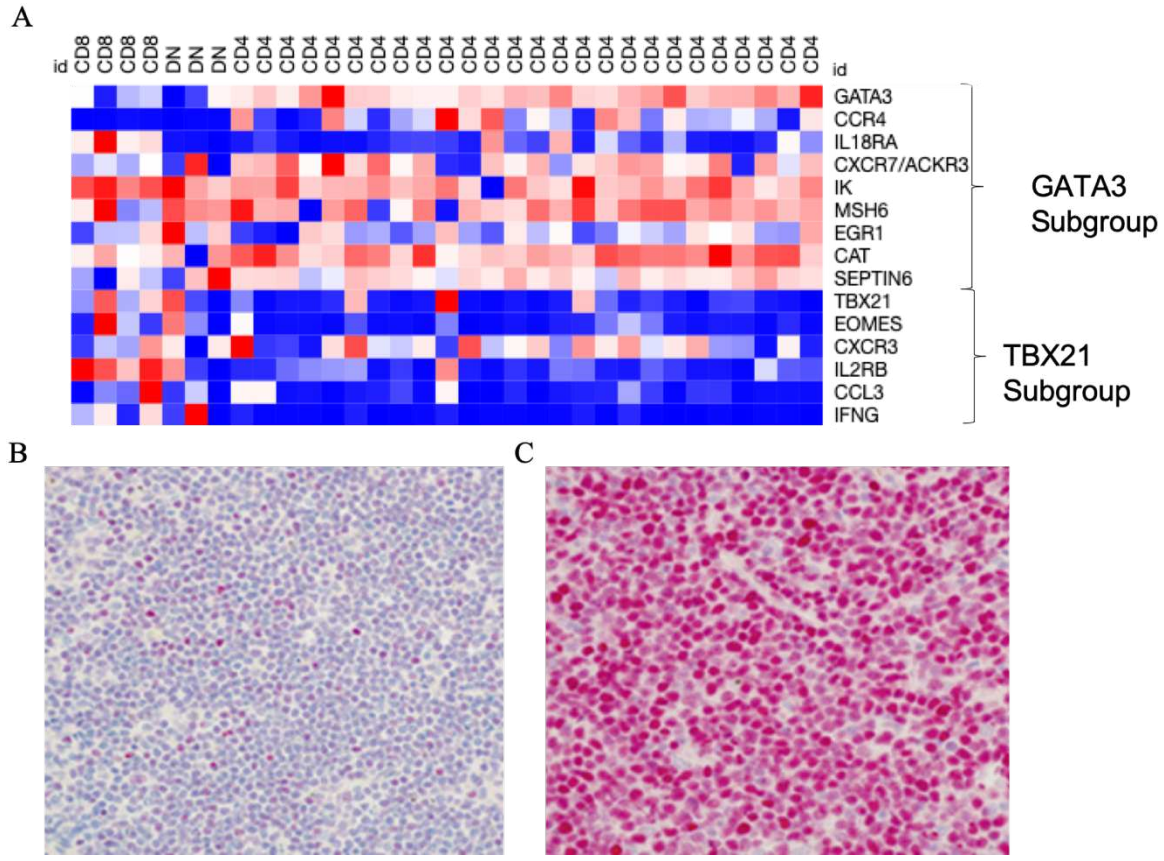

Figure 3.6. Canine $CD4^+$ PTCL exhibits a gene expression pattern similar to that of PTCL-GATA3. (A) Expression levels of genes associated with the GATA3 and TBX21 subgroups of PTCL-NOS as defined by Iqbal et al. (2014). $CD4^+$ PTCL cases exhibited upregulation of GATA3 and variable expression of the associated genes. $CD8^+$ and $CD4^-CD8^-$ (DN) cases have more variable expression patterns. A proportion of these cases appear to upregulate several genes associated with the TBX21 subgroup. $CD4^+$ PTCL cases (n=6) exhibit strong upregulation of GATA3 by immunohistochemistry (C) compared to control lymph node tissue (B).

immunohistochemistry. $CD8^+$ and $CD4^-CD8^-$ PTCL cases were more variable in their expression patterns and a portion of these cases upregulated genes associated with the TBX21group.

PI3K-AKT-MTOR pathway activation in canine PTCL

Human PTCL-GATA3 is enriched for the PI3K-AKT pathway and exhibits frequent mutations of PTEN, a negative regulator of PI3K and tumor suppressor gene.[117,119] Canine $CD4^+$ PTCL was significantly enriched for gene signatures associated with downregulation of PTEN (FDR q-value=0.0266) and upregulation of MTOR (FDR q-value=0.0203) (Figure 3.7 A,B). $CD4^+$ PTCL additionally exhibited diffuse expression of phosphorylated AKT compared to lymphocytes within a control lymph node (Figure 3.7 C, D).

An inhibitor of PI3K, LY249002, was then used to evaluate the role of PI3K-AKT signaling in canine PTCL proliferation and survival. OSW, a canine TCL cell line, was treated with LY249002 or DMSO control and grown in a 4-day culture. Cell proliferation was evaluated by loss of CFSE quantified by flow cytometry. Total cell number was also evaluated using counting beads quantified by flow cytometry. Inhibition of PI3K by LY249002 resulted in impaired loss of CFSE and decreased total cell numbers compared to DMSO-treated controls (Figure 3.7 E, F). These findings indicate that inhibition of PI3K results in impaired proliferation of the canine TCL cell line, OSW.

The effects of PI3K inhibition were then evaluated in primary canine $CD4^+$ T-cell lymphoma cells obtained from lymph node fine-needle aspirations. Cells from 8 separate patients were cultured for 48 hours following treatment with LY249002 or DMSO control. Annexin V and PI were quantified by flow-cytometry to measure total cell death. Total cell death was significantly increased in cells treated with LY249002 compared to DMSO controls (p-value 0.0078) (Figure 3.7 G, H). These results support the conclusion that PI3K plays an important role in cell survival of the canine neoplastic T-cells.

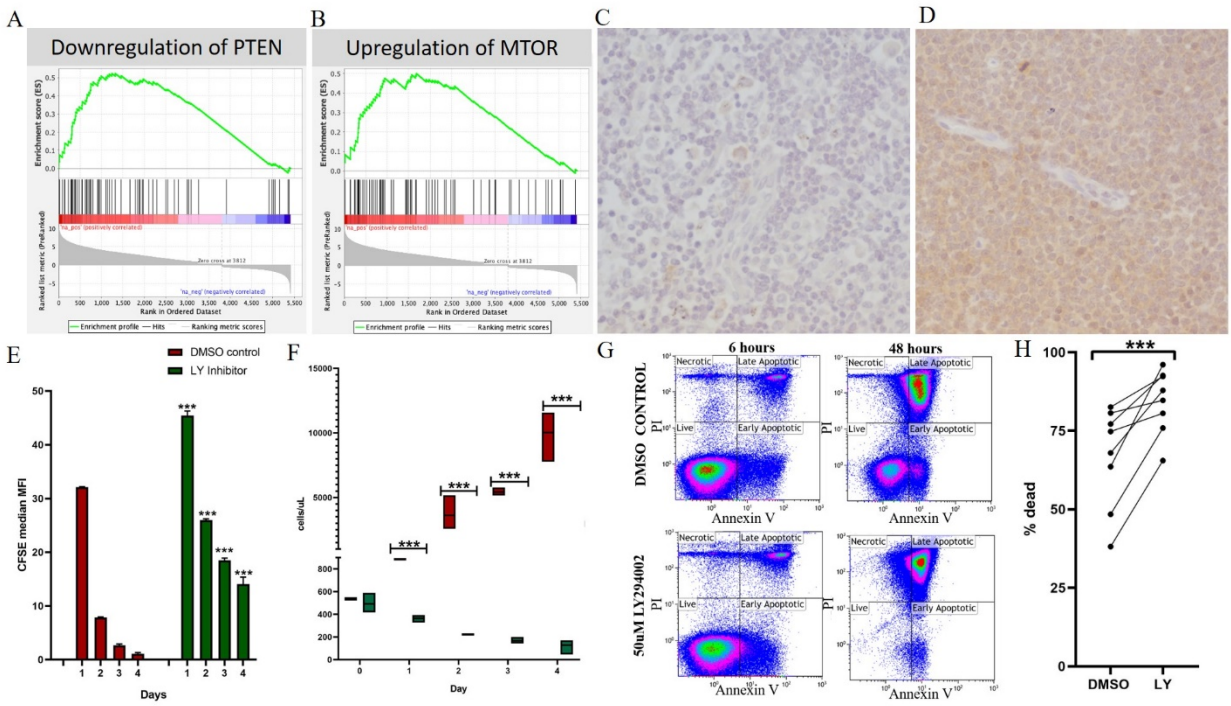

Figure 3.7. Canine PTCL utilizes the PI3K-AKT-MTOR pathway for cell survival and proliferation. (A,B) $CD4^+$ PTCL is significantly enriched for gene signatures associated with downregulation of PTEN (FDR q-value=0.0266) and upregulation of MTOR (FDR q-value=0.0203) using GSEA enrichment analysis. $CD4^+$ PTCL is diffusely and strongly positive for phosphorylated-AKT (D) compared to a non-neoplastic control lymph node (C). OSW, a canine TCL cell line, was treated with LY249002 (green bars in E and F) and a DMSO control (red bars in E and F) and grown in culture over a four-day time period. Cellular proliferation was measured by CFSE loss (E) and changes in total cell number determined by counting beads (F). Both CFSE and counting beads were evaluated using flow cytometry. Treatment with LY249002 resulted in decreased cellular proliferation and well as decreased total cell numbers compared to DMSO treated controls. Primary $CD4^+$ PTCL cells were treated with LY249002 or DMSO control and grown in culture over 48 hours. Cellular death was evaluated by annexin V and PI, measured by flow cytometry. Significantly increased cell death was observed following treatment with LY294002. A representative flow cytometry plot from one individual (G) and the summary of 8 total $CD4^+$ primary patient samples (H). ***=p-value<0.05

Oncogene and tumor suppressor expression in canine PTCL

Differential expression of known cancer associated genes identified using the COSMIC cancer gene census[194] were evaluated in $CD4^+$ PTCL compared to combined $CD4^+$ and $CD8^+$ control T-cells. Genes were classified as oncogene, tumor suppressor gene, or cancer-associated gene based on the classification provided by the Network of Cancer Genes (NCG6.0).[195] To focus on possible tumor drivers, significantly upregulated oncogenes and significantly downregulated tumor suppressor genes were identified and presented in Table 3.2. Specifically,

oncogenes that were upregulated and previously associated with T-cell neoplasms include: STIL, LMO1, LMO2, SET, TAL1 (T-ALL), ALK (ALCL), TNFRSF17 (intestinal T-cell lymphoma), CCR4 (ATLL), and FGFR3 (T-cell lymphoma). Tumor suppressor genes that were downregulated and associated with T-cell neoplasms include: PTPRC, KDM6A (T-ALL), ATM (T-PLL), and FAS (NK/T lymphoma).

Table 3.2 Differentially expressed oncogenes and tumor suppressor genes in CD4$^+$ PTCL

Gene Symbol	Log2FC	Gene Characterization	Tumor Types
FOXA1	7.5954	Oncogene	breast, prostate
TNC	7.3082	Oncogene	SCC, melanoma
SMO	7.0253	Oncogene	skin basal cell
EGFR	6.827	Oncogene	glioma, NSCLC
ETV5	6.509	Oncogene	prostate
MLLT4	6.4	Oncogene	AL
NTRK3	6.3712	Oncogene	congenital fibrosarcoma, secretory breast
PLAG1	6.0526	Oncogene	salivary adenoma, lipoblastoma
FGFR2	5.9778	Oncogene	gastric, NSCLC, endometrial
ERBB2	5.8715	Oncogene	breast, ovarian, other tumour types, NSCLC, gastric
ERG	5.6479	Oncogene	Ewing sarcoma, prostate, AML
MECOM	5.6257	Oncogene	AML, CML, MDS
TCF7L2	5.4784	Oncogene	colorectal
PDGFRA	5.3187	Oncogene	GIST, idiopathic hypereosinophilic syndrome, paediatric glioblastoma
CSF1R	5.0788	Oncogene	MDS, CML, AML, hemangioblastoma, CCRCC
ZNF521	4.8523	Oncogene	ALL
SALL4	4.7209	Oncogene	colorectal cancer, breast cancer, prostate cancer, glioblastoma, melanoma
ACVR1	4.605	Oncogene	DIPG
TAL1	4.5629	Oncogene	lymphoblastic leukaemia/biphasic
MITF	4.5324	Oncogene	melanoma
PREX2	4.4162	Oncogene	melanoma, pancreatic ductal adenocarcinoma
MET	4.4043	Oncogene	papillary renal, head-neck squamous cell
PDGFRB	4.2167	Oncogene	MPN, AML, CMML, CML
SRC	4.2137	Oncogene	colorectal cancer, endometrial carcinoma
CDH17	4.1235	Oncogene	melanoma
PBX1	4.0008	Oncogene	pre B-ALL, myoepithelioma
DDR2	3.9118	Oncogene	squamous cell carcinoma, NSCLC
KIT	3.8839	Oncogene	GIST, AML, TGCT, mastocytosis, mucosal melanoma
ETV1	3.7066	Oncogene	Ewing sarcoma, prostate
CSF3R	3.5277	Oncogene	aCML, CNL, leukaemia lymphoma and MDS associated with severe congenital neutropenia, CMML, de novo AML, MDS
MN1	3.3141	Oncogene	AML, MDS
SIX1	3.2392	Oncogene	Wilms tumour
ALK	3.0931	Oncogene	ALCL, NSCLC, neuroblastoma, inflammatory myofibroblastic tumour, Spitzoid tumour
MYB	2.7905	oncogene	adenoid cystic carcinoma
GATA2	2.7095	Oncogene	AML (CML blast transformation)
KNSTRN	2.7014	Oncogene	SCC
ETV4	2.681	Oncogene	Ewing sarcoma, prostate carcinoma
STIL	2.6465	Oncogene	T-ALL
PDCD1LG2	2.5546	Oncogene	PMBL, Hodgkin lymphoma
LMO1	2.5158	Oncogene	T-ALL, neuroblastoma
TFEB	2.3992	Oncogene	renal cell carcinoma (childhood epithelioid)
PRDM16	2.2653	Oncogene	MDS, AML
CCNE1	2.2578	Oncogene	serous ovarian
MAFB	2.2225	Oncogene	MM
EZH2	2.1319	Oncogene	DLBCL
WHSC1	1.9967	Oncogene	MM
TNFRSF17	1.9482	Oncogene	intestinal T-cell lymphoma
GNAQ	1.9053	Oncogene	uveal melanoma, primary central nervous system melanocytic neoplasms
NUTM1	1.8373	Oncogene	lethal midline carcinoma
CCND2	1.8124	Oncogene	NHL,CLL
CACNA1D	1.7827	Oncogene	adrenal aldosterone producing adenoma
CCR4	1.7119	Oncogene	adult T-cell leukaemia/lymphoma
SGK1	1.5619	Oncogene	Nodular lymphocyte predominant Hodgkin lymphoma
IDH1	1.5286	Oncogene	glioblastoma
SETBP1	1.4985	Oncogene	aCML, sAML, MDS/MPN-U, CMML, JMML
CDK4	1.4638	Oncogene	N.A.
DDIT3	1.4521	Oncogene	liposarcoma
RET	1.4335	Oncogene	medullary thyroid, papillary thyroid, pheochromocytoma, NSCLC, Spitzoid tumour
LMO2	1.3813	Oncogene	T-ALL
FGFR3	1.2785	Oncogene	bladder, MM, T-cell lymphoma
GNAS	1.2276	Oncogene	pituitary adenoma, pancreatic intraductal papillary mucinous neoplasm, fibrous dysplasia
U2AF1	1.0633	Oncogene	CLL, MDS
CALR	1.0376	Oncogene	MPN, MDS
SET	0.90317	Oncogene	T-ALL
NFE2L2	0.90091	Oncogene	NSCLC, HNSCC

HMGA1	0.82618	Oncogene	microfollicular thyroid adenoma, various benign mesenchymal tumours
IDH2	0.8096	Oncogene	glioblastoma
CDK6	0.78141	Oncogene	ALL
RAC1	0.77346	Oncogene	melanoma, carcinoma
RARA	0.72524	Oncogene	APL
IL6ST	0.67061	Oncogene	hepatocellular carcinoma
DEK	0.65948	Oncogene	AML
MTOR	0.55217	Oncogene	endometrial carcinoma, head and neck, clear cell renal cell carcinoma, anaplastic thyroid cancer, urothelial cell carcinoma, central nervous system tumours, testicular germ cell tumours and other tumour types
CTNNB1	0.54209	Oncogene	colorectal, ovarian, hepatoblastoma, pleomorphic salivary gland adenoma, other tumour types
MAP2K1	0.52129	Oncogene	NSCLC, melanoma, colorectal
CRTC1	0.51746	Oncogene	salivary gland mucoepidermoid
HNRNPA2B1	0.46451	Oncogene	prostate
PRKACA	0.42949	Oncogene	fibrolamellar hepatocellular carcinoma, cortisol secreting adrenal adenoma
PTPN11	0.37755	Oncogene	JMML, AML, MDS
BRD3	0.37541	Oncogene	lethal midline carcinoma of young people
SRSF3	0.30357	Oncogene	follicular lymphoma
CDK12	-0.39846	TSG	serous ovarian
STAG2	-0.41288	TSG	bladder carcinoma, glioblastoma, melanoma, Ewing's sarcoma, myeloid neoplasms
ZRSR2	-0.49738	TSG	MDS, CLL
SMAD2	-0.56791	TSG	colorectal carcinoma, hepatocellular carcinoma
RPL22	-0.57979	TSG	AML, CML
KMT2C	-0.61299	TSG	medulloblastoma
ASXL1	-0.61624	TSG	MDS, CMML
POT1	-0.66858	TSG	CLL
WRN	-0.6841	TSG	N.A.
MYH9	-0.71494	TSG	ALCL
PTPRC	-0.72314	TSG	T-ALL
ATM	-0.72502	TSG	T-PLL
XPA	-0.7296	TSG	N.A.
PIK3R1	-0.79664	TSG	glioblastoma, ovarian, colorectal
CYLD	-0.81559	TSG	cylindroma
DDX3X	-0.8222	TSG	CLL, medulloblastoma
FBXO11	-0.84687	TSG	DLBCL
PTEN	-0.8523	TSG	glioma, prostate, endometrial
TRIM33	-0.87116	TSG	papillary thyroid
TNFRSF14	-0.8967	TSG	follicular lymphoma
BTG1	-0.89939	TSG	B-CLL
CHD2	-0.94338	TSG	melanoma, large intestine, CLL, monoclonal B lymphocytosis
PML	-0.96579	TSG	APL, ALL
FANCG	-0.99985	TSG	N.A.
SETD1B	-1.0196	TSG	CRC, endometrium
KAT6B	-1.1178	TSG	AML, leiomyoma
CASP8	-1.1565	TSG	hepatocellular, oral squamous cell, breast
ASXL2	-1.1771	TSG	melanoma, CCRCC, AML
ETNK1	-1.2706	TSG	aCML, CMML, SM-AHD, HES
CIITA	-1.4001	TSG	PMBL, Hodgkin lymphoma
KDM6A	-1.4596	TSG	renal cell carcinoma, bladder carcinoma, oesophageal SCC, MM, medulloblastoma, T-ALL, other tumour types
ZNF331	-1.6499	TSG	follicular thyroid adenoma
MGMT	-1.7333	TSG	glioma
CDKN1B	-1.9996	TSG	breast, small intestine neuroendocrine tumours
BAZ1A	-2.2376	TSG	uterine carcinosarcoma, colon cancer
LRIG3	-2.2729	TSG	NSCLC
PRDM1	-2.3221	TSG	DLBCL
CBLB	-2.3262	TSG	AML
FAS	-3.1527	TSG	TGCT, nasal NK/T lymphoma, skin squamous cell carcinoma-burn scar related

[+]Abbreviations: AEL: Acute eosinophilic leukemia, AL: Acute leukemia, ALCL: Anaplastic large-cell lymphoma, ALL: Acute lymphocytic leukemia, AML: Acute myelogenous leukemia, AML*: Acute myelogenous leukemia (primarily treatment associated), APL: Acute promyelocytic leukemia, B-ALL: B-cell acute lymphocytic leukaemia, B-CLL: B-cell Lymphocytic leukemia, B-NHL: B-cell Non-Hodgkin Lymphoma, CLL: Chronic lymphatic leukemia, CML: Chronic myeloid leukemia, CMML: Chronic myelomonocytic leukemia, CNS: Central nervous system, DFSP: Dermatofibrosarcoma protuberans, DLBL: Diffuse large B-cell lymphoma, DLCL: Diffuse large-cell lymphoma, GIST: Gastrointestinal stromal tumour, JMML: Juvenile myelomonocytic leukemia, L: Leukaemia/lymphoma, MALT: Mucosa-associated lymphoid tissue lymphoma, MDS: Myelodysplastic syndrome, MLCLS: Mediastinal large cell lymphoma with sclerosis, MM: Multiple myeloma, MPD: Myeloproliferative disorder, NHL: Non-Hodgkin lymphoma, NSCLC: Non-small cell lung cancer, PMBL: Primary mediastinal B-cell lymphoma, pre-B All: Pre-B-cell acute lymphoblastic leukaemia, T-ALL: T-cell acute lymphoblastic leukemia. T-CLL: T-cell chronic lymphocytic leukaemia, TGCT: Testicular germ cell tumour, T-PLL: T cell prolymphocytic leukaemia, TSG: Tumor suppressor gene

Discussion

We demonstrate molecular similarity between canine PTCL and human PTCL-NOS. Using RNA-seq, we show that canine $CD4^+$ PTCL has a similar gene expression pattern as human PTCL-NOS. We created a list of the top 200 up-regulated and down-regulated genes in human PTCL-NOS using a previously published microarray study.[128] This study contained

samples from human patients diagnosed with PTCL-NOS, as well as sorted control $CD4^+$ T-cells. The groups in that study were analogous to the samples obtained in our canine study, and therefore served as the optimal group for comparison. A statistically significant enrichment was identified for the list of differentially expressed genes in human PTCL-NOS when compared to control $CD4^+$ T-cells.

We next evaluated the expression of key molecules previously shown to be important in the classification and pathogenesis of PTCL-NOS. CD30 is a TNF-receptor superfamily member and can be expressed on normal and neoplastic lymphocytes.[140,141] Anaplastic large cell lymphoma, a subtype of PTCL, characteristically expresses CD30.[20,196] A proportion of PTCL-NOS cases have been shown to also express CD30, and separation of PTCL-NOS into $CD30^+$ and $CD30^-$ subgroups has been proposed.[142] CD30 is a particularly interesting molecule to evaluate because it can be targeted by the antibody-drug conjugate brentuximab vedotin and has shown promising therapeutic results in treating patients with relapsed or refractory ALCL.[144,145]

The majority of canine PTCL cases did not exhibit upregulation of CD30 gene expression and did not express CD30 using immunohistochemistry. A single PTCL case did have high CD30 expression compared to control lymphocytes. It is therefore possible that a small proportion of PTCL cases in dogs may express CD30. Using hierarchical clustering, this case clustered as an outlier to the other PTCL cases, suggesting it may represent a different T-cell tumor such as anaplastic large cell lymphoma. Nevertheless, CD30 is likely not a valuable therapeutic target in the majority of canine PTCL cases.

PDGFs have been shown to be upregulated in human PTCL-NOS.[128,129] Activation through PDGFRA has been shown to contribute to cellular proliferation and this process is mediated in part by STAT1 and STAT5.[129] Similarly, we demonstrate that PTCL in dogs

expresses PDGFRA and PDGFRB both by gene expression and protein expression. Primary canine PTCL cells, however, were not stimulated to proliferation following exposure to exogenous PDGF. This finding may suggest that constitutive activation of the PDGFR signaling independent of growth factor stimulation, may be driving cellular proliferation. Alternatively, PDGFR signaling may not be a primary oncogenic driver in this tumor. A small clinical trial evaluating the efficacy of imatinib, a RTK inhibitor targeting PDGFRs, in patients with refractory or relapsed PTCL showed no significant improvement in overall survival or progression-free survival.[130] Because of the lack of response to therapy targeting PDGFR, this pathway is not considered a primary therapeutic target. Nevertheless, shared expression of PDGFRs in human and canine PTCLs further supports a similar molecular profile.

A landmark study by Iqbal et al. characterized the GEP of PTCL-NOS and identified two major subgroups, PTCL-GATA3 and PTCL-TBX21.[117] In this study PTCL-GATA3 was characterized by expression of GATA3 and its target genes CCR4, IL18RA, CXCR7, IK, MSH6, EGR1, CAT, and SEPTIN6 and was enriched for MTOR, MYC, and PI3K induced gene signatures. PTCL-TBX21 was characterized by expression of TBX21, EOMES, CXCR3, IL2RB, CCL3, and IFN-ß and was enriched for INFY and NFkB gene signatures. PTCL-GATA3 is associated with a worse prognosis. Expression of GATA3, TBX21 and their downstream targets was evaluated in canine PTCL. All of the evaluated canine $CD4^+$ PTCL cases upregulated GATA3 and variably express the associated genes, suggesting that $CD4^+$ PTCL in dogs exhibits molecular similarity to the PTCL-GATA3 subgroup identified in humans. Canine $CD8^+$ and $CD4^-CD8^-$ PTCL cases had more variable expression of the evaluated markers. A proportion of $CD8^+$ cases express molecules associated with the PTCL-TBX21 subgroup. This finding is

consistent with human PTCL-NOS cases in which the majority of PTCL-GATA3 cases are $CD4^+CD8^-$, while a higher proportion of PTCL-TBX21 cases are $CD4^-CD8^+$.[120]

The PI3K-AKT-MTOR signaling pathway is an important cellular pathway that stimulates cell growth and survival in health. PI3K molecules can phosphorylate and activate AKT which subsequently phosphorylates MTOR. MTOR is a key regulator of proliferation, motility, survival, protein synthesis, autophagy, and cellular transcription. PTEN is a well-known tumor suppressor gene that functions to dephosphorylate and thereby inhibit PI3K.[197] The importance of PTEN in regulating cell growth and survival is highlighted by Cowden syndrome. This is a genetic disease defined by autosomal dominant mutation in PTEN resulting in the presence of multiple hamartomas and increased risk of developing breast, thyroid, and uterine cancers.[197,198] $CD4^+$ PTCL in dogs was significantly enriched for gene signatures associated with upregulation of MTOR and downregulation of PTEN. Activation of this pathway in canine PTCL was further supported by diffuse expression of p-AKT by neoplastic cells. Inhibition of PI3K, using the pan-PI3K inhibitor LY294002 resulted in impaired proliferation of the canine TCL cell line, OSW, as well as increased cell death in primary canine $CD4^+$ TCL cells. Altogether, these results demonstrate a central role of the PI3K-AKT-MTOR pathway in the proliferation and survival of PTCL in dogs. The PI3K-AKT-MTOR pathway has been shown to be enriched in human PTCL-GATA3.[117,119] Furthermore, clinical trials using the PI3K inhibitor duvelisib in patients with refractory or relapsed PTCL have been promising, with reported overall response rate of 50% and complete response rate of 18.8%.[138]

Activation of the PI3K-AKT-MTOR pathway is thought to be at least in part driven by loss of the negative regulator PTEN. PTEN-PI3K and CDKN2A-TP53 pathways have been shown to be frequently mutated in human PTCL-GATA3.[119] Similarly, whole-exome sequencing

of Boxer dogs with T-cell lymphoma identified approximately 25% of cases have mutations in PTEN.[167] A recent study using a Human Cancer Hotspot Panel to identify potential tumor-associated mutations in canine PTCL also identified frequent mutations in *MET, KDR, STK11*, and *BRAF* and missense mutations in *MYC, TP53*, and *MET*.[36] Loss of central tumor-suppressor genes including PTEN and TP53 appear to be key to the oncogenesis of PTCL in both humans and dogs. Loss of these negative regulators is likely to allow uncontrolled cellular proliferation, in part through the PI3K-ATK-MTOR pathway.

In this study, we demonstrate molecular similarities between canine and human PTCL. Canine $CD4^+$ PTCL exhibits significant enrichment for the differentially expressed genes in human PTCL-NOS, including PDGFRs. Furthermore, we show that canine $CD4^+$ PTCL upregulates genes associated with the PTCL-GATA3 gene signature, including strong expression of GATA3. Similar to human PTCL-GATA3, canine $CD4^+$ PTCL is enriched for the PI3K-AKT-MTOR pathway, exhibits constitutive phosphorylation of AKT, and is at least in part dependent upon PI3K for cellular survival and proliferation. Combined, these features suggest that canine $CD4^+$ PTCL has the potential to serve as a valuable model to study PTCL-GATA3. $CD4^+$ PTCL is one of the more common subtypes of NHL in dogs, and therefore provides a unique opportunity to easily accumulate patient-derived tissue for evaluation. The lack of gold-standard veterinary treatments also allows for the design of canine clinical trials which may include the early implementation of novel therapies. Early implementation of novel therapeutics not only aids in more efficient identification of promising new treatments for translation into human patients but also provides therapeutic options to pet dogs and their owners who otherwise would not pursue treatment.

CHAPTER 4 – EVALUATION OF CANINE PTCL CELL OF ORIGIN

Summary

Hematopoietic neoplasms arise from immunological cells at various stages of development and differentiation. Classification of these neoplasms is in part reliant upon identification and characterization of the normal immune counterpart. Identification of the cell of origin provides insights into the underlying pathogenesis and can have prognostic and therapeutic impact. Within the field of B-cell neoplasia, cell of origin has been well studied and characterized. Tumors derived from T-cells, however, are less well-understood and identification of cellular origin is in part complicated by plasticity between normal T-cell subgroups. In this chapter we aim to characterize the cell of origin of canine PTCL. We use flow cytometry to evaluate surface marker expression as well as RNA-seq to evaluate changes in gene expression in PTCL compared to combined control $CD4^+$ and $CD8^+$ T-cells. We specifically evaluate markers of precursor phenotypes, T-cell activation, TCR signaling, and mature $CD8^+$ cytotoxic and $CD4^+$ T-helper subsets. We demonstrate that $CD4^+$ PTCL appears to be derived from a naïve single positive T-cell. This conclusion is supported by lack of expression of markers of activation (MHC class II, CD25, and TCR signaling molecules) as well as lack of upregulation of markers associated with T helper subsets. A portion of $CD4^+$ PTCL cases upregulate markers of immaturity including CD34 and TdT on a gene expression level, however surface CD34 expression is not identified on neoplastic cells. The significance of this finding is therefore undetermined, but may suggest that a portion of these neoplasms are derived from a more immature thymic precursor cell. $CD4^-CD8^-$ tumors are enriched for gene expression profiles associated with a more immature T-cell phenotype, and are therefore thought to most likely

develop from an immature, double negative, thymic precursor cell. $CD8^+$ TCL upregulate molecules associated with activated cytotoxic T-cells, suggesting that at least a subset of $CD8^+$ TCLs may originate from a mature $CD8^+$ effector cell.

Introduction

Identification of the neoplastic cell of origin is a useful way to classify and subtype cancer phenotypes. This is particularly true in hematopoietic tumors which have potential to arise from a wide variety of stages of development and functional capabilities. Identification of the cell of origin has important implications on our understanding of oncogenesis, biologic behavior, epidemiology, and the development of targeted therapies in hematopoietic neoplasms.[20,117,199,200] Tumors derived from B-lymphocytes have been well-studied and a detailed classification system rooted in identification of the normal counterpart has been developed.[199] T-cell lymphomas, on the other hand, are less well characterized and peripheral T-cell lymphomas (PTCLs), in particular, often lack defining diagnostic or cytogenetic markers that allow for definitive identification of the cell of origin.

In humans, PTCL encompasses a heterogenous group of diseases with variable clinical presentations, biologic behaviors, and diagnostic criteria. Angioimmunoblastic T-cell lymphoma (AITL), anaplastic large cell lymphoma (ALCL), extranodal NK/T-cell of nasal type and adult T-cell leukemia/lymphoma (ATLL) are well-described entities that fall within the PTCL classification. Approximately 30-50% of PTCL cases, however, do not fall within specific defined subtypes and are named PTCL-not otherwise specified (PTCL-NOS).[20,110] AITL is the most common PTCL subtype and is characterized by polyclonal hypergammaglobulinemia and autoimmune manifestations.[201] AITL is thought to be derived from T-follicular helper lymphocytes and expresses key Tfh markers including BCL6, CXCR5, CD10, and CXCL13.[95–98]

Adult T-cell leukemia/lymphoma (ATLL) is thought to originate from $CD4^+$ $CD25^+$ FoxP3+ Tregs[104] and patients with ATLL characteristically exhibit T-cell immunodeficiency and frequent opportunistic infections.[20,105]

Recent studies have identified molecular subgroups of PTCL-NOS including PTCL-GATA3 and PTCL-TBX21.[117–120,202] These subgroups appear to be derived from different normal T-cell counterparts with unique oncogenic transcriptional signatures, clinical outcomes, and genetic alterations.[117–119] GATA3 is the master transcriptional regulator to the T-helper 2 (Th2) T-cell subset and T-box 21 (TBX21) is the master regulator of Th-helper 1 (Th1) and cytotoxic T-cell differentiation.[203,204] Given these findings, it has been postulated that these PTCL subgroups are derived from Th2 or Th1 T-cells, respectively. These findings however, are interpreted cautiously due to the plasticity of T-cell differentiation and multiple roles that these key transcriptional regulators play in T-cell development and function.[205]

The cell of origin of canine PTCL has not been previously characterized. In this chapter we seek to determine the normal counterpart for canine PTCL using surface protein expression evaluated by flow cytometry as well as transcriptomic profiling and pathway enrichment analysis.

Materials and Methods

Flow Cytometry

Flow cytometry was performed by the Colorado State University Clinical Immunology Laboratory (CSU-CI) on all cases as previously described.[160] TCL cases were identified by uniform expansion of T-cells characterized by expression of the pan-leukocyte marker CD45, the T-cell markers CD3 with or without CD5, and lack of expression of the B-cell marker CD21. Cases exhibited variable expression of T-cell subset antigens, CD4 and CD8.

Case selection for RNA Sequencing

Fine needle tissue aspirates from 33 dogs submitted to the Colorado State University-Clinical Immunology laboratory for routine diagnostics and diagnosed with $CD4^+$, $CD4^-CD8^-$, or $CD8^+$ TCL by flow cytometry were selected for RNA-seq. TCL cases were identified by uniform expansion of T-cells characterized by expression of the pan-leukocyte marker CD45, the T-cell markers CD3 with or without CD5, and lack of expression of the B-cell marker CD21. Cases exhibited variable expression of T-cell subset antigens, CD4 and CD8. Median purity of neoplastic cells was 91.5% (range 63-99%).

Control $CD4^+$ and $CD8^+$ T lymphocytes were harvested from lymph nodes of healthy dogs utilized for IACUC approved surgical continuing education courses. T-cell subsets were sorted by a MoFlo cell sorter (Beckman Coulter, Brea, CA) using positive selection with anti-CD4 (clone YKIX302.9) or anti-CD8 (clone YCATE55.9). Sorted populations were re-analyzed for purity and were used if greater than 90% of the cells were the desired population.

RNA Extraction and Sequencing

RNA extraction was performed using the Purelink RNA mini Kit (Thermo Fisher Scientific, Waltham, MA) and quality was measured with an Agilent 2100 Bioanalyzer System. All samples had a RIN value greater than 6.3 (median RIN 8.45; range 6.3-9.8). RNA was shipped to Novogene Corporation Inc (Sacramento, CA) where the libraries were constructed and sequenced using an Illumina Hiseq PE150 platform.

Differential Gene Expression

Sequences were aligned to CanFam3.1 genome using HISAT2.[182] HTseq[183] and DESeq2[184] were then used to quantify reads, normalize gene expression, and evaluate differentially expressed genes between tumor samples and controls. P-values were determined

using a negative binomial distribution. A Benjamini-Hochberg procedure was used to correct p-values and padj<0.05 was considered the differentially expressed gene screening standard.

Pathway Enrichment Analysis

Gene set enrichment analysis (GSEA)[186] was used to compare canine PTCL gene expression profiles to various T-cell subset gene signatures. The list of significantly differentially expressed genes for $CD4^+$, $CD8^+$, and $CD4^-CD8^-$ compared to combined control $CD4^+$ and $CD8^+$ T-cells was ranked based on log2foldchange. The pre-ranked gene list was then compared to gene sets identified in the molecular signature database (MSigDB) v7.0.[187] Gene sets with an FDR q-value <0.05 were considered significantly enriched.

Results

Canine PTCL does not express markers of T-cell activation

Canine $CD4^+$, $CD8^+$, and $CD4^-CD8^-$ PTCL are identified as T-cell neoplasms based on expression of the T-cell cell marker CD3. These neoplasms have variable expression of CD5 and can be classified based on their patterns of expression of the T-cell subset markers CD4 and CD8. These neoplasms does not express surface CD34, a hematopoietic stem cell marker that is often used to identify hematopoietic neoplasms of precursor origin (Figures 4.1-4.3).[20,206–208] Neoplastic cells typically exhibit low expression of CD25 and MHC class II (Figures 4.1-4.3). CD25 (IL-2 receptor alpha-chain) is expressed by antigen-exposed, activated T-cells[209,210] and is constitutively expressed by $CD4^+$ regulatory T-cell (Tregs).[211] Similarly, MHC class II is expressed by activated T-cells in multiple species, including dogs.[212–217] This immunophenotypic profile suggests that canine PTCL originates from naïve T-cells.

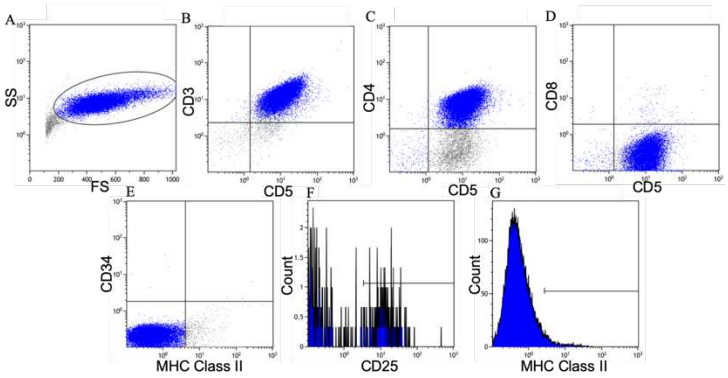

Figure 4.1 CD4$^+$ PTCL immunophenotype. CD4$^+$ PTCL is characterized by a uniform expansion of intermediate to large cells (A) which express the T-cell markers CD3, CD5 and the T-cell subset marker CD4 (B-C). Neoplastic cells do not express CD8 (D), CD34 (E), and have low expression of CD25 (F) and MHC Class II (G).

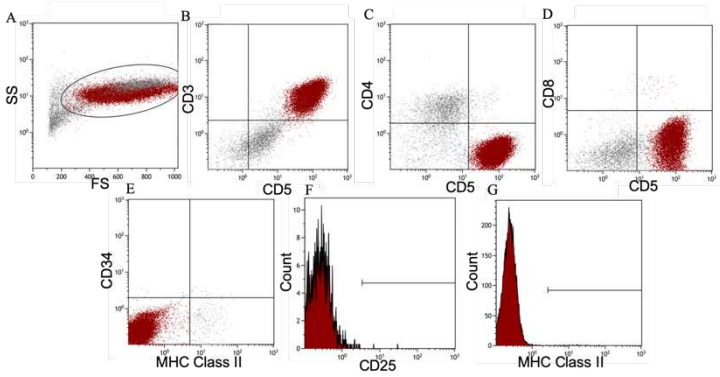

Figure 4.2 CD4$^-$CD8$^-$ PTCL immunophenotype. CD4$^-$CD8$^-$ PTCL is characterized by a uniform expansion of intermediate to large cells (A) which express the T-cell markers CD3 and CD5 (B). Neoplastic cells do not express the T-cell subset antigens CD4 or CD8 (C-D), CD34 (E), and have low expression of CD25 (F) and MHC Class II (G).

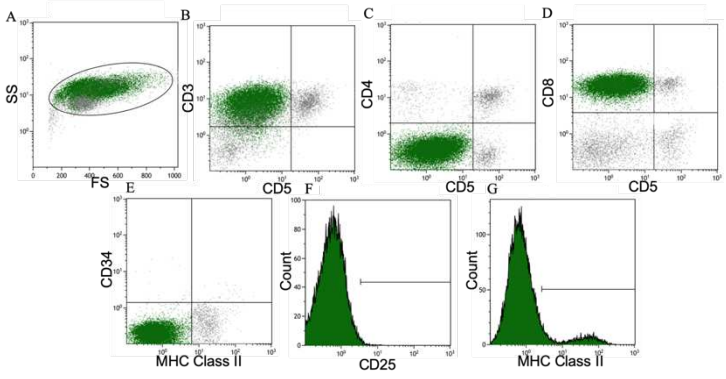

Figure 4.3 CD8$^+$ PTCL immunophenotype. CD8$^+$ PTCL is characterized by a uniform expansion of intermediate to large cells (A) which express the T-cell markers CD3 (B). This case exhibits loss of CD5 (B,C). Neoplastic lymphocytes express the T-cell subset marker CD8 (D). Cells do not express CD4 (C), CD34 (E), and have low expression of CD25 (F) and MHC Class II (G).

To further determine if canine PTCL exhibits a naïve or activated T-cell phenotype, the gene expression profiles of canine PTCL subsets were compared to gene signatures specific to naïve and activated T-cells using GSEA. Gene signatures of naïve and activated T-cell phenotypes were derived from a previous microarray study performed on isolated human immune cell subsets.[218] Evaluated gene sets are listed in table 4.1.

Table 4.1 Naïve and Activated T-cell Subset Gene Lists Used for GSEA Pathway analysis

T-cell activation Subset Gene Sets
Naïve CD4 T-cell vs Memory T-cell_DN
Naïve CD4 T-cell vs Memory T-cell_UP
Naïve CD4 T-cell vs 12h activated Th1_DN
Naïve CD4 T-cell vs 12h activated Th1_UP
Naïve CD4 T-cell vs 12h activated Th2_DN
Naïve CD4 T-cell vs 12h activated Th2_UP
Naïve CD4 T-cell vs 48h activated Th1_DN
Naïve CD4 T-cell vs 48h activated Th1_UP
Naïve CD4 T-cell vs 48h activated Th2_DN
Naïve CD4 T-cell vs 48h activated Th2_UP
Naïve CD8 T-cell vs Memory T-cell_DN
Naïve CD8 T-cell vs Memory T-cell_UP
Naïve vs Memory T-cell_DN
Naïve vs Memory T-cell_UP
Th1 vs Th2_12h activated_DN
Th1 vs Th2_12h activated_UP
Th1 vs Th2_48h activated_DN
Th1 vs Th2_48h activated_UP

The lists of differentially expressed genes in canine $CD4^+$, $CD8^+$, and $CD4^-CD8^-$ PTCL compared to normal $CD4^+/CD8^+$ T-cells were compared to the gene lists defining activated and naïve T-cell subsets. The signature for genes upregulated in naïve CD4 T-cells compared to memory T-cells was significantly upregulated in $CD4^+$ PTCL (FDR q-value=0.035). No gene signatures were enriched at an FDR q-value<0.05 in $CD8^+$ or $CD4^-CD8^-$ PTCL. $CD8^+$ did have moderate enrichment for the gene signatures representing genes upregulated in naïve CD4 or naïve CD8 T-cells compared to memory T-cells (p-value 0.015 and 0.027, respectively), as well as the gene signature representing genes upregulated in Th1 cells compared to Th2 cells following 48 hours of activation (p-value 0.031). (Figure 4.4). Together, the flow cytometry

immunophenotype and gene enrichment analysis focused on signatures of naïve and activated T-cells suggest that these neoplasms originate from a naïve, late thymic or post-thymic T-cells.

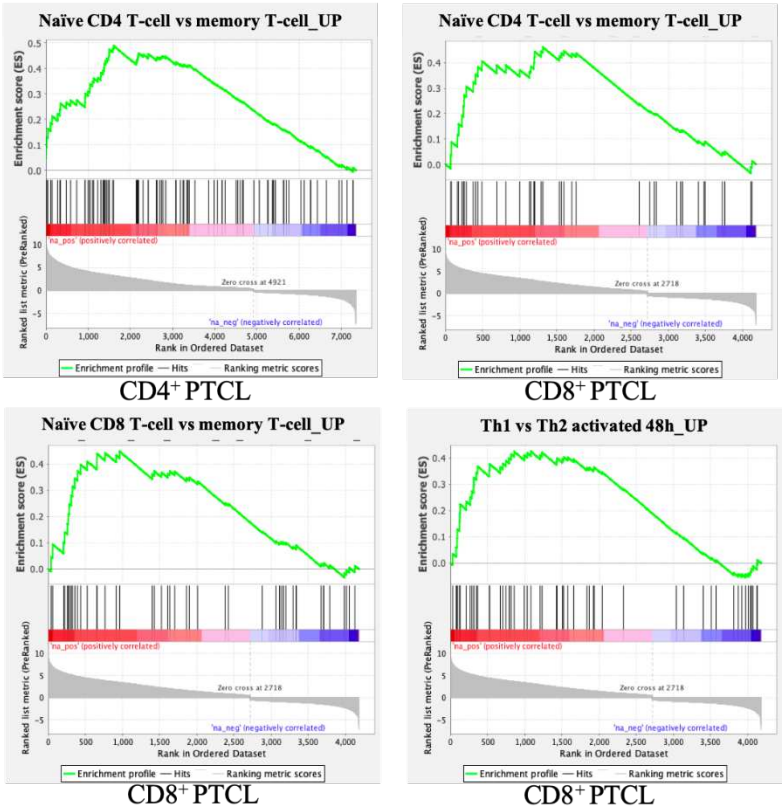

Figure 4.4. Gene set enrichment analysis (GSEA) of canine PTCL subgroups compared to naïve and activated T-cells. $CD4^+$ PTCL was significantly enriched (FDR q-value<0.05) for the gene set that representing genes upregulated in naïve CD4 T-cells compared to memory T-cells. $CD8^+$ PTCL was moderately enriched (p-value <0.05) for signatures associated genes upregulated in naïve CD4 and CD8 T-cells compared to memory T-cells as well as genes upregulated in Th1 cells compared to Th2 cells following 48 hours of activation. GSEA was performed on the list of differentially expressed genes when comparing PTCL cases to combined CD4 and CD8 control T-cells.

To further test our hypothesis that canine PTCL is derived from a naïve T-cell, we sought to evaluate if canine PTCL upregulates genes associated the T-cell receptor (TCR) signal transduction. A simplified schematic of TCR signaling is presented in Figure 4.5.

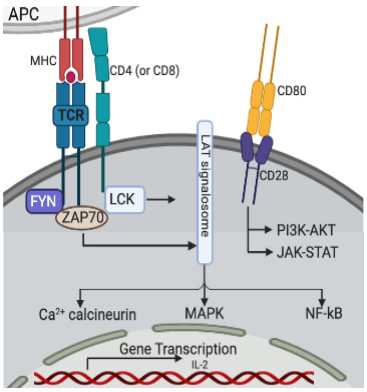

Figure 4.5 Schematic of T-cell signaling adapted from Gaud et al. The TCR signal transduction is initiated by binding of the TCR to antigen-MHC complexes expressed on the surface of antigen-presenting cells (APCs). Upon TCR engagement, the tyrosine kinases LCK and FYN binds to the cytoplasmic domains of the CD4/CD8 co-receptors or CD3, respectively. LCK and FYN phosphorylate immunoreceptor tyrosine-based activation motifs (ITAMs) in the CD3 chains, which allows docking and activation of ZAP70. ZAP70 phosphorylates the transmembrane protein linker for activation of T-cells (LAT), which subsequently recruits a number of adaptor and effector proteins that form the LAT signalosome. The LAT signalosome propagates three major signaling systems including the Ca^{2+}-calcineurin, mitogen-activated protein kinase (MAPK) and nuclear factor-kB (NF-kB). Activation of the T-cell co-receptor CD28 or cytokine receptors additionally results in activation of PI3K-AKT and JAK-STAT signaling pathways.

Differential gene expression of key molecules associated with TCR activation including FYN, LCK, ZAP70, CD3 molecules (CD3G, CD3E, CD3D), CD28, and IL-2 receptor molecules (IL2RG, IL2RB, IL2RA) were evaluated in canine PTCL cases compared to combined $CD4^+$ and $CD8^+$ control T-cells. (Figure 4.6, Table 4.2). The majority of CD3 molecules had significantly lower expression levels or not differentially expressed in PTCL. CD3D expression was modestly elevated in $CD4^+$ PTCL. Similarly, FYN, LCK, ZAP70, CD28, and IL-2 receptor molecules were either significantly downregulated or not differentially expressed in PTCL compared to combined $CD4^+$ and $CD8^+$ control T-cells. IL2RB expression is moderately elevated in $CD8^+$ PTCL and IL2RG expression is modestly elevated in $CD4^+$ PTCL. Taken together, these results suggest that PTCL is not proliferating through enhanced or constitutive TCR signaling and support the hypothesis that in dogs, this neoplasm is derived from naïve-T-cells.

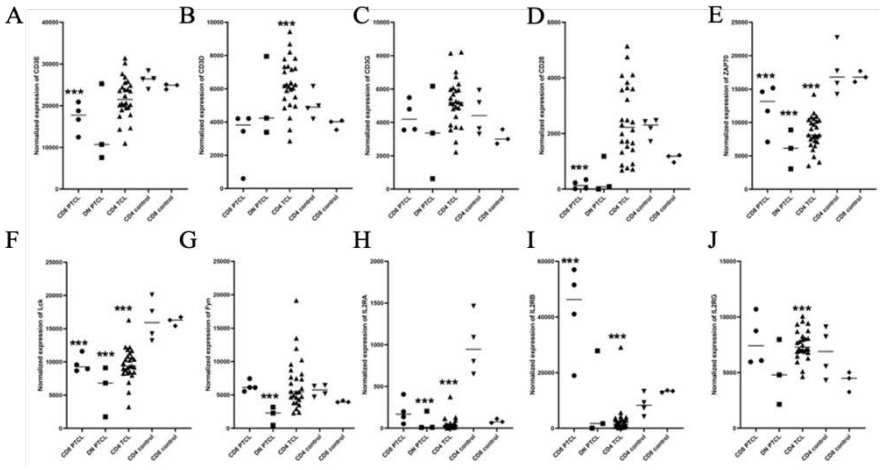

Figure 4.6 Differential gene expression of key molecules associated with TCR signaling. Normalized gene expression for CD3E (A), CD3D (B), CD3G (C), CD28 (D), ZAP70 (E), Lck (F), Fyn (G), IL2RA (H), IL2RB (I), IL2RG (J). Normalized gene expression is derived from DESeq2. ***FDR q-value<0.05

Table 4.2. Summary of differential gene expression of genes associated with TCR signaling

Gene Name	Immunophenotype	Log2(FC)	p-value	padj
CD3E	$CD4^+$	-0.22796	0.089892	0.15403
	CD4-CD8- (DN)	-0.78457	0.024223	0.066383
	CD8+	**-0.66027**	**1.38E-05**	**0.00010555**
CD3D	**$CD4^+$**	**0.46635**	**0.0032487**	**0.0092189**
	CD4-CD8- (DN)	0.20665	0.5088	0.648
	CD8+	-0.61891	0.12739	0.22579
CD3G	$CD4^+$	0.41689	0.023476	0.050206
	CD4-CD8- (DN)	-0.17474	0.74096	0.83353
	CD8+	0.065206	0.79926	0.86438
CD28	$CD4^+$	0.47452	0.1484	0.23099
	CD4-CD8- (DN)	-1.7991	0.03644	0.091337
	CD8+	**-3.3698**	**2.51E-08**	**4.04E-07**
ZAP70	**$CD4^+$**	**-1.0296**	**1.06E-08**	**1.13E-07**
	CD4-CD8- (DN)	**-1.4846**	**4.36E-06**	**4.47E-05**
	CD8+	**-0.59737**	**0.0082548**	**0.024958**
LCK	**$CD4^+$**	**-0.75767**	**4.58E-06**	**2.77E-05**
	CD4-CD8- (DN)	**-1.4095**	**0.00076012**	**0.0038747**
	CD8+	**-0.83077**	**5.03E-08**	**7.50E-07**
FYN	$CD4^+$	0.43756	0.13271	0.21081
	CD4-CD8- (DN)	**-1.2691**	**0.0071247**	**0.02469**
	CD8+	0.25548	0.18938	0.30502
IL2RA	**$CD4^+$**	**-3.3953**	**5.33E-09**	**5.94E-08**
	CD4-CD8- (DN)	**-2.68**	**0.0037583**	**0.014588**
	CD8+	-1.5585	0.034454	0.080649
IL2RB	**$CD4^+$**	**-1.8204**	**0.0023388**	**0.0069277**
	CD4-CD8- (DN)	-0.071857	NA	NA
	CD8+	**1.8689**	**4.55E-07**	**5.25E-06**
IL2RG	**$CD4^+$**	**0.39352**	**0.0076045**	**0.019282**
	CD4-CD8- (DN)	-0.17803	0.68608	0.79088
	CD8+	0.36824	0.23623	0.36233

*Bold and red highlighting indicates significantly upregulated genes and bold and blue highlighting indicates significantly downregulated genes (padj<0.05)

Evaluation of Markers of Immaturity and Thymic Development

Given the suggested naïve cell phenotype, and presence of mediastinal mass in a portion of canine PTCL patients, we next aimed to evaluate if this neoplasm could originate from immature thymic precursor cells. Gene expression levels of markers of immaturity including CD34, TdT, and CD117 (c-KIT) were evaluated (Figure 4.7, Table 4.3). Expression of CD34, TdT, and CD117 were variable among all evaluated cases. Differential gene expression evaluation revealed significantly increased expression of CD34 and CD117 in $CD4^+$ PTCL and $CD8^+$ PTCL. TdT expression was significantly elevated in $CD4^+$ PTCL. Of the seven $CD4^+$ PTCL cases with the highest expression levels of CD34, four of those also expressed high levels of TdT.

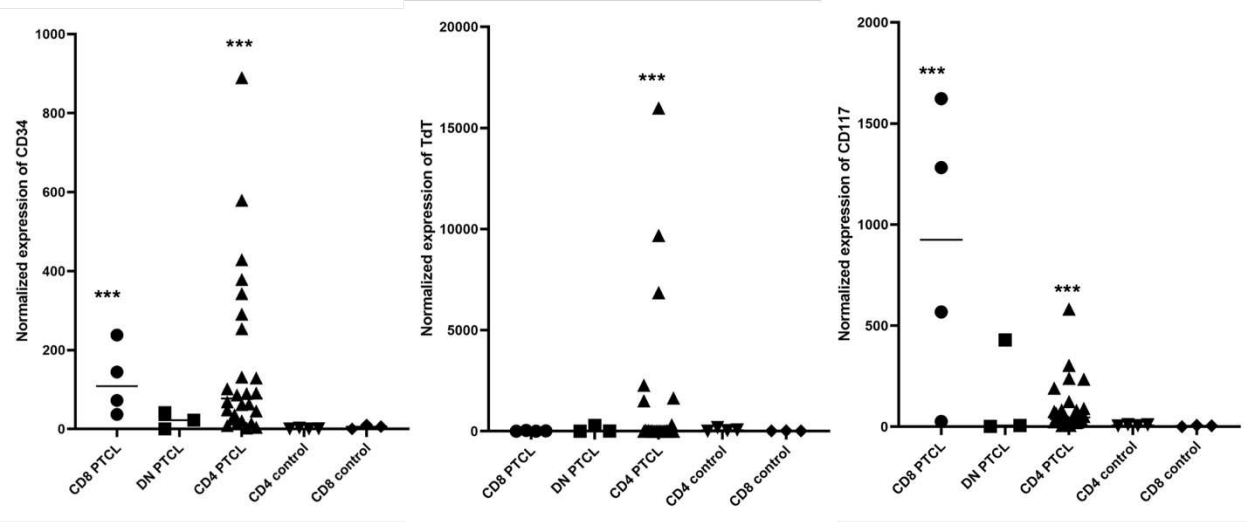

Figure 4.7 Gene expression of markers of immaturity. Normalized gene expression derived from DESeq2 for each PTCL immunophenotype compared to combined $CD4^+$ and $CD8^+$ controls. CD34 and CD117 expression is variable amongst evaluated cases and is significantly increased in $CD4^+$ and $CD8^+$ PTCL (A,C). TdT expression is significantly increased in $CD4^+$ PTCL (B). ***FDR q-value<0.05

Table 4.3 Summary of differential gene expression of precursor markers

Gene Name	Immunophenotype	Log2(FC)	p-value	padj
CD34	**CD4+**	**5.5983**	**3.26E-13**	**8.10E-12**
	CD4-CD8- (DN)	2.2542	0.071822	0.15502
	CD8+	**4.8003**	**2.49E-08**	**4.02E-07**
TdT	**CD4+**	**3.6338**	**0.0015856**	**0.0049431**
	CD4-CD8- (DN)	0.87449	NA	NA
	CD8+	-1.3869	0.11169	0.20409
CD117	**CD4+**	**3.8839**	**3.05E-10**	**4.38E-09**
	CD4-CD8- (DN)	3.9348	NA	NA
	CD8+	**6.5239**	**1.10E-18**	**1.47E-16**

*Bold and red highlighting indicates significantly upregulated genes (padj<0.05)

Table 4.4 Thymic T-cell Subset Gene Lists Used for GSEA Pathway analysis

Thymic Subset Gene Sets
CD4 SP vs CD8 SP Thymocyte_DN
CD4 SP vs CD8 SP Thymocyte_UP
DN vs CD4 SP Thymocyte_DN
DN vs CD4 SP Thymocyte_UP
DN vs CD8 SP Thymocyte_DN
DN vs CD8 SP Thymocyte_UP
DN vs DP Thymocyte_DN
DN vs DP Thymocyte_UP
DN vs immature CD4 SP Thymocyte_DN
DN vs immature CD4 SP Thymocyte_UP
DP vs CD4 SP Thymocyte_DN
DP vs CD4 SP Thymocyte_UP
DP vs CD8 SP Thymocyte_DN
DP vs CD8 SP Thymocyte_UP
Immature CD4 SP vs CD4 SP Thymocyte_DN
Immature CD4 SP vs CD4 SP Thymocyte_UP
Immature CD4 SP vs CD8 SP Thymocyte_DN
Immature CD4 SP vs CD8 SP Thymocyte_UP
Immature CD4 SP vs DN Thymocyte_DN
Immature CD4 SP vs DN Thymocyte_UP

+ Abbreviations: SP: Single positive, DN: Double negative, DP: double positive

GSEA was then utilized to compare the GEP of canine PTCL to gene sets that define stages of thymic development. Gene sets were derived from a previous microarray study that evaluated consecutive T-cell developmental stages in human samples.[219] $CD34^+CD38^-$ $CD1a^-$, $CD34^+CD38^+CD1a^-$, $CD34^+CD38^+CD1a^+$, immature single positive (ISP) $CD4^+$, double positive (DP) $CD3^-$, DP $CD3^+$, single positive (SP) $CD4^+$, and SP $CD8^+$ T-cell subgroups were isolated from human thymi and gene expression was evaluated using Affymetrix microarray analysis.

Results of this microarray study provided 20 gene sets for comparison to PTCL samples (Table 4.4).

The lists of differentially expressed genes in canine $CD4^+$, $CD8^+$, and $CD4^-CD8^-$ PTCL samples were compared to the gene lists defining thymic T-cell subsets. $CD4^+$ PTCL was significantly enriched for two gene sets (FDR q-value <0.05), DN PTCL was significantly enriched for one gene set, and $CD8^+$ PTCL was not enriched for any of the evaluated gene sets. Both $CD4^+$ and DN PTCL were significantly enriched for the genes upregulated in immature CD4 single positive thymocytes compared to double positive thymocytes ($CD4^+$ FDR q-value 0.002; DN FDR q-value 0.005) (Figure 4.8). Immature CD4 single positive thymocytes represent an intermediary thymocyte stage between double negative and double positive thymocytes. $CD4^+$ PTCL was also significantly enriched for the genes upregulated in double positive thymocytes when compared to CD4 single positive thymocytes (FDR q-value 0.027). The gene set enrichment analysis of thymic subsets, as well as upregulation of several markers of immaturity on a gene expression level, suggests that at least a portion of canine PTCL may arise from an immature thymic precursor cell.

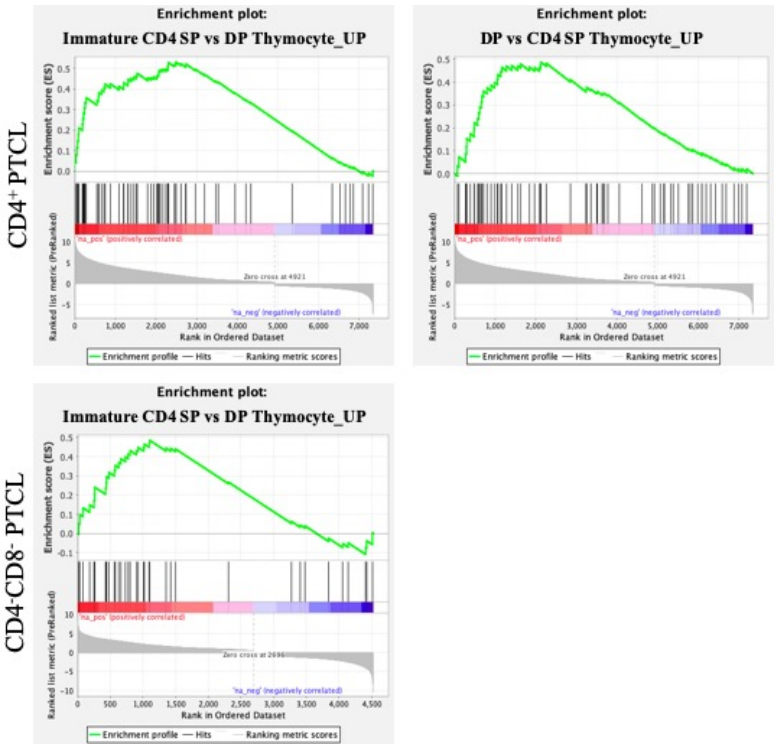

Figure 4.8. Gene set enrichment analysis (GSEA) of canine PTCL subgroups compared to stages of thymic development. Both $CD4^+$ and $CD4^-CD8^-$ PTCL were significantly enriched for the gene set that representing genes upregulated in immature CD4 single positive (SP) thymocytes compared to double positive (DP) thymocytes. $CD4^+$ PTCL was also significantly enriched for the gene set representing genes upregulated in double positive thymocytes versus CD4 single-positive thymocytes.

Expression of T-cell subset markers in canine PTCL

During thymic T-cell development T-cells commit to the CD4 or CD8 lineage upon interaction with MHC class II or MHC class I molecules, respectively. $CD8^+$ T-cells are cytotoxic and act to directly target and destroy virus-infected or tumor cells. $CD4^+$ T-cells perform a variety of functions that aid in propagating an appropriate immune response to the inciting stimulus. Upon antigen exposure, naïve $CD4^+$ T-cells differentiate into T-helper subsets including T helper 1 (Th1), T helper 2 (Th2), T regulatory (Treg), T helper (Th17), and T follicular helper (Tfh) cells. T-cell subsets are defined by major regulatory transcription factor expression and associated secreted cytokines.[220] Differential gene expression analysis of key markers and pathway enrichment analysis for gene signatures associated with the cytotoxic CD8

T-cell as well as the T-helper subsets Th1, Th2, Th17, Treg, and Tfh were performed in canine PTCL groups.

Cytotoxic CD8 T-cells are characterized by the transcription factor EOMES[221–223] and expression of effector molecules TNF, IFNG, perforin, and granzyme-B.[58] $CD8^+$ PTCL significantly upregulates IFNG, TNF, and GZMA (Figure 4.9, Table 4.5). $CD4^+$ PTCL significantly downregulates EOMES, INFG, and GZMB. $CD4^-CD8^-$ PTCL significantly downregulates TNF. GSEA was performed on PTCL subgroups compared to gene sets comparing naïve to activated $CD8^+$ T-cells in mice.[224,225] Significant enrichment for activated $CD8^+$ T-cells was not identified in any of the PTCL groups.

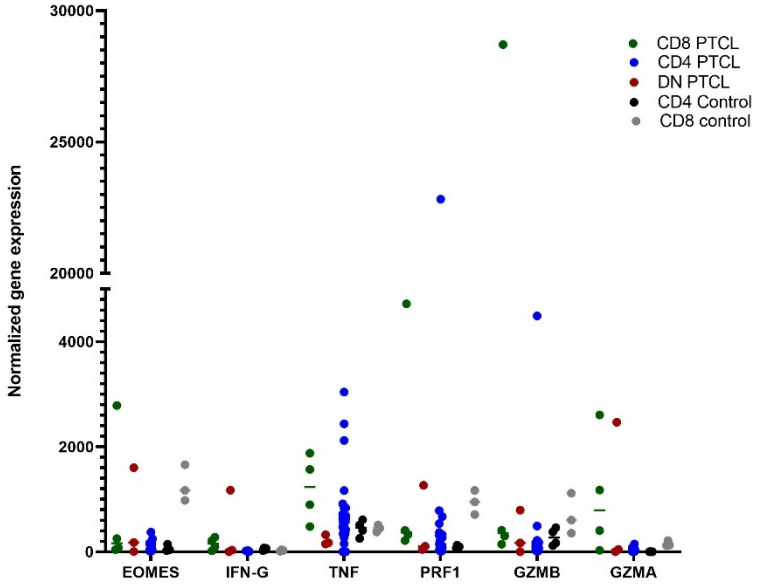

Figure 4.9 Differential gene expression of cytotoxic $CD8^+$ T-cell associated genes. Normalized gene expression for key cytotoxic $CD8^+$ T-cells genes EOMES, INF-G, TNF, PRF1, GZMB, and GZMA. Normalized gene expression is derived from DESeq2.

Table 4.5 Summary of differential gene expression of genes associated with CD8$^+$ phenotype

Gene Name	Immunophenotype	Log2(FC)	p-value	padj
EOMES	**CD4$^+$**	**-3.0752**	**6.67E-06**	**3.88E-05**
	CD4-CD8- (DN)	0.042822	0.97137	0.98263
	CD8+	0.28436	0.78892	0.85699
IFN-G	**CD4$^+$**	**-2.9877**	**1.60E-05**	**8.41E-05**
	CD4-CD8- (DN)	2.8702	NA	NA
	CD8+	**1.761**	**0.0033631**	**0.011743**
TNF	CD4$^+$	0.80452	0.035721	0.071781
	CD4-CD8- (DN)	**-1.0483**	**0.0020806**	**0.0089965**
	CD8+	**1.3218**	**0.00020926**	**0.0011074**
PRF1	CD4$^+$	-1.1285	0.091264	0.15586
	CD4-CD8- (DN)	0.056902	0.95142	0.97053
	CD8+	1.3756	0.10275	0.19112
GZMB	**CD4$^+$**	**-2.3626**	**1.40E-05**	**7.49E-05**
	CD4-CD8- (DN)	-0.46672	0.60128	0.72287
	CD8+	3.2925	NA	NA
GZMA	CD4$^+$	-1.5062	0.068423	0.12325
	CD4-CD8- (DN)	2.5417	NA	NA
	CD8+	**3.0572**	**0.0058024**	**0.018599**

*Bold and red highlighting indicates significantly upregulated genes and bold and blue highlighting indicates significantly downregulated genes (padj<0.05)

The Th1 phenotype is characterized by expression of the master transcription factor TBX21 and downstream molecules INF-γ and TNF.[226] TBX21 and IFN-γ were significantly downregulated in CD4$^+$ PTCL. TNF was significantly downregulated in CD4$^-$CD8$^-$ PTCL. Effector molecules IFN-γ and TNF were significantly upregulated in CD8$^+$ PTCL (Figure 4.10, Table 4.6). The differentially expressed gene lists from canine CD4$^+$, CD8$^+$, or CD4$^-$CD8$^-$ PTCLs were compared to a gene signature associated with Th1 cells using GSEA. The Th1 gene signature was derived from a previous study that compared gene expression profiles of untreated CD4$^+$ T-cell from mice to CD4$^+$ T-cell cultured in Th1 conditions (anti-IL-4, IL-12, and IL-2). Significant enrichment for the Th1 phenotype was not identified an any subset of canine PTCL.

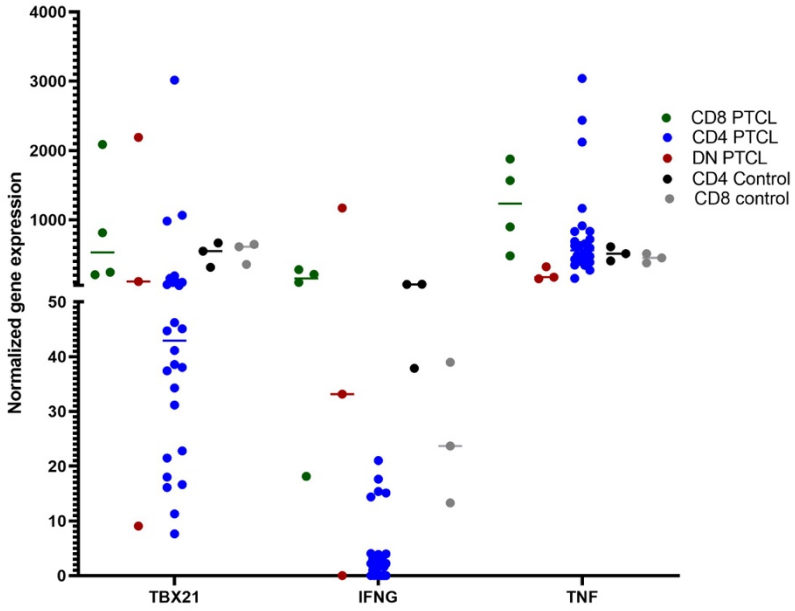

Figure 4.10 Differential gene expression of Th1 associated genes. Normalized gene expression for key Th1-associated molecules TBX21, IFNG, and TNF. Normalized gene expression is derived from DESeq2.

Table 4.6 Summary of differential gene expression of genes associated with Th1 phenotype

Gene Name	Immunophenotype	Log2(FC)	p-value	padj
TBX21	**CD4$^+$**	**-1.8445**	**0.0050847**	**0.01361**
	CD4-CD8- (DN)	0.60217	NA	NA
	CD8+	0.65439	0.22201	0.34526
IFNG	**CD4$^+$**	**-2.9877**	**1.60E-05**	**8.41E-05**
	CD4-CD8- (DN)	2.8702	NA	NA
	CD8+	**1.761**	**0.0033631**	**0.011743**
TNF	CD4$^+$	0.80452	0.035721	0.071781
	CD4-CD8- (DN)	**-1.0483**	**0.0020806**	**0.0089965**
	CD8+	**1.3218**	**0.00020926**	**0.0011074**

*Bold and red highlighting indicates significantly upregulated genes and bold and blue highlighting indicates significantly downregulated genes (padj<0.05)

The Th2 phenotype is characterized by expression of the master transcription factor GATA3 and downstream effectors IL4, IL5, and IL13.[227] GATA3 expression was significantly upregulated in CD4$^+$ PTCL. IL4R, IL5, and IL13 were not differentially expressed in PTCL groups compared to control T-cells (Figure 4.11, Table 4.7). GSEA was then used to compare the differentially expressed gene lists from canine CD4$^+$, CD8$^+$, or CD4$^-$CD8$^-$ PTCLs to the gene

signature associated with Th2 cells. The Th2 gene signature was identified using a previous murine study that compared gene expression profiles of untreated $CD4^+$ T-cells to $CD4^+$ T-cell cultured in Th2 conditions (anti-IFN-γ, anti-IL-12, IL-4, and IL-2). Significant enrichment for the Th2 gene signature was not identified an any subset of canine PTCL.

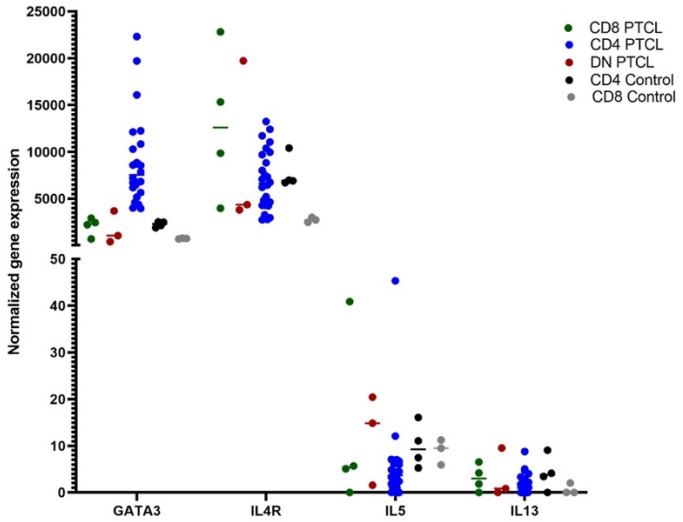

Figure 4.11 Differential gene expression of Th2 associated genes. Normalized gene expression for key Th2-associated molecules GATA3, ILR4, IL5 and IL13. Normalized gene expression is derived from DESeq2.

Table 4.7 Summary of differential gene expression of genes associated with Th2 phenotype

Gene Name	Immunophenotype	Log2(FC)	p-value	padj
GATA3	**$CD4^+$**	**2.4208**	**1.31E-15**	**4.73E-14**
	CD4-CD8- (DN)	0.11384	0.85535	0.91415
	CD8+	0.26511	0.57297	0.69066
IL4R	$CD4^+$	0.30586	0.29803	0.40099
	CD4-CD8- (DN)	0.69255	0.23268	0.37333
	CD8+	1.0865	0.024985	0.061946
IL5	$CD4^+$	-0.83084	0.17792	0.26751
	CD4-CD8- (DN)	0.42228	0.51964	0.65752
	CD8+	0.31264	0.69167	0.78623
IL13	$CD4^+$	-0.71623	0.43155	0.5341
	CD4-CD8- (DN)	0.20327	0.87546	0.92607
	CD8+	0.11264	0.91861	0.94755

*Bold and red highlighting indicates significantly upregulated genes and bold and blue highlighting indicates significantly downregulated genes (padj<0.05)

The Th17 phenotype is characterized by expression of the master transcription factor RORγT and downstream effector IL17. RORC (RORγT), IL17C and IL17F gene expression

levels were compared between canine PTCL and combined $CD4^+$ and $CD8^+$ control T-cells (Figure 4.12, Table 4.8). RORC is significantly downregulated in $CD4^+$, $CD4^-CD8^-$, and $CD8^+$ PTCL. IL17C and IL17F are not differentially expressed in any PTCL subgroup.

GSEA was used to compare the differentially expressed gene lists from canine $CD4^+$, $CD8^+$, or $CD4^-CD8^-$ PTCLs to the gene signature associated with Th17 cells. The Th17 gene signature was derived from a previous study that compared gene expression profiles of untreated $CD4^+$ T-cell from mice to $CD4^+$ T-cell cultured in Th17 conditions (anti-IL-4, inti IFN-γ, anti-IL-12, TGF-B, IL-6, and IL-1B). Significant enrichment was not identified an any subset of canine PTCL.

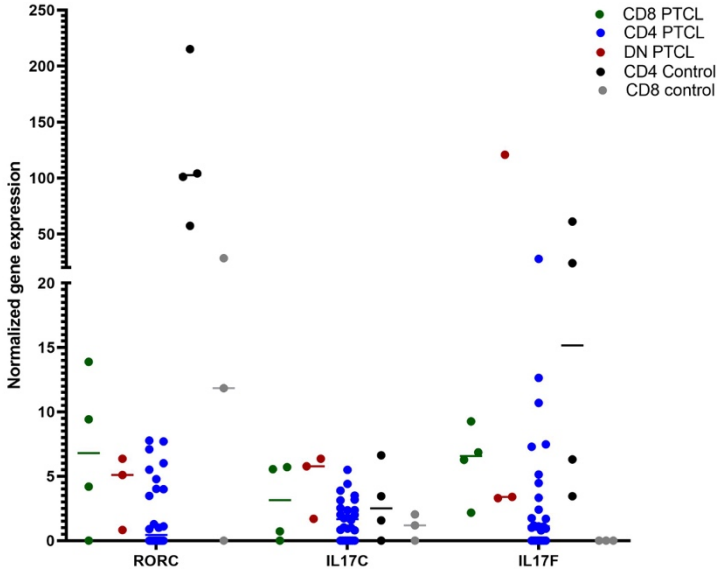

Figure 4.12 Differential gene expression of Th17 associated genes. Normalized gene expression for key Th17-associated molecules RORC, IL17C, IL17F. Normalized gene expression is derived from DESeq2.

Table 4.8 Summary of differential gene expression of genes associated with Th17 phenotype

Gene Name	Immunophenotype	Log2(FC)	p-value	padj
RORC	**$CD4^+$**	**-4.8387**	**2.52E-08**	**2.48E-07**
	CD4-CD8- (DN)	**-3.5621**	**0.00035528**	**0.0020239**
	CD8+	**-2.9855**	**0.0013551**	**0.0054625**
IL17C	$CD4^+$	-0.30732	0.64238	0.72229
	CD4-CD8- (DN)	0.92834	0.37797	0.52651
	CD8+	0.31176	0.76809	0.84342
IL17F	$CD4^+$	-1.7978	0.057487	0.10675
	CD4-CD8- (DN)	1.2193	0.332	0.4821
	CD8+	-0.97185	0.37404	0.50759

*Bold and red highlighting indicates significantly upregulated genes and bold and blue highlighting indicates significantly downregulated genes (padj<0.05)

The Treg phenotype is characterized by expression of the master transcription factor FOXP3 and downstream effectors IL-10, and TGF-β. FOXP3, IL10, and TGFβ1 gene expression levels were compared between canine PTCL and combined $CD4^+$ and $CD8^+$ control T-cells (Figure 4.13, Table 4.9). FoxP3 was significantly downregulated in $CD8^+$ and $CD4^-CD8^-$ PTCL. IL-10 was significantly downregulated in $CD4^+$ PTCL. The differentially expressed gene lists of canine PTCL subgroups were compared to Treg gene signatures using GSEA. Treg gene signatures were derived from a previous murine microarray study which compared naïve $CD4^+$ T-cells to both $CD4^+CD25^{hi}$ natural Tregs or cells cultured under Treg (anti-IL4, anti IFN-γ, TGF-β, and IL-2) conditions.[228] Canine PTCL was not significantly enriched for the induced or natural Treg gene signatures.

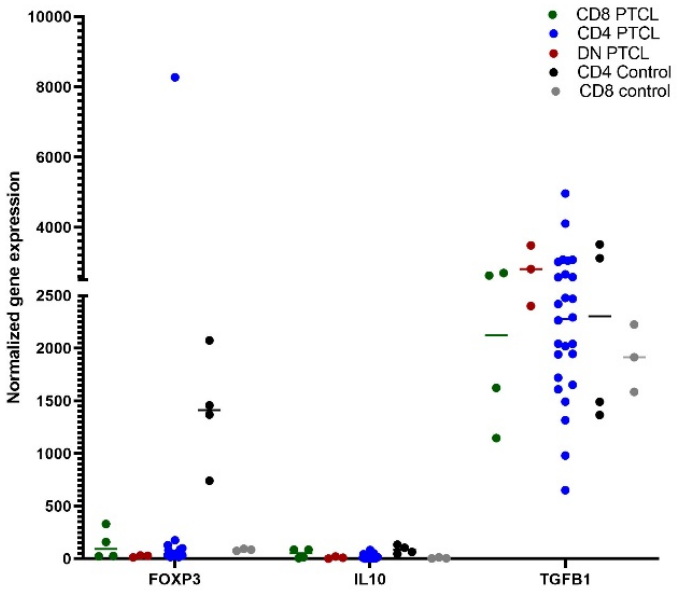

Figure 4.13 Differential gene expression of Treg associated genes. Normalized gene expression for key Treg-associated molecules FOXP3, IL10, and TGFB1. Normalized gene expression is derived from DESeq2.

Table 4.9 Summary of differential gene expression of genes associated with Treg phenotype

Gene Name	Immunophenotype	Log2(FC)	p-value	padj
FOXP3	$CD4^+$	-1.1157	0.21624	0.31199
	CD4-CD8- (DN)	**-4.6035**	**6.76E-08**	**1.12E-06**
	CD8+	**-2.4332**	**0.0033481**	**0.011704**
IL10	**$CD4^+$**	**-1.6448**	**0.0069544**	**0.017856**
	CD4-CD8- (DN)	-2.0471	0.044487	0.10652
	CD8+	-0.18754	0.82702	0.88451
TGFB1	$CD4^+$	0.093982	0.70194	0.77324
	CD4-CD8- (DN)	0.415	0.24123	0.38279
	CD8+	-0.19164	0.57158	0.68976

*Bold and red highlighting indicates significantly upregulated genes and bold and blue highlighting indicates significantly downregulated genes (padj<0.05)

The Tfh phenotype is characterized by expression of the master transcription factor BCL6, downstream effector IL21, as well as CXCL13 and CXCR5. Gene expression levels of BCL6, CXCL13, and CXCR5, and IL21R were compared between canine PTCL and combined $CD4^+$ and $CD8^+$ control T-cells (Figure 4.14, Table 4.10). BCL6 was significantly overexpressed by $CD4^-CD8^-$ PTCL and downregulated in $CD8^+$ PTCL. CXCR5 was significantly downregulated in $CD4^+$ and $CD8^+$ PTCL. GSEA pathway analysis was also performed to

compare the differentially expressed gene lists of canine PTCL subgroups to Tfh gene signatures. Tfh gene signatures were derived from a gene expression microarray study that compared virus-specific Tfh and non-Tfh effector CD4^{+} T-cells in mice.[88] Canine PTCL was not significantly enriched for the Tfh signature.

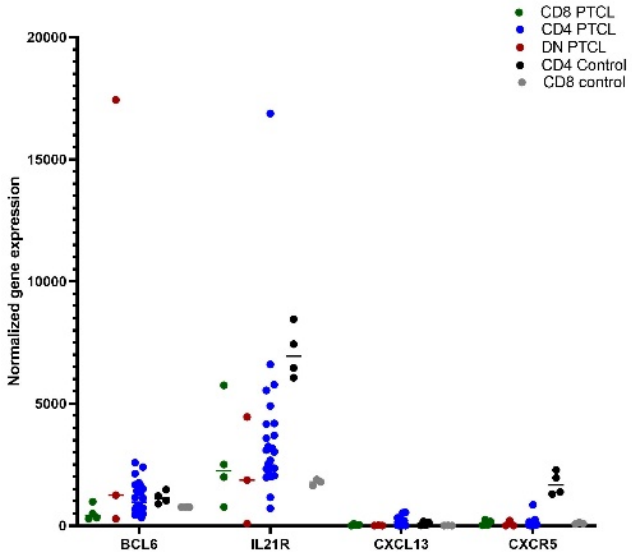

Figure 4.14 Differential gene expression of Tfh associated genes. Normalized gene expression for key Tfh-associated molecules BCL6 and IL21R. Normalized gene expression is derived from DESeq2.

Table 4.10 Summary of differential gene expression of genes associated with Tfh phenotype

Gene Name	Immunophenotype	Log2(FC)	p-value	padj
BCL6	CD4^{+}	0.20706	0.50664	0.60425
	CD4-CD8- (DN)	**2.4693**	**0.0011378**	**0.0054287**
	CD8+	**-0.99223**	**0.0050851**	**0.016638**
IL21R	CD4^{+}	-0.38801	0.30516	0.40861
	CD4-CD8- (DN)	-1.0651	0.16676	0.29298
	CD8+	-0.8549	0.1274	0.22579
CXCL13	CD4^{+}	0.88009	0.31165	0.41556
	CD4-CD8- (DN)	-2.5195	0.023422	0.064633
	CD8+	-0.53066	0.56512	0.6838
CXCR5	**CD4^{+}**	**-3.6176**	**1.31E-07**	**1.12E-06**
	CD4-CD8- (DN)	-2.8713	0.017946	0.052229
	CD8+	**-2.8732**	**0.00066735**	**0.0029892**

Discussion

In this chapter we aim to better understand the normal immunological counterpart of canine PTCL. PTCL expresses T-cell markers CD3 and variably expresses CD5. In thymic development, T-cells gain expression of CD3 following productive rearrangement of the TCR β-chain. Low levels of CD5 are expressed on immature double negative (DN) $CD4^-CD8^-$ thymocytes. CD5 surface expression increases in both the double positive (DP) $CD4^+CD8^+$ and single positive ($CD4^+$ or $CD8^+$) thymocytes. CD5 expression is then maintained on circulating single positive T-cells.[229,230]

Canine PTCL expresses low levels of surface MHC class II and CD25. MHC class II has been shown to be expressed on activated T-cells in a number of species including humans, dogs, horses, and cows. [212–217] CD25 (IL-2 receptor alpha-chain) is expressed by antigen-exposed, activated T-cells[209,210] and is constitutively expressed by $CD4^+$ Tregs.[211] Upon antigen-exposure, naïve T-cells become activated and are able to proliferate through TCR-mediated signaling pathways. CD25, along with other genes associated with TCR signaling, were expressed at lower levels in canine PTCL compared to controls. Lower expression levels of molecules associated with antigen-exposure and T-cell activation in canine PTCL supports a naïve T-cell phenotype. Further supporting a naive T-cell origin, GSEA analysis identified significant enrichment for a gene signature representing genes upregulated in naïve T-cells compared to memory T-cells.

Canine PTCL does not express the surface CD34 molecule. CD34 is a marker of hematopoietic stem cells and hematopoietic progenitor cells. [20,206–208] Evaluation of the canine gene expression profiles, however, identified significant upregulation of several markers of precursor phenotypes including CD34 and TdT. The significance of this upregulation is undetermined. PTCL cases were compared to normal control lymphocytes and a precursor

control was not included in this study. Comparison of CD34 and TdT expression by PTCL to acute leukemia or bone-marrow derived stem cells would provide further insights into the observed upregulation. Based on our gene expression results, a subset of PTCL cases may exhibit a precursor phenotype. Stratification of PTCL cases based on CD34 and TdT gene expression levels and comparison of clinical features, clinical outcome, and gene expression compared to isolated hematopoietic stem cells or acute leukemia cells would be interesting future study directions. TdT protein quantification has been attempted by us and others, however, antibodies that react with canine TdT have yet to be successfully optimized.

Canine $CD4^+$ and $CD4^-CD8^-$ PTCL can present with mediastinal involvement, suggesting that in a portion of cases, neoplastic T-cells may be derived from thymic T-cells. GSEA analysis identified significant enrichment for immature CD4 single positive and double positive thymocytes. Together, these findings imply that canine PTCL may originate from thymic precursors and naïve $CD4^+$ T-cells in various stages of development, a subset of which may be early precursors that maintain expression of CD34 and TdT.

CD117 (c-kit) expression was also evaluated in canine PTCL. CD117 is expressed in several cell types including normal and neoplastic hematopoietic cells.[231] CD117 expression can be seen in both non-neoplastic myeloid and lymphoid lineages, although within the lymphoid lineage expression appears to be restricted to NK-cell and early T-cell precursor subsets.[231] CD117 has also be shown to be expressed in Hodgkin's lymphoma, $CD30^+$ anaplastic large cell lymphoma,[232] multiple myeloma,[233] as well as precursor neoplasms including acute myeloid leukemia,[231] and T-cell acute lymphoblastic leukemia.[234] It is undetermined if CD117 upregulation in canine PTCL is a primary oncogenic pathway or supports derivation from a

precursor lymphocyte. Nevertheless, this finding suggests that receptor tyrosine kinase inhibitors targeting CD117 have potential to be therapeutically beneficial in canine PTCL.[235]

We also assessed expression of key transcription factors and signaling molecules associated with $CD4^+$ T-helper lymphocyte subsets. $CD4^+$ PTCL significantly upregulated the Th2 master regulator GATA3, but did not upregulate downstream effector molecules IL4R, IL5, or IL13. While, GATA3 is best known as the primary transcription factor that directs Th2 differentiation, it has also been shown to have essential roles in early T-cell commitment, β-selection, and $CD4^+$ T-cell development.[236] GATA3 is detectable in hematopoietic stem cells and mRNA levels increase as development proceeds through the lymphoid progenitor, double negative, double positive and single positive stages.[237,238] GATA3 has been shown to be critical for commitment to the $CD4^+$ single positive phenotype. Mice that were conditionally ablated for GATA3 at the double-positive stage result in decreased numbers of CD4 SP thymocytes and increased numbers of CD8 SP thymocytes.[47] Furthermore, enforced expression of GATA3 throughout T-cell development, resulted in reduced numbers of peripheral $CD8^+$ T-cells as well as development of thymic lymphoblastoid neoplasms.[53] These findings support a critical role for GATA3 in the commitment to the $CD4^+$ T-cell lineage and suggest that overexpression of this transcription factor could contribute to oncogenesis of this T-cell subset within the thymus.

Canine PTCL gene expression did not appear to correlate to key molecules associated with Th17, Treg, or Tfh phenotypes. Furthermore, significant enrichment for gene signatures associated with these effector subgroups was not identified. BCL6 was significantly upregulated in $CD4^-CD8^-$ PTCL. The significance of this finding is interpreted with caution, given the low sample number in this group.

$CD8^+$ cytotoxic T-cell molecules, INF-γ, TNF, and granzyme A were upregulated by $CD8^+$ PTCL, indicating that $CD8^+$ PTCL may originate for a more mature, activated cytotoxic T-cell. This finding is in contrast to significant upregulation of markers of immaturity including CD34 and downregulation of TCR signaling associated molecules in $CD8^+$ PTCL. These contradictory findings could imply that the $CD8^+$ PTCL encompasses a heterogenous group of tumors, some of which arise from an immature naïve T-cell while others originate from a mature effector T-cell. Alternatively, upregulation of these effector molecules could represent a more inflammatory microenvironment in the $CD8^+$ PTCL phenotype compared to the more common $CD4^+$ PTCL group. In human PTCL-NOS, the PTCL-TBX21 subgroup is associated with an enhanced mixed inflammatory background compared to PTCL-GATA3.[120]

Based on the findings of this study, we propose that $CD4^+$ PTCL originates from a naïve single positive T-cell that does not signal through the TCR and does not represent an activated T-helper phenotype. At least a proportion of $CD4^+$ PTCL appear to upregulate markers of immaturity, including CD34 and TdT, and are enriched for gene signatures of early thymic development. Based on these findings, it is possible that a subset of these neoplasms are consistent with a lymphoblastic lymphoma derived from precursor cells. Further stratification of canine PTCL based on markers of immaturity may be helpful to better characterize the biologic significance of these findings. Evaluation of the origin of $CD4^-CD8^-$ and $CD8^+$ PTCL is limited by the low sample numbers in this study. We hypothesize that $CD4^-CD8^-$ PTCL originates from a double negative thymic precursor, prior to commitment to a single-positive lineage. Our results also imply that $CD8^+$ PTCL may encompass a more heterogenous tumor group, some of which may be derived from naïve $CD8^+$ T-cells and other from activated cytotoxic $CD8^+$ T-cells. Characterization of the cellular origin of PTCL gives us insights into underlying pathogenesis of

these neoplasms and helps to direct further studies focused on more advanced classification of this group of neoplasms.

CHAPTER 5 – DISCOVERY OF FUSION GENE CANDIDATES IN CANINE PTCL

Summary

Chromosome aberrations and rearrangements are common in a wide variety of cancers. One of the consequences of chromosomal rearrangements is the formation of gene fusions. Fusion genes are particularly common drivers of hematologic malignancies and serve as useful diagnostic markers, as well as therapeutic targets. Identification of novel driving chromosomal translocations and fusion genes offers new targets to investigate disease pathogenesis and treatment. In this chapter we aim to discover fusion gene candidates in 26 canine PTCL cases using an RNA-seq based discovery pipeline. We utilized FusionCatcher to identify fusion transcripts in PTCL cases and control canine lymphocytes. We specifically focused on recurrent fusion genes in which the 3' fusion partner was identified in more than one candidate. Following strict filtering criteria, a total of 591 fusion transcripts were identified in the 26 cases. Recurrent fusion genes involving 11 different 3' fusion partners were chosen for further evaluation of the genome structure and fusion event. Recurrent fusion genes involving DGKZ-MDK and LMO4 with several 5' fusion partners were particularly interesting due to the 3' gene partners' potential roles in driving oncogenesis. This study identifies a list of potential fusion gene candidates in canine PTCL, and lays the groundwork for future efforts to validate these targets.

Introduction

Chromosomal rearrangements that juxtapose two different genes can result in a fusion gene that has potential to drive uncontrolled cellular proliferation and survival. Structural chromosomal rearrangements that yield fusion genes include translocations, inversions, amplifications and deletions. Fusion genes can also form by non-structural aberrations including cis- and trans- splicing or transcriptional read-through.[239,240] Fusion genes and chromosomal translocations are valuable molecular diagnostic markers for tumor identification and classification, particularly in tumors that lack useful cell surface markers. Oncogenic translocations also represent potential therapeutic targets.

Fusion genes can alter cell biology through a number of mechanisms. Among the most common mechanisms is overexpression of an oncogene due to promoter exchange. In this case, a chromosomal rearrangement brings the 3' gene's expression under control of the 5' gene's promoter. The IGH-MYC fusions identified in Burkitt lymphoma is an example in which the promoter of immunoglobulin heavy locus is fused with the MYC proto-oncogene.[241]

Fusion events can also alter oncogene expression by replacing the 3'UTR. The 3' UTR is a regulatory domain that influences the localization, export, stability, and translation efficiency of mRNA. The 3' UTR also contains various sequences that are involved in gene expression, including microRNA (miRNA) response elements, AU-rich elements, and the poly-A tail. MYB-NFIB fusion identified in adenoid cystic carcinoma results in elevated MYB protein levels due to loss of miRNA binding sites as a result of the fusion event.[242]

Chimeric proteins can also form during a fusion gene event. Alterations in the protein structure may result in constitutive activation, altered signaling mechanisms to change downstream signaling events, or inhibition of normal cellular function. BCR-ABL1 is a

canonical example and is identified in greater than 90% of human patients with chronic myelogenous leukemia (CML).[243] BCR-ABL1 fusions result in constitutively active ABL1 kinase by enabling BCR-ALB1 oligomerization via the coiled-coil domain present in BCR.[244]

Fusion genes are frequent drivers of human hematopoietic malignancies. Studies focused on PTCL in humans have identified several recurrent fusion proteins. Anaplastic large cell lymphoma (ALCL) is one of the more common PTCL subtypes and encompasses several distinct entities based on the presence or absence of ALK (anaplastic lymphoma kinase) gene rearrangements. ALK-positive ALCL generally affects a younger patient population than ALK-negative ALCL or other PTCL subtypes.[20] The most common rearrangement involves a t(2;5)(p23;q35) translocation that results in the fusion of nucleophosmin (NPM1) to ALK.[245] This translocation and fusion protein is identified in approximately 75-85% of ALK-positive ALCLs. Fewer ALK-positive ALCLs involve more than 20 other ALK fusion partners.[20,246] ALK fusion proteins result in constitutive ALK tyrosine kinase activity which promotes cancer cell proliferation and survival.[247] Pharmacologic ALK inhibition is an effective therapeutic strategy for patients with ALK-positive ALCL, including patients with relapsed/refractory disease.[248–251] With conventional cytotoxic therapy or ALK targeted therapy, ALK-positive ALCL has a better prognosis than ALK-negative ALCL, as well as most other PTCL subtypes, with 5-year overall survival rates of 70-85%.[251,252]

Recurrent chromosomal translocations appear to occur within a smaller proportion of individuals with other types of PTCL. CTLA4-CD28 fusion genes have been identified in variable numbers of angioimmunoblastic T-cell lymphomas (AITL), PTCL-NOS, and extranodal NK/T cell lymphomas.[253–255] Additionally, a recurrent t(5;9)(q33;q22) translocation resulting in ITK-SYK fusion has been identified in a subset of PTCLs with a follicular growth pattern and

Tfh phenotype, and rarely in AITL. This fusion results in overexpression and activation of spleen tyrosine kinase (SYK).[256–259] The identification of this recurrent fusion gene has contributed to the development of the Tfh-derived PTCL categories, previously discussed.

Recurrent fusions involving VAV1 with varying partners have been identified in 7% of PTCL, including PTCL-NOS as well as ALK-negative ALCL.[260] In vitro ectopic expression of VAV1 fusion was shown to promote cell proliferation and migration in a RAC1-dependent manner. RAC1 inhibitors are clinically available and potentially useful therapeutics for patients with VAV1 fusion proteins.[260]

While fusion genes have been well-characterized in a wide-range of human tumors, the roles of chromosomal translocations and functional fusion genes in canine malignancies are not well understood. There have been few reported oncogenic fusion genes in canine tumors including: IGK-CCND3 in B-cell lymphoma, MPB-BRAF in glioma, COL3A1-PDGFRB in dermatofibrosarcoma protuberans-like, BCR-ABL in chronic lymphocytic leukemia, and IGH-MYC translocation in Burkitt lymphoma.[261,262]

RNA-seq offers a powerful tool for the discovery of fusion genes. A number of algorithms and programs have been developed for fusion detection using RNA-Seq data. These programs generally work by identifying the split reads in discordant read pairs that map to two distinct genes. The exact fusion point is then determined from the split reads where a single mate reads overlap the fusion junction, with the fusion-encompassing reads used as supporting evidence (summarized in Figure 5.1).[263,264]

In this chapter, we aim to identify fusion genes that may be driving canine PTCL using RNA-seq derived transcriptomic data. After applying strict filtering criteria, 591 fusion transcripts were identified in the 26 cases. Recurrent fusion genes involving 11 different 3’

fusion partners were chosen for further evaluation. The structural features of these proposed chromosomal rearrangements and subsequent fusion transcripts were subsequently modeled. This study identifies a list of potential fusion gene candidates in canine PTCL, and lays the groundwork for future efforts to validate these targets.

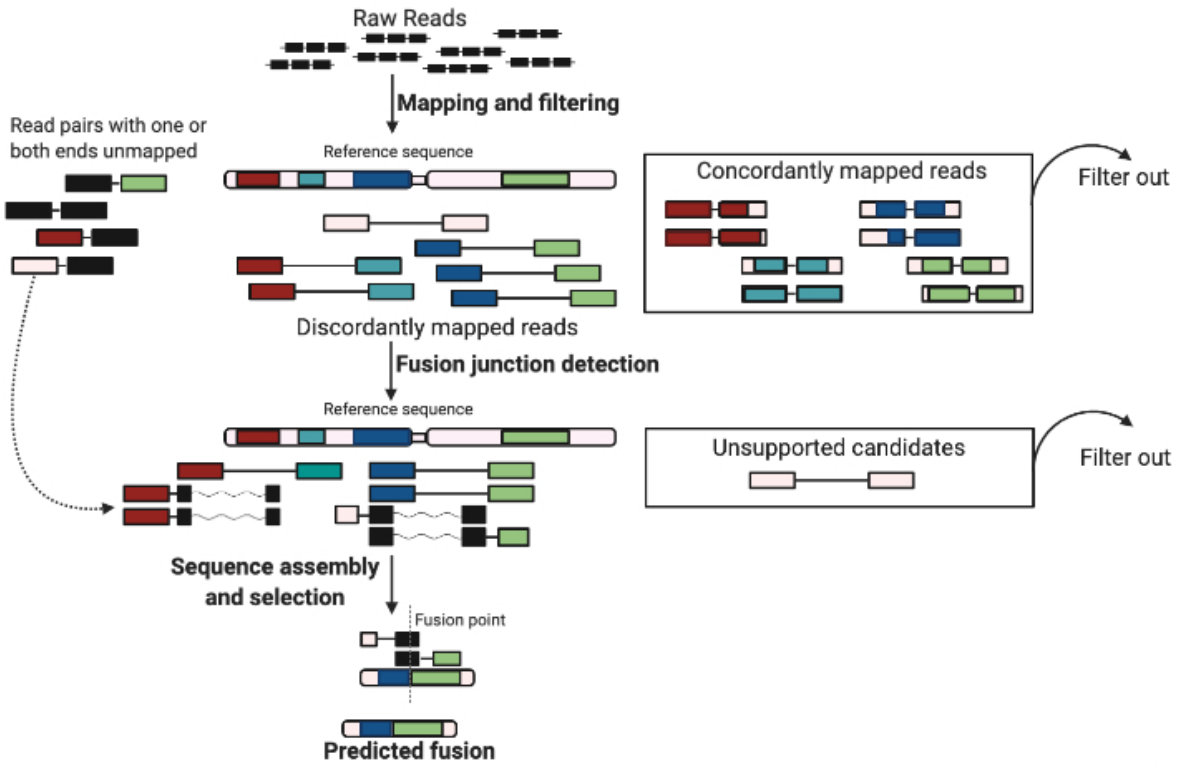

Figure 5.1 Summary of RNA-seq gene fusion detection from paired-end mapping. The reference sequence includes two chromosomes with four different genes represented by colored boxes. Reads are first mapped to the reference sequence and reads that map concordantly are discarded. Reads that map to the reference sequence are colored with the region to which they are aligned to. Unmapped reads are colored black. Reads that map discordantly are used to determine approximate fusion boundaries. In cases with reads in which at least one end is unaligned to the reference sequence, the unmapped read is cut into multiple segments (curved lined) to be aligned independently to the approximate fusion boundaries. Fusion junctions are identified through these 'split-reads' in which the two segments are mapped to two different chromosomes or genes. The sequences of the fusion candidates are then assembled and those with the highest likelihood to be real fusions are selected as final outputs (adapted from Zhoa et al. 2013).

Materials and Methods

Case selection for RNA-Seq

Fine needle tissue aspirates from 26 dogs submitted to the Colorado State University-Clinical Immunology laboratory for routine diagnostics and diagnosed with $CD4^+$ PTCL by flow cytometry were selected for RNA-seq. PTCL cases were identified by uniform expansion of T-cells characterized by expression of the pan-leukocyte marker CD45, the T-cell markers CD3 with or without CD5, the T-cell subset marker CD4, and lack of expression of the B-cell marker CD21.

Control $CD4^+$ and $CD8^+$ T lymphocytes were harvested from lymph nodes of healthy dogs utilized for IACUC approved surgical continuing education courses. T-cell subsets were sorted by a MoFlo cell sorter (Beckman Coulter, Brea, CA) using positive selection with anti-CD4 (clone YKIX302.9). Sorted populations were re-analyzed for purity and were used if greater than 90% of the cells were the desired population.

RNA Extraction and Sequencing

RNA extraction was performed using the Purelink RNA mini Kit (Thermo Fisher Scientific, Waltham, MA) and quality was measured with an Agilent 2100 Bioanalyzer System. RNA was shipped to Novogene Corporation Inc (Sacramento, CA) where the unstranded libraries were constructed and sequenced using an Illumina Hiseq PE150 platform. Quality parameters of the sequencing are summarized in Table 5.1. The median number of raw reads of samples used for fusion discovery was 57,422,874 (range: 46,655,240-71,686,242 reads). The error rates ranged from 0.02-0.03%.

Table 5.1. RNA-seq Quality Control Summary

Sample name	Sample Type	Raw reads	Clean reads	Raw bases	Clean bases	Error rate(%)	Q20(%)	Q30(%)	GC content(%)
107029	CD4 Control	71686242	69323150	10.8G	10.4G	0.03	97.79	94.01	51.21
63500	CD4 Control	49892460	48111496	7.5G	7.2G	0.03	97.78	93.97	51.04
77877	CD4 Control	68020740	65801830	10.2G	9.9G	0.03	97.92	94.25	51.61
80398	CD4 Control	70986464	68679512	10.6G	10.3G	0.03	97.73	93.81	51.3
100641	CD4 PTCL	49548966	47959446	7.4G	7.2G	0.03	97.68	93.62	50.23
100850	CD4 PTCL	48707294	47190500	7.3G	7.1G	0.03	97.52	93.31	50.58
100993	CD4 PTCL	52926966	51138812	7.9G	7.7G	0.03	97.73	93.85	49.89
101786	CD4 PTCL	64708040	63022640	9.7G	9.5G	0.03	97.7	93.8	49.92
104029	CD4 PTCL	54004842	52430952	8.1G	7.9G	0.03	97.76	93.97	50.53
60342	CD4 PTCL	46655240	45027580	7G	6.8G	0.03	97.75	93.88	51.37
65026	CD4 PTCL	49907106	48214140	7.5G	7.2G	0.03	97.77	93.94	49.84
67283	CD4 PTCL	56817058	55231380	8.5G	8.3G	0.03	97.91	94.22	50.87
67308	CD4 PTCL	64997916	62882384	9.7G	9.4G	0.03	97.8	94.03	51.06
69996	CD4 PTCL	50074724	48315878	7.5G	7.2G	0.03	97.87	94.16	50.61
71175	CD4 PTCL	62740124	60789720	9.4G	9.1G	0.03	97.78	93.95	51.31
71312	CD4 PTCL	55758818	53882748	8.4G	8.1G	0.03	97.83	94.03	51.14
71508	CD4 PTCL	55384306	53636026	8.3G	8G	0.03	97.64	93.65	51.57
71605	CD4 PTCL	59408924	57461946	8.9G	8.6G	0.03	97.8	94.03	50.51
71779	CD4 PTCL	60828100	58535460	9.1G	8.8G	0.03	97.25	92.59	50.49
76055	CD4 PTCL	67319066	65041220	10.1G	9.8G	0.03	97.75	93.88	50.62
76392	CD4 PTCL	57422874	55688672	8.6G	8.4G	0.03	97.78	93.95	50.82
95512	CD4 PTCL	60838638	58502090	9.1G	8.8G	0.03	97.85	94.1	50.9
95591	CD4 PTCL	67189882	65277158	10.1G	9.8G	0.03	97.61	93.57	51.67
95593	CD4 PTCL	47484046	46006612	7.1G	6.9G	0.03	97.82	94.14	51.42
96300	CD4 PTCL	58334394	56604978	8.8G	8.5G	0.03	97.86	94.12	50.4
97074	CD4 PTCL	66146888	62293732	9.9G	9.3G	0.03	97.78	93.96	50.99
97336	CD4 PTCL	64768664	62833840	9.7G	9.4G	0.03	97.72	93.86	51.73
97568	CD4 PTCL	62849258	60771456	9.4G	9.1G	0.03	97.77	93.95	50.46
97578	CD4 PTCL	50640402	49050588	7.6G	7.4G	0.03	97.83	94.11	50.57
98458	CD4 PTCL	57844072	55828494	8.7G	8.4G	0.03	97.72	93.85	51.18
107031	CD8 Control	55899102	54070548	8.4G	8.1G	0.03	97.74	93.88	51.05
107032	CD8 Control	56832496	55029784	8.5G	8.3G	0.03	97.82	94.05	50.77
63491	CD8 Control	51380682	49598884	7.7G	7.4G	0.02	97.94	94.36	51.14

Abbreviations: PTCL-peripheral T-cell lymphoma, DN-Double negative (CD4-CD8-)

Definitions: (1) Raw reads: read counts from the raw data.
(2) Clean reads: read counts filtered from raw data (removed reads containing N, low quality reads, reads containing adapter)
(3) Raw bases: # of raw reads X sequence length
(4) Clean bases: # of clean bases X sequence length
(5) Error rate (%): base error rate of whole sequencing
(6) Q20 (%): (Base number of Phred values > 20) / (Total base number) *100
(7) Q30 (%): (Base number of Phred values > 30) / (Total base number) *100
(8) GC content (%): (G&C base number) / (Total base number)*100

Fusion Gene Discovery

Candidate fusion genes in $CD4^+$ PTCL cases as well as control sorted $CD4^+$ and $CD8^+$ lymphocytes were identified using FusionCatcher[265] v1.10 with default parameters. Strict filtering criteria was applied to identify the most biologically-relevant fusion genes in tumor samples. To identify tumor-specific fusion candidates, fusion pairs found in the control lymphocyte groups were excluded from tumor samples. A total of 697 unique fusion pairs were

identified in the control group. Having removed fusion transcripts present in control tissues, a total of 2,399 fusion candidates were identified in the 26 PTCL samples. In a given tumor, fusions with multiple predicted breakpoints involving the same gene partners were considered a single event, as previously described.[266]

Next, fusion genes were filtered on two criteria: fusion description and predicted effect. The fusion description is an output of FusionCatcher that describes the type of fusion event. Fusion candidates that were described as having a high probability of being a false positive were excluded from the candidate list. A list of the fusion descriptions that are associated with a high likelihood of false positivity and were used to excluded cases is provided in Table 5.2.

Candidate fusion genes were further selected to include only those involving exonic, coding sequence (CDS), and/or untranslated regions (UTR). Fusions that are considered in-frame have persevered reading frames for both partners, and are therefore potentially functional if translated. UTR's often contain regulatory elements that can alter the expression of genes they are positioned next to and therefore, a fusion event involving a UTR and protein-coding sequence also has potential to form a functional protein. Candidate fusions in which one of the gene partners was intergenic or intronic were removed from evaluation.

Fusion candidates that were recurrent or involved at least one cancer-associated gene were selected for further evaluation. Fusions were considered recurrent if the 3' fusion partner was identified in two or more tumor samples. To identify fusions in which one or both partners were cancer-associated genes, candidates were screened using the COSMIC cancer-gene census[194]. Fusion gene structure was evaluated using Geneious Prime 2020.0.5.

Table 5.2 Description of fusion events with high probability of being a false positive

Fusion Description Title	Description
Adjacent/Readthrough	Both genes forming the fusion are on the same strand and there are no other genes situated between them
Short_repeats	The sequence of the fusion junction contains a highly repetitive region containing repeating short sequences or polyA/C/G/T
Long_repeats	The sequence of the fusion junction contains a highly repetitive region containing repeating long sequences or polyA/C/G/T
Mt	One or both genes are situated on mitochondrion
Ribosomal	One or both gene is a gene encoding for ribosomal protein
Ensemble_partially overlapping	The genes forming the fusion gene are partially overlapping (on same strand or on different strands) according the Ensembl database.
Rt_circ_RNA	Reciprocal fusion genes which are also readthrough
Pseudo	One or both of the genes is a pseudogene

Differential Gene Expression

Sequences were aligned to CanFam3.1 genome using HISAT2.[182] HTseq[183] and DESeq2[184] were then used to quantify reads, normalize gene expression, and evaluate differentially expressed genes between tumor samples and controls. P-values were determined using a negative binomial distribution. A Benjamini-Hochberg procedure was used to correct p-values and padj<0.05 was considered the differentially expressed gene screening standard. Normalized gene expression of cancer-associated fusion partners was compared between cases with the fusion identified, cases without the fusion identified, and control T-cells.

Results

Fusion gene candidates were identified using FusionCatcher.[265] After applying the strict filtering criteria, 591 fusion candidates were identified in the 26 tumor samples.

Recurrent fusion events in which the 3'fusion partner was identified in more than one fusion candidate are summarized in Table 5.3. Fusion candidates with one gene partner encoding long non-coding RNA (lncRNA), retrotransposable elements, or fusions between two genes from similar gene families with similar functions were considered unlikely to be biologically significant, and removed from the analysis. Forty-three genes were identified as recurrent 3' fusion partners. The most commonly identified 3' fusion partners were MDK, PTMA, GNAS, EEF2, GATD3A, HMGB1, and MYH9.

The counts of common mapping reads, spanning pairs, spanning unique reads, and longest anchor found are listed for each fusion candidate in Table 5.3. The counts of common mapping reads identify the number of reads mapping simultaneously on both genes which form the fusion gene. This metric indicates the similarity of the DNA/RNA sequences of the two fusion gene partners. If the two genes forming the fusion have completely different sequences, this value should be zero, indicating a higher chance of being a true fusion event. All selected recurrent fusions have a count of common mapping reads of zero.

The spanning pairs metric counts the pairs of reads that support the fusion, including the multimapping reads. These reads map to the gene partners involved in the proposed fusion. The spanning unique reads is a count of the unique reads that map to the fusion junction. The longest anchor found indicates the longest sequence hangover found among the unique reads mapping on the fusion junction. Higher values for the spanning pairs, spanning unique reads, and longest anchor found help to remove false positives (Figure 5.2).[265,267]

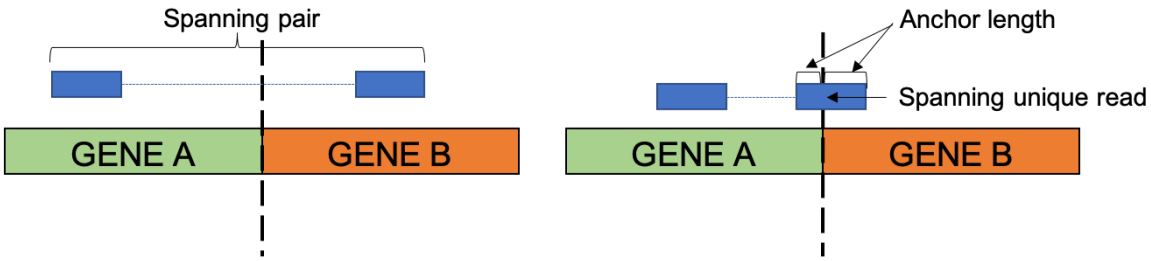

Figure 5.2 Schematics illustrating metrics used to characterize fusion candidates including spanning pairs, spanning unique reads, and longest anchor found. Adapted from Liu et al. 2016.

Normalized gene expression of the recurrent 3' fusion genes was subsequently evaluated in cases in which the fusion gene was identified compared to cases without the candidate fusion gene and control lymphocytes (Figure 5.3). Genes which exhibited aberrant expression in the cases with the fusion identified were considered more likely to produce possible driver fusion proteins. LSP1, TRIM8, GATD3A, and PTMA all exhibited increased expression in at least one of the patient samples with a fusion candidate involving the respective gene. Other fusion candidates of interest include 3' cancer-associated genes: GNAS, MYH9, XPO1, IKZF1, LMO4, JUN, and MDK (Table 5.4).

Table 5.3 Recurrent fusion genes identified in canine CD4$^+$ PTCL

CN	Fusion Candidate	5' Gene	3' Gene	CM	SP	SU	LA	5' Fusion_point	3' Fusion_point
76055	ENSCAFG00000000661-ENSCAFG00000000336	EZR	HNRNPH1	0	8	3	32	1:48176970:-	11:2059687:+
71779	ENSCAFG00000016306-ENSCAFG00000000336	ARAP2	HNRNPH1	0	3	3	29	3:75657733:+	11:2055916:+
71175	ENSCAFG00000006794-ENSCAFG00000000458	GTF3A	RAB21	0	6	2	34	25:12183372:-	10:13325416:+
71779	ENSCAFG00000017975-ENSCAFG00000000458	FAM219B	RAB21	0	3	2	40	30:37947583:-	10:13216897:+
60342	ENSCAFG00000013633-ENSCAFG00000010077	B2M	LSP1	0	9	3	27	30:11331865:+	18:46126859:+
69996	ENSCAFG00000014396-ENSCAFG00000010077	PPY	LSP1	0	10	2	34	9:19395171:+	18:46087948:+
71508	ENSCAFG00000000638-ENSCAFG00000000580	KLF10	YWHAZ	0	8	2	24	13:4223542:-	13:2760450:-
97578	ENSCAFG00000000638-ENSCAFG00000000580	KLF10	YWHAZ	0	13	3	29	13:4223542:-	13:2760450:-
71508	ENSCAFG00000000580-ENSCAFG00000000638	YWHAZ	KLF10	0	8	7	30	13:2763430:-	13:4220105:-
97578	ENSCAFG00000000580-ENSCAFG00000000638	YWHAZ	KLF10	0	13	3	26	13:2763430:-	13:4220105:-
71508	ENSCAFG00000000689-ENSCAFG00000000718	TUBGCP6	BRD1	0	11	3	25	10:17008020:+	10:17393422:+
71779	ENSCAFG00000000689-ENSCAFG00000000718	TUBGCP6	BRD1	0	9	3	22	10:17008020:+	10:17393422:+
100850	ENSCAFG00000014172-ENSCAFG00000000718	ZDHHC8	BRD1	0	7	2	30	26:29207807:-	10:17393422:+
69996	ENSCAFG00000018898-ENSCAFG00000001324	TAOK1	ATF4	0	6	2	32	9:43631429:+	10:25529195:-
100850	ENSCAFG00000019288-ENSCAFG00000001324	SSR4	ATF4	0	3	2	39	X:121613669:+	10:25530976:-
95512	ENSCAFG00000012315-ENSCAFG00000001630	TFAM	MYH9	0	6	4	34	4:10597916:+	10:28110256:+
71779	ENSCAFG00000016150-ENSCAFG00000001630	NR1D1	MYH9	0	4	2	35	9:22468461:+	10:28116611:+
104029	ENSCAFG00000017416-ENSCAFG00000001630	DENND4B	MYH9	0	5	2	31	7:43194960:+	10:28122813:+
95512	ENSCAFG00000017809-ENSCAFG00000001630	BCL11B	MYH9	0	8	3	34	8:67622861:-	10:28122190:+
71779	ENSCAFG00000003374-ENSCAFG00000023756	IKZF1	GNAS	0	6	2	30	18:1683965:+	24:43643409:+
100850	ENSCAFG00000016589-ENSCAFG00000023756	SRSF5	GNAS	0	7	3	36	8:43514223:+	24:43643409:+
100993	ENSCAFG00000016589-ENSCAFG00000023756	SRSF5	GNAS	0	6	3	37	8:43514223:+	24:43643409:+
97568	ENSCAFG00000013633-ENSCAFG00000023756	B2M	GNAS	0	6	6	40	30:11331865:+	24:43643409:+
97578	ENSCAFG00000019693-ENSCAFG00000023756	PTBP1	GNAS	0	6	2	37	20:57811498:-	24:43643409:+
67283	ENSCAFG00000024818-ENSCAFG00000023756	RACK1	GNAS	0	10	3	32	11:430867:-	24:43643409:+
100993	ENSCAFG00000005428-ENSCAFG00000002656	DYRK1B	EEF1A1	0	4	2	30	1:113798304:+	12:35577281:-
100993	ENSCAFG00000000336-ENSCAFG00000002656	HNRNPH1	EEF1A1	0	12	2	37	11:2059763:+	12:35579054:-
95591	ENSCAFG00000014413-ENSCAFG00000003050	SPOCK2	XPO1	0	4	3	37	4:22752884:-	10:61542482:-
100850	ENSCAFG00000028707-ENSCAFG00000003050	ITM2C	XPO1	0	5	3	24	25:42830052:+	10:61585054:-
65026	ENSCAFG00000032596-ENSCAFG00000006597	PTMA	HMGB1	0	10	9	29	25:43563385:+	25:9554184:+
97568	ENSCAFG00000032596-ENSCAFG00000006597	PTMA	HMGB1	0	5	2	27	25:43563385:+	25:9554184:+
100993	ENSCAFG00000032596-ENSCAFG00000006597	PTMA	HMGB1	0	16	10	29	25:43563385:+	25:9554184:+
101786	ENSCAFG00000032596-ENSCAFG00000006597	PTMA	HMGB1	0	10	4	28	25:43563385:+	25:9554184:+
100850	ENSCAFG00000003422-ENSCAFG00000003374	GRB10	IKZF1	0	38	3	28	18:1970944:-	18:1676646:+
100850	ENSCAFG00000016762-ENSCAFG00000003374	PCGF3	IKZF1	0	3	2	36	3:91676726:-	18:1732840:+
65026	ENSCAFG00000003374-ENSCAFG00000006889	IKZF1	CD44	0	9	3	28	18:1683965:+	18:32789707:-

97336	ENSCAFG00000003422-ENSCAFG00000006889	GRB10	CD44	0	6	2	30	18:1970944:-	18:32751720:-
100993	ENSCAFG00000016589-ENSCAFG00000031003	SRSF5	PTTG1IP	0	6	3	37	8:43514223:+	31:38503255:-
100993	ENSCAFG00000011049-ENSCAFG00000031003	FAM207A	PTTG1IP	0	19	2	29	31:38591996:+	31:38506663:-
71508	ENSCAFG00000005312-ENSCAFG00000005190	PGS1	SEPTIN9	0	6	2	21	9:2812326:-	9:3506846:-
60342	ENSCAFG00000009917-ENSCAFG00000005190	ABHD14A	SEPTIN9	0	4	2	23	20:37744387:-	9:3506846:-
69996	ENSCAFG00000001345-ENSCAFG00000013165	MATR3	PRPF6	0	3	2	34	11:26789895:+	24:47450709:+
71779	ENSCAFG00000011777-ENSCAFG00000013165	APH1A	PRPF6	0	4	2	39	17:59511020:-	24:47477399:+
71508	ENSCAFG00000010627-ENSCAFG00000006413	RASSF1	NCKAP1L	0	4	2	29	20:39016878:+	27:805784:-
69996	ENSCAFG00000009248-ENSCAFG00000006413	DGKZ	NCKAP1L	0	4	2	27	18:43088545:-	27:805656:-
60342	ENSCAFG00000009248-ENSCAFG00000020060	DGKZ	MDK	0	10	5	37	18:43088838:-	9:55100533:+
67308	ENSCAFG00000009248-ENSCAFG00000020060	DGKZ	MDK	0	18	2	40	18:43088833:-	9:55100533:+
97074	ENSCAFG00000009248-ENSCAFG00000020060	DGKZ	MDK	0	11	3	41	18:43088723:-	9:55100533:+
97336	ENSCAFG00000009248-ENSCAFG00000020060	DGKZ	MDK	0	8	2	31	18:43088838:-	9:55100533:+
100850	ENSCAFG00000009248-ENSCAFG00000020060	DGKZ	MDK	0	14	9	34	18:43088838:-	9:55100533:+
95591	ENSCAFG00000010551-ENSCAFG00000008933	CHEK1	NLRC5	0	4	2	40	5:8879255:-	2:59285583:-
95512	ENSCAFG00000023756-ENSCAFG00000008933	GNAS	NLRC5	0	6	2	34	24:43651280:+	2:59280850:-
97568	ENSCAFG00000009354-ENSCAFG00000020233	TOX2	LMO4	0	5	3	28	24:31523443:+	6:60906444:-
65026	ENSCAFG00000016589-ENSCAFG00000020233	SRSF5	LMO4	0	8	3	25	8:43514227:+	6:60906444:-
71779	ENSCAFG00000032596-ENSCAFG00000020233	PTMA	LMO4	0	7	4	28	25:43563385:+	6:60906444:-
69996	ENSCAFG00000010155-ENSCAFG00000010232	NFKB2	TRIM8	0	457	26	33	28:14910267:+	28:15136432:+
76055	ENSCAFG00000017764-ENSCAFG00000010232	KRI1	TRIM8	0	3	2	37	20:50613993:+	28:15135460:+
100850	ENSCAFG00000010899-ENSCAFG00000010865	HSPE1-MOB4	HSPD1	0	12	4	29	37:7035913:+	37:7020338:-
100993	ENSCAFG00000010899-ENSCAFG00000010865	HSPE1-MOB4	HSPD1	0	9	4	27	37:7035913:+	37:7020338:-
71508	ENSCAFG00000016034-ENSCAFG00000016010	TNRC18	FSCN1	0	9	3	28	6:12521202:+	6:12363346:-
95512	ENSCAFG00000048528-ENSCAFG00000016010	STAT1	FSCN1	0	4	2	34	37:1514448:-	6:12370804:-
76055	ENSCAFG00000005876-ENSCAFG00000012143	TACC1	NPEPL1	0	6	3	36	16:26710648:-	24:43470151:+
101786	ENSCAFG00000001546-ENSCAFG00000012143	MROH1	NPEPL1	0	9	2	21	13:37647046:+	24:43467691:+
100850	ENSCAFG00000001546-ENSCAFG00000041383	MROH1	GATD3A	0	8	3	27	13:37690507:+	31:38035219:+
97578	ENSCAFG00000004722-ENSCAFG00000041383	JPT1	GATD3A	0	6	3	29	9:5321847:+	31:38035219:+
100850	ENSCAFG00000013072-ENSCAFG00000041383	TPD52L2	GATD3A	0	8	4	30	24:47363544:+	31:38035219:+
101786	ENSCAFG00000019693-ENSCAFG00000041383	PTBP1	GATD3A	0	9	2	30	20:57818279:-	31:38035219:+
65026	ENSCAFG00000013054-ENSCAFG00000032596	ATG4B	PTMA	0	14	2	29	25:51514673:+	25:43566003:+
65026	ENSCAFG00000011037-ENSCAFG00000032596	NCL	PTMA	0	10	2	26	25:43340008:-	25:43566003:+
100993	ENSCAFG00000011037-ENSCAFG00000032596	NCL	PTMA	0	20	9	28	25:43340008:-	25:43566003:+
97568	ENSCAFG00000006597-ENSCAFG00000032596	HMGB1	PTMA	0	5	2	28	25:9552010:+	25:43566003:+
100993	ENSCAFG00000006597-ENSCAFG00000032596	HMGB1	PTMA	0	16	2	21	25:9556607:+	25:43566390:+
100993	ENSCAFG00000009885-ENSCAFG00000032596	JARID2	PTMA	0	7	2	24	35:14477306:+	25:43566003:+
95512	ENSCAFG00000031204-ENSCAFG00000032596	RGS10	PTMA	0	5	4	35	28:29688064:-	25:43563253:+
100993	ENSCAFG00000013689-ENSCAFG00000032596	RFC4	PTMA	0	3	2	40	34:19374779:-	25:43563189:+
97074	ENSCAFG00000001709-ENSCAFG00000032596	MCM5	PTMA	0	4	2	35	10:28722768:-	25:43567242:+
100993	ENSCAFG00000016589-ENSCAFG00000032596	SRSF5	PTMA	0	13	3	35	8:43514223:+	25:43566003:+
97074	ENSCAFG00000005437-ENSCAFG00000013054	SLCO2B1	ATG4B	0	3	2	37	21:23372107:-	25:51517290:+
100850	ENSCAFG00000032596-ENSCAFG00000013054	PTMA	ATG4B	0	6	2	35	25:43563385:+	25:51504539:+
60342	ENSCAFG00000007137-ENSCAFG00000014309	TOX	RASGRP2	0	6	2	29	29:9841497:-	18:52414263:+
71779	ENSCAFG00000032596-ENSCAFG00000014309	PTMA	RASGRP2	0	9	3	26	25:43563385:+	18:52414263:+
100850	ENSCAFG00000032596-ENSCAFG00000014309	PTMA	RASGRP2	0	9	2	27	25:43563385:+	18:52414263:+
71779	ENSCAFG00000013013-ENSCAFG00000014309	RNF168	RASGRP2	0	6	2	21	33:29627903:-	18:52414263:+
100850	ENSCAFG00000019517-ENSCAFG00000014309	MAN1B1	RASGRP2	0	7	2	26	9:48540410:+	18:52414263:+
100850	ENSCAFG00000016628-ENSCAFG00000016129	EIF4A1	EIF5A	0	6	2	28	5:32492527:+	5:32270433:+
71508	ENSCAFG00000016984-ENSCAFG00000016129	PER1	EIF5A	0	7	2	24	5:32968315:-	5:32270433:+
100993	ENSCAFG00000018147-ENSCAFG00000016129	SS18	EIF5A	0	6	3	28	7:62491489:+	5:32270433:+
67283	ENSCAFG00000012916-ENSCAFG00000016568	S100A11	ADAM10	0	6	3	38	17:61021556:-	30:23607379:-
95512	ENSCAFG00000001399-ENSCAFG00000016568	HNRNPK	ADAM10	0	5	3	35	1:75510496:+	30:23635480:-
97568	ENSCAFG00000011659-ENSCAFG00000016762	ATP9A	PCGF3	0	4	2	25	24:37817969:-	3:91684117:-
100850	ENSCAFG00000015152-ENSCAFG00000016762	CAPZB	PCGF3	0	4	2	23	2:79296763:+	3:91704666:-
71508	ENSCAFG00000017516-ENSCAFG00000018285	CALM1	KLC1	0	9	3	23	8:61398437:+	8:71443489:+
76392	ENSCAFG00000010450-ENSCAFG00000018285	SLC37A1	KLC1	0	3	2	28	31:36828738:+	8:71443489:+
97568	ENSCAFG00000008921-ENSCAFG00000018437	NEK4	RAI1	0	4	2	37	20:37091735:+	5:41699555:-
97568	ENSCAFG00000043502-ENSCAFG00000018437	OBSCURIN	RAI1	0	4	3	38	14:737566:-	5:41703579:-
101786	ENSCAFG00000007215-ENSCAFG00000018897	YTHDF3	JUN	0	3	3	36	29:13240194:+	5:50967308:-
67283	ENSCAFG00000019639-ENSCAFG00000018897	VBP1	JUN	0	9	4	40	X:123216276:+	5:50968371:-
100993	ENSCAFG00000032596-ENSCAFG00000019158	PTMA	EEF2	0	5	2	34	25:43567427:+	20:55581740:+
98458	ENSCAFG00000012687-ENSCAFG00000019158	EIF4G1	EEF2	0	8	3	39	34:17204102:+	20:55585972:+
71508	ENSCAFG00000015532-ENSCAFG00000019158	MYO9B	EEF2	0	6	2	33	20:45525613:-	20:55580985:+
71312	ENSCAFG00000016522-ENSCAFG00000019158	PLOD1	EEF2	0	8	2	33	2:84326004:-	20:55578680:+
95591	ENSCAFG00000032222-ENSCAFG00000019158	DLA-12	EEF2	0	10	2	35	12:935460:+	20:55578635:+
71175	ENSCAFG00000042696-ENSCAFG00000019158	THYMOSIN BETA 4	EEF2	0	7	2	40	20:6016910:-	20:55583511:+
60342	ENSCAFG00000005204-ENSCAFG00000019346	CTNNB1	SRRM2	0	4	2	41	23:10572354:+	6:38306369:+
97336	ENSCAFG00000007875-ENSCAFG00000019346	TMSB10	SRRM2	0	6	2	36	17:40048895:-	6:38301717:+
101786	ENSCAFG00000012045-ENSCAFG00000019448	PCNT	ABHD17A	0	3	2	30	31:39626139:+	20:57086800:+
65026	ENSCAFG00000019648-ENSCAFG00000019448	TMEM259	ABHD17A	0	3	2	24	20:57695359:+	20:57086800:+
71175	ENSCAFG00000013589-ENSCAFG00000025045	IVNS1ABP	HNRNPD	0	6	2	27	7:18443461:-	32:6323770:-
69996	ENSCAFG00000001704-ENSCAFG00000025045	APOL6	HNRNPD	0	8	3	39	10:28535182:-	32:6340742:-
95512	ENSCAFG00000009389-ENSCAFG00000025145	NISCH	ZNF777	0	3	2	29	20:37312413:-	16:14388958:-
97568	ENSCAFG00000010958-ENSCAFG00000025145	RIN3	ZNF777	0	5	2	30	8:1746136:+	16:14388958:-
100993	ENSCAFG00000001181-ENSCAFG00000025145	TRAPPC9	ZNF777	0	4	2	22	13:34686848:-	16:14388958:-
95591	ENSCAFG00000029183-ENSCAFG00000029191	EIF1B	STMN1	0	6	2	36	23:9800563:+	2:74042893:+
96300	ENSCAFG00000001618-ENSCAFG00000029191	CCND3	STMN1	0	6	2	28	12:10599352:-	2:74042952:+
100850	ENSCAFG00000005692-ENSCAFG00000031449	RPTOR	UBE2I	0	5	2	25	9:1028499:-	6:39447817:-
100993	ENSCAFG00000019581-ENSCAFG00000031449	UNKL	UBE2I	0	24	9	41	6:39394207:+	6:39447817:-
98458	ENSCAFG00000029086-ENSCAFG00000032222	ARF4	DLA-12	0	4	2	40	20:32870570:+	12:935192:+
69996	ENSCAFG00000049487-ENSCAFG00000032222	NRM	DLA-12	0	6	2	35	12:490872:-	12:983548:+

Abbreviations: CN: Case number, CM: counts of common mapping reads, SP: spanning pairs, SU: spanning unique reads, LA: longest anchor found

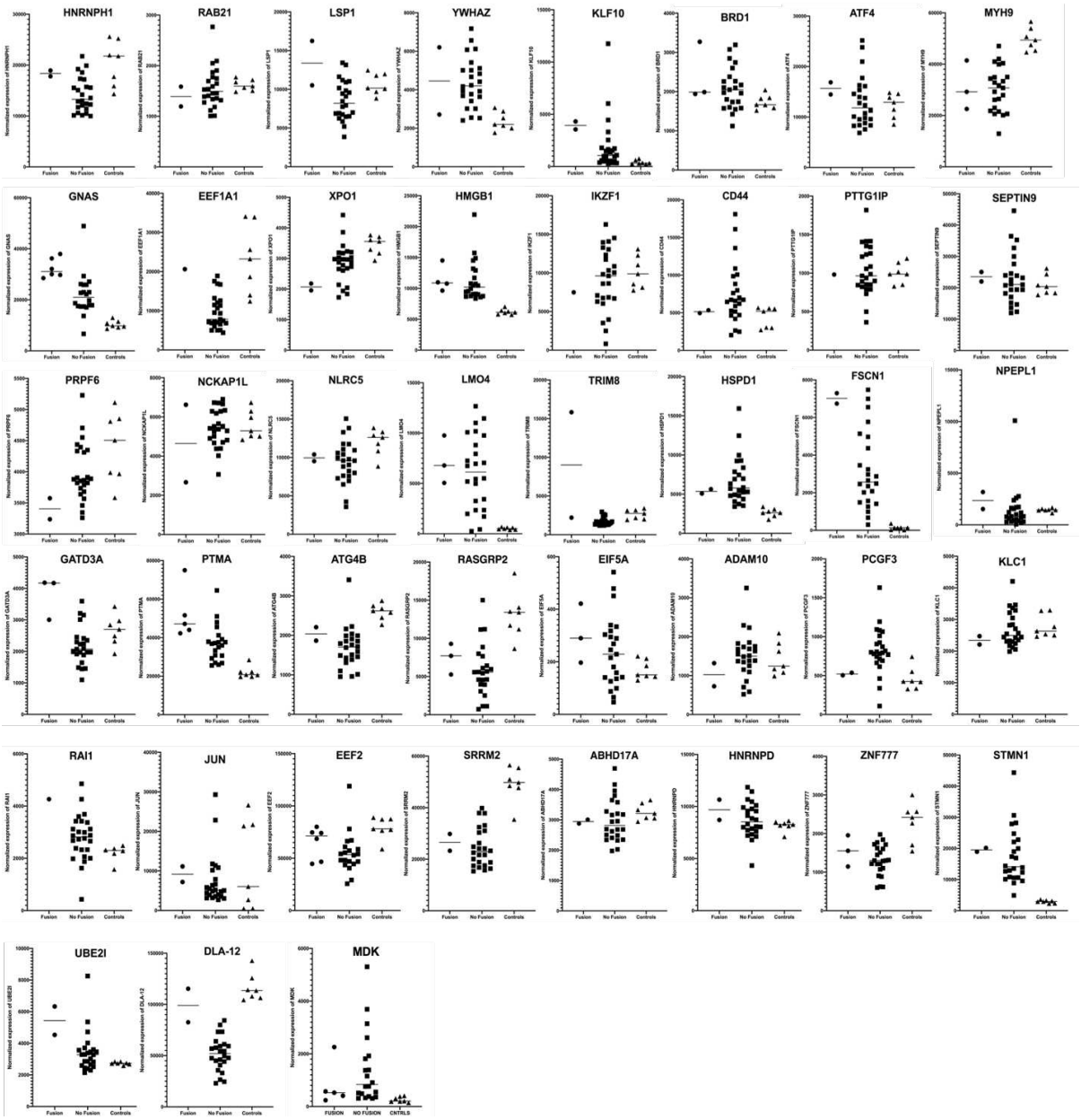

Figure 5.3 Expression of recurrent 3' fusion partners. 43 recurrent 3' fusion partners were identified. Normalized gene expression levels (DESeq2) were compared between cases in which the fusion was identified (circles), cases without the fusion (squares), and control lymphocytes (triangles).

Table 5.4. Selected recurrent candidate fusion genes

CN	5' Gene	3' Gene	5' Fusion_point	3' Fusion_point	Fusion Sequence
101786	YTHDF3	JUN	29:13240194:+	5:50967308:-	CTGCTGTGAGTGCTCGGGGAGAGGCCCAGGCGGCGGCGGCGGCGGCGGC*G AGCTTTGCAAAAGTTCGCTCCGGGACCCGGGCCACTCGTCCCCTGTGCT
67283	VBP1	JUN	X:123216276:+	5:50968371:-	GATACAGTGCTGAAGAAGCTGGATGAACAGTACCAGAAGTACAAGTTTAT*C CGCTGCTCAGCGCGCCCGGGTTGAAGTTGCTGAGGTTGGCGTAGACCGG
65026	ATG4B	PTMA	25:51514673:+	25:43566003:+	CAGCAGGATGAGCATCGGGGAGCTCGACCCGTCCATTGCCGTG*GACTTAAA GGAGAAGAAGGAAGTTGTGGAGGAGGCAGAGAATG
65026	NCL	PTMA	25:43340008:-	25:43566003:+	CACTCCGCCGGCATAAGCCGCCATCATGGTGAAGCTCGCAAAG*GACTTAAA GGAGAAGAAGGAAGTTGTGGAGGAGGCAGAGAATG
100993	NCL	PTMA	25:43340008:-	25:43566003:+	CACTCCGCCGGCATAAGCCGCCATCATGGTGAAGCTCGCAAAG*GACTTAAA GGAGAAGAAGGAAGTTGTGGAGGAGGCAGAGAATG
97568	HMGB1	PTMA	25:9552010:+	25:43566003:+	TGAGAGCCAGACGGGCACTGGGCGACTCTGTGCCTCGCTGAGG*GACTTAAA GGAGAAGAAGGAAGTTGTGGAGGAGGCAGAGAATG
100993	HMGB1	PTMA	25:9556607:+	25:43566390:+	AAGACGAGGAGGATGAAGAGGATGAGGAGGAGGAAGAAGATGAAGAAGAT* GAAGAAGAGGAGGAGGAGGAAGGTGATGGTGAGTAGCCTTGTTTGTCTCC
100993	JARID2	PTMA	35:14477306:+	25:43566003:+	GAGCAAGGAAAGACCCAAGAGGAATATCATTCAGAAGAAATAC*GACTTAAA GGAGAAGAAGGAAGTTGTGGAGGAGGCAGAGAATG
95512	RGS10	PTMA	28:29688064:-	25:43563253:+	ACAAGTCAACGTCGAGGGGCAGTCCCGGCTCAATGAGAAGATACTGGAAG*C CGCGGACTCCGGCAGCTCCCTCGCCAGAGTCCTCGAACTCTTGCTCTCT
100993	RFC4	PTMA	34:19374779:-	25:43563189:+	AAACCACCACTGAAGGATCGAGGAATAGCTGCCACAGCTGGAAGCAGTGG*G CATTGTTCCTGTGTCCGGCTCCCCGTTCGCCGCAACCACCTCCGCCGCG
97074	MCM5	PTMA	10:28722768:-	25:43567242:+	GCTTTACCAGCCAGGAGGACCAGGAGCTTCTGAGCCGCATCGAGAAGCAG*G ACGTCGACACCAAGAAGCAGAAGACTGATGAGGATGACTAGACAGCAAA
100993	SRSF5	PTMA	8:43514223:+	25:43566003:+	CGTCGCAGACTACGGACCTCTCTGGTCTCAGCTGCCAAAGATCCTGTCCG*GA CTTAAAGGAGAAGAAGGAAGTTGTGGAGGAGGCAGAGAATGGAAGAGA
97568	TOX2	LMO4	24:31523443:+	6:60906444:-	GCCGGCCGGCCTGGCGCACCTGGACTATTACCACTGCGGCAAG*ACCATGGTG AATCCGGGCAGCAGCTCACAGCCGCCCCCCGTGA
65026	SRSF5	LMO4	8:43514227:+	6:60906444:-	ACGGACCTCTCTGGTCTCAGCTGCCAAAGATCCTGTCCGGTAG*ACCATGGTG AATCCGGGCAGCAGCTCACAGCCGCCCCCCGTGA
71779	PTMA	LMO4	25:43563385:+	6:60906444:-	GTCAGACGCGGCCGTGGACACCAGCTCCGAGATCACCACCAAG*ACCATGGT GAATCCGGGCAGCAGCTCACAGCCGCCCCCCGTGA
69996	NFKB2	TRIM8	28:14910267:+	28:15136432:+	CCCCCTGAGCCACCAGGAGGGCTCTGCCATGGGCACCCCCAGCCTCAG*AAC ACCAAGTCTGTGAAAATCCTAATGGACAGGTGAGCAGATGACCACTG
76055	KRI1	TRIM8	20:50613993:+	28:15135460:+	ATCCTCCGTGCGCCGCAAGGATGAGCGCAGGAAGGAGAAGAGAGAGGAGA* TGCTGGATGAGGACCTGCGGCAGACGGTTGAGGTCCTGGACAAGGCCCAG
60342	DGKZ	MDK	18:43088838:-	9:55100533:+	AGCACTACCAGATGATCCAGCGGGAGGACCAAGAGACGGCCGTGTAGCTG*A TGCAGCTCCGAGGCTTCCTCCTCCTCGCCCTCCCCACCCTGCTGGCGCT
67308	DGKZ	MDK	18:43088833:-	9:55100533:+	TACCAGATGATCCAGCGGGAGGACCAAGAGACGGCCGTGTAGCTGTGAGG*A TGCAGCTCCGAGGCTTCCTCCTCCTCGCCCTCCCCACCCTGCTGGCGCT
97074	DGKZ	MDK	18:43088723:-	9:55100533:+	TGCACTGCCACATTCCAGTCGGACTGCCACGGGGGGACCCAGGCCCCAGG*A TGCAGCTCCGAGGCTTCCTCCTCCTCGCCCTCCCCACCCTGCTGGCGCT
97336	DGKZ	MDK	18:43088838:-	9:55100533:+	AGCACTACCAGATGATCCAGCGGGAGGACCAAGAGACGGCCGTGTAGCTG*A TGCAGCTCCGAGGCTTCCTCCTCCTCGCCCTCCCCACCCTGCTGGCGCT
100850	DGKZ	MDK	18:43088838:-	9:55100533:+	AGCACTACCAGATGATCCAGCGGGAGGACCAAGAGACGGCCGTGTAGCTG*A TGCAGCTCCGAGGCTTCCTCCTCCTCGCCCTCCCCACCCTGCTGGCGCT
100850	GRB10	IKZF1	18:1970944:-	18:1676646:+	CCAGGCTTCCCGGCGCCGGCCGACCGGCTCACAGGCCACCAGG*ATAACCTG AGGACAATGGATGCTGATGAGGGTCAAGACATGTC
100850	PCGF3	IKZF1	3:91676726:-	18:1732840:+	AACACTTCACAGTCTCAGCGGCCGGAGAGGCGCCTCTCGCAGACTAGATG*G GGAGCGGCCCTTCCAGTGCAACCAGTGCGGCGCCTCCTTCACGCAGAAG
95591	SPOCK2	XPO1	4:22752884:-	10:61542482:-	TGGTTCCAGCTCCTTCATGAGAACGCCAAGCAGAATGGCTCGGCCGGCAG*G GATATTTGTCGACCAAAATGATGCCAATTTGTAAATTAAAATGTCACCT
100850	ITM2C	XPO1	25:42830052:+	10:61585054:-	GGCCCCGGCTCCGGCCGCTGAGATCCTGCTGACGCCGGCTCGG*TAATCTATG CCAGCAATTATGACAATGTTAGCAGACCATGCAG
71779	IKZF1	GNAS	18:1683965:+	24:43643409:+	TTCCACCACATCTGGCGGACAGCAGACCTCCAAGAATGAGAGAGGCGTGG*G TGCCGGAGAATCTGGTAAAAGCACCATTGTGAAGCAGATGAGGATCCTG
100850	SRSF5	GNAS	8:43514223:+	24:43643409:+	CGTCGCAGACTACGGACCTCTCTGGTCTCAGCTGCCAAAGATCCTGTCCG*GT GCCGGAGAATCTGGTAAAAGCACCATTGTGAAGCAGATGAGGATCCTG
100993	SRSF5	GNAS	8:43514223:+	24:43643409:+	CGTCGCAGACTACGGACCTCTCTGGTCTCAGCTGCCAAAGATCCTGTCCG*GT GCCGGAGAATCTGGTAAAAGCACCATTGTGAAGCAGATGAGGATCCTG
97568	B2M	GNAS	30:11331865:+	24:43643409:+	GGCCTTGCTCCTCATCCTCCTCGCTGCGTGCCGCCTGGATGCCGTGCAGC*GTG CCGGAGAATCTGGTAAAAGCACCATTGTGAAGCAGATGAGGATCCTG
97578	PTBP1	GNAS	20:57811498:-	24:43643409:+	CTCTGGCGACAGCCAGCCCTCGCTGGACCAGACCATGGCTGCTGCCTTCG*GT GCCGGAGAATCTGGTAAAAGCACCATTGTGAAGCAGATGAGGATCCTG
67283	RACK1	GNAS	11:430867:-	24:43643409:+	GATCGCCACCACTCCCCAATTCCCAGACATGATACTGTCTGCTTCTCGAG*GT GCCGGAGAATCTGGTAAAAGCACCATTGTGAAGCAGATGAGGATCCTG
95512	TFAM	MYH9	4:10597916:+	10:28110256:+	GTTATTATAATGAAATGAAATCTTGGGAAGAAACAGATGATGGAAGTCGGA*G GGGACTCCACCGACCTCAATGACCAGATCGCCGAGCTGCAGGCTCAGAT
71779	NR1D1	MYH9	9:22468461:+	10:28116611:+	GGGAGCCTGGACGTGTGTGGCCTGTTCGGGGAAGGAGAATGGCCCTGTGG*G ATGGAGGCTGAGCTGGAGGACGAGAAGAAGCAGCGCTCGATGGCTGTGG
104029	DENND4B	MYH9	7:43194960:+	10:28122813:+	TCCTTCCCGCCGCTCCCCCGCCTCTCATGTTCCCCCACCTGAGCTGCCCC*CCA GTTGCTGTCACAAAGGAGTGAACGGAGCTCCCAGCCCCACCCCTTTT
95512	BCL11B	MYH9	8:67622861:-	10:28122190:+	TGTGCAACTACGCGTGCGCGCAGAGCAGCAAGCTCACGCGCCACATGAAG*G CGCCACTGTCCCCTCCTGTTTCTAAAGTGTCTCAAGTGCAATGACGACC
60342	B2M	LSP1	30:11331865:+	18:46126859:+	CTCCTCATCCTCCTCGCTGCGTGCCGCCTGGATGCCGTGCAGC*CTCTCCTGAG ACTACAGGTGCCTCTGGCAGCAGCGTCCACGTC
69996	PPY	LSP1	9:19395171:+	18:46087948:+	ACCAGAGCAGATGGCCCAGTACGCGGCTGAGCTCCGCAGATACATCAACA*C GACGCCAGCCCAATGGCCGAGGCTCCGAGCCACCCCAGCTCCGAGGAGC
100850	MROH1	GATD3A	13:37690507:+	31:38035219:+	CGGTGGTCACCAGCCTCCTGGGAAGCCCCCTGCCCTTTGACAG*CTTGTGCTG CATCGCGTCTGTCCTCGCAGCCAAAGTGCTCCAT
97578	JPT1	GATD3A	9:5321847:+	31:38035219:+	CCACCTTCAAGGGAGTCGATCCCAACAGCAGGAATAGCTCTCG*CTTGTGCTG CATCGCGTCTGTCCTCGCAGCCAAAGTGCTCCAT

100850	TPD52L2	GATD3A	24:47363544:+	31:38035219:+	CCACCGTGGGCTCCGCCATTAGCAGGAAGCTCGGGGATATGAG*CTTGTGCTG CATCGCGTCTGTCCTCGCAGCCAAAGTGCTCCAT
101786	PTBP1	GATD3A	20:57818279:-	31:38035219:+	TCCACTCCGTCCCCTGCGGGTCTCCTCTGTGTGCAATGGACGG*CTTGTGCTGC ATCGCGTCTGTCCTCGCAGCCAAAGTGCTCCAT

Structural Analysis of Fusion Genes

The structural features of the selected fusion candidates from Table 5.3 were evaluated using Geneious Prime 2020.0.5 software. For each fusion partner, the fusion junction sequence was mapped to the reference genome (CanFam3.1). The chromosomal alignment and junction point were identified and junction sequences for both gene sequences were concatenated to create the complete fusion junction sequence.

DGKZ-MDK, was identified in 5 of the 26 evaluated cases (19%). The predicted fusion sequence is illustrated in Figure 5.4. MDK is an oncogene that is highly expressed by a number of tumors.[268,269] DGKZ is located on the reverse strand of chromosome 18 and MDK is located on the forward strand of chromosome 9. Therefore, the formation of a functional fusion transcript would require an inversion event. Among the 5 cases, there were 3 different breakpoints for the DGKZ gene and a single, recurrent breakpoint for the MDK gene. The breakpoint involving MDK is at the beginning of the coding sequence of this protein. This gene has 1 exon and 1 splice variant and therefore, transcription of the entire coding sequence (CDS) of this gene is likely occur.

Of the five total cases, three cases have a DGKZ breakpoint on chromosome 18 at 43088838. The other two breakpoints are within the same region of the gene (18:43088833 and 18:43088723). The fusion junction in all cases of DGKZ involves the 3' UTR with or without the end of the CDS of this gene. Two of the five samples (60342 and 100850) have greater than or equal to 5 spanning unique reads, supportive of a higher likelihood of being a true positive. Because the fusion transcripts involve the entire DGKZ CDS and a portion of the 3' UTR, the

DGKZ stop codon (TAG) is present within the fusion sequence. This finding has the potential to complicate effective translation of the fusion protein.

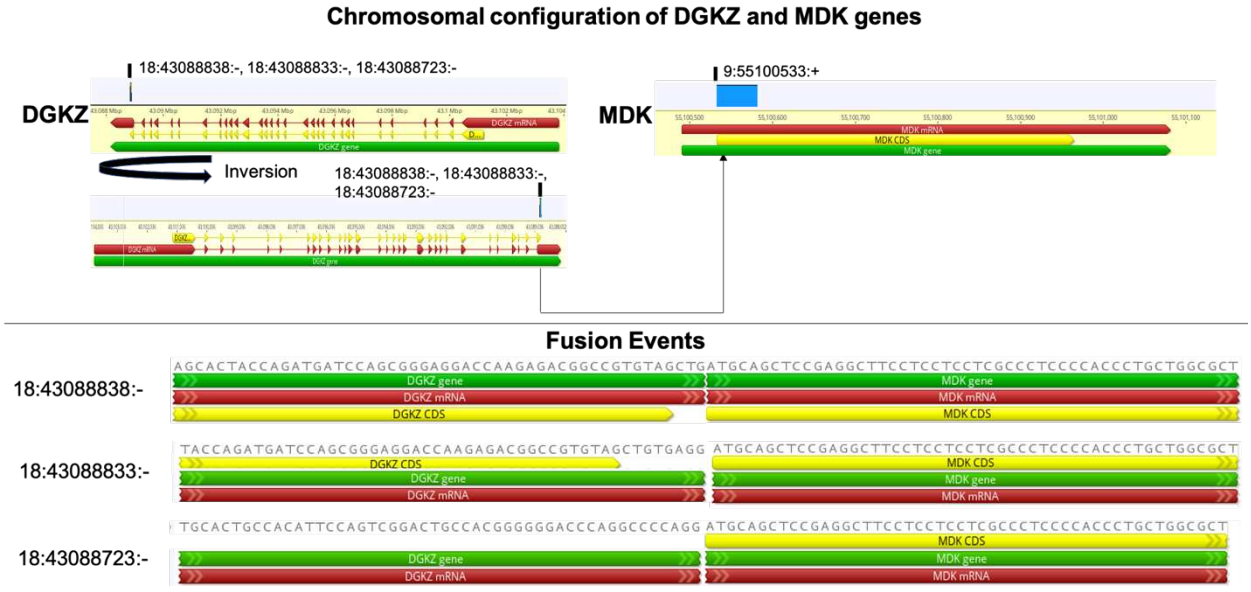

Figure 5.4. Structure of the DGKZ-MDK fusion gene. The gene structures of DGKZ and MDK are shown with the gene sequences in green, mRNA in red, and coding sequence in yellow. The alignment of the mRNA sequence identified by RNA-seq is shown in blue and the fusion junction points are shown on the top of the aligned sequences. DGKZ is on the reverse strand of chromosome 18 and MDK is on the forward strand of chromosome 9. An inversion of DGKZ is therefore necessary for the fusion gene to form. The predicted fusion junction sequence is shown for the three different junction points of the 5' DGKZ fusion partner.

PTMA (prothymosin-alpha) was identified as a 3' fusion partner in 10 fusion candidates from 5 patients. PTMA is present in both lymphoid and non-lymphoid organs and has dual roles controlling the cell cycle and modulating immune responses.[270] Eight different genes (ATG4B, HMGB1, JARID2, MCM5, NCL, SRSF5, RFC4, RGS10) were identified as fusion partners. The predicted fusion sequences are illustrated in Figure 5.5.

The predicted fusions involving ATG4B-PTMA, NCL-PTMA, JARID2-PTMA, and MCM5-PTMA are comprised of the 5'UTR and 5' CDS of the first fusion partner joining with the truncated CDS and 3' UTR of PTMA. This type of fusion construct could result in the regulatory elements of the 5' gene driving expression of the 3' gene. Alternatively, a chimeric protein could be formed. Because the PTMA CDS is truncated, evaluation of the open reading

frame and alterations of the protein structure and function would need to be evaluated. The number of spanning unique reads of the NCL-PTMA fusion is greater than 5, supporting a higher likelihood of being a true positive. Additionally, 1 of the 5 individuals (97568) with the candidate fusion gene involving a 3' PTMA partner exhibited concurrent upregulation of PTMA compared to other cases and control T-cells (Figure 5.3). The 5' fusion partner in this case was MCM5.

The SRSF5-PTMA fusion involves only the 5' UTR joining with the truncated PTMA CDS. This construct could also functionally enable PTMA expression to be driven by the SRSF5 5' regulatory units. The RGS10-PTMA and RFC4-PTMA fusion candidates involve the 5' ends of RGS10 or RFC4 fusing to the 5' UTR of PTMA. In these cases, the complete PTMA CDS has potential to be translated and form a complete PTMA protein, if the open-reading frame remains in-tact.

One of the fusion transcripts involving HMGB1-PTMA (5' fusion breakpoint 25:9556607) involves the 5' end of HMGB1 CDS fusing to the shortened PTMA CDS. The other HMGB1-PTMA fusion transcript (5' fusion breakpoint 25:9552010) involves the fusion of the HMGB1 3' UTR to the truncated PTMA CDS. This fusion would likely involve a fully transcribed HMGB1 gene with an intact stop codon. It is therefore, uncertain, if translation would continue beyond the HMGB1 stop codon.

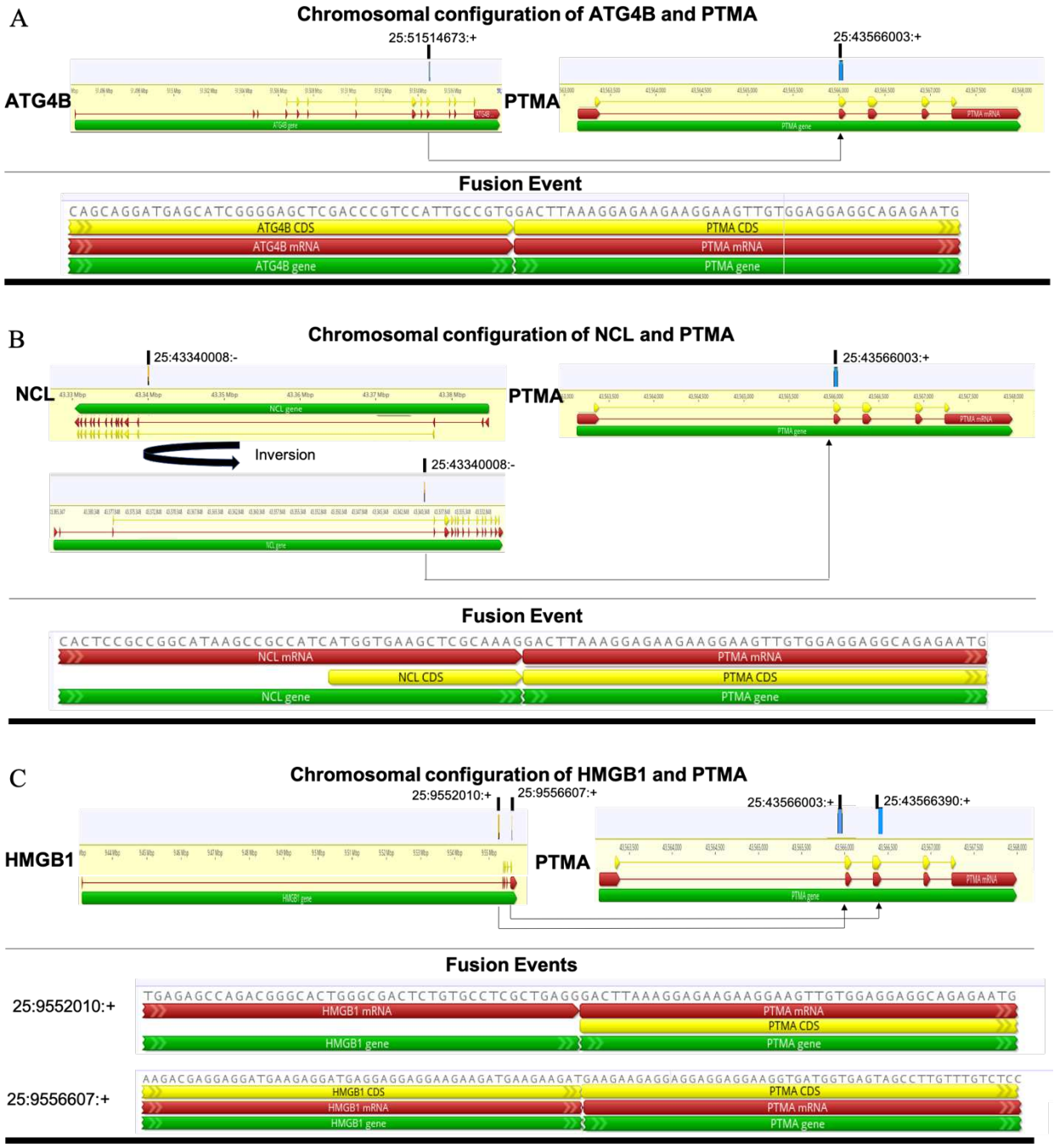
A
Chromosomal configuration of ATG4B and PTMA
25:51514673:+
25:43566003:+
ATG4B
PTMA
Fusion Event
CAGCAGGATGAGCATCGGGGAGCTCGACCCGTCCATTGCCGTGGACTTAAAGGAGAAGAAGGAAGTTGTGGAGGAGGCAGAGAATG
ATG4B CDS
PTMA CDS
ATG4B mRNA
PTMA mRNA
ATG4B gene
PTMA gene
B
Chromosomal configuration of NCL and PTMA
25:43340008:-
25:43566003:+
NCL
PTMA
Inversion
25:43340008:-
Fusion Event
CACTCCGCCGGCATAAGCCGCCATCATGGTGAAGCTCGCAAAGGACTTAAAGGAGAAGAAGGAAGTTGTGGAGGAGGCAGAGAATG
NCL mRNA
PTMA mRNA
NCL CDS
PTMA CDS
NCL gene
PTMA gene
C
Chromosomal configuration of HMGB1 and PTMA
25:9552010:+
25:9556607:+
25:43566003:+
25:43566390:+
HMGB1
PTMA
Fusion Events
25:9552010:+
TGAGAGCCAGACGGGCACTGGGCGACTCTGTGCCTCGCTGAGGGACTTAAAGGAGAAGAAGGAAGTTGTGGAGGAGGCAGAGAATG
HMGB1 mRNA
PTMA mRNA
PTMA CDS
HMGB1 gene
PTMA gene
25:9556607:+
AAGACGAGGAGGATGAAGAGGATGAGGAGGAGGAAGAAGATGAAGAAGATGAAGAAGAGGAGGAGGAAGGTGATGGTGAGTAGCCTTGTTTGTCTCC
HMGB1 CDS
PTMA CDS
HMGB1 mRNA
PTMA mRNA
HMGB1 gene
PTMA gene

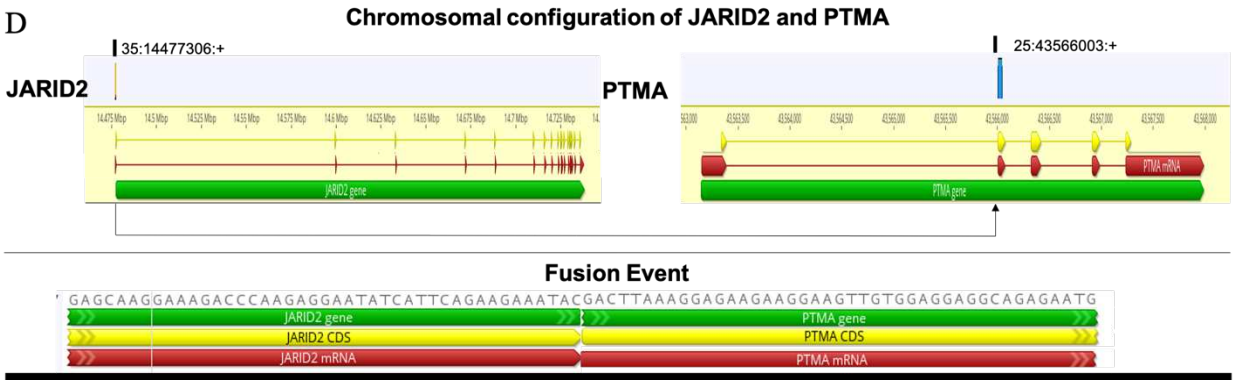
D
Chromosomal configuration of JARID2 and PTMA
JARID2
35:14477306:+
PTMA
25:43566003:+
JARID2 gene
PTMA mRNA
PTMA gene
Fusion Event
GAGCAAGGAAAGACCCAAGAGGAATATCATTCAGAAGAAATACGACTTAAAGGAGAAGAAGGAAGTTGTGGAGGAGGCAGAGAATG
JARID2 gene
JARID2 CDS
JARID2 mRNA
PTMA gene
PTMA CDS
PTMA mRNA

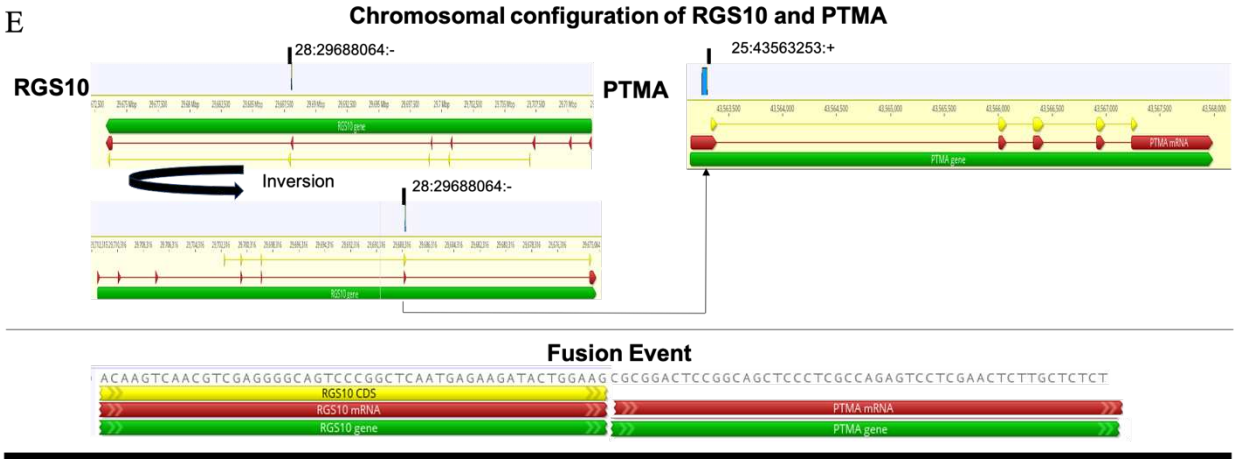
E
Chromosomal configuration of RGS10 and PTMA
RGS10
28:29688064:-
PTMA
25:43563253:+
Inversion
28:29688064:-
RGS10 gene
PTMA mRNA
PTMA gene
Fusion Event
ACAAGTCAACGTCGAGGGGCAGTCCCGGCTCAATGAGAAGATACTGGAAGCGCGGACTCCGGCAGCTCCCTCGCCAGAGTCCTCGAACTCTTGCTCTCT
RGS10 CDS
RGS10 mRNA
RGS10 gene
PTMA mRNA
PTMA gene

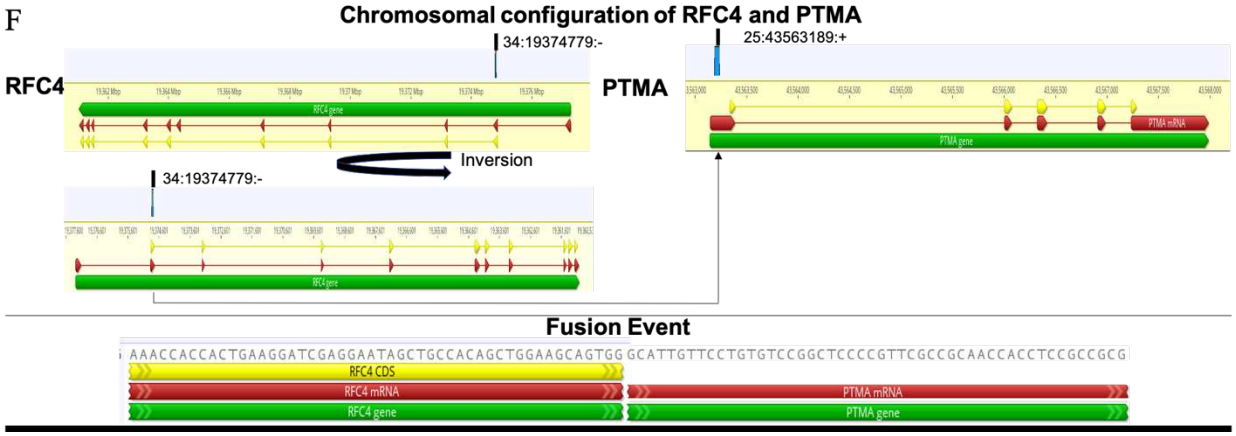
F
Chromosomal configuration of RFC4 and PTMA
RFC4
34:19374779:-
PTMA
25:43563189:+
Inversion
34:19374779:-
RFC4 gene
PTMA mRNA
PTMA gene
Fusion Event
AAACCACCACTGAAGGATCGAGGAATAGCTGCCACAGCTGGAAGCAGTGGGCATTGTTCCTGTGTCCGGCTCCCCGTTCGCCGCAACCACCTCCGCCGCG
RFC4 CDS
RFC4 mRNA
RFC4 gene
PTMA mRNA
PTMA gene

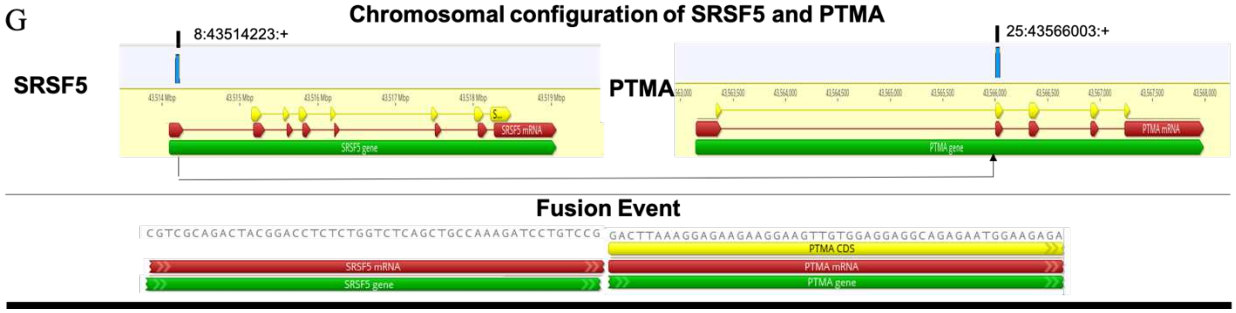
G
Chromosomal configuration of SRSF5 and PTMA
SRSF5
8:43514223:+
PTMA
25:43566003:+
SRSF5 mRNA
SRSF5 gene
PTMA mRNA
PTMA gene
Fusion Event
CGTCGCAGACTACGGACCTCTCTGGTCTCAGCTGCCAAAGATCCTGTCCGGACTTAAAGGAGAAGAAGGAAGTTGTGGAGGAGGCAGAGAATGGAAGAGA
PTMA CDS
SRSF5 mRNA
SRSF5 gene
PTMA mRNA
PTMA gene

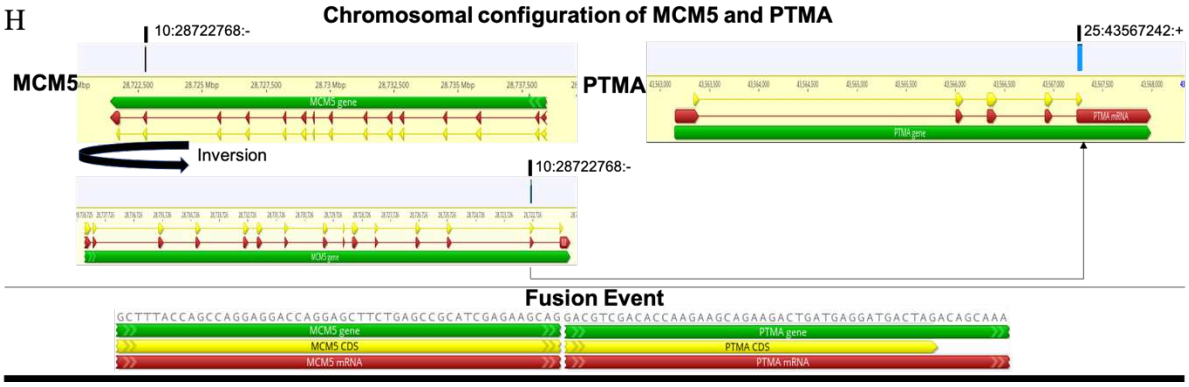

Figure 5.5. Structure of the fusion genes involving PTMA as a 3' fusion partner. The gene structures and predicted fusion junction sequence is illustrated from the following fusion genes ATG4B-PTMA (A), NCL-PTMA (B), HMGB1-PTMA (C), JARID2-PTMA (D), RGS10-PTMA (E), RFC4-PTMA (F), SRSF5-PTMA (G), MCM5-PTMA (H). The gene structures of are shown with the gene sequences in green, mRNA in red, and coding sequence in yellow. The alignment of the mRNA sequence identified by RNA-seq is shown in blue and the fusion junction points are shown on the top of the aligned sequences. The fusion junction sequence is shown below.

JUN, a well-established oncogenic transcription factor, and key regulator of cell cycle progression, was identified as a 3' fusion partner in two cases. JUN was partnered with YTHDF3 and VBP1, respectively (Figure 5.6). The fusion junction sequence identified by RNA-seq involves the reverse complement sequence, suggesting that an inversion event and complex chromosomal rearrangement likely took place. Alternatively, this finding could be an artifact of an unstranded library preparation. In the YTHDF3-JUN fusion, it is predicted that the 5' UTR of YTHDF3 combines with the 5'UTR of JUN. In the VBP1-JUN fusion, it is predicted that the 5' CDS and UTR of VBP1 would fuse with the truncated CDS of JUN. In these fusions, JUN could function under the YTHDF3 or VBP1 5' regulatory elements or could form a chimeric JUN protein.

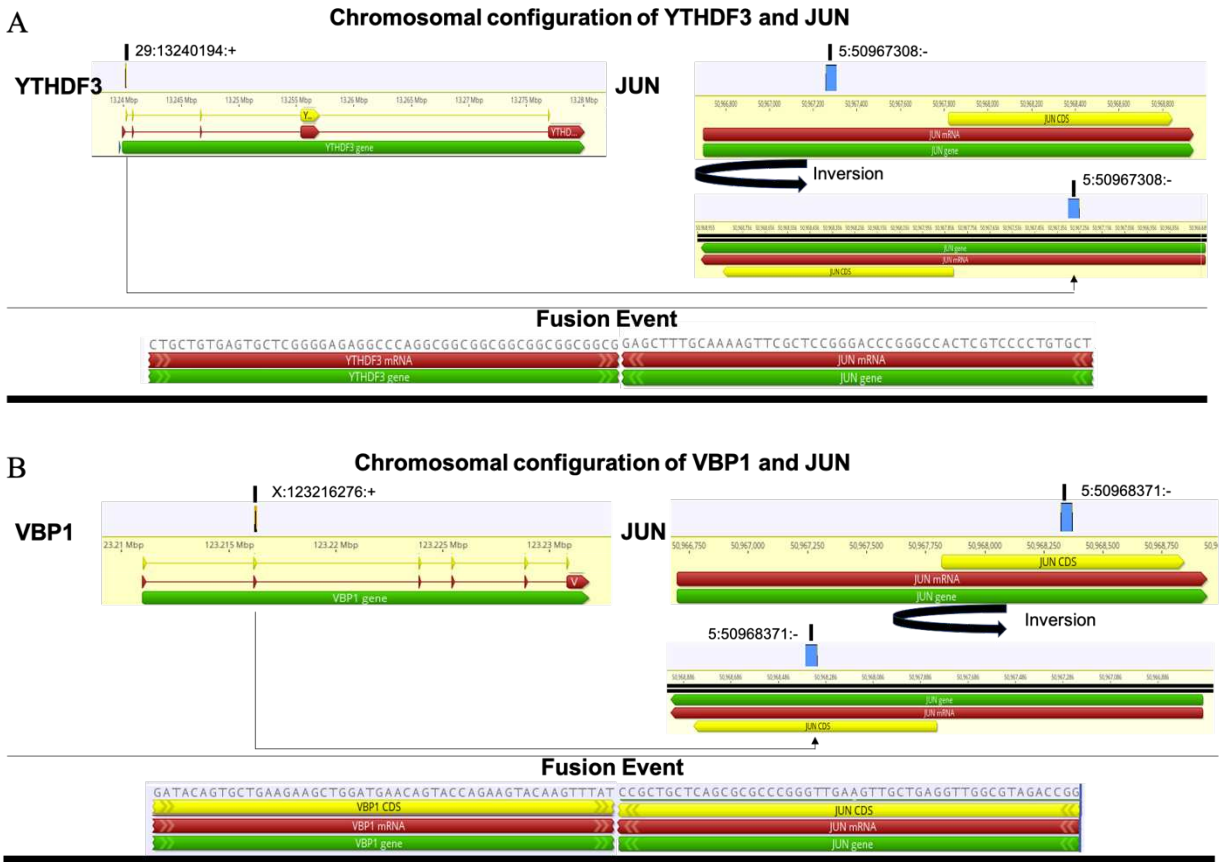

Figure 5.6. Structure of the fusion genes involving JUN as a 3' fusion partner. The gene structures and predicted fusion junction sequence is illustrated from the following fusion genes YTHDF3-JUN(A), VBP1-JUN (B). The gene structures of are shown with the gene sequences in green, mRNA in red, and coding sequence in yellow. The alignment of the mRNA sequence identified by RNA-seq is shown in blue and the fusion junction points are shown on the top of the aligned sequences. The fusion junction sequence is shown below.

LMO4 was identified as a recurrent 3' fusion partner with 3 different 5' genes (TOX2, SRSF5, and PTMA) in three different dogs. LMO4 is a member of the LIM domain-only genes and has been shown to be an oncogene in a number of malignancies, including breast cancer.[271] The structures of the proposed fusion genes are shown in Figure 5.7. LMO4 is located on the reverse strand of chromosome 6 and the 5' fusion partners are on the forward strands of

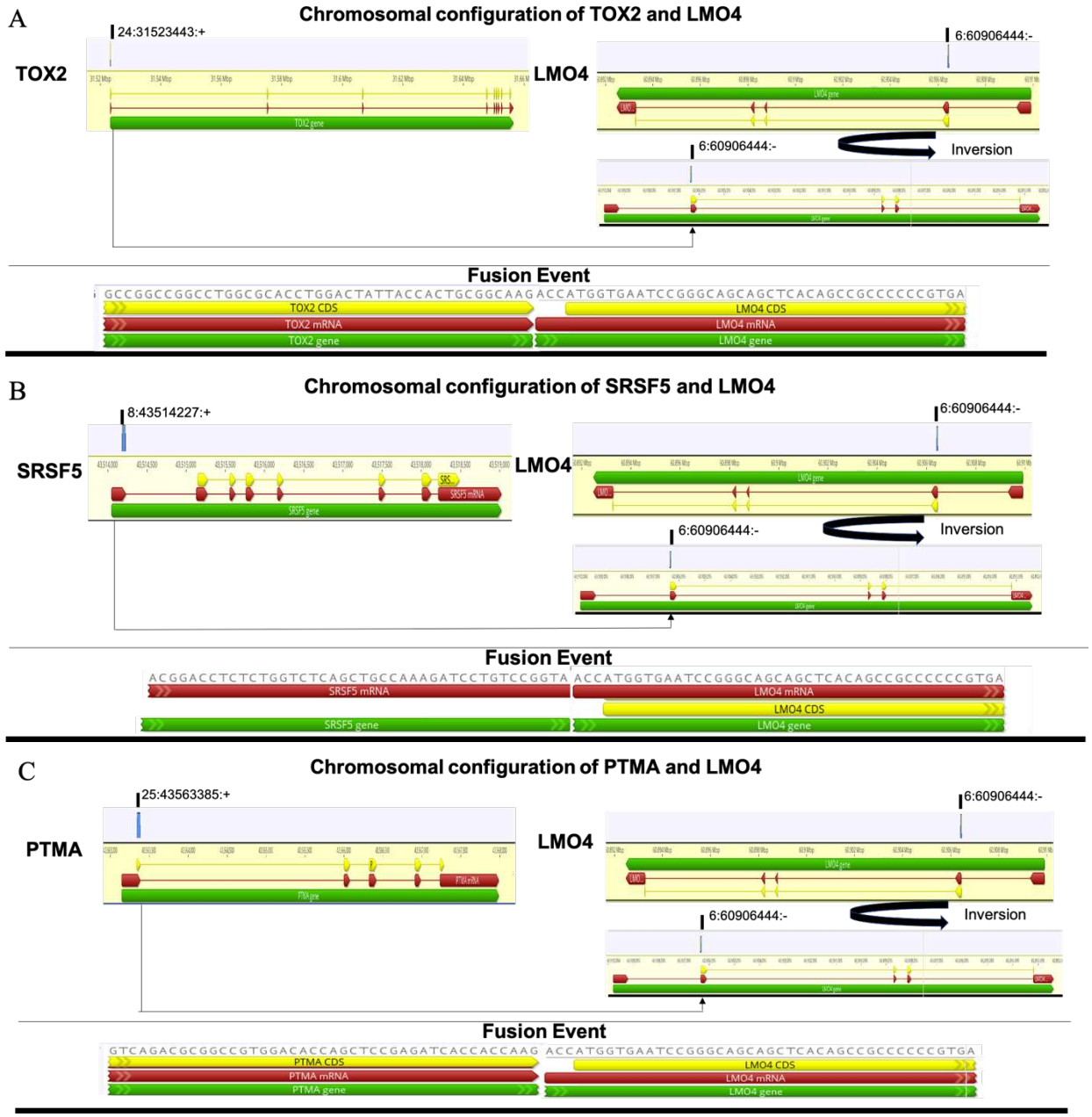

Figure 5.7. Structure of the fusion genes involving LMO4 as a 3' fusion partner. The gene structures and predicted fusion junction sequence is illustrated from the following fusion genes TOX2-LMO4(A), SRSF5-LMO4 (B), and PTMA-LMO4 (C). The gene structures of are shown with the gene sequences in green, mRNA in red, and coding sequence in yellow. The alignment of the mRNA sequence identified by RNA-seq is shown in blue and the fusion junction points are shown on the top of the aligned sequences. The fusion junction sequence is shown below.

chromosome 24, 8, and 25, respectively. An inversion event of the LMO4 gene is therefore required to form these predicted fusion genes. The fusion gene constructs would involve the 5' UTR (SRSF5) and 5' UTR and 5' CDS (PTMA and TOX2) to juxtapose the beginning of the

LMO4 CDS. These events have the potential for complete transcription and translation of LMO4, driven by the 5' fusion partners regulatory elements, or the formation of a chimeric protein.

TRIM8 was identified as the 3' fusion partner in two different dogs (Figure 5.8). TRIM8 was paired with either NFKB2 or KRI1 as 5' gene partners. TRIM8 has been shown to work as an oncogene through positive regulation of the NF-κB pathway or as a tumor suppressor by regulating p53 activity.[272] TRIM8 and NFKB2 are both located on the forward strand of chromosome 28 and KRI1 is located on the forward strand of chromosome 20. The 5' UTR and 5' CDS of NFKB2 or KRI1 would be juxtaposed to the truncated CDS and 3' UTR of TRIM8, allowing TRIM8 expression to be under the control of the 5' gene partner. It is also possible that the 3' UTR of TRIM8 allows for enhanced mRNA stability or altered translational regulation of the 5' gene partner. One case (69996) exhibited increased expression of TRIM8 compared to other cases and control lymphocytes. The NFKB2-TRIM8 candidate fusion gene was identified in this individual. Additionally, the number of spanning unique reads in the NFKB2-TRIM8 fusion was 26, supporting a possible true fusion event.

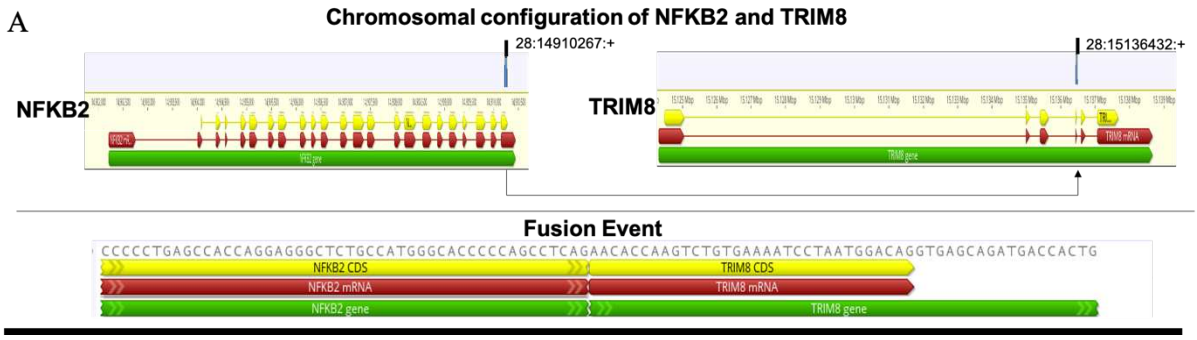

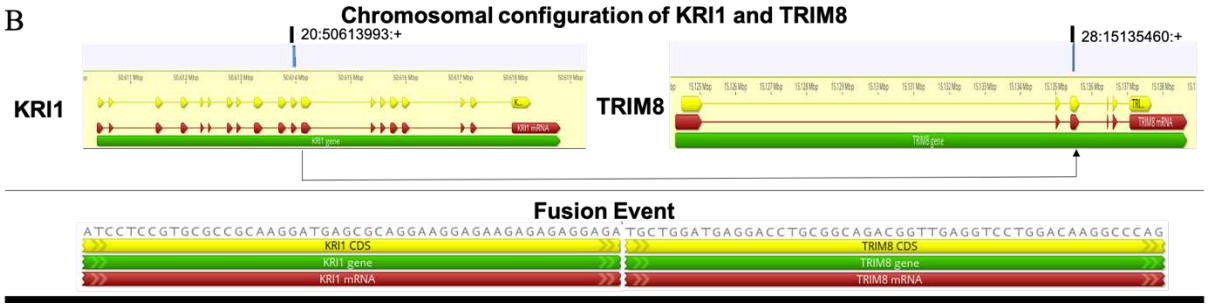

Figure 5.8. Structure of the fusion genes involving TRIM8 as a 3' fusion partner. The gene structures and predicted fusion junction sequence is illustrated from the following fusion genes NFKB2-TRIM8 (A), and KRI1-TRIM8 (B). The gene structures of are shown with the gene sequences in green, mRNA in red, and coding sequence in yellow. The alignment of the mRNA sequence identified by RNA-seq is shown in blue and the fusion junction points are shown on the top of the aligned sequences. The fusion junction sequence is shown below.

IKZF1 was identified as a 3' fusion partner with two separate 5' partners (GRB10 and PCGF3) (Figure 5.9). Both of these candidate fusion genes were identified in the same individual patient (100850), suggesting multiple chromosomal alterations may have taken place at this site. An inversion event of the 5' fusion partner is required for either of these fusion events to occur. The fusion transcripts predict that the 5' UTR and 5' CDS of GRB10 would juxtapose the CDS of IKZF1. The 3' UTR of PCGF3 would juxtapose the CDS of IZKF1. A truncated IKZF1 CDS would result from the fusion event. Evaluation of the open reading frame would aid in determining if this fusion event would result in a potentially functional protein. IKZF1encodes the lymphoid transcription factor IKAROS, and genetic alterations involving this gene have been described in acute lymphoblastic leukemia in humans.[273]

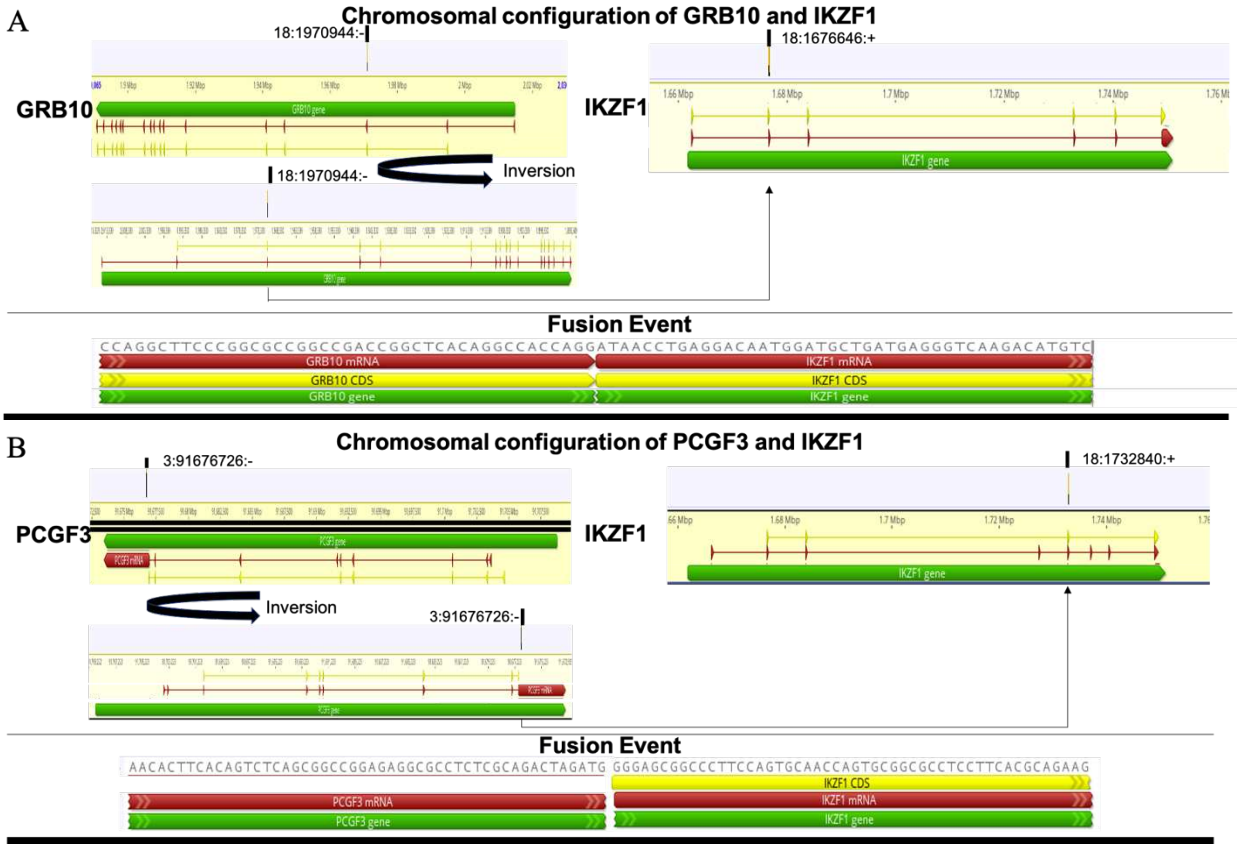

Figure 5.9. Structure of the fusion genes involving IKZF1 as a 3' fusion partner. The gene structures and predicted fusion junction sequence is illustrated from the following fusion genes GRB10-IKZF1 (A), and PCGF3-IKZF1 (B). The gene structures of are shown with the gene sequences in green, mRNA in red, and coding sequence in yellow. The alignment of the mRNA sequence identified by RNA-seq is shown in blue and the fusion junction points are shown on the top of the aligned sequences. The fusion junction sequence is shown below.

Two fusion candidates involving the 3' partner of XPO1 were identified in two different dogs (Figure 5.10). XPO1 encodes a critical nuclear export protein, exportin-1, and plays a role in oncogenesis of several types of cancer, including B-cell malignancies.[274–276] SPOCK2 and XPO1 are located on the reverse strands of chromosome 4 and 10, respectively. Inversions of both genes would be necessary to form the fusion junction sequence identified by RNA-seq. The fusion construct would involve the 5' CDS of SPOCK2 juxtaposed to the 3' UTR of XPO1. This fusion, therefore, does not contain the XPO1 CDS. Alternatively, regulatory elements within the 3' UTR of XPO1, including miRNA binding sites, may have an effect on expression of

SPOCK2. The ITM2C-XPO1 fusion event would result in the 5' UTR and beginning of the 5' CDS of ITM2C juxtaposed to the 5' UTR and CDS of XPO1. In this case, complete translation of the XPO1 CDS could take place and XPO1 expression could be altered by the regulatory elements in the ITM2C 5' UTR.

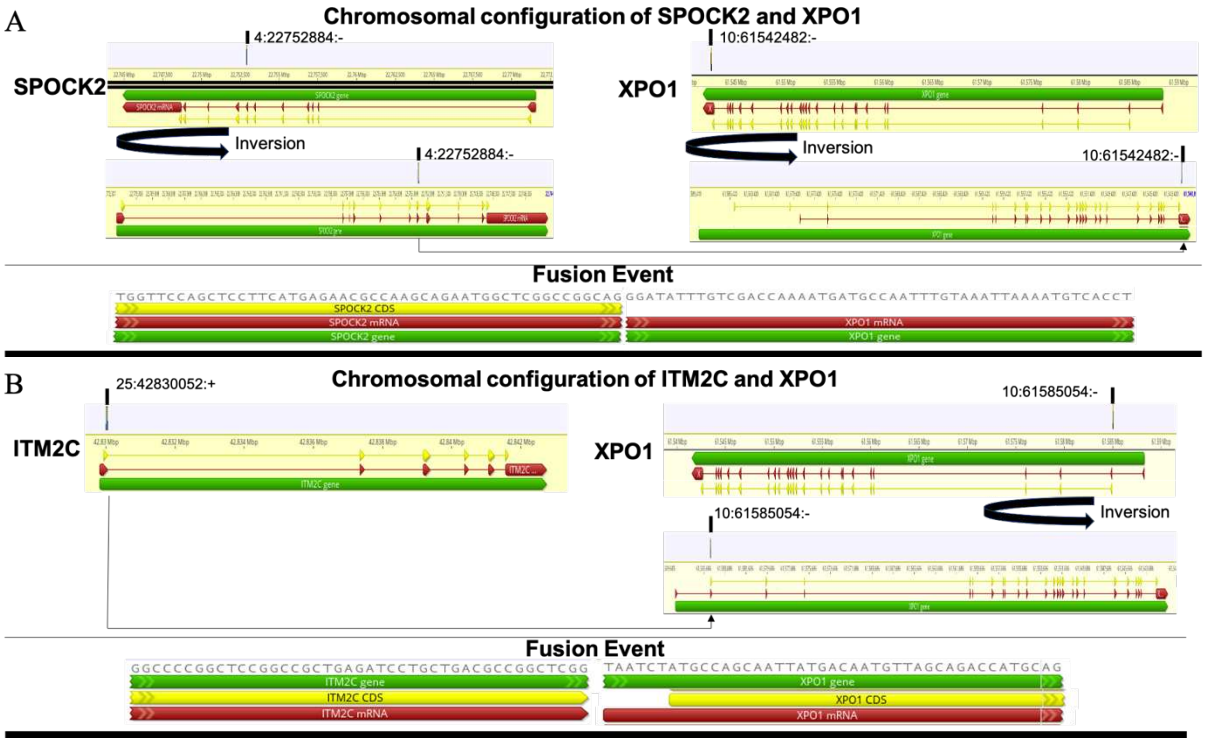

Figure 5.10. Structure of the fusion genes involving XPO1 as a 3' fusion partner. The gene structures and predicted fusion junction sequence is illustrated from the following fusion genes SPOCK2-XPO1 (A), and ITM2C-XPO1 (B). The gene structures of are shown with the gene sequences in green, mRNA in red, and coding sequence in yellow. The alignment of the mRNA sequence identified by RNA-seq is shown in blue and the fusion junction points are shown on the top of the aligned sequences. The fusion junction sequence is shown below.

Fusion genes involving GNAS as the 3' partner were identified in 6 different dogs (Figure 5.11). The SRSF5-GNAS fusion gene was identified to two different patients, with consistent fusion junction sequences and fusion points. GNAS encodes the G protein Gαs and has been shown to have oncogenic or tumor suppressor functions, depending on the microenvironmental context.[277–279] The fusion candidate involving a B2M-GNAS fusion had

greater than 5 spanning unique reads, supporting a possible true fusion event. All predicted fusion events would involve the 5' UTR or 5' UTR and CDS of the 5' gene partner juxtaposed to the beginning of the GNAS CDS. This model would predict that expression of GNAS could be regulated by the 5' UTR of the upstream fusion gene partner or result in a chimeric protein.

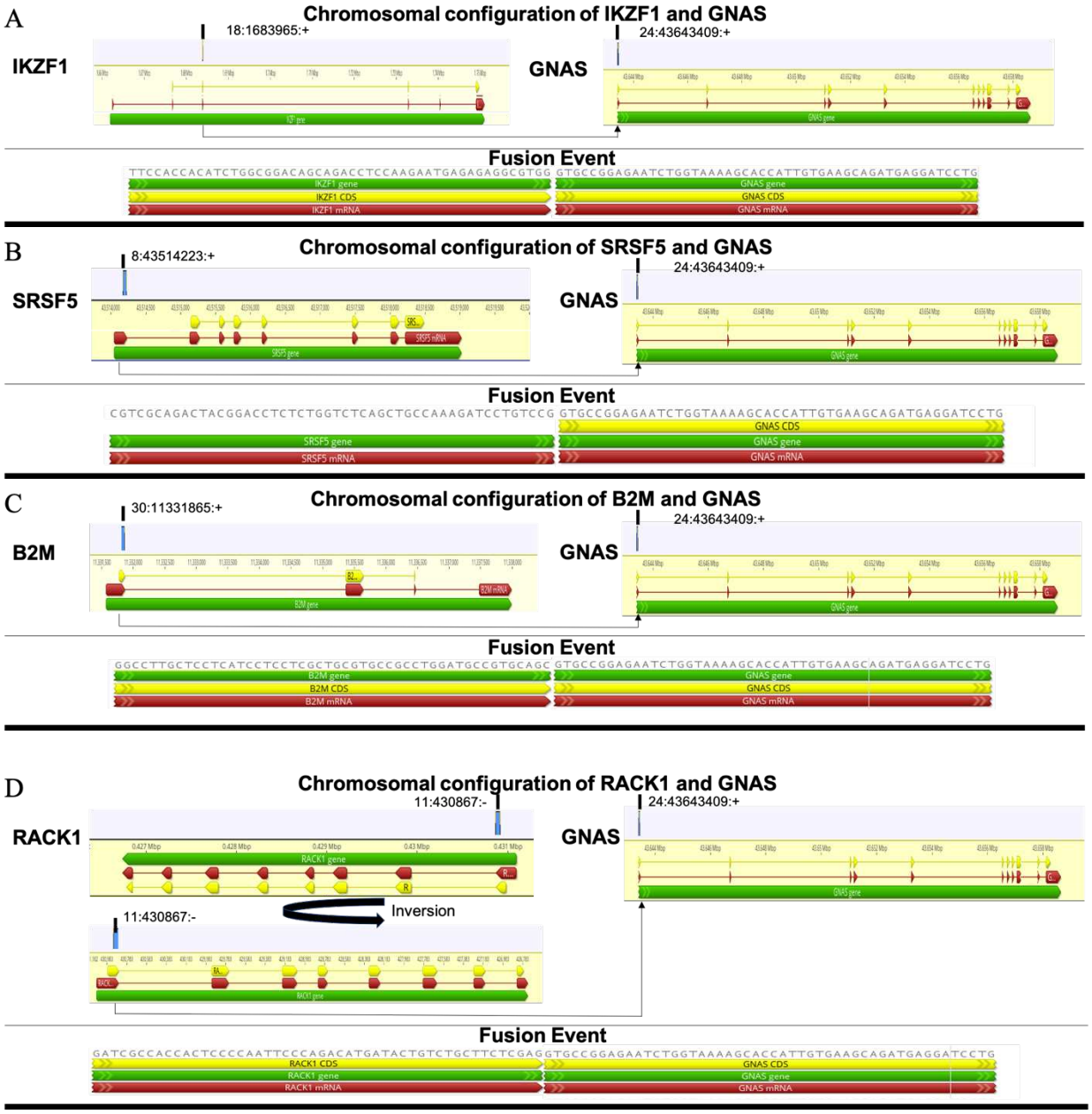

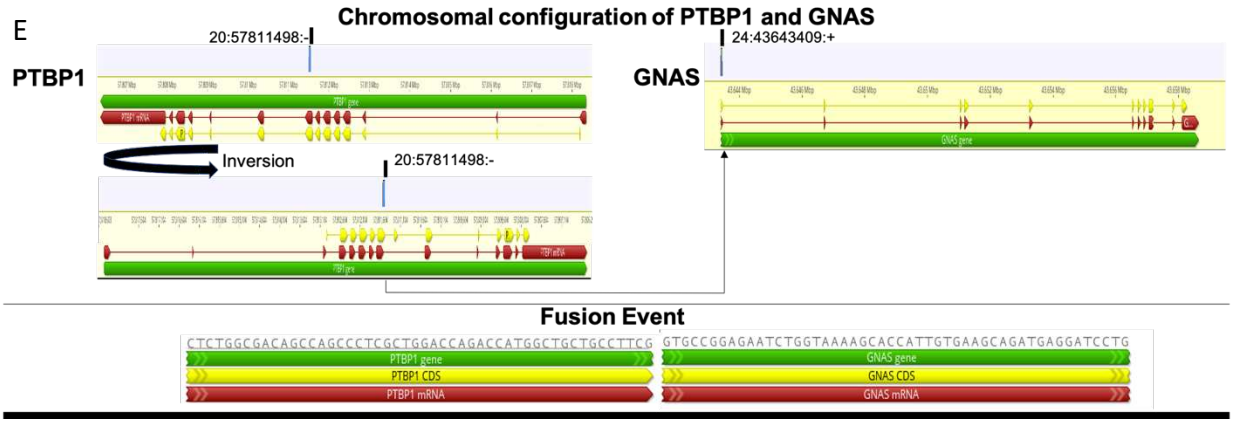

Figure 5.11. Structure of the fusion genes involving GNAS as a 3' fusion partner. The gene structures and predicted fusion junction sequence is illustrated from the following fusion genes IKZF1-GNAS (A), SRSF5-GNAS (B), B2M-GNAS (C), RACK1-GNAS (D), PTBP1-GNAS (E). The gene structures of are shown with the gene sequences in green, mRNA in red, and coding sequence in yellow. The alignment of the mRNA sequence identified by RNA-seq is shown in blue and the fusion junction points are shown on the top of the aligned sequences. The fusion junction sequence is shown below.

MYH9 was a 3' fusion partner in 4 different fusion gene candidates in 4 different dogs (Figure 5.12). MYH9 has been shown to play a role in cancer through modulating cytoskeletal reorganization and cellular migration.[280,281] High expression levels of MYH9 have been identified in a number of human malignancies.[282] The TFAM-MYH9 and NR1D1-MYH9 fusion events are predicted to result in the 5' UTR and CDS of the 5' fusion partner placed adjacent to a truncated MYH9 CDS. The DENND4B-MYH9 and BCL11B-MYH9 fusion candidates, on the other hand, involved the 5' UTR and CDS of the 5' fusion partner placed adjacent to the 3' UTR of MYH9. It is possible that regulatory elements within the 3' UTR of MYH9 may exert their effects on the upstream fusion partner, but transcription and translation of the MYH9 CDS is not expected in these cases.

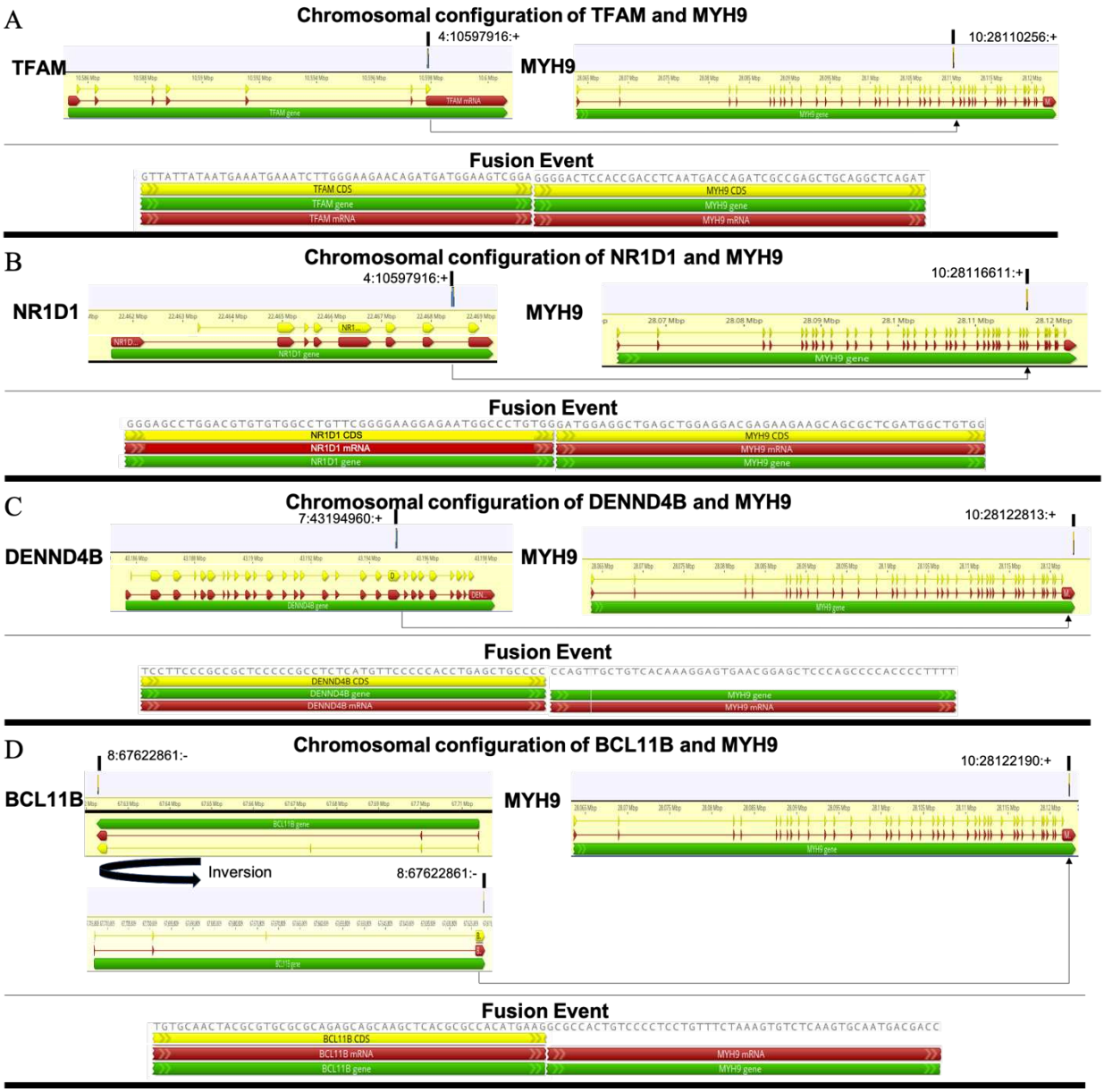

Figure 5.12. Structure of the fusion genes involving MYH9 as a 3' fusion partner. The gene structures and predicted fusion junction sequence is illustrated from the following fusion genes TFAM-MYH9 (A), NR1D1-MYH9 (B), DENND4B-MYH9 (C), and BCL11B-MYH9 (D). The gene structures of are shown with the gene sequences in green, mRNA in red, and coding sequence in yellow. The alignment of the mRNA sequence identified by RNA-seq is shown in blue and the fusion junction points are shown on the top of the aligned sequences. The fusion junction sequence is shown below.

LSP1 was identified as the 3' fusion partner in 2 different patients. The 5' fusion partners were B2M and PPY (Figure 5.13). LSP1 encodes lymphocyte specific protein 1and LSP1

downregulation, mutation, or deletion has been shown to play a role in multiple cancer types, including lymphomas, breast cancer, and hepatocellular carcinoma.[283–285] The B2M-LSP1 fusion involves juxtaposition of the 5' UTR and beginning of the B2M CDS to the 3' UTR of LSP1. Therefore, a functional LSP1 protein is unlikely to result from this fusion event. It is also possible for the 3' UTR regulatory elements to alter expression of B2M. Regardless of these structural features, LSP1 expression was markedly increased in the case (60342) with the B2M-LSP1 fusion gene identified compared to other cases and control T-cells. The PPY-LSP1 fusion results in juxtaposition of the 5' UTR and CDS of PPY and the 5' UTR and complete CDS of LSP1. As a result, LSP1 expression could be driven by the PPY 5' UTR.

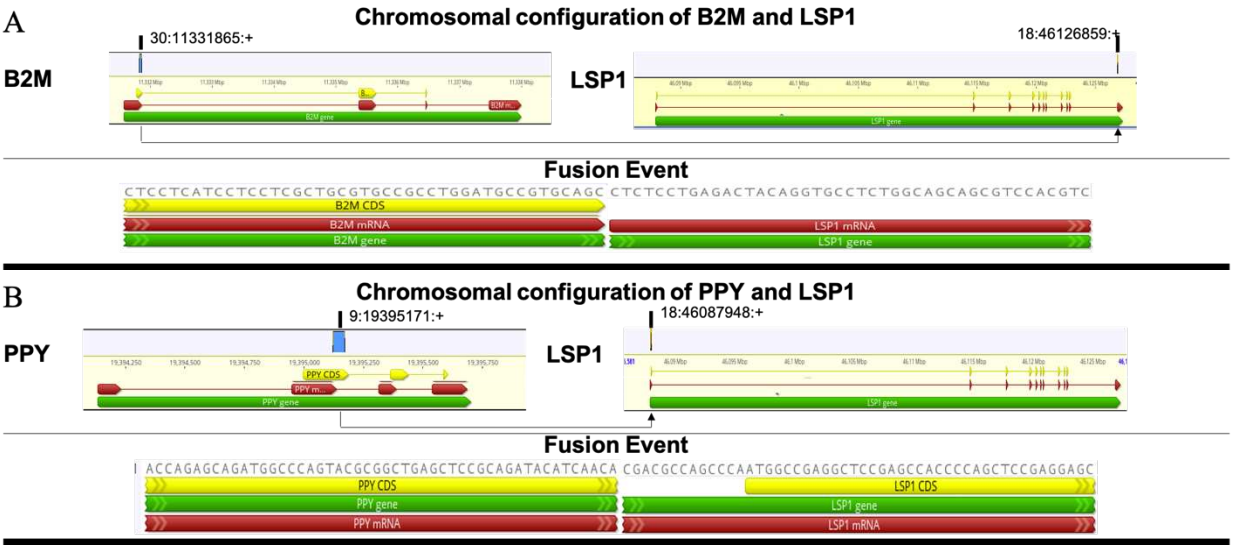

Figure 5.13. Structure of the fusion genes involving LSP1 as a 3' fusion partner. The gene structures and predicted fusion junction sequence is illustrated from the following fusion genes B2M-LSP1 (A), and PPY-LSP1 (B). The gene structures of are shown with the gene sequences in green, mRNA in red, and coding sequence in yellow. The alignment of the mRNA sequence identified by RNA-seq is shown in blue and the fusion junction points are shown on the top of the aligned sequences. The fusion junction sequence is shown below.

GATD3A (C31H21orf33) was the 3' fusion partner in 4 fusion gene candidates from 3 different dogs (Figure 5.14). Two fusion genes, MRPH1-GATD3A and TPD52L2-GATD3A, were identified in a single dog (100850). This patient (100850) and one other individual (97578)

with a JPT1-GATD3A exhibited higher expression levels of GATD3A compared to other cases or control T-cells (Figure 5.3). The role of this gene as a potential genetic driver of cancer is not well explored. In all cases, the fusion breakpoint of GATD3A is conserved and results in truncation of the GATD3A CDS. This 3' fusion partner is juxtaposed to the 5' UTR and CDS of the 5' fusion partner genes.

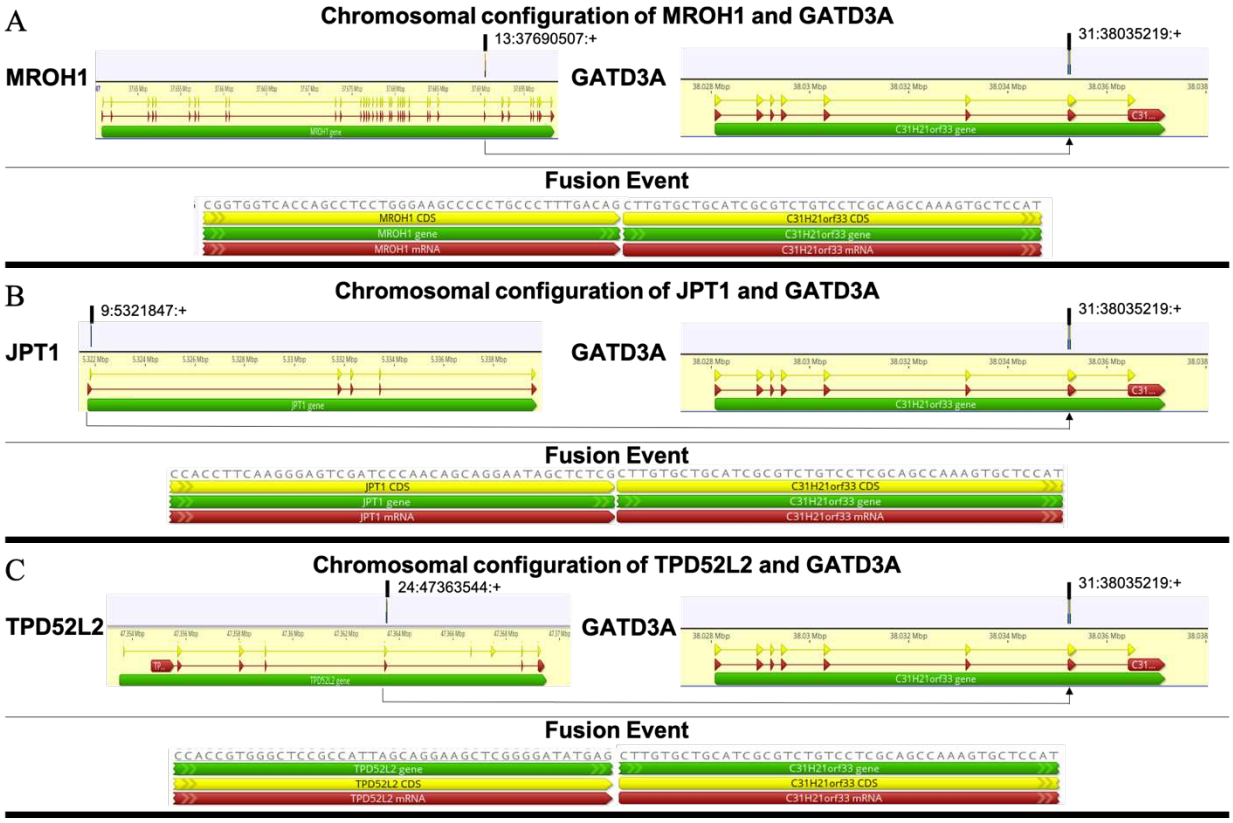

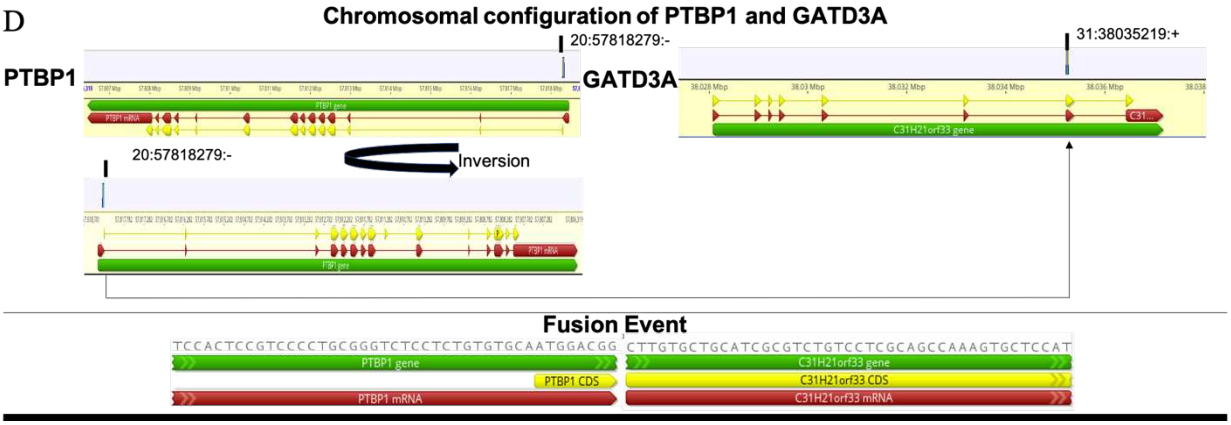

Figure 5.14. Structure of the fusion genes involving GATD3A(C31H21orf33) as a 3' fusion partner. The gene structures and predicted fusion junction sequence is illustrated from the following fusion genes MROH1-GATD3A (A), JPT1-GATD3A (B), TPD52L2-GATD3A (C), and PTBP1-GATD3A (D).The gene structures of are shown with the gene sequences in green, mRNA in red, and coding sequence in yellow. The alignment of the mRNA sequence identified by RNA-seq is shown in blue and the fusion junction points are shown on the top of the aligned sequences. The fusion junction sequence is shown below.

Discussion

A recurrent fusion gene present in the majority of PTCL cases was not identified using our RNA-seq derived fusion gene discovery pipeline. This finding is not unique to canine PTCL. The prevalence of known fusion genes in different human malignancies varies greatly, with the majority of recurrent fusion genes occurring at low frequencies.[240,286]

We identified 43 genes that were recurrently identified as 3' fusion partners from 26 cases of canine PTCL. This list was subsequently narrowed to 11 target genes that have been previously described as cancer-associated and/or genes in which at least one of the patients with the fusion candidate exhibited aberrant expression of the 3' fusion partner. This list of fusion candidates warrants validation studies to confirm the presence of the fusion gene in the patient samples used for RNA-seq using PCR. Further screening of a larger cohort of new patients may also provide greater insights into the prevalence of identified fusion candidates within the population of canine patients with PTCL.

The DGKZ-MDK fusion gene is of particular interest since it was among the most frequently encountered fusion candidates, identified in 19% of cases. This fusion gene was one of the few in which both the 5' and 3' partners occurred repetitively in different patients. Additionally, within 2 of the 5 evaluated cases the spanning unique read count was greater than 5, further supporting the possibility that this is a true fusion event. Diacylglycerol kinase zeta (DGKZ) functions at the TCR complex following TCR/CD28 engagement and works as a negative regulator of DAG-mediated signals.[287] Midkine (MDK) is heparin-binding growth factor that can act as an oncogene and promotes multiple hallmarks of cancer including cell growth, survival, metastasis, migration, and angiogenesis.[269]

The fusion breakpoint of the MDK partner occurred at the same location in all cases and was located at the start of the CDS, beginning with the start codon ATG. The MDK gene is simple with 1 exon and 1 splice variant. Therefore, the entire coding sequence of this protein would be expected to be translated. The 5' UTR of MDK is lost, and consequently this gene is likely to regulated by of the 5' UTR of DGKZ. Because DGKZ can be expressed downstream of the TCR, regulation under the DGKZ could result in subsequent upregulation of MDK in the neoplastic T-cells.

Three different junction points were identified in the DGKZ gene, with 3 cases sharing the same junction point. The fusion breakpoint involves the 3' end of the CDS and 3' UTR in two of the junction breakpoints. One junction breakpoint involves only the 3' UTR. Successful translation of this fusion transcript is challenged by the presence of a stop codon within the upstream DGKZ gene. Translation of this fusion protein would be dependent on uninterrupted translation of both proteins, despite the presence of the DGKZ stop codon or re-initiation of translation using the start codon for MDK. Interestingly, despite the presence of the stop codon

in this fusion transcript, non-sense mediated decay did not take place to remove the mRNA transcripts from the sequencing evaluation. It is possible the disruption of the DGKZ 3' UTR alters RNA stability or normal regulation of translation. In vitro validation of the presence of this fusion transcript and fusion protein is warranted to better understand if this transcript is a true potential driving fusion gene or a false positive result.

Another candidate of interest involves recurrent fusions to LMO4. Genes within the LMO family, particularly LMO1, LMO2, and LMO3, have been shown to frequently participate in chromosomal translocations that drive T-acute lymphoblastic lymphoma (T-ALL).[288] The role of LMO4 in T-cell development and function, however, is less well understood. LMO4 is widely expressed in mouse tissues, including T-cells within the embryonic and adult thymus.[289] LMO4 has been shown to drive cellular proliferation in other tumor types, including breast cancer, by working as a downstream target of ErbB2 and PI3K.[271,290] In this study, three fusion gene candidates involving LMO4 were identified in three different dogs. The 5' fusion partners in these cases were TOX2, SRSF5, and PTMA. The LMO4 fusion breakpoint was conserved in all cases and was located 3 nucleotides before the start codon of the LMO4 CDS. Therefore, the entire LMO4 CDS is predicted to be translated, increasing the likelihood of the formation of a functional LMO4 protein. The fusion breakpoint of TOX2 and PTMA involve the 5' UTR and the beginning of the 5' CDS. The fusion breakpoint of SRSF5 involves only the 5' UTR. These fusion constructs are predicted to result in expression of LMO4 being driven by the 5' UTR of the fusion partner.

The 5' fusion partner genes are expressed by T-cells and/or neoplastic cells. TOX2 is a transcription factor belonging to the thymocyte selection-associated high mobility group box protein family (TOX).[291] TOX2 plays multiple roles in T-cell development and differentiation,

including transition from the double-positive to single-positive stage of thymic development.[292–295] TOX2 is also highly expressed in Tfh cells and is a key regulator of Tfh development.[292,294] PTMA encodes the protein thymosin $\alpha 1$. Thymosin $\alpha 1$ is a thymic peptide that primarily works to augment T-cell function.[296] SRSF5 is a member of the serine/arginine-rich protein (SR) family and works to regulate pre-mRNA alternative splicing. SRSF5 has been shown to play a role in oncogenesis, and is upregulated by neoplastic cells in a number of cancers.[297,298] Other members of SR family, including SRSF1, also play a role in regulating expression of the T-cell receptor-associated CD3 signaling.[299] Validation of the LMO4 fusion genes in patient samples using PCR is warranted to better understand if the identified fusion transcripts may be potential oncogenic drivers of canine PTCL.

RNA-seq is considered the preferred methodology for oncologic fusion gene identification for several reasons including: 1) RNA-seq only sequences regions of the genome that are transcribed and spliced into mature mRNA, therefore rearrangements resulting in non-sense mediated decay would not be included 2) RNA-seq is practical with relatively low cost, fast turnaround time, and computational efficiency and 3) RNA-seq fusion discovery identifies candidates based on the presence of a potential fusion transcript and allows for detection of multiple alternative splice variants resulting from a fusion event.

Despite these advantages, there are several drawbacks to RNA-seq based fusion discovery. A major challenge of identifying fusion genes using RNA-seq derived fusion discovery are the high rates of false positivity. Differentiation between fusions of interest from artifacts is extremely challenging due to the high prevalence of gene readthrough events and other false-positive candidates.[263]. Therefore, stringent filtering techniques must be applied in an

attempt to identify the most biologically relevant fusion transcripts. In applying this technique, however, it is possible to filter-out potentially relevant candidates.

Additionally, the tissue-specificity, dynamic range of expression, and variable transcription of genes in different tissues and cellular stages within the canine transcriptome complicates evaluation of fusion transcripts. RNA-seq is dependent upon alignment to the reference genome as well as reference transcriptome for gene annotation. Fusion gene discovery in the dog is exceptionally challenging due to poor annotation accuracy and incompleteness of the canine genome. In particular, the genes encoding the T-cell receptor (TCR) are not well annotated and incompletely identified in the dog. It is possible that fusion gene transcripts that involve TCR genes are not identified by our fusion gene discovery pipeline, which relies on the CanFam3.1 genome.

The fusion discovery was performed on an unstranded library in this study. An unstranded library does not maintain the coding DNA strand (sense and antisense) for the transcript that is sequenced. An unstranded library may produce artifacts if there are small overlapping regions of isoforms of two genes located on opposite strands.

In our study we identified several samples in which multiple fusions were detected with the same 3' partner paired to different 5' partners. Formation of fusion genes involving multiple fusion partners is possible in the event of massive chromosomal disruptions such as chromothripsis. Chromothripsis describes a process in which there are tens to thousands of clustered chromosomal rearrangements confined to a localized genomic region.[300]

Additional studies using combined whole genome sequencing (WGS) and RNA-seq with paired somatic and germline tissues from a large number of canine PTCL cases may be helpful to better understand the chromosomal alterations that are driving this disease. In addition to

confirming the presence of RNA-seq identified fusion events, WGS may provide an opportunity to identify chromosomal translocations involving untranscribed regions and those that result in loss of tumor suppressor genes. Additionally, WGS would be helpful to characterize chromosomal deletions or amplification events that may be occurring in these tumors.

In this study we performed fusion gene discovery and identified a candidate list for further validation in canine PTCL. From an initial list of 591 fusion candidates, we selected 11 recurrent fusions of interest for structural evaluation. This list was selected based on aberrant expression of the 3' fusion partner and/or cancer-related 3' gene partners. We specifically identified fusions involving DGKZ-MDK and LMO4 as potential oncogenic drivers. This work seeks to begin to understand that roles of chromosomal alterations and fusion genes as drivers of canine hematopoietic malignancies.

CONCLUSIONS

The overarching goals of this dissertation were to better understand the pathobiology underlying peripheral T-cell lymphomas in dogs, and to determine if the dog could serve as a naturally occurring translational model for this aggressive disease in people. Through this work we aimed to better establish a canine disease model to foster the concept of 'One Health' and promote the shared goals of veterinarians, medical physicians, and researchers to understand and treat diseases in a comparative and translational capacity. We were able to build a strong foundation to inform future studies focused on the molecular drivers of canine and human PTCL.

Characterization of $CD4^+$, $CD8^+$, and $CD4^-CD8^-$ subtypes of canine PTCL

We began our investigation into canine PTCL by characterizing the histologic and clinical features of the $CD4^+$, $CD8^+$, and $CD4^-CD8^-$ TCLs. Previous work focused on these tumor subtypes in dogs is scarce in the literature. Perhaps most importantly, we established that these neoplasms, regardless of immunophenotype appear to behave aggressively. This prognostic information can be used by veterinarians to treat and manage these patients. Prospective clinical studies in which patient treatment is standardized would be greatly beneficial in further evaluating potential differences in biologic behaviors within these tumor subgroups.

By looking at the presenting clinical signs and expression of cell surface markers by flow cytometry, we show that $CD4^-CD8^-$ TCLs share clinical and diagnostic features with the more common $CD4^+$ TCLs, suggesting a common pathogenesis. $CD8^+$ TCLs, on the other hand exhibit unique clinical features and prognostic indicators suggesting that these tumors may be have a different pathobiology. This conclusion is further strengthened by hierarchical clustering of tumor samples based on RNA-seq derived gene expression profiles. $CD8^+$ tumors clustered

separately from the $CD4^+$ tumors whereas, $CD4^-CD8^-$ tumors were split between the $CD8^+$ and $CD4^+$ groups. Histologic and cytologic morphologies of the $CD8^+$ and $CD4^-CD8^-$ tumor types were more variable than the $CD4^+$ subtype, and therefore it is possible that different subgroups with unique pathogeneses may exist within these less common immunophenotypic subgroups.

Using gene expression profiling and cell surface marker expression by flow cytometry we then attempted to better understand the cell of origin of these subtypes. We concluded that $CD4^+$ PTCL appears to be derived from a naïve single positive T-cell and $CD4^-CD8^-$ PTCL appears to be derived from a slightly more immature naïve double negative T-cell. A subset of these cases expressed markers of immaturity, suggesting that at least a portion of PTCL may originate from a more immature thymic precursor, consistent with lymphoblastic lymphoma. Additional studies, looking at protein expression of markers of immaturity, including TdT, in a large group of these tumors would be useful next steps. Because optimizing antibodies for protein expression in dogs can be challenging, evaluating mRNA levels of CD34 and TdT and correlating to any differences in histomorphology, clinical presentation, or outcome in those patients with higher expression levels may also provide further insights.

$CD8^+$ TCLs upregulated molecules associated with activated cytotoxic T-cells, suggesting that at least a subset of $CD8^+$ TCLs may originate from a mature $CD8^+$ effector cell. Additional gene expression profiling studies, including larger numbers of dogs with $CD8^+$ and $CD4^-CD8^-$ tumors may provide further information about possible molecular subtypes within these groups.

Interestingly, one $CD4^+$ PTCL case exhibited increased gene expression of CD30 and this case clustered separately from the rest of the PTCL samples. This finding suggests that this individual tumor may represent an uncommon $CD30^+$ subgroup of PTCL, or perhaps may

represent an anaplastic large cell lymphoma, which in humans are characteristically $CD30^+$. Evaluation of CD30 expression in a large cohort of new patients may be helpful in better determining the significance of this finding.

Molecular drivers of canine PTCL and development of a translational model

We were able to show molecular similarities between canine $CD4^+$ PTCL and the human PTCL-GATA3 subtype. This finding lays the groundwork to use the dog as a naturally occurring model. The dog may be particularly useful in this capacity because studies in PTCL in people are limited by the scarcity of patients for enrollment in large clinical trials and difficulty in acquiring adequate patient material for molecular studies. We show that like PTCL-GATA3, this neoplasm in dogs is driven in part by PI3K-AKT-MTOR signaling. Both human and canine PTCL exhibit frequent loss of the tumor suppressor gene PTEN, which likely contributes to the key oncogenic role of this pathway. PI3K inhibitors have already been used in human PTCL, with promising results. Implementation of clinical studies looking at the effects of various PI3K inhibitors in dogs diagnosed with $CD4^+$ PTCL may provide further insights into therapeutic benefits of this targeted treatment.

To further understand the molecular drivers of this neoplasm, we sought to identify potential fusion genes using an RNA-seq discovery platform. Because many hematopoietic tumors are driven by chromosomal translocations and subsequent fusion genes, we hypothesized that a recurrent fusion gene would be discovered in the majority of cases. Fusion genes and driving chromosomal translocations are well described in human tumors and cytogenetic analysis of tumors is a routine diagnostic modality. Chromosomal translocation and fusion genes in canine cancers, however, are poorly described with only few individual cases referenced in the literature. We did not identify a recurrent fusion gene present in the majority of cases.

Nevertheless, we did identify a number of candidate fusion genes present in a minority of the PTCL samples. Of particular interest were DGKZ-MDK fusions and fusions involving LMO4 with multiple partners. Next steps include validation of the presence of these fusion transcripts in the samples used for RNA-seq by conventional PCR and subsequent screening of a larger, independent patient cohort for the presence of the fusion genes of interest. Developing methods to identify canine fusion genes is a valuable endeavor and can lead to enhanced classification and diagnostic accuracy of canine tumors, development of targeted treatment options, and identification of novel fusions present in human tumors.

Future studies involving paired whole-genome sequencing and RNA-seq on a large group of tumors would facilitate better understanding of the molecular drivers of canine PTCL. Having both genomic and transcriptomic data would allow for detailed evaluation of the mutational profile and chromosomal aberrations which could be directly correlated to the mRNA transcript levels. Additionally, because PTCL in dogs exhibits strong breed predilections with Boxer dogs being overrepresented in the patient population, genome-wide association studies may provide useful insights into predisposing genetic factors that are novel to both dogs and humans.

In this dissertation we begin to understand the molecular and genetic drivers of PTCL and correlate these findings to the human counterpart. We contribute to the development of a naturally occurring canine cancer model, with the hopes of promoting collaborations between veterinarians, biomedical researchers, and physicians to enhance our understanding of cancer biology and cancer treatment through a translational and comparative approach.

REFERENCES

1. Germain RN. T-cell development and the CD4–CD8 lineage decision. *Nat Rev Immunol*. 2002;2(5):309-322.
2. Lind EF, Prockop SE, Porritt HE, Petrie HT. Mapping Precursor Movement through the Postnatal Thymus Reveals Specific Microenvironments Supporting Defined Stages of Early Lymphoid Development. *J Exp Med*. 2001;194(2):127-134.
3. Koch U, Radtke F. Mechanisms of T Cell Development and Transformation. *Annu Rev Cell Dev Biol*. 2011;27(1):539-562.
4. Galy A,Verma S, Bárcena A, Spits H. Precursors of CD3+CD4+CD8+ cells in the human thymus are defined by expression of CD34. Delineation of early events in human thymic development. *J Exp Med*. 1993;178(2):391-401.
5. Civin CI, Strauss LC, Brovall C, Fackler MJ, Schwartz JF, Shaper JH. Antigenic analysis of hematopoiesis. III. A hematopoietic progenitor cell surface antigen defined by a monoclonal antibody raised against KG-1a cells. *J Immunol*. 1984;133(1):157 LP - 165.
6. Andrews RG, Singer JW, Bernstein ID. Precursors of colony-forming cells in humans can be distinguished from colony-forming cells by expression of the CD33 and CD34 antigens and light scatter properties. *J Exp Med*. 1989;169(5):1721-1731.
7. Terstappen LW, Huang S, Picker LJ. Flow cytometric assessment of human T-cell differentiation in thymus and bone marrow. *Blood*. 1992;79(3):666-677.
8. von Freeden-Jeffry U, Vieira P, Lucian LA, McNeil T, Burdach SE, Murray R. Lymphopenia in interleukin (IL)-7 gene-deleted mice identifies IL-7 as a nonredundant cytokine. *J Exp Med*. 1995;181(4):1519-1526.
9. van Lent AU, Dontje W, Nagasawa M, et al. IL-7 Enhances Thymic Human T Cell Development in “Human Immune System” Rag2-/-IL-2Rgammac-/- Mice without Affecting Peripheral T Cell Homeostasis. *J Immunol*. 2009;183(12):7645-7655.
10. Napolitano LA, Stoddart CA, Hanley MB, Wieder E, McCune JM. Effects of IL-7 on Early Human Thymocyte Progenitor Cells In Vitro and in SCID-hu Thy/Liv Mice. *J Immunol*. 2003;171(2):645-654.
11. Peschon JJ, Morrissey PJ, Grabstein KH, et al. Early lymphocyte expansion is severely impaired in interleukin 7 receptor-deficient mice. *J Exp Med*. 1994;180(5):1955-1960.
12. Mazzucchelli RI, Riva A, Durum SK. The human IL-7 receptor gene: Deletions, polymorphisms and mutations. *Semin Immunol*. 2012;24(3):225-230.
13. Puel A, Ziegler SF, Buckley RH, Leonard. WJ. Defective IL7R expression in T-B+NK+ severe combined immunodeficiency. *Nat Genet*. 1998;20(4):394-397.
14. García-León MJ, Fuentes P, de la Pompa JL, Toribio ML. Dynamic regulation of NOTCH1 activation and Notch ligand expression in human thymus development. *Development*. 2018;145(16):dev165597.
15. Felli MP, Maroder M, Mitsiadis TA, et al. Expression pattern of Notch1, 2 and 3 and Jagged1 and 2 in lymphoid and stromal thymus components: distinct ligand–receptor interactions in intrathymic T cell development. *Int Immunol*. 1999;11(7):1017-1025.
16. Koch U, Fiorini E, Benedito R, et al. Delta-like 4 is the essential, nonredundant ligand for Notch1 during thymic T cell lineage commitment . *J Exp Med*. 2008;205(11):2515-2523.
17. Hozumi K, Mailhos C, Negishi N, et al. Delta-like 4 is indispensable in thymic

environment specific for T cell development. *J Cell Biol*. 2008;183:i2-i2.
18. Radtke F, Wilson A, Stark G, et al. Deficient T cell fate specification in mice with an induced inactivation of Notch1. *Immunity*. 1999;10(5):547-558.
19. Pui JC, Allman D, Xu L, et al. Notch1 expression in early lymphopoiesis influences B versus T lineage determination. *Immunity*. 1999;11(3):299-308.
20. Swerdlow SH, Campo E, Harris NL, et al. *WHO Classification of Tumours of the Haematopoietic and Lymphoid Tissues*. Vol 4.; 2017.
21. Orazi A, Cattoretti G, John K, Neiman RS. Terminal deoxynucleotidyl transferase staining of malignant lymphomas in paraffin sections. *Mod Pathol*. 1994;7(5):582-586.
22. Patel JL, Smith LM, Anderson J, et al. The immunophenotype of T-lymphoblastic lymphoma in children and adolescents: a Children's Oncology Group report. *Br J Haematol*. 2012;159(4):454-461.
23. Ellisen LW, Bird J, West DC, et al. TAN-1, the human homolog of the Drosophila Notch gene, is broken by chromosomal translocations in T lymphoblastic neoplasms. *Cell*. 1991;66(4):649-661.
24. Weng AP, Ferrando AA, Lee W, et al. Activating Mutations of NOTCH1 in Human T Cell Acute Lymphoblastic Leukemia. *Science*. 2004;306(5694):269-271.
25. Starr TK, Jameson SC, Hogquist KA. Positive and Negative Selection of T Cells . *Annu Rev Immunol*. 2003;21(1):139-176.
26. Miller JFAP. The discovery of thymus function and of thymus-derived lymphocytes. *Immunol Rev*. 2002;185:7-14.
27. Godfrey DI, Kennedy J, Suda T, Zlotnik A. A developmental pathway involving four phenotypically and functionally distinct subsets of CD3-CD4-CD8- triple-negative adult mouse thymocytes defined by CD44 and CD25 expression. *J Immunol*. 1993;150(10):4244-4252.
28. MacDonald HR, Radtke F, Wilson A. T cell fate specification and αβ/γδ lineage commitment. *Curr Opin Immunol*. 2001;13(2):219-224.
29. Kang J, Raulet DH. Events that regulate differentiation of αβ TCR+ and γδ TCR+ T cells from a common precursor. *Semin Immunol*. 1997;9(3):171-179.
30. MacDonald HR, Wilson A, MacDonald HR, Wilson A. The role of the T-cell receptor (TCR) in αβ/γδ lineage commitment: clues from intracellular TCR staining. *Immunol Rev*. 1998;165(1):87-94.
31. Fehling, Hans Jorg Gilfillian, Susan Ceredig R. aB/yD lineage Commitment in the Thymus of Normal and Genetically Manipulated Mice. *Adv Immunol*. 1998;71:1-76.
32. Turka LA, Schatz DG, Oettinger MA, et al. Thymocyte expression of RAG-1 and RAG-2: termination by T cell receptor cross-linking. *Science*. 1991;253(5021):778-781.
33. Gilfillan S, Dierich A, Lemeur M, Benoist C, Mathis D. Mice lacking TdT: Mature animals with an immature lymphocyte repertoire. *Science*. 1993;261(5125):1175- 1178.
34. Capone M, Hockett RD, Zlotnik A. Kinetics of T cell receptor β, γ, and δ rearrangements during adult thymic development: T cell receptor rearrangements are present in CD44+CD25+ Pro-T thymocytes. *Proc Natl Acad Sci*. 1998;95(21):12522-12527.
35. Saint-Ruf C, Ungewiss K, Groettrup M, Bruno L, Fehling HJ, von Boehmer H. Analysis and expression of a cloned pre-T cell receptor gene. *Science*. 1994;266(5188):1208 -1212.
36. von Boehmer H, Fehling HJ. Structure and Function of the Pre-T Cell Receptor. *Annu Rev Immunol*. 1997;15(1):433-452.
37. Wilson A, Held W, MacDonald HR. Two waves of recombinase gene expression in

developing thymocytes. *J Exp Med*. 1994;179(4):1355-1360.
38. Levelt CN, Eichmann K. Receptors and signals in early thymic selection. *Immunity*. 1995;3(6):635-646.
39. Groettrup M, von Boehmer H. A role for a pre-T-cell receptor in T-cell development. *Immunol Today*. 1993;14(12):610-614.
40. Levelt CN, Mombaerts P, Iglesias A, Tonegawa S, Eichmann K. Restoration of early thymocyte differentiation in T-cell receptor beta-chain-deficient mutant mice by transmembrane signaling through CD3 epsilon. *Proc Natl Acad Sci*. 1993;90(23):11401-11405.
41. Petrie HT, Livak F, Schatz DG, Strasser A, Crispe IN, Shortman K. Multiple rearrangements in T cell receptor alpha chain genes maximize the production of useful thymocytes. *J Exp Med*. 1993;178(2):615-622.
42. Xiong N, Raulet DH. Development and selection of γδ T cells. *Immunol Rev*. 2007;215(1):15-31.
43. Falk I, Nerz G, Haidl I, Krotkova A, Eichmann K. Immature thymocytes that fail to express TCRβ and/or TCRγ δ proteins die by apoptotic cell death in the CD44-CD25- (DN4) subset. *Eur J Immunol*. 2001;31(11):3308-3317.
44. Vasseur F, Le Campion A, Pénit C. Scheduled kinetics of cell proliferation and phenotypic changes during immature thymocyte generation. *Eur J Immunol*. 2001;31(10):3038-3047.
45. Ferreri AJM, Govi S, Pileri SA. Hepatosplenic gamma-delta T-cell lymphoma. *Crit Rev Oncol Hematol*. 2012;83(2):283-292.
46. Cooke CB, Krenacs L, Stetler-Stevenson M, et al. Hepatosplenic T-cell lymphoma: A distinct clinicopathologic entity of cytotoxic γδ T-cell origin. *Blood*. 1996;88(11):4265-4274.
47. Pai SY, Truitt ML, Ting CN, Leiden JM, Glimcher LH, Ho IC. Critical Roles for Transcription Factor GATA-3 in Thymocyte Development. *Immunity*. 2003;19(6):863-875.
48. Anderson G, Hare KJ, Jenkinson EJ. Positive selection of thymocytes: the long and winding road. *Immunol Today*. 1999;20(10):463-468.
49. Teh HS, Kisielow P, Scott B, et al. Thymic major histocompatibility complex antigens and the αβ T-cell receptor determine the CD4/CD8 phenotype of T cells. *Nature*. 1988;335(6187):229-233.
50. Kaye J, Hsu M-L, Sauron M-E, Jameson SC, Gascoigne NRJ, Hedrick SM. Selective development of CD4+ T cells in transgenic mice expressing a class II MHC-restricted antigen receptor. *Nature*. 1989;341(6244):746-749.
51. He X, He X, Dave VP, et al. The zinc finger transcription factor Th-POK regulates CD4 versus CD8 T-cell lineage commitment. *Nature*. 2005;433(7028):826-833.
52. Kappes DJ, He X, He X. Role of the transcription factor Th-POK in CD4:CD8 lineage commitment. *Immunol Rev*. 2006;209(1):237-252.
53. Nawijn MC, Ferreira R, Dingjan GM, et al. Enforced Expression of GATA-3 During T Cell Development Inhibits Maturation of CD8 Single-Positive Cells and Induces Thymic Lymphoma in Transgenic Mice. *J Immunol*. 2001;167(2):715-723.
54. Avitahl N, Winandy S, Friedrich C, Jones B, Ge Y, Georgopoulos K. Ikaros Sets Thresholds for T Cell Activation and Regulates Chromosome Propagation. *Immunity*. 1999;10(3):333-343.

55. Urban JA, Winandy S. Ikaros Null Mice Display Defects in T Cell Selection and CD4 versus CD8 Lineage Decisions. *J Immunol*. 2004;173(7):4470-4478.
56. Aliahmad P, Kaye J. Development of all CD4 T lineages requires nuclear factor TOX. *J Exp Med*. 2008;205(1):245-256.
57. Woolf E, Xiao C, Fainaru O, et al. Runx3 and Runx1 are required for CD8 T cell development during thymopoiesis. *Proc Natl Acad Sci*. 2003;100(13):7731-7736.
58. Cruz-Guilloty F, Pipkin M, Djuretic I, et al. Runx3 and T-box proteins cooperate to establish the transcriptional program of effector CTLs. *J Exp Med*. 2009;206:51-59.
59. Nossal GJ. Negative selection of lymphocytes. *Cell*. 1994;76(2):229-239.
60. Palmer E. Negative selection-clearing out the bad apples from the T-cell repertoire. *Nat Rev Immunol*. 2003;3(5):383-391.
61. Sims TN, Dustin ML. The immunological synapse: integrins take the stage. *Immunol Rev*. 2002;186(1):100-117.
62. Geijtenbeek TBH, Torensma R, van Vliet SJ, et al. Identification of DC-SIGN, a Novel Dendritic Cell-Specific ICAM-3 Receptor that Supports Primary Immune Responses. *Cell*. 2000;100(5):575-585.
63. Montoya MC, Sancho D, Bonello G, et al. Role of ICAM-3 in the initial interaction of T lymphocytes and APCs. *Nat Immunol*. 2002;3(2):159-168.
64. Rudd CE. Upstream-downstream: CD28 co-signaling pathways and T cell function. *Immunity*. 1996;4(6):527-534.
65. Alegre M-L, Frauwirth KA, Thompson CB. T-cell regulation by CD28 and CTLA-4. *Nat Rev Immunol*. 2001;1(3):220-228.
66. van Oers NS, Killeen N, Weiss A. Lck regulates the tyrosine phosphorylation of the T cell receptor subunits and ZAP-70 in murine thymocytes. *J Exp Med*. 1996;183(3):1053-1062.
67. Au-Yeung BB, Deindl S, Hsu L-Y, et al. The structure, regulation, and function of ZAP-70. *Immunol Rev*. 2009;228(1):41-57.
68. Macian F. NFAT proteins: key regulators of T-cell development and function. *Nat Rev Immunol*. 2005;5(6):472-484.
69. Huang Y, Wange RL. T cell receptor signaling: Beyond complex complexes. *J Biol Chem*. 2004;279(28):28827-28830.
70. Taniguchi T, Minami Y. The IL-2 IL-2 receptor system: A current overview. *Cell*. 1993;73(1):5-8.
71. Kadin M. Common Activated Helpter T-cell Origin for Lymphomatoid Papulosis, Mycosis Fungoides, and Some Types of Hodgkin's Disease. *Lancet*. 1985;326(8460):864-865.
72. Wong P, Pamer EG. CD8 T Cell Responses to Infectious Pathogens. *Annu Rev Immunol*. 2003;21(1):29-70.
73. Harty JT, Tvinnereim AR, White DW. CD8+ T Cell Effector Mechanisms in Resistance to Infection. *Annu Rev Immunol*. 2000;18(1):275-308.
74. Langerak AW, Sandberg Y, van Dongen JJM. Spectrum of T-large granular lymphocyte lymphoproliferations: ranging from expanded activated effector T cells to T-cell leukaemia. *Br J Haematol*. 2003;123(3):561-562.
75. Alekshun TJ, Sokol L. Diseases of Large Granular Lymphocytes. *Cancer Control*. 2007;14(2):141-150.
76. Lamy T, Moignet A, Loughran Jr TP. LGL leukemia: from pathogenesis to treatment. *Blood*. 2017;129(9):1082-1094.

77. Clemente MJ, Wlodarski MW, Makishima H, et al. Clonal drift demonstrates unexpected dynamics of the T-cell repertoire in T-large granular lymphocyte leukemia. *Blood*. 2011;118(16):4384-4393.
78. Szabo SJ, Kim ST, Costa GL, Zhang X, Fathman CG, Glimcher LH. A novel transcription factor, T-bet, directs Th1 lineage commitment. *Cell*. 2000;100(6):655-669.
79. Ansel KM, Djuretic I, Tanasa B, Rao A. Regulation of the TH2 Differentiation and Il4 Locus Accessibility. *Annu Rev Immunol*. 2006;24(1):607-656.
80. Swain SL, Weinberg AD, English M, Huston G. IL-4 directs the development of Th2-like helper effectors. *J Immunol*. 1990;145(11):3796-3806.
81. Mowen KA, Glimcher LH. Signaling pathways in Th2 development. *Immunol Rev*. 2004;202(1):203-222.
82. Glimcher LH, Murphy KM. Lineage commitment in the immune system: The T helper lymphocyte grows up. *Genes Dev*. 2000;14(14):1693-1711.
83. Khader SA, Bell GK, Pearl JE, et al. IL-23 and IL-17 in the establishment of protective pulmonary CD4+ T cell responses after vaccination and during Mycobacterium tuberculosis challenge. *Nat Immunol*. 2007;8(4):369-377.
84. Huang W, Na L, Fidel PL, Schwarzenberger P. Requirement of Interleukin-17A for Systemic Anti-Candida albicans Host Defense in Mice. *J Infect Dis*. 2004;190(3):624-631.
85. Rudner XL, Happel KI, Young EA, Shellito JE. Interleukin-23 (IL-23)-IL-17 cytokine axis in murine Pneumocystis carinii infection. *Infect Immun*. 2007;75(6):3055-3061.
86. Ivanov II, McKenzie BS, Zhou L, et al. The Orphan Nuclear Receptor RORγt Directs the Differentiation Program of Proinflammatory IL-17+ T Helper Cells. *Cell*. 2006;126(6):1121-1133.
87. Zenobia C, Hajishengallis G. Basic biology and role of interleukin-17 in immunity and inflammation. *Periodontol 2000*. 2015;69(1):142-159.
88. Johnston RJ, Poholek AC, DiToro D, et al. Bcl6 and Blimp-1 Are Reciprocal and Antagonistic Regulators of T Follicular Helper Cell Differentiation. *Science.* 2009;325(5943):1006-1010.
89. Nurieva RI, Chung Y, Martinez GJ, et al. Bcl6 Mediates the Development of T Follicular Helper Cells. *Science*. 2009;325(5943):1001-1005.
90. Nurieva RI, Chung Y, Hwang D, et al. Generation of T Follicular Helper Cells Is Mediated by Interleukin-21 but Independent of T Helper 1, 2, or 17 Cell Lineages. *Immunity*. 2008;29(1):138-149.
91. Yu D, Rao S, Tsai LM, et al. The Transcriptional Repressor Bcl-6 Directs T Follicular Helper Cell Lineage Commitment. *Immunity*. 2009;31(3):457-468.
92. Moser B, Schaerli P, Loetscher P. CXCR5+ T cells: follicular homing takes center stage in T-helper-cell responses. *Trends Immunol*. 2002;23(5):250-254.
93. Rolf J, Bell SE, Kovesdi D, et al. Phosphoinositide 3-Kinase Activity in T Cells Regulates the Magnitude of the Germinal Center Reaction. *J Immunol*. 2010;185(7):4042-4052.
94. Linterman MA, Beaton L, Yu D, et al. IL-21 acts directly on B cells to regulate Bcl-6 expression and germinal center responses. *J Exp Med*. 2010;207(2):353-363. \
95. Attygalle A, Al-Jehani R, Diss TC, et al. Neoplastic T cells in angioimmunoblastic T-cell lymphoma express CD10. *Blood*. 2002;99(2):627-633.
96. Dupuis J, Boye K, Martin N, et al. Expression of CXCL13 by Neoplastic Cells in Angioimmunoblastic T-Cell Lymphoma (AITL): A New Diagnostic Marker Providing Evidence That AITL Derives From Follicular Helper T Cells. *Am J Surg Pathol*.

2006;30(4):490-494.
97. Grogg KL, Attygalle AD, Macon WR, Remstein ED, Kurtin PJ, Dogan A. Angioimmunoblastic T-cell lymphoma: a neoplasm of germinal-center T-helper cells? *Blood*. 2005;106(4):1501-1502.
98. Krenacs L, Schaerli P, Kis G, Bagdi E. Phenotype of neoplastic cells in angioimmunoblastic T-cell lymphoma is consistent with activated follicular B helper T cells. *Blood*. 2006;108(3):1110-1111.
99. Frizzera G, Moran EM, Rappaport H. Angio-immunoblastic lymphadenopathy with dysproteinaemia. *Lancet*. 1974;303(7866):1070-1073.
100. Federico M, Rudiger T, Bellei M, et al. Clinicopathologic characteristics of angioimmunoblastic T-cell lymphoma: analysis of the international peripheral T-cell lymphoma project. *J Clin Oncol*. 2013;31(2):240-246.
101. Chen W, Konkel JE. TGF-beta and "adaptive" Foxp3(+) regulatory T cells. *J Mol Cell Biol*. 2010;2(1):30-36.
102. Hori S, Nomura T, Sakaguchi S. Control of Regulatory T Cell Development by the Transcription Factor Foxp3. *Science*. 2003;299(5609):1057-1061.
103. Horwitz DA, Zheng SG, Wang J, Gray JD. Critical role of IL-2 and TGF-β in generation, function and stabilization of Foxp3+CD4+ Treg. *Eur J Immunol*. 2008;38(4):912-915.
104. Karube K, Ohshima K, Tsuchiya T, et al. Expression of FoxP3, a key molecule in CD4+CD25+ regulatory T cells, in adult T-cell leukaemia/lymphoma cells. *Br J Haematol*. 2004;126(1):81-84.
105. Barros N, Woll F, Watanabe L, Montes M. Are increased Foxp3+ regulatory T cells responsible for immunosuppression during HTLV-1 infection? Case reports and review of the literature. *BMJ Case Rep*. 2012:1-5.
106. Matsubara Y, Hori T, Morita R, Sakaguchi S, Uchiyama T. Phenotypic and functional relationship between adult T-cell leukemia cells and regulatory T cells. *Leukemia*. 2005;19(3):482-483.
107. Uchiyama, T Yodoi, J Sagawa, K Takatsuki, K Uchino H. Adult T-cell leukemia: clinical and hematologic features of 16 cases. *Blood*. 2016;128(24):481-492.
108. Weisenburger DD, Savage KJ, Harris NL, et al. Peripheral T-cell lymphoma, not otherwise specified: A report of 340 cases from the International Peripheral T-cell Lymphoma Project. *Blood*. 2011;117(12):3402-3408.
109. Broccoli A, Zinzani PL. Peripheral T-cell lymphoma , not otherwise specified. *Blood*. 2017;129(9):1103-1112.
110. Vose JM, Neumann M, Harris ME. International peripheral T-cell and natural killer/T-cell lymphoma study: Pathology findings and clinical outcomes international T-cell lymphoma project. *J Clin Oncol*. 2008;26(25):4124-4130.
111. Pizzi, Marco Margolskee, Elizabeth Inghirami G. Pathogenesis of Peripheral T Cell Lymphoma. *Annu Rev Pathol Mech Dis*. 2018;13:293-320.
112. de Leval, L Parrens, M Le Bras F et al. Angioimmunoblastic T-cell lymphoma is the most common T-cell lymphoma in two distinct French information data sets. *Haematologica*. 2015;100(9):361-364.
113. Lemonnier F, Couronné L, Parrens M, et al. Recurrent TET2 mutations in peripheral T-cell lymphomas correlate with TFH-like features and adverse clinical parameters. *Blood*. 2012;120(7):1466-1469.
114. Sakata-Yanagimoto M, Enami T, Yoshida K, et al. Somatic RHOA mutation in

angioimmunoblastic T cell lymphoma. *Nat Genet*. 2014;46(2):171-175.
115. Palomero T, Couronne L, Khiabanian H, et al. Recurrent mutations in epigenetic regulators, RHOA and FYN kinase in peripheral T cell lymphomas. *Nat Genet*. 2014;46(2):166-170.
116. Watatani Y, Sato Y, Miyoshi H, et al. Molecular heterogeneity in peripheral T-cell lymphoma, not otherwise specified revealed by comprehensive genetic profiling. *Leukemia*. 2019:2867-2883.
117. Iqbal J, Wright G, Wang C, et al. Gene expression signatures delineate biologic and prognostic subgroups in peripheral T-cell lymphoma. *Blood*. 2014;123(19):2915-2924.
118. Wang T, Feldman AL, Wada DA, et al. GATA-3 expression identifies a high-risk subset of PTCL,NOS with distinct molecular and clinical features. *Blood*. 2014;123(19):3007-3015.
119. Heavican TB, Bouska A, Yu J, et al. Genetic drivers of oncogenic pathways in molecular subgroups of peripheral T-cell lymphoma. *Blood*. 2019;133(15):1664-1676.
120. Amador C, Greiner TC, Heavican TB, et al. Reproducing the Molecular Subclassification of Peripheral T-cell Lymphoma-NOS by Immunohistochemistry. *Blood*. 2019.
121. Abate F, da Silva-Almeida AC, Zairis S, et al. Activating mutations and translocations in the guanine exchange factor VAV1 in peripheral T-cell lymphomas. *Proc Natl Acad Sci*. 2017;114(4):764-769.
122. Streubel B, Vinatzer U, Willheim M, Raderer M, Chott A. Novel t(5;9)(q33;q22) fuses ITK to SYK in unspecified peripheral T-cell lymphoma. *Leukemia*. 2006;20(2):313-318.
123. Feldman AL, Sun DX, Law ME, et al. Overexpression of Syk tyrosine kinase in peripheral T-cell lymphomas. *Leukemia*. 2008;22(6):1139-1143.
124. Vasmatzis G, Johnson SH, Knudson RA, et al. Genome-wide analysis reveals recurrent structural abnormalities of TP63 and other p53-related genes in peripheral T-cell lymphomas. *Blood*. 2012;120(11):2280-2289.
125. Farooqi AA, Siddik ZH. Platelet-derived growth factor (PDGF) signalling in cancer: rapidly emerging signalling landscape. *Cell Biochem Funct*. 2015;33(5):257-265.
126. Pietras K, Sjöblom T, Rubin K, Heldin CH, Östman A. PDGF receptors as cancer drug targets. *Cancer Cell*. 2003;3(5):439-443.
127. Demoulin J-B, Essaghir A. PDGF receptor signaling networks in normal and cancer cells. *Cytokine Growth Factor Rev*. 2014;25(3):273-283.
128. Piccaluga PP, Agostinelli C, Califano A, et al. Gene expression analysis of peripheral T cell lymphoma , unspecified , reveals distinct profiles and new potential therapeutic targets. *J Clin Invest.* 2007;117(3):823-834.
129. Piccaluga PP, Rossi M, Agostinelli C, et al. Platelet-derived growth factor alpha mediates the proliferation of peripheral T-cell lymphoma cells via an autocrine regulatory pathway. *Leukemia*. 2014;28(8):1687-1697.
130. Jacobsen E, Pozdnyakova O, Redd R, et al. Imatinib mesylate lacks efficacy in relapsed/refractory peripheral T cell lymphoma. *Leuk Lymphoma*. 2015;56(4):993-998.
131. Martini M, De Santis MC, Braccini L, Gulluni F, Hirsch E. PI3K/AKT signaling pathway and cancer: an updated review. *Ann Med*. 2014;46(6):372-383.
132. Fruman DA, Rommel C. PI3K and cancer: lessons, challenges and opportunities. *Nat Rev Drug Discov*. 2014;13(2):140-156.
133. Hanahan D, Weinberg RA. Hallmarks of Cancer: The Next Generation. *Cell*. 2011;144(5):646-674.

134. Beagle B, Fruman DA. A lipid kinase cousin cooperates to promote cancer. *Cancer Cell*. 2011;19(6):693-695.
135. Hirsch E, Ciraolo E, Franco I, Ghigo A, Martini M. PI3K in cancer–stroma interactions: bad in seed and ugly in soil. *Oncogene*. 2014;33(24):3083-3090.
136. Soler A, Serra H, Pearce W, et al. Inhibition of the p110α isoform of PI3-kinase stimulates nonfunctional tumor angiogenesis. *J Exp Med*. 2013;210(10):1937-1945.
137. Samuels Y, Ericson K. Oncogenic PI3K and its role in cancer. *Curr Opin Oncol*. 2006;18(1):77-82.
138. Horwitz SM, Koch R, Porcu P, et al. Activity of the PI3K-δ,γ inhibitor duvelisib in a phase 1 trial and preclinical models of T-cell lymphoma. *Blood*. 2018;131(8):888-898.
139. Bachow SH, O'Connor OA. Emerging therapies in relapsed and refractory peripheral T-cell lymphoma. *Clin Adv Hematol Oncol*. 2015;13(12):837-846.
140. Chiarle R, Podda A, Prolla G, Gong J, Thorbecke GJ, Inghirami G. CD30 in normal and neoplastic cells. *Clin Immunol*. 1999;90(2):157-164.
141. Buchan SL, Al-Shamkhani A. Distinct Motifs in the Intracellular Domain of Human CD30 Differentially Activate Canonical and Alternative Transcription Factor NF-κB Signaling. *PLoS One*. 2012;7(9).
142. Bisig B, de Reyniès A, Bonnet C, et al. CD30-positive peripheral T-cell lymphomas share molecular and phenotypic features. *Haematologica*. 2013;98(8):1250-1258.
143. Younes A, Bartlett NL, Leonard JP, et al. Brentuximab vedotin (SGN-35) for relapsed CD30-positive lymphomas. *N Engl J Med*. 2010;363(19):1812-1821.
144. Pro B, Advani R, Brice P, et al. Brentuximab Vedotin (SGN-35) in Patients With Relapsed or Refractory Systemic Anaplastic Large-Cell Lymphoma: Results of a Phase II Study. *J Clin Oncol*. 2012;30(18):2190-2196.
145. Horwitz SM, Advani RH, Bartlett NL, et al. Objective responses in relapsed T-cell lymphomas with single-agent brentuximab vedotin. *Blood*. 2014;123(20):3095-3100.
146. Dorn CR, Taylor DO, Schneider R, Hibbard HH, Klauber MR. Survey of animal neoplasms in Alameda and Contra Costa Counties, California. II. Cancer morbidity in dogs and cats from Alameda County. *J Natl Cancer Inst*. 1968;40(2):307-318.
147. Dorn CR, Taylor DO, Hibbard HH. Epizootiologic characteristics of canine and feline leukemia and lymphoma. *Am J Vet Res*. 1967;28(125):993-1001.
148. Dobson JM, Samuel S, Milstein H, Rogers K, Wood JLN. Canine neoplasia in the UK: estimates of incidence rates from a population of insured dogs. *J Small Anim Pract*. 2002;43(6):240-246.
149. Merlo DF, Rossi L, Pellegrino C, et al. Cancer Incidence in Pet Dogs: Findings of the Animal Tumor Registry of Genoa, Italy. *J Vet Intern Med*. 2008;4:976-984.
150. Edwards DS, Henley WE, Harding EF, Dobson JM, Wood JLN. Breed incidence of lymphoma in a UK population of insured dogs. *Vet Comp Oncol*. 2003;1(4):200-206.
151. Howlader N, Noone AM, Krapcho M, Miller D, Bishop K, Kosary CL, Yu M, Ruhl J, Tatalovich Z, Mariotto A, Lewis DR, Chen HS, Feuer EJ CK (eds). SEER Cancer Statistics Review, 1975-2014. *Natl Cancer Institute; Bethesda MD, USA*. 2016.
152. Valli VE, San Myint M, Barthel a, et al. Classification of canine malignant lymphomas according to the World Health Organization criteria. *Vet Pathol*. 2011;48(1):198-211.
153. Modiano JF, Breen M, Burnett RC, et al. Distinct B-Cell and T-Cell Lymphoproliferative Disease Prevalence among Dog Breeds Indicates Heritable Risk. *Cancer Res*. 2005;65(13):5654-5662.

154. Priester WA. Canine Lymphoma: Relative Risk in the Boxer Breed. *JNCI J Natl Cancer Inst*. 1967;39(5):833-845.
155. Pastor M, Chalvet-Monfray K, Marchal T, et al. Genetic and environmental risk indicators in canine non-Hodgkin's lymphomas: Breed associations and geographic distribution of 608 cases diagnosed throughout France over 1 year. *J Vet Intern Med*. 2009;23(2):301-310.
156. Seelig D, Avery A, Ehrhart E, Linden M. The Comparative Diagnostic Features of Canine and Human Lymphoma. *Vet Sci*. 2016;3(2):11.
157. Ito D, Frantz AM, Modiano JF. Canine lymphoma as a comparative model for human non-Hodgkin lymphoma: Recent progress and applications. *Vet Immunol Immunopathol*. 2014;159(3-4):192-201.
158. Valli VE, Kass PH, Myint MS, Scott F. Canine Lymphomas: Association of Classification Type , Disease Stage , Tumor Subtype , Mitotic Rate , and Treatment With Survival. 2013;50(5):738-748.
159. Harris LJ, Hughes KL, Ehrhart EJ, Labadie JD, Yoshimoto J, Avery AC. Canine CD4+ T-cell lymphoma identified by flow cytometry exhibits a consistent histomorphology and gene expression profile. *Vet Comp Oncol*. 2019.
160. Seelig DM, Avery P, Webb T, et al. Canine t-zone lymphoma: Unique immunophenotypic features, outcome, and population characteristics. *J Vet Intern Med*. 2014;28(3):878-886.
161. Pittaway R, Wu Y, Szladovits B, et al. Diagnosis of anaplastic large-cell lymphoma in a dog using CD30 immunohistochemistry. *J Vet Diagnostic Investig*. 2018;30(3):455-458.
162. Ponce F, Marchal T, Magnol JP, et al. A morphological study of 608 cases of canine malignant lymphoma in France with a focus on comparative similarities between canine and human lymphoma morphology. *Vet Pathol*. 2010;47(3):414-433.
163. Avery PR, Burton J, Bromberek JL, Seelig DM, Elmslie R, Correa S, Ehrhart EJ, Morley PS, Avery AC. Flow Cytometric Characterization and Clinical Outcome of CD4 + T-Cell Lymphoma in Dogs: 67 Cases. *J Vet Intern Med*. 2014;28(2):538-546.
164. Deravi N, Berke O, Woods JP, Bienzle D. Specific immunotypes of canine T cell lymphoma are associated with different outcomes. *Vet Immunol Immunopathol*. 2017;19:5-13.
165. Lurie DM, Milner RJ, Suter SE, Vernau W. Immunophenotypic and cytomorphologic subclassification of T-cell lymphoma in the boxer breed. *Vet Immunol Immunopathol*. 2008;125(1-2):102-110.
166. Fournel-Fleury C, Ponce F, Felman P, et al. Canine T-cell lymphomas: a morphological, immunological, and clinical study of 46 new cases. *Vet Pathol*. 2002;39(1):92-109.
167. Elvers I, Turner-Maier J, Swofford R, et al. Exome sequencing of lymphomas from three dog breeds reveals somatic mutation patterns reflecting genetic background. *Genome Res*. 2015;25(11):1634-1645.
168. Wong CH, Siah KW, Lo AW. Estimation of clinical trial success rates and related parameters. *Biostatistics*. 2019;20(2):273-286.
169. Gordon I, Paoloni M, Mazcko C, Khanna C. The Comparative Oncology Trials Consortium : Using Spontaneously Occurring Cancers in Dogs to Inform the Cancer Drug Development Pathway. *PLoS Med.* 2009;6(10):2-6.
170. Khanna C, Lindblad-Toh K, Vail D, London C, Bergman P, Barber L et al. The dog as a cancer model. *Nat Biotechnol*. 2006;24(9):1065.
171. Simpson S, Dunning MD, de Brot S, Grau-Roma L, Mongan NP, Rutland CS.

Comparative review of human and canine osteosarcoma: morphology, epidemiology, prognosis, treatment and genetics. *Acta Vet Scand*. 2017;59(1):71.
172. *Losartan + Sunitinib in Treatment of Osteosarcoma*; 2020. https://clinicaltrials.gov/ct2/show/NCT03900793.
173. Regan DP, Coy JW, Chahal KK, et al. The Angiotensin Receptor Blocker Losartan Suppresses Growth of Pulmonary Metastases via AT1R-Independent Inhibition of CCR2 Signaling and Monocyte Recruitment. *J Immunol*. 2019;202(10):3087-3102.
174. Martini V, Marconato L, Poggi a, et al. Canine small clear cell/T-zone lymphoma: clinical presentation and outcome in a retrospective case series. *Vet Comp Oncol*. 2016;14:1-9.
175. Ponce F, Magnol JP, Marchal T, et al. High-grade canine T-cell lymphoma / leukemia with plasmacytoid morphology: a clinical pathological study of nine cases. *J Vet Diagn Invest.* 2003;15(4):330-337.
176. Tasca S, Carli E, De Lorenzi D, Furlanello T. Use of fine needle aspirates and flow cytometry for the diagnosis, classification, and immunophenotyping of canine lymphomas. *J Vet Diagn Invest.* 2005;17(4)323-330.
177. Vernau W, Moore PF. An immunophenotypic study of canine leukaemias and preliminary assessment of clonality by Polymerase Chain Reaction. *Vet Immol Immunopathol*. 1999;69(2-4):145-164.
178. Martini V, Melega M, Riondato F, et al. A retrospective study of flow cytometric characterization of suspected extranodal lymphomas in dogs. *J Vet Diagnostic Investig*. 2018;30(6):830-836.
179. Moore PF, Olivry T, Naydan D. Canine cutaneous epitheliotropic lymphoma (mycosis fungoides) is a proliferative disorder of CD8+ T Cells. *Am J Pathol.* 1994;144(2):421-429.
180. Keller SM, Vernau W, Hodges J, et al. Hepatosplenic and Hepatocytotropic T-Cell Lymphoma: Two Distinct Types of T-Cell Lymphoma in Dogs. *Vet Pathol*. 2013;50(2):281-290.
181. Oluwasanjo A, Kartan S, Johnson W, et al. Peripheral T-Cell Lymphoma, not Otherwise Specified (PTCL-NOS). In: Querfeld C, Zain J, Rosen ST, eds. *T-Cell and NK-Cell Lymphomas: From Biology to Novel Therapies*. Springer International Publishing; 2019:83-98.
182. Kim D, Paggi JM, Park C, Bennett C, Salzberg SL. Graph-based genome alignment and genotyping with HISAT2 and HISAT-genotype. *Nat Biotechnol*. 2019;37(8):907-915.
183. Anders S, Pyl PT, Huber W. Genome analysis HTSeq — a Python framework to work with high-throughput sequencing data. *Bioinformatics.*2015;31(2):166-169.
184. Love MI, Huber W, Anders S. Moderated estimation of fold change and dispersion for RNA-seq data with DESeq2. *Genome Biol.* 2014;15(550):1-21.
185. Gould J. Morpheus. https://software.broadinstitute.org/morpheus/.
186. Subramanian A, Tamayo P, Mootha VK, Mukherjee S, Ebert BL. Gene set enrichment analysis : A knowledge-based approach for interpreting genome-wide. *PNAS.* 2005;102(43):15545-15550.
187. Liberzon A, Birger C, Thorvaldsdóttir H, Ghandi M, Mesirov JP, Tamayo P. The Molecular Signatures Database Hallmark Gene Set Collection. *Cell Syst*. 2015;1(6):417-425.
188. Kisseberth WC, Nadella MVP, Breen M, et al. A novel canine lymphoma cell line: A translational and comparative model for lymphoma research. *Leuk Res*. 2007;31(12):1709-

1720.
189. Hawkins ED, Hommel M, Turner ML, Battye FL, Markham JF, Hodgkin PD. Measuring lymphocyte proliferation, survival and differentiation using CFSE time-series data. *Nat Protoc*. 2007;2(9):2057-2067.
190. Croft D, Mundo AF, Haw R, et al. The Reactome Pathway Knowledgebase. *Nucleic Acids Res.* 2014;42(D2):D472-D477.
191. Fabregat A, Jupe S, Matthews L, et al. The Reactome Pathway Knowledgebase. *Nucleic Acids Res* 2018;46(D1):D649-D655.
192. Jassal B, Matthews L, Viteri G, et al. The Reactome Pathway Knowledgebase. *Nucleic Acids Res*. 2019;48(D1):D498-D503.
193. Bauer K, Hadzijusufovic E, Cerny-Reiterer S, et al. IL-4 downregulates expression of the target receptor CD30 in neoplastic canine mast cells. *Vet Comp Oncol*. 2016:1-17.
194. Sondka Z, Bamford S, Cole CG, Ward SA, Dunham I, Forbes SA. The COSMIC Cancer Gene Census: describing genetic dysfunction across all human cancers. *Nat Rev Cancer*. 2018;18(11):696-705.
195. Repana D, Nulsen J, Dressler L, et al. The Network of Cancer Genes (NCG): a comprehensive catalogue of known and candidate cancer genes from cancer sequencing screens. *Genome Biol*. 2019;20(1).
196. Stein H, Foss H, Du H, et al. CD30 (+) anaplastic large cell lymphoma : A review of its histopathologic, genetic, and clinical features. *Blood.* 2000;96(12):3681-3695.
197. Song MS, Salmena L, Pandolfi PP. The functions and regulation of the PTEN tumour suppressor. *Nat Rev Mol Cell Biol*. 2012;13(5):283-296.
198. Pilarski R, Burt R, Kohlman W, Pho L, Shannon KM, Swisher E. Cowden syndrome and the PTEN hamartoma tumor syndrome: Systematic review and revised diagnostic criteria. *J Natl Cancer Inst*. 2013;105(21):1607-1616.
199. Shaffer AL, Young RM, Staudt LM. Pathogenesis of Human B Cell Lymphomas. *Annu Rev Immunol*. 2012;30(1):565-610.
200. Rosenwald A, Wright G, Chan WC, et al. The use of molecular profiling to predict survival after chemotherapy for diffuse large-B-cell lymphoma. *N Engl J Med*. 2002;346(25):1937-1947.
201. Federico M, Rudiger T, Bellei M, et al. Clinicopathologic characteristics of angioimmunoblastic t-cell lymphoma: Analysis of the international peripheral t-cell lymphoma project. *J Clin Oncol*. 2013;31(2):240-246.
202. Iqbal J, Weisenburger DD, Greiner TC, et al. Molecular signatures to improve diagnosis in peripheral T-cell lymphoma and prognostication in angioimmunoblastic T-cell lymphoma. *Blood.* 2010;115(5):1026-1036.
203. Kanhere A, Hertweck A, Bhatia U, et al. T-bet and GATA3 orchestrate Th1 and Th2 differentiation through lineage-specific targeting of distal regulatory elements. *Nat Commun*. 2012;3(1):1268.
204. Yagi R, Zhu J, Paul WE. An updated view on transcription factor GATA3-mediated regulation of Th1 and Th2 cell differentiation. *Int Immunol*. 2011;23(7):415-420.
205. Shea JJO, Paul WE, Cells CDT. Commitment and Plasticity of Helper. *Science.* 2012;1098(2010):1098-1103.
206. Andrews RG, Singer JW, Bernstein ID. Precursors of Colony-Forming Cells in Humans Can Be Distinguished From Colony-Forming Cells by Expression of the CD33 and CD34 Antigens and Light Scatter Properties. *J Exp Med.* 1989;169(5):1721-31.

207. Berenson RJ, Andrews RG, Bensinger WI, et al. Antigen CD34+ marrow cells engraft lethally irradiated baboons. *J Clin Invest*. 1988;81(3):951-955.
208. Sato T, Laver JH, Ogawa M. Reversible Expression of CD34 by Murine Hematopoietic Stem Cells. *Blood*. 1999;94(8):2548-2554.
209. Smith-Garvin JE, Koretzky GA, Jordan MS. T cell activation. *Annual Review of Immunology*. 2009;27(1):591-619.
210. Shatrova AN, Mityushova E V., Vassilieva IO, et al. Time-dependent regulation of IL-2R α-chain (CD25) expression by TCR signal strength and IL-2-induced STAT5 signaling in activated human blood T lymphocytes. *PLoS One*. 2016;11(12):1-19.
211. Kelley TW, Parker CJ. CD4(+)CD25(+)Foxp3(+) regulatory T cells and hematologic malignancies. *Front Biosci*. 2010;2:980-992.
212. Ko HS, Fu SM, Winchester RJ, Yu DT, Kunkel HG. Ia determinants on stimulated human T lymphocytes. Occurrence on mitogen- and antigen-activated T cells. *J Exp Med*. 1979;150(2):246-255.
213. Isaacson JA, Flaming KP, Roth JA. Increased MHC class II and CD25 expression on lymphocytes in the absence of persistent lymphocytosis in cattle experimentally infected with bovine leukemia virus. *Vet Immunol Immunopathol*. 1998;64(3):235-248.
214. Bendali-Ahcène S, Cadore JL, Fontaine M, Monier JC. Anti-α chain monoclonal antibodies of equine MHC class-II antigens: Applications to equine infectious anaemia. *Res Vet Sci*. 1997;62(2):99-104.
215. Hammond SA, Issel CJ, Montelaro RC. General method for the detection and in vitro expansion of equine cytolytic T lymphocytes. *J Immunol Methods*. 1998;213(1):73-85.
216. Doveren RF, Buurman WA, Schutte B, Groenewegen G, van der Linden CJ. Class II antigens on canine T lymphocytes. *Tissue Antigens*. 1985;25(5):255-265.
217. Doveren RF, van der Linden CJ, Spronken EEM, Groenewegen G, Buurman WA. Canine MHC-class II antigens on B and T lymphocytes. *Tissue Antigens*. 1986;27(2):87-98.
218. Abbas AR, Baldwin D, Ma Y, et al. Immune response in silico (IRIS): immune-specific genes identified from a compendium of microarray expression data. *Genes Immun*. 2005;6(4):319-331.
219. Dik WA, Pike-Overzet K, Weerkamp F, et al. New insights on human T cell development by quantitative T cell receptor gene rearrangement studies and gene expression profiling . *J Exp Med*. 2005;201(11):1715-1723.
220. Kanno Y, Vahedi G, Hirahara K, Singleton K, O'Shea JJ. Transcriptional and Epigenetic Control of T Helper Cell Specification: Molecular Mechanisms Underlying Commitment and Plasticity. *Annu Rev Immunol*. 2012;30(1):707-731.
221. Kaech SM, Cui W. Transcriptional control of effector and memory CD8+ T cell differentiation. *Nat Rev Immunol*. 2012;12(11):749-761.
222. Intlekofer AM, Takemoto N, Wherry EJ, et al. Effector and memory CD8+ T cell fate coupled by T-bet and eomesodermin. *Nat Immunol*. 2005;6(12):1236-1244.
223. Pipkin ME, Sacks JA, Cruz-Guilloty F, Lichtenheld MG, Bevan MJ, Rao A. Interleukin-2 and Inflammation Induce Distinct Transcriptional Programs that Promote the Differentiation of Effector Cytolytic T Cells. *Immunity*. 2010;32(1):79-90.
224. Yamada T, Park CS, Mamonkin M, Lacorazza HD. Transcription factor ELF4 controls the proliferation and homing of CD8+ T cells via the Krüppel-like factors KLF4 and KLF2. *Nat Immunol*. 2009;10(6):618-626.
225. Gil MP, Ploquin MJY, Watford WT, et al. Regulating type 1 IFN effects in CD8 T cells

during viral infections: changing STAT4 and STAT1 expression for function. *Blood*. 2012;120(18):3718-3728.
226. Szabo SJ, Sullivan BM, Peng SL, Glimcher LH. Molecular Mechanisms Regulating Th1 Immune Responses. *Annu Rev Immunol*. 2003;21(1):713-758.
227. Zhu J, Yamane H, Cote-Sierra J, Guo L, Paul WE. GATA-3 promotes Th2 responses through three different mechanisms: induction of Th2 cytokine production, selective growth of Th2 cells and inhibition of Th1 cell-specific factors. *Cell Res*. 2006;16(1):3-10.
228. Wei G, Wei L, Zhu J, et al. Global Mapping of H3K4me3 and H3K27me3 Reveals Specificity and Plasticity in Lineage Fate Determination of Differentiating CD4+ T Cells. *Immunity*. 2009;30(1):155-167.
229. Azzam BHS, Grinberg A, Lui K, Shen H, Shores EW, Love PE. CD5 Expression is Developmentally Regulated by T Cell Receptor (TCR) Signals and TCR Avidity. *J Exp Med*. 1998;188(12):2301-2311.
230. Fowlkes BJ, Edison L, Mathieson BJ, Chused TM. Early T lymphocytes. Differentiation in vivo of adult intrathymic precursor cells. *J Exp Med*. 1985;162(3):802-822.
231. Escribano L, Ocqueteaub M, Almeida J, Orfao A, Migue JFS. Expression of the c-kit (CD117) Molecule in Normal and Malignant Hematopoiesis. *Leuk Lymphoma*. 1998;30(5-6):459-466.
232. Pinto A, Gloghini A, Gattei V, Aldinucci D, Zagonel V, Carbone A. Expression of the c-kit receptor in human lymphomas is restricted to Hodgkin's disease and CD30+ anaplastic large cell lymphomas. *Blood*. 1994;83(3):785-792.
233. Ocqueteau M, Orfao A, García-Sanz R, Almeida J, Gonzalez M, San Miguel JF. Expression of the CD117 antigen (C-Kit) on normal and myelomatous plasma cells. *Br J Haematol*. 1996;95(3):489-493.
234. Sykora KW, Tomeczkowski J, Reiter A. C-Kit receptors in childhood malignant lymphoblastic cells. *Leuk Lymphoma*. 1997;25(3-4):201-216.
235. Ashman LK, Griffith R. Therapeutic targeting of c-KIT in cancer. *Expert Opin Investig Drugs*. 2013;22(1):103-115.
236. Ho IC, Tai TS, Pai SY. GATA3 and the T-cell lineage: essential functions before and after T-helper-2-cell differentiation. *Nat Rev Immunol*. 2009;9(2):125-135.
237. David-Fung ES, Yui MA, Morales M, et al. Progression of regulatory gene expression states in fetal and adult pro-T-cell development. *Immunol Rev*. 2006;209(1):212-236.
238. Tydell CC, David-Fung ES, Moore JE, Rowen L, Taghon T, Rothenberg EV. Molecular Dissection of Prethymic Progenitor Entry into the T Lymphocyte Developmental Pathway. *J Immunol*. 2007;179(1):421-438.
239. Dai X, Theobard R, Cheng H, Xing M, Zhang J. Fusion genes: A promising tool combating against cancer. *Biochim Biophys Acta - Rev Cancer*. 2018;1869(2):149-160.
240. Mitelman F, Johansson B, Mertens F. The impact of translocations and gene fusions on cancer causation. *Nat Rev Cancer*. 2007;7(4):233-245.
241. Dalla-Favera R, Bregni M, Erikson J, Patterson D, Gallo RC, Croce CM. Human c-myc onc gene is located on the region of chromosome 8 that is translocated in Burkitt lymphoma cells. *Proc Natl Acad Sci U S A*. 1982;79(24):7824-7827.
242. Persson M, Andrén Y, Mark J, Horlings HM, Persson F, Stenman G. Recurrent fusion of MYB and NFIB transcription factor genes in carcinomas of the breast and head and neck. *Proc Natl Acad Sci*. 2009;106(44):18740-18744.
243. Shtivelman E, Lifshitz B, Gale RP, Canaani E. Fused transcript of abl and bcr genes in

chronic myelogenous leukaemia. *Nature*. 1985;315(6020):550-554.
244. McWhirter JR, Galasso DL, Wang JY. A coiled-coil oligomerization domain of Bcr is essential for the transforming function of Bcr-Abl oncoproteins. *Mol Cell Biol*. 1993;13(12):7587-7595.
245. Morris SW, Kirstein MN, Valentine MB, et al. Fusion of a kinase gene, ALK, to a nucleolar protein gene, NPM, in non-Hodgkins lymphoma. *Science*. 1994;263(5151):1281-1284.
246. Xing X, Feldman AL. Anaplastic Large Cell Lymphomas: ALK Positive, ALK Negative, and Primary Cutaneous. *Adv Anat Pathol*. 2015;22(1):29-49.
247. Hapgood G, Savage KJ. The biology and management of systemic anaplastic large cell lymphoma. *Blood*. 2015;126(1):17-25.
248. Piccaluga PP, Tabanelli V, Pileri SA. Molecular genetics of peripheral T-cell lymphomas. *Int J Hematol*. 2014;99(3):219-226.
249. Mossé YP, Lim MS, Voss SD, et al. Safety and activity of crizotinib for paediatric patients with refractory solid tumours or anaplastic large-cell lymphoma: a Children's Oncology Group phase 1 consortium study. *Lancet Oncol*. 2013;14(6):472-480.
250. Gambacorti-Passerini C, Messa C, Pogliani EM. Crizotinib in Anaplastic Large-Cell Lymphoma. *N Engl J Med*. 2011;364(8):775-776.
251. Savage KJ, Harris NL, Vose JM, et al. ALK− anaplastic large-cell lymphoma is clinically and immunophenotypically different from both ALK+ ALCL and peripheral T-cell lymphoma, not otherwise specified: report from the International Peripheral T-Cell Lymphoma Project. *Blood*. 2008;111(12):5496-5504.
252. Gascoyne RD, Aoun P, Wu D, et al. Prognostic Significance of Anaplastic Lymphoma Kinase (ALK) Protein Expression in Adults With Anaplastic Large Cell Lymphoma. *Blood*. 1999;93(11):3913-3921.
253. Yoo HY, Kim P, Kim WS, et al. Frequent CTLA4-CD28 gene fusion in diverse types of T-cell lymphoma. *Haematologica*. 2016;101(6):757-763.
254. Yoo HY, Kim P, Kim WS, et al. Author reply to Comment on: Frequent CTLA4-CD28 gene fusion in diverse types of T-cell lymphoma, by Yoo et al. *Haematologica*. 2016;101(6):e271-e271.
255. Gong Q, Wang C, Rohr J, Feldman AL, Chan WC, McKeithan TW. Comment on: Frequent CTLA4-CD28 gene fusion in diverse types of T-cell lymphoma, by Yoo et al. *Haematologica*. 2016;101(6):e269-e270.
256. Huang Y, Moreau A, Dupuis J, et al. Peripheral T-cell lymphomas with a follicular growth pattern are derived from follicular helper T cells (TFH) and may show overlapping features with angioimmunoblastic T-cell lymphomas. *Am J Surg Pathol*. 2009;33(5):682-690.
257. Streubel B, Vinatzer U, Willheim M, Raderer M, Chott A. Novel t(5;9)(q33;q22) fuses ITK to SYK in unspecified peripheral T-cell lymphoma. *Leukemia*. 2006;20(2):313-318.
258. Dierks C, Adrian F, Fisch P, et al. The ITK-SYK fusion oncogene induces a T-cell lymphoproliferative disease in mice mimicking human disease. *Cancer Res*. 2010;70(15):6193-6204.
259. Attygalle A, Feldman A, Dogan A. ITK/SYK Translocation in Angioimmunoblastic T-cell Lymphoma. *Am J Surg Pathol*. 2013;37:1456-1457.
260. Boddicker RL, Razidlo GL, Dasari S, et al. Integrated mate-pair and RNA sequencing identifies novel, targetable gene fusions in peripheral T-cell lymphoma. *Blood*.

2016;128(9):1234-1245.
261. Ulvé R, Rault M, Bahin M, et al. Discovery of Human-Similar Gene Fusions in Canine Cancers. *Cancer Res*. 2017;77(21):5721-5727.
262. Breen M, Modiano JF. Evolutionarily conserved cytogenetic changes in hematological malignancies of dogs and humans – man and his best friend share more than companionship. *Chromosom Res*. 2008;16(1):145-154.
263. Kim P, Jang YE, Lee S. Fusionscan: Accurate prediction of fusion genes from RNA-seq data. *Genomics and Informatics*. 2019;17(3):1-12.
264. Wang Q, Xia J, Jia P, Pao W, Zhao Z. Application of next generation sequencing to human gene fusion detection: computational tools, features and perspectives. *Brief Bioinform*. 2013;14(4):506-519.
265. Nicorici D, Şatalan M, Edgren H, et al. FusionCatcher– a tool for finding somatic fusion genes in paired-end RNA-sequencing data. *bioRxiv*. 2014:11650.
266. Earp MA, Raghavan R, Li Q, et al. Characterization of fusion genes in common and rare epithelial ovarian cancer histologic subtypes. *Oncotarget*. 2017;8(29):46891-46899.
267. Liu S, Tsai W-H, Ding Y, et al. Comprehensive evaluation of fusion transcript detection algorithms and a meta-caller to combine top performing methods in paired-end RNA-seq data. *Nucleic Acids Res*. 2016;44(5):e47-e47.
268. Jono H, Ando Y. Midkine: a novel prognostic biomarker for cancer. *Cancers*. 2010;2(2):624-641.
269. Filippou PS, Karagiannis GS, Constantinidou A. Midkine (MDK) growth factor: a key player in cancer progression and a promising therapeutic target. *Oncogene*. 2020;39(10):2040-2054.
270. Ioannou K, Samara P, Livaniou E, Derhovanessian E, Tsitsilonis OE. Prothymosin alpha: a ubiquitous polypeptide with potential use in cancer diagnosis and therapy. *Cancer Immunol Immunother*. 2012;61(5):599-614.
271. Sutherland KD, Visvader JE, Choong DYH, Sum EYM, Lindeman GJ, Campbell IG. Mutational analysis of the LMO4 gene, encoding a BRCA1-interacting protein, in breast carcinomas. *Int J Cancer*. 2003;107(1):155-158.
272. Caratozzolo MF, Marzano F, Mastropasqua F, Sbisà E, Tullo A. TRIM8: Making the Right Decision between the Oncogene and Tumour Suppressor Role. *Genes.* 2017;8(12):354.
273. Mullighan CG, Xiaoping S, Zhang J, et al. Deletion of IKZF1 and Prognosis in Acute Lymphoblastic Leukemia. *N Engl J Med*. 2009;360(5):470-480.
274. Camus V, Miloudi H, Taly A, Sola B, Jardin F. XPO1 in B cell hematological malignancies: from recurrent somatic mutations to targeted therapy. *J Hematol Oncol*. 2017;10(1):47.
275. Jain P, Kanagal-Shamanna R, Wierda W, et al. Clinical and molecular characteristics of XPO1 mutations in patients with chronic lymphocytic leukemia. *Am J Hematol*. 2016;91(11):E478-E479.
276. Kim J, McMillan E, Kim HS, et al. XPO1-dependent nuclear export is a druggable vulnerability in KRAS-mutant lung cancer. *Nature*. 2016;538(7623):114-117.
277. Wilson CH, McIntyre RE, Arends MJ, Adams DJ. The activating mutation R201C in GNAS promotes intestinal tumourigenesis in ApcMin/+ mice through activation of Wnt and ERK1/2 MAPK pathways. *Oncogene*. 2010;29(32):4567-4575.
278. Zhang B, Sun N, Mu X, et al. G Protein Alpha S Subunit Promotes Cell Proliferation of

Renal Cell Carcinoma with Involvement of Protein Kinase A Signaling. *DNA Cell Biol*. 2017;36(3):237-242.
279. He X, Zhang L, Chen Y, et al. The G protein α subunit Gαs is a tumor suppressor in Sonic hedgehog−driven medulloblastoma. *Nat Med*. 2014;20(9):1035-1042.
280. Morimura S, Suzuki K, Takahashi K. Nonmuscle myosin IIA is required for lamellipodia formation through binding to WAVE2 and phosphatidylinositol 3,4,5-triphosphate. *Biochem Biophys Res Commun*. 2011;404(3):834-840.
281. Mu Y, Chen Y, Zhang G, et al. Identification of stromal differentially expressed proteins in the colon carcinoma by quantitative proteomics. *Electrophoresis*. 2013;34(11):1679-1692.
282. Wang Y, Liu S, Zhang Y, Yang J. Myosin Heavy Chain 9: Oncogene or Tumor Suppressor Gene? *Med Sci Monit*. 2019;25:888-892.
283. Marafioti T, Mancini C, Ascani S, et al. Leukocyte-specific phosphoprotein-1 and PU.1: two useful markers for distinguishing T-cell-rich B-cell lymphoma from lymphocyte-predominant Hodgkin's disease. *Haematologica*. 2004;89(8):957-964.
284. Zhang H, Wang Y, Liu Z, et al. Lymphocyte-specific protein 1 inhibits the growth of hepatocellular carcinoma by suppressing ERK1/2 phosphorylation. *FEBS Open Bio*. 2016;6(12):1227-1237.
285. Lim U, Kocarnik JM, Bush WS, et al. Pleiotropy of cancer susceptibility variants on the risk of non-Hodgkin lymphoma: the PAGE consortium. *PLoS One*. 2014;9(3):e89791-e89791.
286. Rheinbay E, Nielsen MM, Abascal F, et al. Analyses of non-coding somatic drivers in 2,658 cancer whole genomes. *Nature*. 2020;578(7793):102-111.
287. Gharbi SI, Rincón E, Avila-Flores A, et al. Diacylglycerol kinase ζ controls diacylglycerol metabolism at the immunological synapse. *Mol Biol Cell*. 2011;22(22):4406-4414.
288. Rabbitts TH. LMO T-cell translocation oncogenes typify genes activated by chromosomal translocations that alter transcription and developmental processes. *Genes Dev*. 1998;12(17):2651-2657.
289. Grutz G, Forster A, Rabbitts TH. Identification of the LMO4 gene encoding an interaction partner of the LIM-binding protein LDB1/NLI1: a candidate for displacement by LMO proteins in T cell acute leukaemia. *Oncogene*. 1998;17(21):2799-2803.
290. Montañez-Wiscovich ME, Seachrist DD, Landis MD, Visvader J, Andersen B, Keri RA. LMO4 is an essential mediator of ErbB2/HER2/Neu-induced breast cancer cell cycle progression. *Oncogene*. 2009;28(41):3608-3618.
291. Tessema M, Yingling CM, Grimes MJ, et al. Differential epigenetic regulation of TOX subfamily high mobility group box genes in lung and breast cancers. *PLoS One*. 2012;7(4):e34850.
292. Vong QP, Leung W-H, Houston J, et al. TOX2 regulates human natural killer cell development by controlling T-BET expression. *Blood*. 2014;124(26):3905-3913.
293. Seo H, Chen J, González-Avalos E, et al. TOX and TOX2 transcription factors cooperate with NR4A transcription factors to impose CD8+ T cell exhaustion. *Proc Natl Acad Sci USA*. 2019;116(25):12410-12415.
294. Xu W, Zhao X, Wang X, et al. The Transcription Factor Tox2 Drives T Follicular Helper Cell Development via Regulating Chromatin Accessibility. *Immunity*. 2019;51(5):826-839.
295. Park JE, Botting RA, Conde CD, et al. A cell atlas of human thymic development defines

T cell repertoire formation. *Science.* 2020;367(6480):eaay3224.
296. Pierluigi B, D'Angelo C, Fallarino F, et al. Thymosin α1: the regulator of regulators? *Ann N Y Acad Sci*. 2010;1194(1):1-5.
297. Yang S, Jia R, Bian Z. SRSF5 functions as a novel oncogenic splicing factor and is upregulated by oncogene SRSF3 in oral squamous cell carcinoma. *Biochim Biophys Acta - Mol Cell Res*. 2018;1865(9):1161-1172.
298. Liu J, Huang B, Xiao Y, et al. Aberrant Expression of Splicing Factors in Newly Diagnosed Acute Myeloid Leukemia. *Oncol Res Treat*. 2012;35(6):335-340.
299. Moulton VR, Tsokos GC. Alternative splicing factor/splicing factor 2 regulates the expression of the ζ subunit of the human T cell receptor-associated CD3 complex. *J Biol Chem*. 2010;285(17):12490-12496.
300. Forment J V, Kaidi A, Jackson SP. Chromothripsis and cancer: causes and consequences of chromosome shattering. *Nat Rev Cancer*. 2012;12(10):663-670.